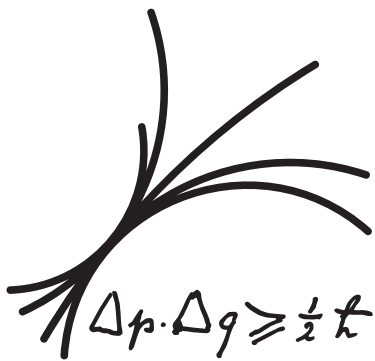


Higher-Order Predictions for Supersymmetric Particle Decays

Ananda Demian Patrick Landwehr



Technische Universität München

Max-Planck-Institut für Physik
(Werner-Heisenberg-Institut)

Higher-Order Predictions for Supersymmetric Particle Decays

Ananda Demian Patrick Landwehr

Vollständiger Abdruck der von der Fakultät für Physik
der Technischen Universität München
zur Erlangung des akademischen Grades eines
Doktors der Naturwissenschaften (Dr. rer. nat.)
genehmigten Dissertation.

Vorsitzender: Univ.-Prof. Dr. L. Oberauer

Prüfer der Dissertation: 1. Hon.-Prof. Dr. W. F. L. Hollik
2. Univ.-Prof. Dr. A. Ibarra

Die Dissertation wurde am 28.03.2012
bei der Technischen Universität München eingereicht und
durch die Fakultät für Physik am 12.06.2012 angenommen.

Zusammenfassung

In dieser Arbeit untersuchen wir QCD und elektroschwache Korrekturen auf Ein-Schleifen-Ordnung zu Squark-, Gluino- und Higgs-Boson-Zerfällen im Rahmen des Minimalen Supersymmetrischen Standard Modells (MSSM). Wir erläutern die technischen Details, die für Ein-Schleifen-Rechnungen benötigt werden und werten die Zerfälle inklusive deren Korrekturen in verschiedenen Benchmark-Szenarien aus.

Falls das MSSM an der TeV Skala realisiert ist, haben Squarks und Gluinos hohe Produktionsraten an Hadronkollider wie dem LHC. Da diese Teilchen umgehend nach der Produktion wieder zerfallen, und die Unsicherheiten in Verbindung mit den dazugehörigen Zerfallsbreiten auf niedrigster Ordnung beträchtlich sind, ist es essentiell Korrekturen in nächst höherer Ordnung zu berechnen. Daher untersuchen wir im ersten Teil dieser Arbeit QCD und elektroschwache Ein-Schleifen-Korrekturen zu den Squark Zerfällen nach Quark-Gluino, Quark-Neutralino und Quark-Chargino für Squarks aller drei Generationen. Aufgrund der großen Yukawa-Kopplungen der Quarks der dritten Generation müssen Mischungen für deren Superpartner berücksichtigt werden. Des Weiteren können die Massenunterschiede der Squark Masseneigenzustände beträchtlich sein. Daher sind für die Squarks der dritten Generation zusätzlich zu den obengenannten Zerfällen noch die Zerfälle in Squark-W/Z-Eichboson und Squark-Higgs-Boson kinematisch erlaubt. Für den Fall, dass die Gluinos schwerer sind als die Squarks, werden die Gluino Zerfälle nach Quark und Squark berechnet.

Im Gegensatz zum Higgs Sektor des Standard Modells, beinhaltet der Higgs Sektor des MSSM fünf physikalische Higgs Bosonen. Zusätzlich zu deren Zerfälle in SM Teilchen müssen auch deren Zerfälle in MSSM Teilchen betrachtet werden. Daher untersuchen wir Ein-Schleifen-Korrekturen zu Higgs Zerfällen in Neutralinos und Charginos. Als Letztes berechnen wir Korrekturen zu den Zerfällen von Higgs Bosonen in Squarks und Sleptonen.

Abstract

We study QCD and electroweak next-to-leading-order (NLO) corrections to two-body decays of squarks, the gluino and Higgs bosons within the Minimal Supersymmetric Standard Model (MSSM). The technical details needed to calculate NLO corrections to these processes are presented in this thesis. Finally the aforementioned decays and their corrections are evaluated at different benchmark scenarios.

If the MSSM is realized at the TeV scale, squarks and gluinos have large production cross sections at hadron colliders such as the LHC. Since these particles decay immediately after their production and the uncertainties connected to the decay widths on lowest order are sizeable, it is necessary to compute the corrections at NLO. In this work we examine the QCD and electroweak NLO corrections to the decays of squarks into quark-gluino, quark-neutralino and quark-chargino for the first two squark generations. Because of the large Yukawa couplings of third generation quarks, mixing effects for their superpartners, the squarks, become relevant and the mass-difference between the two mass-eigenstates can be large. This potentially opens the decays channels of third generation squarks into squark plus W/Z -boson and squark plus Higgs-boson. Lastly, we compute the gluino decay into quark plus squark, which becomes dominant when the gluino mass is larger than the squark masses.

In contrast to the Higgs sector of the Standard Model, the Higgs sector of the MSSM includes five physical Higgs bosons. In addition to their decay modes into SM particles, the decays into supersymmetric particles have to be taken into account. We examine NLO corrections to Higgs decays into neutralinos and charginos. Furthermore, we also calculate corrections to the decays of Higgs bosons into squarks and sleptons.

Contents

1	Introduction	1
2	Theoretical framework	5
2.1	The Standard Model of particle physics	5
2.1.1	Shortcomings	9
2.2	Supersymmetry and the MSSM	10
2.2.1	Motivation	10
2.2.2	From SUSY to the MSSM	11
2.2.3	The particle spectrum of the MSSM	16
3	Decay widths and branching ratios	23
3.1	Tree-level	23
3.2	Next-to-leading order	24
4	Methods in perturbation theory	27
4.1	Ultraviolet singularities	27
4.1.1	Regularization schemes	28
4.1.2	Renormalization	28
4.1.3	Renormalization of the MSSM	31
4.1.4	Resummation in the b / \tilde{b} sector	53
4.2	Infrared singularities	53
4.2.1	Soft bremsstrahlung	54
4.2.2	Collinear bremsstrahlung	55
4.3	Dependent masses in higher order calculations	56
4.4	Computation methods	56
5	Squark decays: introduction	59
5.1	Squarks at the LHC	59
5.2	Squark decays: phenomenological overview	60
5.3	Squark decays: calculations	62
6	Squark decays: process-specific calculations	65
6.1	$\tilde{q}_a \rightarrow q' \tilde{\chi}_i^\pm$ and $\tilde{q}_a \rightarrow q \tilde{\chi}_i^0$	65

6.1.1	Counterterm Lagrangian	65
6.1.2	Feynman diagrams	67
6.1.3	Partial decay widths and branching ratios	67
6.2	$\tilde{q}_a \rightarrow q\tilde{g}$	69
6.2.1	Counterterm Lagrangian	69
6.2.2	Feynman diagrams	70
6.2.3	Partial decay width and branching ratios	71
6.2.4	Color factors	72
6.3	$\tilde{q}_a \rightarrow \tilde{q}_b Z$ and $\tilde{q}_a \rightarrow \tilde{q}'_b W^\pm$	73
6.3.1	Feynman diagrams	73
6.3.2	Partial decay width and branching ratios	74
6.3.3	Dependent masses in squark–squark–Goldstone vertices	76
6.4	$\tilde{q}_a \rightarrow \tilde{q}_b h^0, H^0, A^0$ and $\tilde{q}_a \rightarrow \tilde{q}'_b H^\pm$	77
6.4.1	Counterterm Lagrangian	77
6.4.2	Feynman diagrams	80
6.4.3	Partial decay widths and branching ratios	81
6.4.4	$\tilde{q}_a \rightarrow \tilde{q}_b (h^0, H^0)$	82
6.4.5	Real radiation	83
6.4.6	$\tilde{q}_a \rightarrow \tilde{q}'_b (A^0, H^\pm)$	84
7	Squark decays: numerical evaluation	87
7.1	Input parameters	87
7.1.1	Soft and collinear cuts	92
7.2	Numerical evaluation	93
7.2.1	Dependent masses	97
7.3	Parameter dependences	99
7.3.1	Scale dependence	99
7.3.2	Dependence on $\tan\beta$	99
7.3.3	Dependence on m_{A^0}	102
7.3.4	Dependence on A_t and A_b	104
7.3.5	Parameter scan over M_{SUSY} and M_3	105
7.4	Quark jet p_T distribution	112
7.5	Comparison with SFOLD	115
8	Gluino decays	119
8.1	Overview	119
8.2	Decay width	119
8.3	Numerical evaluation	121
8.4	Dependence on the squark masses	123

9	Higgs-boson decays into sfermions, neutralinos and charginos	127
9.1	Overview	127
9.2	Amplitudes	128
9.2.1	$H \rightarrow \tilde{q}_i^* \tilde{q}'_j$	128
9.2.2	$H \rightarrow \tilde{l}_i \tilde{l}'_j$	128
9.2.3	$H \rightarrow \tilde{\chi} \tilde{\chi}$	130
9.3	Decay widths	136
9.3.1	$h^0/H^0 \rightarrow ab$	136
9.3.2	$A^0/H^\pm \rightarrow ab$	137
9.4	Numerical evaluation	137
9.4.1	$H^0 \rightarrow \tilde{\chi} \tilde{\chi}$	140
9.4.2	$h^0 \rightarrow \tilde{\chi}_1^0 \tilde{\chi}_1^0$	141
9.4.3	$H^0 \rightarrow \tilde{t}_1 \tilde{t}_1$	143
9.4.4	$H^0 \rightarrow \tilde{\tau}_1 \tilde{\tau}_1^*$	143
9.5	Comparison with HFOLD	145
10	Conclusions	147
A	Bremsstrahlung integrals	151
B	Renormalization constants	153
B.1	$\tilde{q}_a^* \tilde{q}' \tilde{\chi}_i$	153
B.2	$\tilde{q}_a^* \tilde{q}'_b V$	154
B.3	$\tilde{q}_a^* \tilde{q}'_b S$	154
B.4	$S \tilde{\chi}_i \tilde{\chi}_j$	156
C	Feynman rules	157
C.1	$\tilde{q}_s \tilde{q}' \tilde{\chi}_k$	157
C.2	$\tilde{q}_s \tilde{q} \tilde{g}^a$	158
C.3	$\tilde{q}'_s \tilde{q}_t^* V$	159
C.4	$\tilde{q}'_s \tilde{q}_t^* S$	159
C.5	$S \tilde{\chi}_n \tilde{\chi}_l$	160
D	Input parameters	163
	Acknowledgments	179

Chapter 1

Introduction

In the 20th century, our understanding of the fundamental structure of nature improved dramatically. The theories of special relativity [1] and quantum mechanics [2,3] became the corner stones to describe physics at the subatomic level. Today, all empirically known elementary particles and their interactions can be described within one theoretical framework – the Standard Model of elementary particle physics (SM) [4–8]. The SM incorporates the quarks and leptons of three generations and the gauge bosons going along with the strong, weak, and electromagnetic force. All these constituents have been detected and identified in numerous experiments. In order to provide a mathematically consistent description of these elementary particles, a scalar field which breaks the symmetry of the SM Lagrangian spontaneously, has to be introduced [9]. After this spontaneous symmetry breaking, the particles acquire masses and a further elementary particle emerges – the Higgs boson. It is the only constituent of the SM which has not been detected in high-energy experiments so far, although very recently first hints might have been observed [10,11].

In spite of the SM being in excellent agreement with most experimental data, unresolved issues remain. For example, the gravitational force cannot be included in the framework of the SM. It also lacks to describe the dark matter observed in the universe and the CP-violation necessary to explain the asymmetry between matter and antimatter. There are also issues of more theoretical nature such as the hierarchy problem connected to the Higgs-boson mass, the non-unification of gauge couplings, and the origin and nature of quark and lepton masses. These issues are strong hints that the SM is an effective theory of a more fundamental one, i.e. that it only describes phenomena for currently available energies but has to be extended in order to explain physics at higher energy scales. There are numerous such extensions of the SM amongst which supersymmetric extensions [12] are of particular interest.

Supersymmetry (SUSY) is a theory which relates bosons with fermions. The minimal supersymmetric extension of the SM (MSSM) [13,14] postulates scalar partners to the SM fermions – the sfermions – and fermionic partners to the SM gauge and Higgs bosons – the gauginos and higgsinos. If SUSY was an exact symmetry, SUSY partners would have the same masses as their SM partner particles and would have been detected by now. Since no SUSY particle has been observed so far, SUSY has to be broken at lower energies in

order to allow for heavier SUSY particles. If the masses of the SUSY particles are at the TeV scale, the hierarchy problem is solved owing to the existing particles of different spin statistics of SUSY particles and the SM gauge couplings unify at high energies due to the enlarged particle spectrum. In order to circumvent problems with proton decay, an additional discrete symmetry called R-parity [15] is introduced. Besides avoiding terms yielding fast proton decay, it renders the lightest SUSY particle (LSP) stable, which in large regions of parameter space is a viable dark matter candidate. Finally, gravity can potentially be included by promoting SUSY to a local symmetry.

Up to now, there are no direct hints of SUSY particles. The absence of direct evidence at high-energy particle accelerators such as LEP and the Large Hadron Collider (LHC) gives lower bounds on their masses [16]. On the other hand, indirect hints from precision observables such as the mass of the W boson M_W , the anomalous magnetic moment of the muon $(g - 2)_\mu$ or B-physics observables at low energies provide a powerful tool for testing the MSSM (or other models) with empirical data [17]. However, with the LHC still acquiring data and eventually moving to higher energies, it will be possible to detect or exclude supersymmetric particles at higher mass scales which is one of the main goals of the LHC. If SUSY is realized at the TeV scale, production of superpartners of quarks and gluons – squarks and gluinos – is among the most important production channels of SUSY particles. Since, in general, squarks and gluinos have very short life-times, it is important to have precise knowledge about their decays. Studying these decays will be important in order to determine the couplings and parameters associated with these particles. Since the predictions for decays are significantly affected by QCD and electroweak higher-order effects, the computation of next-to-leading order (NLO) contributions is necessary. Hence, in the first part of this thesis, we give precise calculations including all electroweak and QCD NLO contributions to decay widths of squark and gluino two-body decays. In order to study these decays and the associated NLO contributions, the general results are evaluated numerically in specific benchmark scenarios.

SUSY also enriches the phenomenology of Higgs physics. In order to get a consistent theory, the MSSM has to include two scalar doublets, which after spontaneous symmetry breaking result in five physical Higgs bosons. Since these Higgs bosons can also decay into SUSY particles, they have complex decay signatures in the MSSM. Precise predictions for Higgs-boson decays are substantial for probing the nature of electroweak and SUSY breaking. Therefore, in the second part of this thesis, two-body decays of Higgs bosons into SUSY particles including NLO QCD and electroweak corrections will be examined.

The outline of this thesis is as follows:

- In Chapter 2, the theoretical framework is introduced. First, the building blocks of the SM and some of its open questions are reviewed. Then, construction of supersymmetric theories is shortly sketched. This chapter is concluded by presenting the Lagrangian and field-content of the MSSM.
- Relevant physical observables are then introduced in Chapter 3. The definitions of decay widths and branching ratios at the tree-level and at NLO in perturbation

theory are given.

- In Chapter 4, first, possible divergencies for high internal loop momenta are addressed. We shortly mention the different regularization schemes and give the regularization procedure used throughout this work. Furthermore, we give an detailed description of the renormalization of the MSSM. Finally, treatment of soft and collinear divergencies is discussed.
- In Chapter 5, a phenomenological overview over squark decays is given. We discuss the different decay modes of squarks and give a survey over the different computations performed so far.
- The specific details for the computation of radiative corrections to the different squark decays are presented in Chapter 6. We list the Lagrangians and derive counterterm Lagrangians for the different squark interactions, picture the Feynman diagrams needed to calculate the NLO amplitudes and write down the decay widths for the different squark decays.
- The numerical evaluation of the preceding calculation is presented in Chapter 7. The decay widths and branching ratios of squarks are evaluated in different benchmark scenarios and dependences on different MSSM parameters are shown. Finally, we also present the p_T distributions of the quark jet in squark decays into quark plus neutralino.
- In Chapter 8, gluino decays are discussed. We begin with a very brief phenomenological overview. The calculation is performed in analogy to the one for squark decays. In the last section the numerical evaluation including parameter dependence studies is presented.
- Higgs-boson decays into SUSY particles are the topic of Chapter 9. As before we give a short introduction and present the details of the computations including the derivation of the counterterm Lagrangians, Feynman diagrams contributing to these processes, and decay widths for the different Higgs-boson decay channels. Again, we conclude this chapter with a numerical survey at specific benchmark points.
- Finally, in Chapter 10 we summarize our work. In the appendices, we provide needed analytical formulas for bremsstrahlung integrals. We also list detailed expressions appearing in the counterterm Lagrangians in Chapters 6 and 9 and the Feynman rules relevant for the computed processes. Finally, more details are given on obtaining low-energy input parameters for the numerical evaluations.

Chapter 2

Theoretical framework

In this chapter, the Standard Model of elementary particle physics (SM) and its supersymmetric extension, the Minimal Supersymmetric Standard Model (MSSM), are introduced. In Section 2.1, the SM Lagrangian and its particle spectrum are discussed and in the last part, the most prominent shortcomings of the SM are pointed out.

Supersymmetric theories represent a class of the most prominent models to explain some of the open problems of the SM. They are introduced in Section 2.2. First, the general idea of supersymmetric theories is roughly sketched and the MSSM is elaborated in more detail. The different sectors are then discussed separately and the tree-level mass spectrum of all particles in the MSSM is worked out.

2.1 The Standard Model of particle physics

All particles and interactions known today – apart from gravity – can be described within one framework, the Standard Model of elementary particles (SM) [4–8]. It has high predictive power and is compatible with most experimental data.

The SM is a renormalizable field theory [18] with the Poincaré group of space-time transformations as outer symmetry. Matter – electrons and quarks – is described by chiral fermions, whereas their interactions are incorporated by imposing local gauge invariance under the direct product $SU(3)_C \times SU(2)_L \times U(1)_Y$. Interactions of the different fermions are defined by their charges under the different gauge groups.

$SU(3)_C$ is the gauge group of strong interactions also known as quantum chromodynamics (QCD) with the Gell-Mann matrices T^a ($a = 1, \dots, 8$) as generators. Electromagnetic and weak interactions are incorporated into the unified group $SU(2)_L \times U(1)_Y$ with the respective generators I^i ($i = 1, 2, 3$) and Y . The different generators fulfill the commutation relations

$$[T^a, T^b] = if^{abc}T^c, \quad [I^i, I^j] = i\varepsilon^{ijk}I^k, \quad [Y, Y] = 0. \quad (2.1)$$

The electric charge Q is connected to the third component of the weak isospin (I^3) and hyperweak charge (Y) through the Gell-Mann–Nishijima relation, which, after electroweak

	1st generation	2nd generation	3rd generation	I	I^3	Y	Q
quarks	$\begin{pmatrix} u \\ d \end{pmatrix}_L$	$\begin{pmatrix} c \\ s \end{pmatrix}_L$	$\begin{pmatrix} t \\ b \end{pmatrix}_L$	$1/2$	$1/2$	$1/3$	$2/3$
	u_R	c_R	t_R	$1/2$	$-1/2$	$1/3$	$-1/3$
	d_R	s_R	b_R	0	0	$4/3$	$2/3$
				0	0	$-2/3$	$-1/3$
leptons	$\begin{pmatrix} \nu_e \\ e \end{pmatrix}_L$	$\begin{pmatrix} \nu_\mu \\ \mu \end{pmatrix}_L$	$\begin{pmatrix} \nu_\tau \\ \tau \end{pmatrix}_L$	$1/2$	$1/2$	$1/3$	$2/3$
				$1/2$	$-1/2$	$1/3$	$-1/3$

Table 2.1: Fermion (spin $1/2$) fields of the SM and their quantum numbers: the weak isospin I , its third component I^3 , the weak hypercharge Y and the electromagnetic charge Q . The last three charges are related via the Gell-Mann-Nishijima relation (2.2).

symmetry breaking, will turn out to be

$$Q = I^3 + \frac{Y}{2}. \quad (2.2)$$

The charges and transformation properties of the fermions under the gauge groups define their interactions with the associated forces or rather gauge bosons. Quarks carry “color” charge and are arranged in $SU(3)_C$ triplets, whereas the color-neutral leptons are $SU(3)_C$ singlets. In order to correctly describe parity violation of the weak interaction, left-handed fermions are arranged in $SU(2)_L$ doublets whereas right-handed fermions are $SU(2)_L$ singlets. The complete list of matter fields can be found in Tab. 2.1.

A local $SU(3)_C \times SU(2)_L \times U(1)_Y$ transformation can be written as the exponentiation of the generators

$$U(x) = e^{-i(g_s \theta_s^a(x) T^a + g_2 \theta_2^i(x) I^i + g_1 \theta_1(x) Y)} \quad (2.3)$$

with the space-time dependent parameters $\theta_s(x)$, $\theta_2(x)$ and $\theta_1(x)$. Fermions then transform under this function as

$$\Psi \rightarrow \Psi' = U(x)\Psi. \quad (2.4)$$

In order to maintain the invariance of the SM Lagrangian under this transformation, the covariant derivative D_μ has to be introduced,

$$D_\mu = \partial_\mu + ig_s T^a G_\mu^a + ig_2 I^i W_\mu^i + ig_1 \frac{Y}{2} B_\mu \quad (2.5)$$

with the local spin-1 gauge fields for the strong (G_μ^a), weak (W_μ^i) and hyperweak (B_μ) interaction. They are defined to transform as

$$A_\mu \rightarrow A'_\mu = U(x)(A_\mu + i\partial_\mu)U^{-1}(x), \quad (2.6)$$

where A_μ stands for any of the three gauge fields. With these ingredients the kinetic terms for fermions and gauge fields can be written down,

$$\mathcal{L}_{\text{fermion}} = q_L^\dagger \not{D} q_L + l_L^\dagger \not{D} l_L + u_R^\dagger \not{D} u_R + d_R^\dagger \not{D} d_R + e_R^\dagger \not{D} e_R, \quad (2.7a)$$

$$\mathcal{L}_{\text{gauge}} = -\frac{1}{4} G^{a\mu\nu} G_{\mu\nu}^a - \frac{1}{4} W^{i\mu\nu} W_{\mu\nu}^i - \frac{1}{4} B^{\mu\nu} B_{\mu\nu}, \quad (2.7b)$$

where the sum over the three generations has been emitted. The field-strength tensors in (2.7b) are defined as

$$G_{\mu\nu}^a = \partial_\mu G_\nu^a - \partial_\nu G_\mu^a - g_s f_{abc} G_\mu^b G_\nu^c, \quad (2.8a)$$

$$W_{\mu\nu}^i = \partial_\mu W_\nu^i - \partial_\nu W_\mu^i - g_2 \epsilon^{ijk} G_\mu^j G_\nu^k, \quad (2.8b)$$

$$B_{\mu\nu} = \partial_\mu B_\nu - \partial_\nu B_\mu. \quad (2.8c)$$

Gauge-invariance forbids explicit mass terms for fermions and gauge bosons. The solution has been elaborated by Brout, Englert, Guralnik, Hagen, Higgs, and Kibble – the Higgs mechanism [9]. They postulate a two-component complex scalar field $H^T = (\phi^+, \phi^0)$ – the Higgs field – which is a doublet under $SU(2)_L$ with hypercharge $Y = +1$. Due to the scalar potential

$$V(H) = -\mu^2 H^\dagger H + \frac{\lambda}{4} (H^\dagger H)^2, \quad \mu^2, \lambda > 0 \quad (2.9)$$

the Higgs field acquires a non-vanishing vacuum state which spontaneously brakes the $SU(2)_L \times U(1)_Y$ symmetry down to $U(1)_{\text{em}}$. The minimum is obtained for $|\langle H \rangle|^2 = 2\mu^2/\lambda \equiv v/2$, with the vacuum expectation value (vev) v . In the unitarity gauge, the Higgs ground state is given by $\langle H^T \rangle = (0, v/\sqrt{2})$. Furthermore, Yukawa couplings between the fermion fields and the scalar Higgs field are introduced. This yields the Lagrangian

$$\begin{aligned} \mathcal{L}_{\text{Higgs}} &= (D_\mu H)^\dagger (D^\mu H) - V(H) \\ &\quad - \sum_{i,j=1}^3 \left[y_d^{ij} q_L^{i\dagger} H d_R^j + y_u^{ij} q_L^{i\dagger} H^c u_R^j + y_{ij}^l l_L^{i\dagger} H e_R^j \right], \end{aligned} \quad (2.10)$$

where the charge conjugation of the Higgs field is defined as $H^c = i\sigma^2 H^*$.

The Higgs field can be expanded around its ground state $\langle H \rangle$

$$H(x) = \begin{pmatrix} \phi^+(x) \\ \frac{1}{\sqrt{2}}(v + h(x) + i\chi(x)) \end{pmatrix}, \quad \phi^-(x) \equiv (\phi^+(x))^\dagger. \quad (2.11)$$

The field $h(x)$ then describes the physical Higgs boson, $\phi^\pm(x)$ and $\chi(x)$, the would-be Goldstone bosons of the broken $SU(2)_L \times U(1)_Y$, turn out to be unphysical degrees of freedom, which will disappear from the physical spectrum in order to render the W^\pm and Z bosons massive. Choosing an appropriate gauge (unitarity gauge) this would-be Goldstone bosons disappear and only $h(x)$ remains.

Inserting the expansion (2.11) into the Lagrangian (2.10), the $SU(2)_L \times U(1)_Y$ symmetry is broken down to $U(1)_{\text{em}}$ whose generator Q is given by (2.2). The emerging mass matrix

for the gauge fields W_μ^i and B_μ has to be diagonalized leading to the physical gauge fields W_μ^\pm , Z_μ and A_μ , which are linear combinations of W_μ^i and B_μ ,

$$W_\mu^\pm = \frac{1}{\sqrt{2}} (W_\mu^1 \pm W_\mu^2), \quad (2.12a)$$

$$\begin{pmatrix} Z_\mu \\ A_\mu \end{pmatrix} = \begin{pmatrix} \cos \theta_W & -\sin \theta_W \\ \sin \theta_W & \cos \theta_W \end{pmatrix} \begin{pmatrix} W_\mu^3 \\ B_\mu \end{pmatrix}. \quad (2.12b)$$

The weak mixing angle θ_W is given by

$$c_W \equiv \cos \theta_W = \frac{g_2}{\sqrt{g_1^2 + g_2^2}}, \quad s_W \equiv \sin \theta_W = \frac{g_1}{\sqrt{g_1^2 + g_2^2}}. \quad (2.13)$$

W^\pm gauge bosons have a charge of ± 1 under Q , whereas the Z boson and the photon are electrically neutral. Furthermore, the masses of these gauge bosons turn out as

$$M_W = \frac{g_2 v}{2}, \quad M_Z = \frac{v}{2} \sqrt{g_1^2 + g_2^2}. \quad (2.14)$$

The photon stays massless, since it is the gauge boson connected to the unbroken symmetry $U(1)_{\text{em}}$. Its gauge coupling, the electrical charge e , is related to the couplings g_1 and g_2 via $e = g_1 g_2 / \sqrt{g_1^2 + g_2^2}$. Since the masses of the gauge bosons are known, the vev is fixed to $v \approx 246$ GeV. Moreover, the physical Higgs field $h(x)$ acquires a mass term

$$M_h = \sqrt{2} \mu = \frac{v \lambda}{2}, \quad (2.15)$$

which is determined by the quadratic coupling μ . Hence, the Higgs-boson mass is a free parameter in the SM and remains the only parameter of the SM which has not been measured yet.

Fermion masses are generated by the Yukawa couplings in (2.10). After insertion of the ground state $\langle H \rangle$ complex-valued mass matrices $M_{ij}^f = 1/\sqrt{2} y_{ij}^f v$ for the fermions emerge. They can be diagonalized by a bi-unitary transformation. The resulting mass eigenstates for the fermionic fields and their masses are

$$f_L^i = \sum_{k=1}^3 U_{ik}^{f,L} f_L^k, \quad f_R^i = \sum_{k=1}^3 U_{ik}^{f,R} f_R^k, \quad (2.16a)$$

$$m_{f,i} = \frac{v}{\sqrt{2}} \sum_{k,m=1}^3 U_{ik}^{f,L} y_{km}^f \left(U_{mi}^{f,R} \right)^\dagger \equiv \frac{v}{\sqrt{2}} \lambda_i^f, \quad (2.16b)$$

where $U_{ik}^{f,L}$ and $U_{ik}^{f,R}$ are the unitarity matrices for the left- and right-handed fields $f_i = u_i, d_i, e_i$. Considering interactions between fermions and gauge bosons, these unitarity matrices enter when expressing the gauge eigenstates by the mass eigenstates (2.16b). However, in interactions with neutral gauge bosons, these matrices drop out due to their unitarity. Hence, there are no flavor-changing neutral currents (FCNC) at tree-level. Since

the W^\pm boson connects up- and down-type fermions, products of up- and down-type matrices emerge. The Cabibbo-Kobayashi-Maskawa (CKM) mixing matrix,

$$V_{\text{CKM}} = U^{u,L} (U^{d,L})^\dagger \quad (2.17)$$

remains in charged current interaction. It can be parameterized by four parameters, three angles and one CP-violating phase. Together with the strong CP-violating term of QCD, this phase is the only source of CP-violation within the SM.

2.1.1 Shortcomings

The SM is very successful in describing experimental data, it inhibits all known elementary particles and their interactions [16] and fits experimental precision observables¹ well [20,21]. The parameters of the SM that remain to be determined are the Higgs-boson mass and associated couplings.

Despite of its experimental success, there are theoretical and experimental considerations, which consolidates the assumption that there is a more fundamental theory at higher energies. Furthermore, the SM does not account for all fundamental phenomena. The most prominent being its lacking of describing gravitational interactions, which become important at energies reaching the Planck scale $\Lambda_{\text{Planck}} \sim 10^{18}$ GeV. If the SM was valid up to this scale, it would have to describe gravitational interactions.

A further deficiency of the SM is given by cosmological observations, the most prominent being the measurement of rotation curves of galaxies. For large distances from the center of the galaxy, the velocity of a star is expected to behave as $v^2 \sim 1/R$, where R is the distance between the star and the center of the galaxy. However, for the outer stars the rotation curves are almost constant with respect to R . This behavior can be reproduced by surrounding the galaxy with non-luminous (electrically neutral) matter – dark matter (DM). The existence of DM is reinforced by precision measurements of the cosmic microwave background. The only electrically neutral particle in the SM is the neutrino. However, because of its small mass it does not reproduce the right small-scale structure of the universe and therefore is not a viable DM candidate.

In addition, there are also theoretical considerations which motivate extensions at higher energies. If the SM was valid up to high energy scales, i.e. the Planck scale $\Lambda_{\text{Planck}} \sim 10^{18}$ GeV, the smallness of the weak scale compared to the Planck scale would have to be explained. This is addressed as the hierarchy problem. This hierarchy expresses itself when considering the Higgs-boson mass and its radiative corrections. From electroweak symmetry breaking, one expects the Higgs-boson mass to be of the order of the weak scale. However, it gets corrections due to Higgs self-couplings and couplings to heavy fermions and gauge bosons. The dominant contributions are

$$\Delta M_h^2 = \frac{3\Lambda_{\text{cut}}^2}{8\pi v^2} (M_h^2 + 2M_W^2 + M_Z^2 - 4m_t^2), \quad (2.18)$$

¹The largest deviation is measured for the anomalous magnetic moment of the muon $g_\mu - 2$. Its measurement differs over three standard deviations from high-precision computations [19].

where integrals over the loop-momenta are cut at the scale Λ_{cut} where new physics enters. If the SM is valid up to high scales such as the GUT scale $\Lambda_{\text{GUT}} \sim 10^{15}$ GeV or the Planck scale $\Lambda_{\text{Planck}} \sim 10^{18}$ GeV the corrections would be up to 30 orders of magnitude larger than the expected Higgs-boson mass, i.e. $\Delta M_h^2/M_h^2 \sim 10^{30}$. The Higgs-boson mass would suffer under an unnaturally severe fine-tuning. Therefore this is known as the fine-tuning or naturalness problem.

2.2 Supersymmetry and the MSSM

In this section, supersymmetry (SUSY) is introduced and motivated relying on [22, 23]. The formal derivations of supersymmetric Lagrangians are kept to a minimum. Detailed elaborations can be found in [22] on which our discussion is based. More space will be given to the Minimal Supersymmetric Standard Model (MSSM) and its renormalization.

2.2.1 Motivation

Coleman and Mandula showed that any group combining an internal symmetry group with the Poincaré group can only be built of their direct product with commuting operators [24]. This no-go theorem can be circumvented by supersymmetric groups, whose generators fulfill commutator as well as anti-commutator relations,

$$\{Q_A, Q_B\} = \{\bar{Q}^{\dot{A}}, \bar{Q}^{\dot{B}}\} = 0, \quad (2.19a)$$

$$\{Q_A, \bar{Q}_{\dot{B}}\} = 2(\sigma^\mu)_{A\dot{B}} P_\mu, \quad (2.19b)$$

$$[Q_A, P_\mu] = [\bar{Q}^{\dot{A}}, P_\mu] = 0, \quad (2.19c)$$

$$[M_{\mu\nu}, Q_A] = -(\sigma_{\mu\nu})^B_A Q_B, \quad (2.19d)$$

$$[M_{\mu\nu}, \bar{Q}^{\dot{A}}] = -(\sigma_{\mu\nu})^{\dot{A}}_{\dot{B}} \bar{Q}^{\dot{B}}, \quad (2.19e)$$

where the two-component Weyl-spinor notation of [22] has been adapted and P_μ , $M_{\mu\nu}$ are the generators of the Poincaré group. Q_A and $\bar{Q}^{\dot{A}}$ represent the SUSY generators and their conjugate. When acting on a particle, it changes its spin by 1/2, i.e. bosons are transformed into fermions and vice versa. In general, N independent SUSY generators can be assumed. However, in four-dimensional field theory, $N > 1$ SUSY theories do not allow for chiral fermions. Therefore, in this thesis – and for most phenomenological studies – the case $N = 1$ is considered, where only one SUSY generator is present. In $N = 1$ supersymmetric models, each SM spin-1/2 particle is accompanied by a spin-0 SUSY partner and vice versa. They are arranged in chiral superfields. The spin-1 vector-bosons get a spin-1/2 partner and are arranged in vector superfields. By construction, the superpartners have the same couplings to gauge bosons and the same masses as their SM partners. The equivalence of the masses will be canceled by the soft SUSY-breaking terms which are introduced when constructing the Minimal Supersymmetric Standard Model (MSSM).

In Subsection 2.1.1 a selection of the most important drawbacks of the SM has been discussed. They can all be addressed by supersymmetric models. Concerning the naturalness or fine-tuning problem emerging from the hierarchy problem, supersymmetry provides a very elegant solution. For each diagram contributing to the Higgs-boson mass corrections (2.18) diagrams containing the supersymmetric partner particles are present. In exact SUSY these contributions from SM particles and their SUSY partners exactly cancel due to different spin statistics. In the phenomenological relevant models with softly broken SUSY, the Higgs-boson mass corrections are proportional to the squared-mass differences between SM and SUSY partners and only grow logarithmically with the cutoff scale,

$$\Delta M_h^2 = \frac{m_f^2}{4\pi v^2} (m_f^2 - m_s^2) \log \left(\frac{\Lambda_{\text{cut}}}{m_s} \right). \quad (2.20)$$

The masses of the fermionic SM particles are denoted as m_f and the mass of their supersymmetric partners as m_s . Hence, for SUSY masses m_s up to the TeV scale the naturalness problem is solved.

Moreover, many SUSY models – especially the MSSM – provide for a lightest supersymmetric particle (LSP). In many models it fulfills the conditions for a stable, massive, weakly interacting particle and therefore is a viable DM candidate.

A further nice feature of SUSY models with a particle spectrum at the TeV scale is that they alter the renormalization group equations for the gauge couplings in such a way, that the three couplings meet at one point, i.e. at the grand unification (GUT) scale $\Lambda_{\text{GUT}} \sim 10^{16}$ GeV and allow for unification of the electroweak and strong forces.

2.2.2 From SUSY to the MSSM

Theoretical concepts of SUSY

At this point, the construction of $N = 1$ supersymmetric theories is sketched. An elegant way is to adapt the superfield formalism introduced in [25]. In superspace, four-dimensional space-time is extended by two anti-commuting, spinor-like Grassmann variables θ^A and $\bar{\theta}_{\dot{A}}$. Acting on this superspace, superfields $\Phi(x, \theta, \bar{\theta})$ can be defined consisting of irreducible representations, the chiral and vector superfields. Chiral superfields contain a spin-0 complex scalar and a spin- $1/2$ Weyl spinor field, whereas vector superfields describe spin- $1/2$ Weyl spinor and spin-1 vector fields. In addition to these physical fields, each superfield contains an additional auxiliary field, such that there are the same number of bosonic and fermionic degrees of freedom in both super-multiplets. They are denoted as F-term for chiral and D-term for vector superfields. These auxiliary fields have no dynamical degrees of freedom and can be eliminated using their equations of motion. Under SUSY transformations they transform as total derivatives and hence lead to a SUSY invariant action when surface terms are discarded.

In order to construct a general renormalizable supersymmetric Lagrangian, only terms with mass dimension less or equal four are allowed. For multiple fields denoted by an index

i , these are the superfield Φ_i and the products $\Phi_i\Phi_j$ and $\Phi_i\Phi_j\Phi_k$. As a matter of fact, both products are chiral superfields again. They can be combined to the superpotential

$$\mathcal{W} = h_i\Phi_i + \frac{1}{2}m_{ij}\Phi_i\Phi_j + \frac{1}{3!}f_{ijk}\Phi_i\Phi_j\Phi_k, \quad (2.21)$$

where the mass terms m_{ij} and couplings f_{ijk} are symmetric in their indices. In order not to spoil supersymmetry, only the F-term of the superpotential is taken to construct the interaction Lagrangian

$$\mathcal{L}_{\text{int}} = [\mathcal{W} + \text{hc}]_F, \quad (2.22)$$

where ‘‘hc’’ denotes the hermitian conjugate.

For the kinetic terms, the product of a chiral superfield with its complex-conjugate is taken, which is a vector superfield. Thus, supersymmetry invariance requires that the Lagrangian only contains the D-term of this product. In order to maintain gauge-invariance, gauge transformations for chiral superfields $\Phi \rightarrow e^{-i2g\Lambda^a(z)T^a}$ and vector superfields $e^{2gV} \rightarrow e^{-i2g\Lambda^\dagger} e^{2gV} e^{i2g\Lambda}$ are needed. T^a is the generator of a $SU(N)$ gauge group obeying $[T^a, T^b] = if^{abc}T^c$ and $\Lambda(z)$ is a chiral superfield specifying the local gauge transformation. Thus, the kinetic term can be written as

$$\mathcal{L}_{\text{kin}} = [\Phi^\dagger e^{2gV} \Phi]_D. \quad (2.23)$$

The kinetic terms for gauge bosons and their spin- $1/2$ partners are constructed with help of the supersymmetric field strength tensor W_A , which is defined as

$$W_A = -\frac{1}{4}\bar{D}_{\dot{A}}\bar{D}^{\dot{A}}D_A V \quad \text{and} \quad W_A = -\frac{1}{4}\bar{D}_{\dot{A}}\bar{D}^{\dot{A}}e^{-2gV}D_A e^{2gV}, \quad (2.24)$$

for abelian and non-abelian gauge groups, respectively. Here

$$D_A = \partial/\partial\theta^A - i\sigma_{AB}^\mu \bar{\theta}^{\dot{B}} \partial_\mu \quad \text{and} \quad \bar{D}_{\dot{A}} = -\partial/\partial\bar{\theta}^{\dot{A}} + i\theta^B \sigma_{BA}^\mu \partial_\mu \quad (2.25)$$

are the supersymmetric covariant derivatives, where σ_{AB}^μ denote the Pauli matrices and $\partial/\partial\theta^A$ the derivative with respect to the Grassmann number θ^A . Hence, the supersymmetric field strength is given by

$$\mathcal{L}_{\text{gauge}} = \left[\frac{1}{16g^2} \text{Tr} (W^A W_A) + \text{hc} \right]_F. \quad (2.26)$$

Since W_A is a chiral field, the F-term of the above expression has to be taken, such that SUSY is conserved.

With these ingredients the supersymmetric Lagrange density can be constructed. By convention it is grouped into F- and D-terms

$$\mathcal{L} = \mathcal{L}_F + \mathcal{L}_D, \quad (2.27a)$$

$$\mathcal{L}_F = \mathcal{L}_{\text{int}} + \mathcal{L}_{\text{gauge}} = \left[(\mathcal{W} + \text{hc}) + \frac{1}{16g^2} (\text{Tr}(W^A W_A) + \text{hc}) \right]_F, \quad (2.27b)$$

$$\mathcal{L}_D = \mathcal{L}_{\text{kin}} = [\Phi^\dagger e^{2gV} \Phi]_D. \quad (2.27c)$$

The F-term contains the superpotential and the kinetic terms for the vector superfields, whereas the kinetic terms for the chiral superfields are collected in the D-term of the Lagrangian.

Field content of the MSSM

The MSSM is a $N = 1$ supersymmetric extension of the SM based on the theoretical framework presented in the previous subsection. It is minimal in the sense, that it introduces the least number of particles, such that the theory is invariant under the SM gauge groups $SU(3)_C \times SU(2)_L \times U(1)_Y$ and only has one SUSY generator Q_A .

As aforementioned, SM particles and their supersymmetric partner particles (sparticles) are arranged in chiral and vector supermultiplets. In general, spin-0 superpartners of fermionic particles are denoted with a precedent “s-” and spin- $1/2$ superpartners of bosonic particles with an appended “-ino”. The quarks and squarks as well as the leptons and sleptons are arranged in chiral superfields, generally denoted as fermions and sfermions. Since the left- and right-handed SM fermions are separate Weyl spinor they get their own superpartners, denoted as left- and right-handed sfermions. The SM gauge fields, the gluon, W- and B-boson get spin- $1/2$ superpartners called gluino, wino, and bino, respectively. Special care has to be taken when constructing the Higgs sector of the MSSM. In the SM it is possible to give masses to up- and down-type fermions with one Higgs doublet field by writing down Yukawa terms containing H and H^c . The Yukawa terms in the MSSM stem from the superpotential \mathcal{W} which has to be an analytic function of chiral superfields. Hence, it cannot contain H and H^c simultaneously. Therefore, two Higgs doublets H_u and H_d with hypercharge $Y = 1$ and -1 have to be introduced, which give mass to up- and down-type fermions separately. These Higgs doublet fields and their spin- $1/2$ superpartners, the higgsinos, are described by chiral superfields. The field content of the MSSM is collected in Tab. 2.2.

R-parity

A general superpotential for the MSSM would contain terms which violate baryon (B) and lepton number (L). Such terms are severely constrained, since B- and L-violating processes have not been seen experimentally. The most prominent constraint is given by the non-observation of proton decay. Therefore, in the MSSM a further symmetry – R-parity [15] – is added, which eliminates these possible B- and L-violating terms in the superpotential and soft-breaking terms.

R-parity is a multiplicatively conserved quantum number, which is assigned to each particle,

$$P_R = (-1)^{3(B-L)+2s}, \quad (2.28)$$

where s denotes the particle’s spin. Accordingly, SM and Higgs particles obtain an positive R-parity $P_R = +1$ and their supersymmetric partners carry $P_R = -1$. R-parity conservation then implies that all vertices in the theory contain an even number of supersymmetric ($P_R = -1$) particles. This has important phenomenological consequences. First, the LSP

	Name	Label	Bosonic field	Fermionic field	$(SU(3)_C, SU(2)_L, U(1)_Y)$
chiral superfields		Q	$\tilde{q}_L = (\tilde{u}_L, \tilde{d}_L)$	$q_L = (u_L, d_L)$	$(\mathbf{3}, \mathbf{2}, +1/3)$
	(s)quarks	\bar{U}	\tilde{u}_R^*	$\bar{u}_L = u_R^c$	$(\bar{\mathbf{3}}, \mathbf{1}, -4/3)$
		\bar{D}	\tilde{d}_R^*	$\bar{d}_L = d_R^c$	$(\bar{\mathbf{3}}, \mathbf{1}, +2/3)$
	(s)leptons	L	$\tilde{l}_L = (\tilde{\nu}_L, \tilde{e}_L)$	$l_L = (\nu_L, e_L)$	$(\mathbf{1}, \mathbf{2}, -1)$
		\bar{E}	\tilde{e}_R^*	$\bar{e}_L = e_R^c$	$(\mathbf{1}, \mathbf{1}, +2)$
	Higgs(ino)	H_u	$h_u = (h_u^+, h_u^0)$	$\tilde{h}_u = (\tilde{h}_u^+, \tilde{h}_u^0)$	$(\mathbf{1}, \mathbf{2}, +1)$
	H_d	$h_d = (h_d^0, h_d^-)$	$\tilde{h}_d = (\tilde{h}_d^0, \tilde{h}_d^-)$	$(\mathbf{1}, \mathbf{2}, -1)$	
vector superfield	gluon/gluino	G	g^a	\tilde{g}^a	$(\mathbf{8}, \mathbf{1}, 0)$
	W(ino)	W	W^i	\tilde{W}^i	$(\mathbf{1}, \mathbf{3}, 0)$
	B(ino)	B	B^i	\tilde{B}^i	$(\mathbf{1}, \mathbf{1}, 0)$

Table 2.2: Field content of the MSSM. As a convention, superfields are labeled with capital letters and the superpartners of SM field are denoted with a tilde. The gauge group representation (bold numbers) and the hyperweak charge are arranged as $(SU(3)_C, SU(2)_L, U(1)_Y)$. The indices $a = 1 \dots 8$ and $i = 1 \dots 3$ denote the $SU(3)_C$ and the $SU(2)_L$ quantum numbers, whereas the color and generation indices have been suppressed.

must be stable, since its decay into SM particles would violate R-parity conservation. If the LSP is electrically neutral, it is an attractive DM candidate, whereas charged LSPs are excluded by cosmological constraints. Second, supersymmetric particles decay through possibly long decay chains ending up in usually one LSP. Lastly, at collider experiments always an even number of sparticles is produced resulting in final states with an even number of LSPs (if the decays are fast enough).

SUSY-breaking and the softly broken MSSM

It was mentioned before that in SUSY-conserving theories masses of particles in identical supermultiplets are the same. In the MSSM, this would imply mass equality between SM particles and their superpartners. In that case, SUSY particles would already have been detected. Hence, in a realistic supersymmetric extension SUSY has to be broken. From a theoretical point of view, SUSY is expected to be broken spontaneously. Hence the underlying Lagrangian is invariant under SUSY transformations whereas the vacuum state is not, such that SUSY is hidden at low scales. SUSY breaking in the MSSM sector is

phenomenologically ruled out. Thus, it typically occurs in an unknown (hidden) sector and then is mediated to the MSSM sector. In the MSSM, our ignorance how SUSY breaking specifically happens is parameterized by the soft-breaking parameters. These soft-breaking terms are chosen such that they introduce no new quadratic divergent corrections to scalar masses in order not to reintroduce the naturalness problem. The most general soft-SUSY-breaking, R-parity conserving Lagrangian is given by [26],

$$\begin{aligned}
\mathcal{L}_{\text{soft}} = & -\frac{1}{2} \left(M_1 \tilde{B} \tilde{B} + M_2 \tilde{W} \tilde{W} + M_3 \tilde{g}^a \tilde{g}^a + \text{hc} \right) \\
& - \left(\tilde{u}_{i,R}^* a_{ij}^u \tilde{q}_{j,L} \cdot h_u - \tilde{d}_{i,R}^* a_{ij}^d \tilde{q}_{j,L} \cdot h_d - \tilde{e}_{i,R}^* a_{ij}^e \tilde{l}_{j,L} \cdot h_d + \text{hc} \right) \\
& - \tilde{q}_{i,L}^\dagger (M_{\tilde{q}_L}^2)_{ij} \tilde{q}_{j,L} - \tilde{u}_{i,R}^* (M_{\tilde{u}_R}^2)_{ij} \tilde{u}_{j,R} - \tilde{d}_{i,R}^* (M_{\tilde{d}_R}^2)_{ij} \tilde{d}_{j,R} \\
& - \tilde{l}_{i,L}^\dagger (M_{\tilde{l}_L}^2)_{ij} \tilde{l}_{j,L} - \tilde{e}_{i,R}^* (M_{\tilde{e}_R}^2)_{ij} \tilde{e}_{j,R} \\
& - m_{h_u}^2 h_u^\dagger h_u - m_{h_d}^2 h_d^\dagger h_d - (b h_u \cdot h_d + \text{hc}), \tag{2.29}
\end{aligned}$$

where $a = 1, \dots, 8$ denotes the color, $i = 1, 2, 3$ the generation indices, and $a \cdot b \equiv \epsilon^{ij} a^i b^j$. The first line in (2.29) contains the gaugino mass terms, the second line the trilinear Higgs–sfermion–sfermion interactions, the third and fourth line the sfermion and slepton mass terms, and the fifth line the Higgs mass terms and bilinear couplings. The gaugino mass terms $M_{1,2,3}$ and the bilinear Higgs interaction term b are in general complex numbers, whereas the Higgs mass parameters $m_{h_{u,d}}$ have real values. Sfermion mass- and trilinear coupling-parameters are 3×3 Hermitian matrices in generation space. It is common to express the trilinear couplings in terms of the Yukawa couplings,

$$a_{ij}^{u,d,e} = y_{ik}^{u,d,e} (A_{u,d,e})_{kj}. \tag{2.30}$$

Including all possible complex-valued soft-breaking terms, the MSSM counts 105 parameters in addition to the 19 SM parameters.

Most of these parameters allow for FCNC or introduce new sources of CP violation, which are heavily constrained. Therefore a great deal of the parameter space is phenomenologically excluded. All these FCNC and CP-violating effects can be evaded in minimal flavor violation (MFV), where SUSY breaking is assumed to be flavor-blind and the only source of CP violation is given by the CKM matrix in the SM. Thus, all MSSM parameters are set to be real and the sfermion mass matrices M_f^2 and the trilinear couplings A_f diagonal in flavor space,

$$(M_f^2)_{ij} = \delta_{ij} M_{f_i}^2, \quad (A_f)_{ij} = \delta_{ij} A_{f_i}. \tag{2.31}$$

This reduces the total number of parameters of the MSSM to 49. In the following chapters we will refer to the MSSM as the MSSM within the MFV scenario real parameters.

The Lagrangian of the MSSM

The supersymmetric Lagrangian of the MSSM consists of F-, D- and the soft-breaking-terms (2.29),

$$\mathcal{L}_{\text{MSSM}} = \mathcal{L}_D + \mathcal{L}_F + \mathcal{L}_{\text{soft}} = \mathcal{L}_{\text{kin}} + \mathcal{L}_{\text{gauge}} + \mathcal{L}_{\text{int}} + \mathcal{L}_{\text{soft}}, \tag{2.32}$$

where the D-term provides for the kinetic terms of the chiral superfields (\mathcal{L}_{kin}) and the F-term contains the gauge- ($\mathcal{L}_{\text{gauge}}$) and interaction-Lagrange densities (\mathcal{L}_{int}). In terms of the superfields in Tab. 2.2 and the supersymmetric field strength tensors (2.24) they are given by

$$\begin{aligned} \mathcal{L}_{\text{kin}} = & \left[Q^\dagger e^{2(g_1 B + g_2 W + g_s G)} Q + \bar{U}^\dagger e^{2(g_1 B + g_s G)} \bar{U} + \bar{D}^\dagger e^{2(g_1 B + g_s G)} \bar{D} \right. \\ & + L^\dagger e^{2(g_1 B + g_2 W)} L + \bar{E}^\dagger e^{2g_1 B} \bar{E} \\ & \left. + H_u^\dagger e^{2(g_1 B + g_2 W)} H_u + H_d^\dagger e^{2(g_1 B + g_2 W)} H_d \right]_D, \end{aligned} \quad (2.33a)$$

$$\begin{aligned} \mathcal{L}_{\text{gauge}} = & \frac{1}{16} \left[\frac{1}{g_s^2} \text{Tr} [(W_G)^A (W_G)_A] + \frac{1}{g_2^2} \text{Tr} [(W_W)^A (W_W)_A] \right. \\ & \left. + \frac{1}{g_1^2} \text{Tr} [(W_B)^A (W_B)_A] + \text{hc} \right]_F \end{aligned} \quad (2.33b)$$

$$\mathcal{L}_{\text{int}} = [\mu H_u \cdot H_d - y_{ij}^u \bar{U}_i Q_j \cdot H_u - y_{ij}^d \bar{D}_i Q_j \cdot H_d - y_{ij}^e \bar{E}_i L_j \cdot H_d + \text{hc}]_F, \quad (2.33c)$$

where the expression in the squared brackets of the last line is given by the R-parity conserving superpotential \mathcal{W}_R .

2.2.3 The particle spectrum of the MSSM

The Higgs sector

The Higgs sector of the MSSM contains two complex scalar $SU(2)$ -doublet fields h_u and h_d with hypercharge $Y = -1$ and $Y = 1$, respectively. Contrary to the SM, the Higgs potential of the MSSM V_H emerges naturally from the F-, D- and the soft breaking terms. It depends on the SUSY-breaking parameters m_{h_u} , m_{h_d} , b , the higgsino mass parameter μ , and the gauge couplings g_1 and g_2 :

$$\begin{aligned} V_H = & (m_{h_d}^2 + |\mu|^2) h_d^\dagger h_d + (m_{h_u}^2 + |\mu|^2) h_u^\dagger h_u - b^2 (\epsilon_{ab} h_d^a h_u^b + \text{hc}) \\ & + \frac{g_1^2 + g_2^2}{8} (h_d^\dagger h_d - h_u^\dagger h_u)^2 + \frac{g_2^2}{2} |h_d^\dagger h_u|^2, \end{aligned} \quad (2.34)$$

where $\epsilon_{12} = -\epsilon_{21} = -1$ and $\epsilon_{11} = \epsilon_{22} = 0$. Unlike in the Higgs potential of the SM (2.34), the quartic couplings of the Higgs fields are given by the gauge couplings g_1 and g_2 – i.e. they are no free parameters of the theory. This has important consequences for the masses of the Higgs bosons as it will be discussed later. Analogously to the SM, the Higgs-doublet fields are required to acquire non-vanishing expectation values

$$\langle h_d \rangle = \begin{pmatrix} v_d \\ 0 \end{pmatrix}, \quad \langle h_u \rangle = \begin{pmatrix} 0 \\ v_u \end{pmatrix}, \quad (2.35)$$

with the vevs v_d and v_u . With an appropriate choice of phases for the Higgs-doublet fields, v_d and v_u are real and non-negative. In order to ensure electroweak symmetry breaking

the potential has to be bounded from below. This imposes the following conditions:

$$m_{h_d}^2 + m_{h_u}^2 + 2|\mu|^2 > 2|b|, \quad (2.36a)$$

$$(m_{h_d}^2 + |\mu|^2)(m_{h_u}^2 + |\mu|^2) < b^2. \quad (2.36b)$$

Thus, electroweak symmetry breaking requires broken SUSY, since for an unbroken theory (i.e. $m_{h_d} = m_{h_u} = b = 0$) the conditions (2.36) are not fulfilled. In complete analogy to the SM, the gauge boson's masses are obtained,

$$M_W^2 = \frac{g_2^2}{2}(v_d^2 + v_u^2), \quad M_Z^2 = \frac{g_1^2 + g_2^2}{2}(v_d^2 + v_u^2). \quad (2.37)$$

At this point one usually defines $v = \sqrt{v_d^2 + v_u^2} = 246$ GeV and $\tan \beta = v_u/v_d$ with $0 < \beta < \pi/2$. The Higgs doublets then can be expanded around these ground states yielding

$$h_d = \begin{pmatrix} v_d + \frac{1}{\sqrt{2}}(\phi_1^0 - i\chi_1^0) \\ -\phi_1^- \end{pmatrix}, \quad h_u = \begin{pmatrix} \phi_2^+ \\ v_u + \frac{1}{\sqrt{2}}(\phi_2^0 + i\chi_2^0) \end{pmatrix}, \quad (2.38)$$

with the CP-even neutral fields $\phi_{1/2}^0$, the charged fields $\phi_{1/2}^\pm$ and the CP-odd fields $\chi_{1/2}^0$. For vanishing fields, the potential (2.34) has to acquire the minimum (2.35). Essentially, the linear terms in the fields $\phi_{1/2}^0$, $\phi_{1/2}$ and $\chi_{1/2}^0$ have to vanish giving the minimization conditions

$$\left. \begin{array}{l} T_{\phi_1} \phi_1^0 = 0 \\ T_{\phi_2} \phi_2^0 = 0 \end{array} \right\} \implies \left\{ \begin{array}{l} (|\mu|^2 + m_{h_d}^2) = b \frac{v_u}{v_d} - \frac{g_1^2 + g_2^2}{4} \frac{v_d^2 - v_u^2}{v_d}, \\ (|\mu|^2 + m_{h_u}^2) = b \frac{v_d}{v_u} - \frac{g_1^2 + g_2^2}{4} \frac{v_d^2 - v_u^2}{v_u}, \end{array} \right. \quad (2.39)$$

where the linear terms in the fields are given by the tadpole parameters,

$$T_{\phi_1} = - \left(\sqrt{2} (m_1^2 + \mu^2) v_d - \sqrt{2} b^2 v_u + \frac{v_d (g_1^2 + g_2^2) (v_d^2 - v_u^2)}{2\sqrt{2}} \right), \quad (2.40a)$$

$$T_{\phi_2} = - \left(\sqrt{2} (m_2^2 + \mu^2) v_u - \sqrt{2} b^2 v_d - \frac{v_u (g_1^2 + g_2^2) (v_d^2 - v_u^2)}{2\sqrt{2}} \right). \quad (2.40b)$$

(2.39) can be used to eliminate $m_{h_d}^2$ and $m_{h_u}^2$ in terms of $\tan \beta$ and m_{A^0} . However, the fields in (2.38) are no gauge eigenstates. In fact, fields with the same quantum numbers mix, which is manifest by writing down the bilinear terms after inserting the expansion (2.38) into the Higgs potential (2.34),

$$V_H^{\text{bil}} = +\frac{1}{2}(\phi_1^0, \phi_2^0) \mathcal{M}_{\phi_{1,2}^0} \begin{pmatrix} \phi_1^0 \\ \phi_2^0 \end{pmatrix} + \frac{1}{2}(\chi_1^0, \chi_2^0) \mathcal{M}_{\chi_{1,2}^0} \begin{pmatrix} \chi_1^0 \\ \chi_2^0 \end{pmatrix} + (\phi_1^+, \phi_2^+) \mathcal{M}_{\phi_{1,2}^\pm} \begin{pmatrix} \phi_1^- \\ \phi_2^- \end{pmatrix}. \quad (2.41a)$$

The mass matrices read

$$\mathcal{M}_{\phi_{1,2}^0} = \begin{pmatrix} m_{h_d}^2 + |\mu|^2 + \frac{1}{4}\hat{g}^2(3v_d^2 - v_u^2) & -(b^2 + \frac{1}{2}\hat{g}^2 v_d v_u) \\ -(b^2 + \frac{1}{2}\hat{g}^2 v_d v_u) & m_{h_u}^2 + |\mu|^2 - \frac{1}{4}\hat{g}^2(v_d^2 - 3v_u^2) \end{pmatrix}, \quad (2.41b)$$

$$\mathcal{M}_{\chi_{1,2}^0} = \begin{pmatrix} m_{h_d}^2 + |\mu|^2 + \frac{1}{4}\hat{g}^2(v_d^2 - v_u^2) & -b^2 \\ -b^2 & m_{h_u}^2 + |\mu|^2 - \frac{1}{4}\hat{g}^2(v_d^2 - v_u^2) \end{pmatrix}, \quad (2.41c)$$

$$\mathcal{M}_{\phi_{1,2}^\pm} = \begin{pmatrix} m_{h_d}^2 + |\mu|^2 + \frac{1}{4}(\hat{g}^2 v_d^2 + \bar{g}^2 v_u^2) & -(b^2 - \frac{1}{2}g_2^2 v_d v_u) \\ -(b^2 - \frac{1}{2}g_2^2 v_d v_u) & m_{h_u}^2 + |\mu|^2 + \frac{1}{4}(\hat{g}^2 v_u^2 + \bar{g}^2 v_d^2) \end{pmatrix}, \quad (2.41d)$$

where $\hat{g}^2 = g_1^2 + g_2^2$ and $\bar{g}^2 = g_2^2 - g_1^2$. Diagonalizing the mass matrices, one obtains the Higgs mass-eigenstates,

$$\begin{pmatrix} h^0 \\ H^0 \end{pmatrix} = U_{\phi_{1,2}^0} \begin{pmatrix} \phi_1^0 \\ \phi_2^0 \end{pmatrix}, \quad \text{where} \quad U_{\phi_{1,2}^0} = \begin{pmatrix} -\sin \alpha & \cos \alpha \\ \cos \alpha & \sin \alpha \end{pmatrix}, \quad (2.42a)$$

$$\begin{pmatrix} A^0 \\ G^0 \end{pmatrix} = U_{\chi_{1,2}^0} \begin{pmatrix} \chi_1^0 \\ \chi_2^0 \end{pmatrix}, \quad \text{where} \quad U_{\chi_{1,2}^0} = \begin{pmatrix} -\sin \beta_n & \cos \beta_n \\ \cos \beta_n & \sin \beta_n \end{pmatrix}, \quad (2.42b)$$

$$\begin{pmatrix} H^\pm \\ G^\pm \end{pmatrix} = U_{\phi_{1,2}^\pm} \begin{pmatrix} \phi_1^\pm \\ \phi_2^\pm \end{pmatrix}, \quad \text{where} \quad U_{\phi_{1,2}^\pm} = \begin{pmatrix} -\sin \beta_c & \cos \beta_c \\ \cos \beta_c & \sin \beta_c \end{pmatrix}. \quad (2.42c)$$

There are five physical Higgs fields: two neutral and CP-even Higgs fields h^0 and H^0 , the neutral and CP-odd Higgs field A^0 , and the two charged fields H^\pm . The CP-odd field G^0 and the charged fields G^\pm are the would-be Goldstone bosons.

At tree-level the mixing angles β_n , β_c and the ratio of the Higgs vevs β are equal

$$\beta = \beta_n = \beta_c. \quad (2.43)$$

However, β has to be renormalized, whereas β_n and β_c need not. Therefore it will be important to distinguish β , β_n and β_c when carrying out renormalization transformations. At certain points, especially when encountering lengthy expressions, the notation $s_\beta \equiv \sin \beta$, $c_\beta \equiv \cos \beta$ and $t_\beta \equiv \tan \beta$ will be adopted. The diagonal Higgs mass matrices are given by

$$\mathcal{D}_{h^0 H^0} = U_{\phi_{1,2}^0} \mathcal{M}_{\phi_{1,2}^0} U_{\phi_{1,2}^0}^\dagger = \begin{pmatrix} m_{h^0}^2 & 0 \\ 0 & m_{H^0}^2 \end{pmatrix}, \quad (2.44a)$$

$$\mathcal{D}_{A^0 G^0} = U_{\chi_{1,2}^0} \mathcal{M}_{\chi_{1,2}^0} U_{\chi_{1,2}^0}^\dagger = \begin{pmatrix} m_{A^0}^2 & 0 \\ 0 & m_{G^0}^2 \end{pmatrix}, \quad (2.44b)$$

$$\mathcal{D}_{H^\pm G^\pm} = U_{\phi_{1,2}^\pm} \mathcal{M}_{\phi_{1,2}^\pm} U_{\phi_{1,2}^\pm}^\dagger = \begin{pmatrix} m_{H^\pm}^2 & 0 \\ 0 & m_{G^\pm}^2 \end{pmatrix}. \quad (2.44c)$$

At tree-level, the Higgs mass eigenvalues are

$$m_{h^0, H^0}^2 = \frac{1}{2} \left(b^2 (\tan \beta + \cot \beta) + M_Z^2 \mp \sqrt{(b^2 (\tan \beta - \cot \beta) + M_Z^2 \cos(2\beta))^2 + (2b^2 + M_Z^2 \sin(2\beta))^2} \right), \quad (2.45a)$$

$$m_{A^0}^2 = b^2 (\tan \beta + \cot \beta), \quad (2.45b)$$

$$m_{H^\pm}^2 = b^2 (\tan \beta + \cot \beta) + M_W^2. \quad (2.45c)$$

The Goldstone bosons G^0 and G^\pm acquire their masses through the gauge-fixing terms and depend on the chosen gauge. Using (2.39) and (2.45b) the Higgs sector at the tree level is determined by only two new SUSY parameters. They are usually defined to be m_{A^0} and $\tan \beta$. In terms of these parameters and the tree-level Higgs-boson mass m_{h^0} the mixing angle α reads as follows,

$$\alpha = \arctan \left[\frac{-(m_{A^0}^2 + M_Z^2) \sin \beta \cos \beta}{M_Z^2 \cos^2 \beta + m_{A^0}^2 \sin^2 \beta - m_{h^0}^2} \right], \quad -\frac{\pi}{2} < \alpha < 0. \quad (2.46)$$

From (2.45a) and (2.45c) constraints on the Higgs-boson masses emerge,

$$m_{h^0} < \min(m_{A^0}, M_Z), \quad (2.47a)$$

$$m_{H^0} > \max(m_{A^0}, M_Z), \quad (2.47b)$$

$$m_{H^\pm} > \max(m_{A^0}, M_W). \quad (2.47c)$$

In contrast to the SM, the tree-level masses of the neutral CP-even and charged Higgs bosons are no free parameters. This is due to the quartic couplings in the MSSM which are fixed by the D-terms. Remarkably, the tree-level mass of the lightest Higgs boson h^0 is lower than the Z mass, which is in contradiction with the current lower bound from LEP, $m_{h^0} > 93$ GeV [27]. Since the lightest CP-even Higgs-boson mass is not a free parameter, radiative corrections [28] have to be included. These are dominated by the fourth power of the top-quark Yukawa coupling owing to the incomplete cancellation of loops involving top quarks and their supersymmetric partners. With the one-loop and dominating two-loop contributions [29] the lightest Higgs-boson mass can be shifted up to $m_{h^0} \lesssim 140$ GeV without facing a severe fine-tuning problem again.

Sfermion sector

Generally, sfermions of different families mix via the soft breaking terms leading to 6×6 mixing matrices for squarks and charged sleptons and 3×3 matrices for the sneutrinos. As mentioned in Subsection 2.2.2 we are restricting our-self to the minimal flavor-violation scenario where the 6×6 matrices reduce to block-diagonal matrices with 2×2 blocks. Since only left-handed sneutrinos are included in the MSSM they do not mix. The sfermion mass-term for a given species of sfermions $\tilde{f} = \tilde{u}, \tilde{d}, \tilde{e}$ can be written as

$$\mathcal{L}_{\tilde{f}\text{-mass}} = - \left(\tilde{f}_L^*, \tilde{f}_R^* \right) \mathcal{M}_{\tilde{f}} \begin{pmatrix} \tilde{f}_L \\ \tilde{f}_R \end{pmatrix}, \quad (2.48)$$

where the generation indices have been omitted. The mass matrix $\mathcal{M}_{\tilde{f}}$ is given by

$$\mathcal{M}_{\tilde{f}} = \begin{pmatrix} \mathcal{M}_{\tilde{f}}^{\text{LL}} & \mathcal{M}_{\tilde{f}}^{\text{LR}} \\ \mathcal{M}_{\tilde{f}}^{\text{RL}} & \mathcal{M}_{\tilde{f}}^{\text{RR}} \end{pmatrix}, \quad (2.49\text{a})$$

$$\mathcal{M}_{\tilde{f}}^{\text{LL}} = m_f^2 + M_{\tilde{f}_L}^2 + (I_f^3 - Q_f s_W^2) \cos 2\beta M_Z^2, \quad (2.49\text{b})$$

$$\mathcal{M}_{\tilde{f}}^{\text{LR}} = \mathcal{M}_{\tilde{f}}^{\text{RL}} = m_f (A_f + \mu\kappa), \quad (2.49\text{c})$$

$$\mathcal{M}_{\tilde{f}}^{\text{RR}} = m_f^2 + M_{\tilde{q}_R}^2 + Q_f s_W^2 \cos 2\beta M_Z^2, \quad (2.49\text{d})$$

where $\kappa = \cot \beta$ for up-type squarks and $\kappa = \tan \beta$ for down-type squarks and charged sleptons. Since the MSSM only involves left-handed sneutrinos, they are described by the one-dimensional matrix

$$\mathcal{M}_{\tilde{\nu}} = M_{\tilde{L}}^2 + \frac{1}{2} \cos 2\beta M_Z^2 = m_{\tilde{\nu}}^2. \quad (2.50)$$

The soft-breaking mass parameters $M_{\tilde{f}_L}$, $M_{\tilde{f}_R}$ and the trilinear couplings A_f have been introduced in (2.29). Since the left-handed up- and down-type fermions are arranged in the same $SU(2)_L$ doublet the soft-breaking mass parameter $M_{\tilde{f}_L}$ is the same for $\tilde{f}_L = \tilde{u}_L$ and $\tilde{f}_L = \tilde{d}_L$. The parameter $\tan \beta$ was introduced in the Higgs sector and μ will be introduced in the chargino sector. The gauge eigenstates \tilde{f}_L and \tilde{f}_R can be rotated into mass eigenstates with the rotation matrices $U_{\tilde{f}}$,

$$\begin{pmatrix} \tilde{f}_1 \\ \tilde{f}_2 \end{pmatrix} = U_{\tilde{f}} \begin{pmatrix} \tilde{f}_L \\ \tilde{f}_R \end{pmatrix} \quad \rightarrow \quad \mathcal{D}_{\tilde{f}} \equiv U_{\tilde{f}} \mathcal{M}_{\tilde{f}} U_{\tilde{f}}^\dagger = \begin{pmatrix} m_{\tilde{f}_1}^2 & 0 \\ 0 & m_{\tilde{f}_2}^2 \end{pmatrix}. \quad (2.51)$$

\tilde{f}_1 is defined to be the sfermion mass eigenstate with the lower mass: $m_{\tilde{f}_1} < m_{\tilde{f}_2}$. The mixing matrix $U_{\tilde{f}}$ can be parameterized by the mixing angle $\theta_{\tilde{f}}$,

$$U_{\tilde{f}} = \begin{pmatrix} \cos \theta_{\tilde{f}} & \sin \theta_{\tilde{f}} \\ -\sin \theta_{\tilde{f}} & \cos \theta_{\tilde{f}} \end{pmatrix} \quad \text{or} \quad U_{\tilde{f}} = \begin{pmatrix} -\sin \theta_{\tilde{f}} & \cos \theta_{\tilde{f}} \\ \cos \theta_{\tilde{f}} & \sin \theta_{\tilde{f}} \end{pmatrix}, \quad (2.52)$$

where the rotation matrix on the left-hand side has a positive determinant and the determinant of the matrix on the right-hand side is negative. The sign of $\det(U_{\tilde{f}}) = \pm 1$ is chosen such that $m_{\tilde{f}_1} < m_{\tilde{f}_2}$. With (2.51) the mixing angle is related to the soft-breaking parameters

$$\sin 2\theta_{\tilde{f}} = \det(U_{\tilde{f}}) \frac{2m_f (A_f - \mu\kappa)}{m_{\tilde{f}_1}^2 - m_{\tilde{f}_2}^2}. \quad (2.53)$$

Comparing $(U_{\tilde{q}}^\dagger \mathcal{D}_{\tilde{q}} U_{\tilde{q}})_{1,1}$ for up- and down-type squarks yields the following relation between the squark mass eigenvalues

$$(U_{\tilde{d}_{11}})^2 m_{\tilde{d}_1}^2 + (U_{\tilde{d}_{12}})^2 m_{\tilde{d}_2}^2 = (U_{\tilde{u}_{11}})^2 m_{\tilde{u}_1}^2 + (U_{\tilde{u}_{12}})^2 m_{\tilde{u}_2}^2 + m_d^2 - m_u^2 - M_W^2 \cos 2\beta \quad (2.54)$$

for each generation. Thus, one squark mass depends on the residual squark masses. This will be important when imposing on-shell renormalization conditions on the squark masses.

Each squark generation can be described by five free parameters: $M_{\tilde{q}_L}^2$, $M_{\tilde{u}_R}^2$, $M_{\tilde{d}_R}^2$, A_u and A_d . They can be parameterized by three out of the four squark masses $m_{\tilde{u}_1}$, $m_{\tilde{u}_2}$, $m_{\tilde{d}_1}$, $m_{\tilde{d}_2}$ and the two mixing angles $\theta_{\tilde{u}}$, $\theta_{\tilde{d}}$.

Since the squark mixing is proportional to the corresponding quark mass the mixing effects will be particularly interesting for third generation squarks. For the first two generations the quark masses or rather Yukawa couplings will be neglected. This leads to trivial mixing matrices, reducing the number of free parameters from five to three. The free parameters for the first two generations then are $M_{\tilde{q}_L}^2$, $M_{\tilde{u}_R}^2$ and $M_{\tilde{d}_R}^2$, or rather three out of the four squark masses.

Analogously, the slepton masses are connected via

$$(U_{\tilde{e}11})^2 m_{\tilde{e}_1}^2 + (U_{\tilde{e}12})^2 m_{\tilde{e}_2}^2 = m_{\tilde{\nu}}^2 + m_e^2 - M_W^2 \cos 2\beta. \quad (2.55)$$

The free parameters are $M_{\tilde{l}_L}^2$, $M_{\tilde{e}_R}^2$ for the light-flavor sleptons. For the stau sector these parameters are supplemented by the trilinear coupling A_τ .

Chargino and neutralino sector

The charged gauginos $\tilde{W}^\pm = 1/\sqrt{2}(\tilde{W}^1 \pm \tilde{W}^2)$ and higgsinos \tilde{h}_u^+ , \tilde{h}_d^- mix and form mass eigenstates called charginos $\tilde{\chi}_{1,2}^\pm$. So do the neutral gauginos \tilde{B} , \tilde{W}^3 and higgsinos \tilde{h}_u^0 , \tilde{h}_d^0 . Their four mass eigenstates are the neutralinos $\tilde{\chi}_{1,2,3,4}^0$. In terms of gauge eigenstates, the chargino mass-terms in the Lagrangian are given by

$$\mathcal{L}_{\tilde{\chi}^\pm\text{-mass}} = -\frac{1}{2} ((\Psi^R)^T, (\Psi^L)^T) \begin{pmatrix} 0 & \mathcal{M}_{\tilde{\chi}^\pm}^T \\ \mathcal{M}_{\tilde{\chi}^\pm} & 0 \end{pmatrix} \begin{pmatrix} \Psi^R \\ \Psi^L \end{pmatrix} + \text{hc} \quad (2.56)$$

with the mass matrix

$$\mathcal{M}_{\tilde{\chi}^\pm} = \begin{pmatrix} M_2 & g_2 v_u \\ g_2 v_d & \mu \end{pmatrix} = \begin{pmatrix} M_2 & \sqrt{2} M_W \sin \beta \\ \sqrt{2} M_W \cos \beta & \mu \end{pmatrix} \quad (2.57)$$

and

$$\begin{pmatrix} \Psi_1^R \\ \Psi_2^R \end{pmatrix} = \begin{pmatrix} \tilde{W}^+ \\ h_u^+ \end{pmatrix}, \quad \begin{pmatrix} \Psi_1^L \\ \Psi_2^L \end{pmatrix} = \begin{pmatrix} \tilde{W}^- \\ h_d^- \end{pmatrix}. \quad (2.58)$$

The terms originate from the SUSY-breaking Lagrangian (terms proportional to M_1 and M_2), the D-terms (couplings proportional g_2), and the superpotential (term proportional to μ). Diagonalizing the mass matrix $\mathcal{M}_{\tilde{\chi}^\pm}$ with two unitary matrices U and V yields the mass eigenstates,

$$\begin{pmatrix} \chi_1^L \\ \chi_2^L \end{pmatrix} = V \begin{pmatrix} \Psi_1^L \\ \Psi_2^L \end{pmatrix}, \quad \begin{pmatrix} \chi_1^R \\ \chi_2^R \end{pmatrix} = U \begin{pmatrix} \Psi_1^R \\ \Psi_2^R \end{pmatrix}, \quad (2.59)$$

where the Weyl spinors are usually combined into the correspondent chargino Dirac spinors

$$\tilde{\chi}_i^+ = \begin{pmatrix} \chi_i^L \\ \bar{\chi}_i^R \end{pmatrix}, \quad \tilde{\chi}_i^- = \begin{pmatrix} \chi_i^R \\ \bar{\chi}_i^L \end{pmatrix}, \quad i = 1, 2. \quad (2.60)$$

The diagonal mass matrix then is

$$\mathcal{D}_{\tilde{\chi}^\pm} = U^* \mathcal{M}_{\tilde{\chi}^\pm} V^\dagger = \text{diag} \left(m_{\tilde{\chi}_1^\pm}, m_{\tilde{\chi}_2^\pm} \right), \quad (2.61)$$

where U and V can be chosen such that $m_{\tilde{\chi}_{1,2}^\pm}$ are real, positive numbers with $m_{\tilde{\chi}_1^\pm} < m_{\tilde{\chi}_2^\pm}$,

$$m_{\tilde{\chi}_{1,2}^\pm}^2 = \frac{1}{2} \left(M_2^2 + \mu^2 + 2M_W^2 \right) \mp \frac{1}{2} \sqrt{\left(M_2^2 + \mu^2 + 2M_W^2 \right)^2 - 4 \left(\mu M_2 - M_W^2 \sin 2\beta \right)^2}. \quad (2.62)$$

The mass terms for the neutral gauginos and higgsinos read

$$\mathcal{L}_{\tilde{\chi}^0\text{-mass}} = -\frac{1}{2} (\Psi^0)^T \mathcal{M}_{\tilde{\chi}^0} \Psi^0 + \text{hc}, \quad \text{with} \quad (\Psi^0)^T = \left(\tilde{B}^0, \tilde{W}^3, \tilde{h}_d^0, \tilde{h}_u^0 \right)^T, \quad (2.63)$$

where the mass matrix is given by

$$\mathcal{M}_{\tilde{\chi}^0} = \begin{pmatrix} M_1 & 0 & -M_Z s_W \cos \beta & M_Z s_W \sin \beta \\ 0 & M_2 & M_Z c_W \cos \beta & -M_Z c_W \sin \beta \\ -M_Z s_W \cos \beta & M_Z c_W \cos \beta & 0 & -\mu \\ M_Z s_W \sin \beta & -M_Z c_W \sin \beta & -\mu & 0 \end{pmatrix}. \quad (2.64)$$

With the help of the 4×4 unitary matrix N it can be diagonalized resulting in

$$\mathcal{D}_{\tilde{\chi}^0} = N^* \mathcal{M}_{\tilde{\chi}^0} N^\dagger = \text{diag} \left(m_{\tilde{\chi}_1^0}, m_{\tilde{\chi}_2^0}, m_{\tilde{\chi}_3^0}, m_{\tilde{\chi}_4^0} \right), \quad (2.65)$$

where N is chosen in such way that $\mathcal{D}_{\tilde{\chi}^0}$ has real, non-negative entries, which obey $m_{\tilde{\chi}_1^0} \leq m_{\tilde{\chi}_2^0} \leq m_{\tilde{\chi}_3^0} \leq m_{\tilde{\chi}_4^0}$. The neutralino mass eigenstates then are

$$\begin{pmatrix} \chi_1^0 \\ \chi_2^0 \\ \chi_3^0 \\ \chi_4^0 \end{pmatrix} = N \begin{pmatrix} \Psi_1^0 \\ \Psi_2^0 \\ \Psi_3^0 \\ \Psi_4^0 \end{pmatrix}, \quad (2.66)$$

constituting the four Majorana spinors

$$\tilde{\chi}_i^0 = \begin{pmatrix} \chi_i^0 \\ \bar{\chi}_i^0 \end{pmatrix}, \quad i = 1 \dots 4. \quad (2.67)$$

Gluino sector

The superpartner of the gluon is the gluino \tilde{g}^a . Since it has unique color and spin quantum-numbers it does not mix with any other particles. Its mass term in the Lagrangian is given by

$$\mathcal{L}_{\tilde{g}\text{-mass}} = \frac{1}{2} M_3 \tilde{g}^a \tilde{g}^a + \text{hc}, \quad (2.68)$$

and the gluino mass is given by the soft-breaking parameter $m_{\tilde{g}} = M_3$. They are described by the four-component Majorana spinor

$$\Psi_{\tilde{g}} = \begin{pmatrix} \tilde{g} \\ \bar{\tilde{g}} \end{pmatrix}. \quad (2.69)$$

Chapter 3

Decay widths and branching ratios

In this chapter, the general calculation of decay widths and branching ratios and the required notation is introduced. The methods used to compute observables at next-to-leading order (NLO) will then be introduced in Chapter 4.

3.1 Tree-level

The decay width at tree-level for a general two-body decay $a \rightarrow b c$ is given by

$$\begin{aligned}\Gamma_0(a \rightarrow b c) &= \frac{(2\pi)^4}{m_a} \int d\text{PS}_2 |\mathcal{M}_0|^2 \\ &= \frac{\kappa(m_a^2, m_b^2, m_c^2)}{64\pi^2 m_a^3} \int d\phi d\cos\theta |\mathcal{M}_0|^2,\end{aligned}\tag{3.1}$$

where $p_i = (E_i, \mathbf{p}_i)$ are the four-momenta and $m_i = \sqrt{E_i^2 - \mathbf{p}_i^2}$ the masses of particle i . In the second line, the 2-body phase space element $d\text{PS}_2$ is written in terms of the angles ϕ and $\cos\theta$ in the rest frame of the decaying particle. $|\mathcal{M}_0|^2$ is the squared matrix element for the specific process. Since decays of scalar particles are isotropic, the angles $\cos\theta$ and ϕ can be integrated out in this case, which leads to a factor of 4π . The Källén function κ is given by

$$\kappa(x, y, z) = \sqrt{x^2 + y^2 + z^2 - 2(xy + xz + yz)}.\tag{3.2}$$

In the rest frame of the particle a with mass m_0 the absolute values of the outgoing three-momenta are given by

$$|\mathbf{p}_b| = |\mathbf{p}_c| = \frac{\kappa(m_a^2, m_b^2, m_c^2)}{2m_a}.\tag{3.3}$$

Tree-level matrix elements \mathcal{M}_0 are obtained computing the Born diagrams with the Feynman rules deduced from the Lagrangians discussed in Chapters 6 and 9.

The total width of a particle a is obtained by summing all partial widths for all decay channels,

$$\Gamma_0(a) = \sum_{\{b,c\}} \Gamma_0(a \rightarrow b c).\tag{3.4}$$

A relevant quantity for hadron colliders such as the LHC is the branching ratio for a specific decay channel $a \rightarrow bc$,

$$\text{BR}_0(a \rightarrow bc) = \frac{\Gamma_0(a \rightarrow bc)}{\Gamma_0(a)}. \quad (3.5)$$

It gives the probability of a particle a decaying into the particles b and c .

3.2 Next-to-leading order

There are two different kinds of processes contributing to EW/QCD NLO corrections. On the one hand are the virtual corrections consisting of genuine loop-diagrams and counterterm contributions. On the other hand, there are real processes where an additional photon or gluon is radiated. The virtual corrections to the partial decay width for a process $a \rightarrow bc$ are given by

$$\begin{aligned} \Gamma_1^{\text{virt,EW/QCD}}(a \rightarrow bc) &= \frac{(2\pi)^4}{m_a} \int \text{dPS}_2 \, 2\text{Re} \left(\mathcal{M}_0 \mathcal{M}_1^{\text{EW/QCD}} \right) + \Gamma_1^{\text{soft+coll,EW/QCD}} \\ &= \frac{\kappa(m_a^2, m_b^2, m_c^2)}{64\pi^2 m_a^3} \int \text{d}\phi \, \text{d}\cos\theta \, 2\text{Re} \left(\mathcal{M}_0 \mathcal{M}_1^{\text{EW/QCD}} \right) + \Gamma_1^{\text{soft+coll,EW/QCD}} \end{aligned} \quad (3.6)$$

with the same definitions as in (3.1). The decay width $\Gamma_1^{\text{soft+coll,EW/QCD}}$ is added to cure possible infrared (IR) divergencies. In Section 4.2 the calculation of decay widths for soft and collinear photon/gluon radiation is discussed. The computation of the one-loop matrix element $\mathcal{M}_1^{\text{EW/QCD}}$ will be discussed in Chapter 6. In order to cancel the ultraviolet (UV) divergencies, $\mathcal{M}_1^{\text{EW/QCD}}$ contains the genuine one-loop amplitudes $\mathcal{M}_1^{\text{1L,EW/QCD}}$ as well as the counterterm contributions $\mathcal{M}_1^{\text{CT,EW/QCD}}$,

$$\mathcal{M}_1^{\text{EW/QCD}} = \mathcal{M}_1^{\text{1L,EW/QCD}} + \mathcal{M}_1^{\text{CT,EW/QCD}}. \quad (3.7)$$

The one-loop matrix elements $\mathcal{M}_1^{\text{1L,EW/QCD}}$ are obtained computing all one-loop diagrams contributing to the EW/QCD NLO corrections. They involve integrals over the loop momentum. Generally, these integrals are UV- and IR-divergent as it will be discussed in Chapter 4. In order to regularize the UV-divergencies the loop integrals are computed in $D = 4 - 2\epsilon$ dimensions. Referring to [30], we define the general one-loop tensor integral with P integration momenta in the numerator and N propagator factors in the denominator as follows,

$$T_{\mu_1 \dots \mu_P}^N(p_1, \dots, p_{N-1}, m_0, \dots, m_{N-1}) = \frac{(2\pi\mu_R)^{4-D}}{i\pi^2} \int \text{d}^D q \frac{q_{\mu_1} \dots q_{\mu_P}}{D_0 \dots D_{N-1}}, \quad (3.8)$$

where the propagator factors are given by

$$D_0 = q^2 - m_0^2 + i\epsilon, \quad D_i = (q + p_i)^2 - m_i^2 + i\epsilon, \quad i = 1, \dots, N-1. \quad (3.9)$$

The momenta q , $(q + p_i)$ and the masses m_i belong to the particles propagating in the loop and $i\epsilon$ gives rise to the imaginary part of the S-matrix. The parameter μ_R is introduced to preserve the mass dimension of the loop-integral in D dimensions. For NLO corrections to two-body decays integrals up to $N = 3$ are involved. The one-, two-, and three-point integrals will be denoted by A , B and C . One-loop tensor integrals ($P > 0$) can be decomposed to scalar loop integrals ($P = 0$) using the Passarino-Veltman reduction method [31].

For the counterterm matrix elements $\mathcal{M}_1^{\text{CT,EW/QCD}}$, the corresponding counterterm diagrams have to be evaluated. The required Feynman rules are obtained by renormalizing the corresponding parameters (cf. Chapter 4) and inserting them into the relevant part of the Lagrangian (Chapters 6 and 9). From the resulting counterterm Lagrangian, the counterterm Feynman rules can be deduced. They are listed in Appendix C.

The amplitudes for real hard photon/gluon radiation $\mathcal{M}_0^{\text{real,EW/QCD}}$, are of the same order in perturbation theory as the virtual corrections (3.6). The partial decay widths for the real processes $a \rightarrow bcV$, where V denotes the photon or gluon with momentum k , are

$$\Gamma_1^{\text{real,EW/QCD}}(a \rightarrow bcV) = \frac{(2\pi)^4}{m_a} \int d\text{PS}_3 |\mathcal{M}_1^{\text{real,EW/QCD}}|^2, \quad (3.10)$$

where $d\text{PS}_3$ denotes the three particle phase space element. In order to avoid the soft and collinear regions which already have been added to the virtual corrections, integration bounds have to be adjusted such that $|k| > \Delta E$ and $0 < \cos \theta < 1 - \delta_c$, where θ denotes the angle between the emitting massless quark and the photon/gluon in the rest frame of the decaying particle. For the three-body decay, the phase space cannot simply be integrated out as for the two-body decays of scalar particles. In the following computation, we use the phase-space integration of FormCalc 6.0 [32]. FormCalc builds up the n-body phase space iteratively as a sequence of two-body decays (Fig. 3.1).

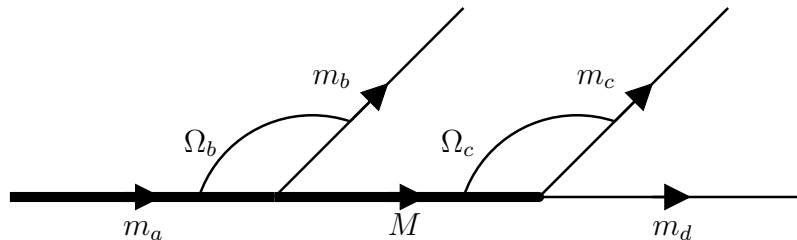


Figure 3.1: Iterative construction of a three-body decay as a sequence of two two-body decays.

For a three-body decay this results in an integration over the invariant mass M and the solid angles $\Omega_i = \cos \theta_i \phi_i$, $i = b, c$, which define the directions of \mathbf{p}_i ($i = b, c$) in the rest frame of the decaying particle,

$$\Gamma_1^{\text{real,EW/QCD}} = \frac{(2\pi)^4}{2m_a^2} \int_{m_c+m_d}^{m_a-m_b} dM d\Omega_b \frac{|\mathbf{p}_b|}{2} \int d\Omega_c \frac{|\mathbf{p}_c|}{2} |\mathcal{M}_1^{\text{real,EW/QCD}}|^2, \quad (3.11)$$

where the momenta $|\mathbf{p}_i|$ are given by

$$|\mathbf{p}_b| = \frac{\kappa(m_a^2, m_b^2, M^2)}{2m_a}, \quad |\mathbf{p}_c| = \frac{\kappa(M^2, m_c^2, m_d^2)}{2M}. \quad (3.12)$$

More details about recursive phase space integration can be found in [33, 34].

Having introduced the different contributions to decays at EW/QCD NLO, the complete partial and total decay widths are given by

$$\Gamma_1^{\text{EW/QCD}}(a \rightarrow bc) = \left[\Gamma_0 + \Gamma_1^{\text{virt,EW/QCD}} + \Gamma_1^{\text{real,EW/QCD}} \right] (a \rightarrow bc), \quad (3.13a)$$

$$\Gamma_1^{\text{EW/QCD}}(a) = \sum_{\{b,c\}} \Gamma_1^{\text{EW/QCD}}(a \rightarrow bc). \quad (3.13b)$$

Finally, the branching ratios with EW/QCD NLO corrections can be computed:

$$\text{BR}_1^{\text{EW/QCD}}(a \rightarrow bc) = \frac{\Gamma_1^{\text{EW/QCD}}(a \rightarrow bc)}{\Gamma_1^{\text{EW/QCD}}(a)}. \quad (3.14)$$

Decay widths and branching ratios including both, EW and QCD corrections are calculated as

$$\Gamma_1(a \rightarrow bc) = \left[\Gamma_0 + \Gamma_1^{\text{virt,EW}} + \Gamma_1^{\text{real,EW}} + \Gamma_1^{\text{virt,QCD}} + \Gamma_1^{\text{real,QCD}} \right] (a \rightarrow bc), \quad (3.15a)$$

$$\Gamma_1(a) = \sum_{\{b,c\}} \Gamma_1(a \rightarrow bc), \quad (3.15b)$$

$$\text{BR}_1(a \rightarrow bc) = \frac{\Gamma_1^{\text{tot}}(a \rightarrow bc)}{\Gamma_1^{\text{tot}}(a)}. \quad (3.15c)$$

Chapter 4

Methods in perturbation theory

While computing radiative corrections in perturbation theory two major obstacles have to be approached. On the one hand, at higher order in perturbation theory the relation between parameters in the Lagrangian and physical observables get altered. At the same time, loop functions arising in NLO computations may diverge at high energies, i.e. they are ultraviolet (UV) divergent. Both problems are addressed within the renormalization procedure.

On the other hand, when a massless particle is emitted or exchanged with vanishing energy, the corresponding amplitude diverges – it is infrared (IR) divergent. Furthermore, collinear singularities appear when a massless particle splits into two massless collinear particles. This can be understood to originate from the unphysical separation of virtual and real corrections and is solved by defining sufficiently inclusive observables.

In this chapter the technical tools are provided to compute sparticle decays at NLO. In Section 4.1 the regularization and renormalization methods to tackle the UV divergencies are discussed. Especially the renormalization procedure of the relevant sectors of the MSSM is presented in Subsection 4.1.3. Finally, the treatment of IR and collinear singularities is given in Section 4.2.

4.1 Ultraviolet singularities

The Lagrangian of a given model introduces free parameters which have to be determined experimentally. At tree-level these free parameters can be chosen in such a way that they directly correspond to physical observables such as masses or couplings. However, at higher order in perturbation theory this direct correspondence is lost. The parameters in the Lagrangian – the “bare” parameters – get contributions from higher-order diagrams. Moreover, these corrections involve loop diagrams which diverge for arbitrarily high energies – they are ultraviolet (UV) divergent. For a consistent mathematical treatment these UV divergencies have to be regularized.

In the renormalization procedure the connection between the bare parameters in the Lagrangian and the physical observables at higher order is fixed. Furthermore, the diver-

gencies appearing in loop amplitudes are absorbed into the bare parameters. In renormalizable theories it is possible to absorb all divergencies order-by-order in perturbation theory with only a finite number of such redefinitions. With a finite number of parameters fixed by measurement all possible physical quantities up to any order may be calculated resulting in a highly predictive theory. Both, the SM and the MSSM are renormalizable theories [18, 35, 36].

4.1.1 Regularization schemes

In order to treat the UV singularities appearing in loop amplitudes analytically, a regularization procedure has to be introduced. The integrals then become finite but depend on an unphysical parameter – the regulator Λ . In the following renormalization procedure the dependence on the regulator Λ will be eliminated.

There is no unique, mathematically consistent method to regularize UV-divergent integrals. In this work the regularization method of use is dimensional reduction (DRED) which is a variant of dimensional regularization (DREG). The idea of DREG is to analytically expand the divergent loop integrals in $D = 4 - 2\epsilon$ dimensions [18, 37]. For $D < 4$ the loop diagrams converge and the singularities appear as poles in $1/\epsilon$ when $D \rightarrow 4$. In DREG space-time coordinates, γ -matrices and vector fields are treated in D dimensions. Special care has to be taken, when generalizing γ_5 to D dimensions. In order to maintain the right mass-dimension of the D -dimensional loop-integrals they have to be multiplied by a factor $(2\pi\mu_R)^{2\epsilon}$ introducing a non-physical mass parameter μ_R . The advantage of DREG is that Lorentz- and gauge-invariance is preserved.

Since in DREG the dimension of vector bosons is altered, the number of degrees of freedom of gauge bosons and gauginos in SUSY theories would not match anymore. Hence, supersymmetry is explicitly broken when DREG is applied. In order to maintain the supersymmetry relations DRED has been introduced [38]. Technically, only the momenta are treated in D dimensions whereas the vector fields and γ matrices remain in four dimensions. However, this definition leads to mathematical inconsistencies [39]. A mathematically consistent formulation has been worked out in [40], where the D -dimensional space is a subspace of a quasi four-dimensional space and the vector fields and γ -matrices remain four-dimensional objects.

4.1.2 Renormalization

In perturbative calculations beyond the tree level bare parameters of the Lagrangian of a given model do not directly correspond to physical observables anymore. They differ by UV-divergent contributions, which after regularization can be absorbed into the bare quantities. In order to express the Lagrangian by UV-finite – renormalized – parameters, the counterterm formalism is applied.

The mass and coupling parameters m_0 and g_0 of a given Lagrangian $\mathcal{L}_0(m_0, g_0, \psi_0)$ are

expressed in terms of the renormalized UV-finite quantities m and g ,

$$m_0 = Z_m m = \left(1 + \delta Z_m^{(1,0)} + \delta Z_m^{(0,1)} + \dots\right) m \equiv m + \delta m^{(1,0)} + \delta m^{(0,1)} + \dots, \quad (4.1a)$$

$$g_0 = Z_g g = \left(1 + \delta Z_g^{(1,0)} + \delta Z_g^{(0,1)} + \dots\right) g \equiv g + \delta g^{(1,0)} + \delta g^{(0,1)} + \dots, \quad (4.1b)$$

where

$$Z_n = 1 + \sum_{i,j=1}^{\infty} \delta Z_n^{(i,j)}. \quad (4.1c)$$

All UV singularities have been absorbed into the renormalization constants Z_m and Z_g . In the second step the multiplicative renormalization constants have been expanded in a power series of the order parameters. In the SM and MSSM these are the coupling constants α and α_s . In this work, one-loop and higher-order EW/QCD contributions are studied. However, for the renormalization procedure, only the first order expansion of the renormalization constants is relevant. According to the LSZ formula [41], the wave functions ψ_0 get renormalized by field renormalization constants Z_ψ ,

$$\psi_0 = \sqrt{Z_\psi} \psi = \left(1 + \frac{1}{2} \left(\delta Z_\psi^{(1,0)} + \delta Z_\psi^{(0,1)}\right) + \dots\right) \psi. \quad (4.2)$$

Inserting the above definitions of the renormalized parameters into the Lagrangian \mathcal{L}_0 allows to split it into a renormalized Lagrangian and a counterterm Lagrangian,

$$\begin{aligned} \mathcal{L}_0(g_0, m_0, \psi_0) &= \mathcal{L}_0 \left(Z_m, Z_g g, \sqrt{Z_\psi} \psi \right) \\ &= \mathcal{L} (m, g, \psi) + \delta \mathcal{L}_{\text{CT}}^{(1,0)} \left(m, g, \psi, \delta m^{(1,0)}, \delta g^{(1,0)}, \delta Z_\psi^{(1,0)} \right) \\ &\quad + \delta \mathcal{L}_{\text{CT}}^{(0,1)} \left(m, g, \psi, \delta m^{(0,1)}, \delta g^{(0,1)}, \delta Z_\psi^{(0,1)} \right) + \dots \end{aligned} \quad (4.3)$$

The Lagrangian \mathcal{L} has the same form as \mathcal{L}_0 but only depends on renormalized parameters. All renormalization constants are included in the counterterm Lagrangian densities $\mathcal{L}_{\text{CT}}^{(i,j)}$ and thus absorb all UV divergencies. The counterterm Lagrangian $\mathcal{L}_{\text{CT}}^{(i,j)}$ defines additional Feynman rules from which counterterm diagrams can be computed. Together with the virtual diagrams they yield a UV-finite result.

The choices of the renormalized parameters and consequently the renormalization constants are only determined up to finite parts. This mathematical arbitrariness has to be fixed by choosing a specific renormalization scheme. In the following paragraphs the used renormalization schemes are presented.

On-shell renormalization

In the on-shell (OS) renormalization scheme the renormalized parameters of the Lagrangian and the physical observables are directly related. Renormalization conditions for the masses are imposed such that the renormalized mass corresponds to the real part of the pole of the

propagator. The field renormalization constants are fixed by requiring the renormalized propagator to have residue one.

In the case of mixing particles the on-shell conditions are imposed on the mass eigenvalues of the mass matrices. The fields are renormalized in such a way that the one-particle irreducible (1PI) two-point functions are diagonal for on-shell external particles.

The OS renormalization condition for the coupling constant of electroweak interactions α is imposed such that the renormalized vertex function at zero momentum transfer exactly reproduces the Thomson limit. This is not applicable for the strong coupling constant α_s , since in the low energy limit the theory gets strongly coupled and cannot be described within perturbation theory anymore. Therefore, a different renormalization scheme for QCD is required. Since the OS conditions fix the scale intrinsically at the mass scale of the renormalized particle, the OS renormalized parameters show no dependence on μ_R . The OS renormalization scheme is applicable for both, the electroweak SM [30,42] and the MSSM [36].

$\overline{\text{MS}}$ and $\overline{\text{DR}}$ renormalization

In the OS scheme the renormalization constants are defined in such a way that the renormalized parameters correspond to physical quantities. In contrast, the renormalization constants in the modified minimal subtraction ($\overline{\text{MS}}$) scheme [43] only absorb the divergences plus universal terms from the differential regularization procedure. Thus, this renormalization scheme relies on DREG where the UV-divergent parts are proportional to $1/\epsilon$. In the $\overline{\text{MS}}$ scheme the expressions proportional to Δ are absorbed into the renormalization constants,

$$\Delta = \frac{1}{\epsilon} - \gamma_E + \log 4\pi, \quad (4.4)$$

where γ_E is the Euler-Mascheroni constant. $\overline{\text{MS}}$ renormalized parameters depend on the unphysical renormalization scale μ_R . When including higher-order contributions this scale dependence gets more and more reduced. On the other hand, the dependence on the scale variation of a calculated quantity gives a hint on the remaining uncertainties coming from higher-order corrections.

Technically, μ_R usually enters the calculations in form of $\log \mu_R^2/Q^2$, where Q is set by the kinematics of the process. Therefore, μ_R should be chosen at the energy scale of the process to keep these arising logarithms small. In decay processes μ_R is usually set to the mass of the decaying particle.

In the same way as the $\overline{\text{MS}}$ renormalization scheme, the $\overline{\text{DR}}$ scheme is defined for the DRED regularization procedure of the divergent integrals. Since in supersymmetric theories DRED is needed to preserve SUSY, this or the OS scheme are the renormalization procedures of choice.

4.1.3 Renormalization of the MSSM

In this subsection the renormalization procedure for the different sectors of the MSSM is discussed. This consists of the following steps. First, the independent parameters of each sector are chosen. Second, the bare parameters and fields are replaced with the renormalized quantities. After applying the chosen renormalization conditions, the expressions for the renormalization constants can be written down.

Generally, we adopt the OS renormalization scheme. Exceptions are the strong coupling constant, the bottom-quark mass, the according trilinear coupling, and parts of the Higgs sector, where the $\overline{\text{DR}}$ renormalization scheme is used.

Electroweak sector

The electroweak sector is renormalized according to [30]. Care has to be taken concerning the definition of the covariant derivative. Other than [30], in this work the definition (2.5) taken from [14] is adopted. This has an impact on the renormalization constants of the electroweak coupling constant and the couplings where W and Z bosons are involved.

The bilinear terms of the Fourier-transformed Lagrangian for the gauge bosons are

$$\begin{aligned} \mathcal{L}_{A,Z,W} = & -A_\mu [g^{\mu\nu} p^2 - p_\mu p^\nu] A_\nu - Z_\mu [g^{\mu\nu} (p^2 - M_Z^2) - p^\mu p^\nu] Z_\nu \\ & + W_\mu^- [g^{\mu\nu} (p^2 - M_W^2) - p^\mu p^\nu] W_\nu^+, \end{aligned} \quad (4.5)$$

where the gauge-fixing parameters have been neglected, since they are not renormalized. The independent parameters of the electroweak gauge-boson sector are the electric charge e , the mass of the W boson M_W , and the mass of the Z boson M_Z . For these parameters the renormalization prescriptions are given by

$$e \rightarrow Z_e e = (1 + \delta Z_e) e, \quad (4.6a)$$

$$M_W^2 \rightarrow M_W^2 + \delta M_W^2, \quad (4.6b)$$

$$M_Z^2 \rightarrow M_Z^2 + \delta M_Z^2. \quad (4.6c)$$

The electroweak mixing angle is given by $c_W = M_W/M_Z$. Hence, its renormalization constant depends on δM_W^2 and δM_Z^2 ,

$$c_W \rightarrow c_W + \delta c_W = c_W + \left[\frac{M_W}{2M_Z} \left(\frac{\delta M_W^2}{M_W^2} - \frac{\delta M_Z^2}{M_Z^2} \right) \right], \quad (4.7a)$$

$$s_W \rightarrow s_W + \delta s_W = s_W + \left[-\frac{c_W M_W}{2s_W M_Z} \left(\frac{\delta M_W^2}{M_W^2} - \frac{\delta M_Z^2}{M_Z^2} \right) \right]. \quad (4.7b)$$

Since the couplings g_1 and g_2 can be expressed by e , s_W , and c_W , their renormalization transformations are given by,

$$g_1 \rightarrow g_1 + \delta g_1 = g_1 + \left(\frac{\delta Z_e}{c_w} - \frac{e \delta c_W}{c_W^2} \right), \quad g_2 \rightarrow g_2 + \delta g_2 = g_2 + \left(\frac{\delta Z_e}{s_w} - \frac{e \delta s_W}{s_W^2} \right). \quad (4.8)$$

For the gauge Fields A_μ , Z_μ and W_μ^\pm the renormalization transformations are

$$W_\mu^\pm \rightarrow \sqrt{Z_W} W_\mu^\pm = \left(1 + \frac{1}{2} \delta Z_W\right) W_\mu^\pm, \quad (4.9a)$$

$$\begin{pmatrix} Z_\mu \\ A_\mu \end{pmatrix} \rightarrow \begin{pmatrix} \sqrt{Z_{ZZ}} & \sqrt{Z_{ZA}} \\ \sqrt{Z_{AZ}} & \sqrt{Z_{AA}} \end{pmatrix} \begin{pmatrix} Z_\mu \\ A_\mu \end{pmatrix} = \begin{pmatrix} 1 + \frac{1}{2} \delta Z_{ZZ} & \frac{1}{2} \delta Z_{ZA} \\ \frac{1}{2} \delta Z_{AZ} & 1 + \frac{1}{2} \delta Z_{AA} \end{pmatrix} \begin{pmatrix} Z_\mu \\ A_\mu \end{pmatrix}. \quad (4.9b)$$

Inserting these renormalization transformations into the gauge-boson Lagrangian (4.5) yields

$$\begin{aligned} \mathcal{L}_{A,Z,W}^{\text{CT}} = & -\frac{1}{2} A_\mu [\delta Z_{AA} (g^{\mu\nu} p^2 - p^\mu p^\nu)] A_\nu \\ & -\frac{1}{2} Z_\mu [\delta Z_{ZZ} [g^{\mu\nu} (p^2 - M_Z^2) - p^\mu p^\nu] - \delta M_Z^2 g^{\mu\nu}] Z_\nu \\ & -\frac{1}{2} A_\mu [\delta Z_{AZ} [g^{\mu\nu} (p^2 - M_Z^2) - p^\mu p^\nu] + \delta Z_{ZA} [g^{\mu\nu} p^2 - p^\mu p^\nu]] Z_\nu \\ & -\frac{1}{2} W_\mu^- [\delta Z_W [g^{\mu\nu} (p^2 - M_W^2) - p^\mu p^\nu] - \delta M_W^2 g^{\mu\nu}] W_\nu^+. \end{aligned} \quad (4.10)$$

The renormalized self-energies $\hat{\Sigma}_{V_i V_j}^{\mu\nu}$ for $V_i, V_j = A, Z, W$ are given by the unrenormalized self-energies plus the derivatives of the counterterm Lagrangian $\mathcal{L}_{A,Z,W}^{\text{CT}}$ with respect to the corresponding fields $V = A, Z$ or W ,

$$\hat{\Sigma}_{V_i V_j}^{\mu\nu}(p) = \Sigma_{V_i V_j}^{\mu\nu}(p) + \frac{\partial}{\partial V_i^*} \frac{\partial}{\partial V_j} \mathcal{L}_{A,Z,W}^{\text{CT}}, \quad (4.11a)$$

$$\hat{\Sigma}_{AA}^{\mu\nu}(p) = \Sigma_{AA}^{\mu\nu}(p) - \delta Z_{AA} [p^2 g^{\mu\nu} - p^\mu p^\nu], \quad (4.11b)$$

$$\hat{\Sigma}_{ZZ}^{\mu\nu}(p) = \Sigma_{ZZ}^{\mu\nu}(p) - [\delta Z_{ZZ} [(p^2 - M_Z^2) g^{\mu\nu} - p^\mu p^\nu] - \delta M_Z^2 g^{\mu\nu}], \quad (4.11c)$$

$$\hat{\Sigma}_{AZ}^{\mu\nu}(p) = \Sigma_{AZ}^{\mu\nu}(p) - \frac{1}{2} [\delta Z_{ZA} [(p^2 - M_Z^2) g^{\mu\nu} - p^\mu p^\nu] + \delta Z_{AZ} [p^2 g^{\mu\nu} - p^\mu p^\nu]], \quad (4.11d)$$

$$\hat{\Sigma}_{WW}^{\mu\nu}(p) = \Sigma_{WW}^{\mu\nu}(p) - [\delta Z_W [(p^2 - M_W^2) g^{\mu\nu} - p^\mu p^\nu] - \delta M_W^2 g^{\mu\nu}]. \quad (4.11e)$$

With the Lorentz decomposition of the self-energy,

$$\Sigma_{V_i V_j}^{\mu\nu}(p) = \Sigma_{V_i V_j}^T(p^2) \left(g^{\mu\nu} - \frac{p^\mu p^\nu}{p^2} \right) + \Sigma_{V_i V_j}^L(p^2) \frac{p^\mu p^\nu}{p^2}, \quad (4.11f)$$

the OS renormalization conditions are given by

$$\widetilde{\text{Re}} \hat{\Sigma}_{AA}^T(0) = 0, \quad \widetilde{\text{Re}} \hat{\Sigma}_{AA}^T'(0) = 0, \quad (4.12a)$$

$$\widetilde{\text{Re}} \hat{\Sigma}_{ZZ}^T(M_Z^2) = 0, \quad \widetilde{\text{Re}} \hat{\Sigma}_{ZZ}^T'(M_Z^2) = 0, \quad (4.12b)$$

$$\widetilde{\text{Re}} \hat{\Sigma}_{AZ}^T(0) = 0, \quad \widetilde{\text{Re}} \hat{\Sigma}_{AZ}^T(M_Z^2) = 0, \quad (4.12c)$$

$$\widetilde{\text{Re}} \hat{\Sigma}_{WW}^T(M_W^2) = 0, \quad \widetilde{\text{Re}} \hat{\Sigma}_{WW}^T'(M_W^2) = 0, \quad (4.12d)$$

where $\Sigma'(m^2) = \partial\Sigma(p^2)/\partial p^2|_{p^2=m^2}$. $\widetilde{\text{Re}}$ is defined such that only the real parts of the loop integrals L_i are selected while all other expressions c_i such as the coupling constants remain complex, i.e. $\widetilde{\text{Re}} \sum c_i L_i \equiv \sum c_i \text{Re} L_i$. This fixes the renormalization constants as follows,

$$\delta Z_{AA} = -\widetilde{\text{Re}} \Sigma_{AA}^T{}'(0), \quad (4.13a)$$

$$\delta Z_{ZZ} = -\widetilde{\text{Re}} \Sigma_{ZZ}^T{}'(M_Z^2), \quad \delta M_Z^2 = \widetilde{\text{Re}} \Sigma_{ZZ}^T(M_Z^2), \quad (4.13b)$$

$$\delta Z_{AZ} = -2\widetilde{\text{Re}} \frac{\Sigma_{AZ}^T(M_Z^2)}{M_Z^2}, \quad \delta Z_{ZA} = 2\widetilde{\text{Re}} \frac{\Sigma_{AZ}^T(0)}{M_Z^2}, \quad (4.13c)$$

$$\delta Z_W = -\Sigma_{WW}^T{}'(M_W^2), \quad \delta M_W^2 = \Sigma_{WW}^T(M_W^2). \quad (4.13d)$$

For the renormalization constant of the electroweak coupling constant e , the Ward identity yields

$$\delta Z_e = -\frac{1}{2} \left(\delta Z_{AA} - \frac{s_W}{c_W} \delta Z_{ZA} \right). \quad (4.14)$$

Higgs sector

The renormalization of the Higgs sector is based on [29], where a hybrid OS/ $\overline{\text{DR}}$ scheme is adopted, i.e. the Higgs fields are renormalized according to the $\overline{\text{DR}}$ prescription, whereas the masses are defined in the OS scheme. The Fourier-transformed Lagrangian for the Higgs fields may be written as

$$\begin{aligned} \mathcal{L}_{\text{Higgs}} = & \frac{1}{2} (h^0, H^0) [p^2 - \mathcal{D}_{h^0 H^0}] \begin{pmatrix} h^0 \\ H^0 \end{pmatrix} + T_h h^0 + T_H H^0 \Big|_{T_h=T_H=0} \\ & + \frac{1}{2} (A^0, G^0) [p^2 - \mathcal{D}_{A^0 G^0}] \begin{pmatrix} A^0 \\ G^0 \end{pmatrix} + (H^+, G^+) [p^2 - \mathcal{D}_{H^\pm G^\pm}] \begin{pmatrix} H^- \\ G^- \end{pmatrix}, \end{aligned} \quad (4.15)$$

with the mass matrices (2.44). The tadpole parameters T_h and T_H ¹ denote the linear terms in the fields h^0 and H^0 ,

$$T_h = \sqrt{2} \left(+m_1^2 v_d s_\alpha - m_2^2 v_u c_\alpha + \frac{1}{4} (g_1^2 + g_2^2) (v_d^2 - v_u^2) (v_d s_\alpha + v_u c_\alpha) \right), \quad (4.16a)$$

$$T_H = \sqrt{2} \left(-m_1^2 v_d c_\alpha - m_2^2 v_u s_\alpha - \frac{1}{4} (g_1^2 + g_2^2) (v_d^2 - v_u^2) (v_d c_\alpha - v_u s_\alpha) \right). \quad (4.16b)$$

They have to vanish at tree-level yielding the minimization conditions (2.39). The free parameters of the Higgs sector can conventionally be chosen as

$$m_{A^0}, \tan \beta, T_h, T_H. \quad (4.17)$$

¹The tadpole parameters of the physical Higgs fields $T_{h/H}$ are related to the tadpole parameters $T_{\phi_{1,2}}$ over $T_{\phi_1} \phi_1^0 + T_{\phi_2} \phi_2^0 = T_h h^0 + T_H H^0$.

For the parameters and fields of the Higgs sector the renormalization conditions are given by

$$m_{A^0}^2 \rightarrow m_{A^0}^2 + \delta m_{A^0}^2, \quad (4.18a)$$

$$T_{h/H} \rightarrow T_{h/H} + \delta T_{h/H}, \quad (4.18b)$$

$$\tan \beta \rightarrow \tan \beta + \delta \tan \beta, \quad (4.18c)$$

$$\mu \rightarrow \mu + \delta \mu. \quad (4.18d)$$

Therewith the renormalization transformations for the mass matrices are obtained,

$$\begin{aligned} \delta \mathcal{D}_{h^0 H^0} \rightarrow \mathcal{D}_{h^0 H^0} + \delta \mathcal{D}_{h^0 H^0} &= \mathcal{D}_{h^0 H^0} + \begin{pmatrix} \delta m_{h^0}^2 & \delta m_{h^0 H^0}^2 \\ \delta m_{h^0 H^0}^2 & \delta m_{H^0}^2 \end{pmatrix} \\ &= \mathcal{D}_{h^0 H^0} + U_{\phi_{1,2}^0} \delta \mathcal{M}_{\phi_{1,2}^0} U_{\phi_{1,2}^0}^\dagger, \end{aligned} \quad (4.19a)$$

$$\begin{aligned} \delta \mathcal{D}_{A^0 G^0} \rightarrow \mathcal{D}_{A^0 G^0} + \delta \mathcal{D}_{A^0 G^0} &= \mathcal{D}_{A^0 G^0} + \begin{pmatrix} \delta m_{A^0}^2 & \delta m_{A^0 G^0}^2 \\ \delta m_{A^0 G^0}^2 & \delta m_{G^0}^2 \end{pmatrix} \\ &= \mathcal{D}_{A^0 G^0} + U_{\chi_{1,2}^0} \delta \mathcal{M}_{\chi_{1,2}^0} U_{\chi_{1,2}^0}^\dagger, \end{aligned} \quad (4.19b)$$

$$\begin{aligned} \delta \mathcal{D}_{H^\pm G^\mp} \rightarrow \mathcal{D}_{H^\pm G^\mp} + \delta \mathcal{D}_{H^\pm G^\mp} &= \mathcal{D}_{H^\pm G^\mp} + \begin{pmatrix} \delta m_{H^\pm}^2 & \delta m_{H^\pm G^\mp}^2 \\ \delta m_{H^\pm G^\mp}^2 & \delta m_{G^\pm}^2 \end{pmatrix} \\ &= \mathcal{D}_{H^\pm G^\mp} + U_{\chi_{1,2}^\pm} \delta \mathcal{M}_{\chi_{1,2}^\pm} U_{\chi_{1,2}^\pm}^\dagger. \end{aligned} \quad (4.19c)$$

The renormalization constants $\delta \mathcal{M}_\phi$ are obtained by expressing the Higgs mass matrices (2.42) in terms of the free parameters (4.17) and applying (4.18). As mentioned in Subsection 2.2.3 the rotation matrices U_ϕ are not renormalized. The explicit values for $\delta \mathcal{D}$ can be found in [29].

For each Higgs doublet (2.38) one renormalization constant is assigned:

$$h_d \rightarrow \left(1 + \frac{1}{2} \delta Z_{h_d}\right) h_d, \quad h_u \rightarrow \left(1 + \frac{1}{2} \delta Z_{h_u}\right) h_u. \quad (4.20)$$

This also fixes the renormalization of $\tan \beta$:

$$\begin{aligned} \tan \beta \rightarrow \tan \beta + \delta \tan \beta &= \tan \beta + \delta \left(\frac{v_u}{v_d}\right) \\ &= \tan \beta \left(\frac{1}{2} (\delta Z_{h_u} - \delta Z_{h_d}) + \frac{\delta v_u}{v_u} - \frac{\delta v_d}{v_d}\right), \end{aligned} \quad (4.21)$$

where the Higgs vevs are renormalized according to

$$v_{u/d} \rightarrow \left(1 + \delta Z_{h_{u/d}}\right) (v_{u/d} + \delta v_{u/d}) = v_{u/d} + \delta v_{u/d} + \frac{1}{2} v_{u/d} \delta Z_{h_{u/d}}. \quad (4.22)$$

In the mass-eigenstate basis the renormalization transformations then are

$$\begin{pmatrix} h^0 \\ H^0 \end{pmatrix} \rightarrow \left(\mathbf{1} + \frac{1}{2} \delta \mathcal{Z}_{h^0 H^0} \right) \begin{pmatrix} h^0 \\ H^0 \end{pmatrix} = \begin{pmatrix} 1 + \frac{1}{2} \delta \mathcal{Z}_{h^0 h^0} & \frac{1}{2} \delta \mathcal{Z}_{h^0 H^0} \\ \frac{1}{2} \delta \mathcal{Z}_{h^0 H^0} & 1 + \frac{1}{2} \delta \mathcal{Z}_{H^0 H^0} \end{pmatrix} \begin{pmatrix} h^0 \\ H^0 \end{pmatrix}, \quad (4.23a)$$

$$\begin{pmatrix} A^0 \\ G^0 \end{pmatrix} \rightarrow \left(\mathbf{1} + \frac{1}{2} \delta \mathcal{Z}_{A^0 G^0} \right) \begin{pmatrix} A^0 \\ G^0 \end{pmatrix} = \begin{pmatrix} 1 + \frac{1}{2} \delta \mathcal{Z}_{A^0 A^0} & \frac{1}{2} \delta \mathcal{Z}_{A^0 G^0} \\ \frac{1}{2} \delta \mathcal{Z}_{A^0 G^0} & 1 + \frac{1}{2} \delta \mathcal{Z}_{G^0 G^0} \end{pmatrix} \begin{pmatrix} A^0 \\ G^0 \end{pmatrix}, \quad (4.23b)$$

$$\begin{pmatrix} H^\pm \\ G^\pm \end{pmatrix} \rightarrow \left(\mathbf{1} + \frac{1}{2} \delta \mathcal{Z}_{H^\pm G^\pm} \right) \begin{pmatrix} H^\pm \\ G^\pm \end{pmatrix} = \begin{pmatrix} 1 + \frac{1}{2} \delta \mathcal{Z}_{H^\pm H^\pm} & \frac{1}{2} \delta \mathcal{Z}_{H^\pm G^\pm} \\ \frac{1}{2} \delta \mathcal{Z}_{H^\pm G^\pm} & 1 + \frac{1}{2} \delta \mathcal{Z}_{G^\pm G^\pm} \end{pmatrix} \begin{pmatrix} H^\pm \\ G^\pm \end{pmatrix}. \quad (4.23c)$$

Applying the renormalization transformations (4.20) and rotating the fields according to (2.42) yields the following expressions for the field-renormalization constants of the fields in the mass-eigenstate basis:

$$\delta \mathcal{Z}_{h^0 h^0} = \sin^2 \alpha \delta \mathcal{Z}_{h_d} + \cos^2 \alpha \delta \mathcal{Z}_{h_u}, \quad (4.24a)$$

$$\delta \mathcal{Z}_{H^0 H^0} = \cos^2 \alpha \delta \mathcal{Z}_{h_d} + \sin^2 \alpha \delta \mathcal{Z}_{h_u}, \quad (4.24b)$$

$$\delta \mathcal{Z}_{h^0 H^0} = \sin \alpha \cos \alpha (\delta \mathcal{Z}_{h_d} - \delta \mathcal{Z}_{h_u}), \quad (4.24c)$$

$$\delta \mathcal{Z}_{A^0 A^0} = \sin^2 \beta \delta \mathcal{Z}_{h_d} + \cos^2 \beta \delta \mathcal{Z}_{h_u}, \quad (4.24d)$$

$$\delta \mathcal{Z}_{G^0 G^0} = \cos^2 \beta \delta \mathcal{Z}_{h_d} + \sin^2 \beta \delta \mathcal{Z}_{h_u}, \quad (4.24e)$$

$$\delta \mathcal{Z}_{A^0 G^0} = \sin \beta \cos \beta (\delta \mathcal{Z}_{h_d} - \delta \mathcal{Z}_{h_u}), \quad (4.24f)$$

$$\delta \mathcal{Z}_{H^- H^+} = \sin^2 \beta \delta \mathcal{Z}_{h_d} + \cos^2 \beta \delta \mathcal{Z}_{h_u}, \quad (4.24g)$$

$$\delta \mathcal{Z}_{G^- G^+} = \cos^2 \beta \delta \mathcal{Z}_{h_d} + \sin^2 \beta \delta \mathcal{Z}_{h_u}, \quad (4.24h)$$

$$\delta \mathcal{Z}_{H^\mp G^\mp} = \delta \mathcal{Z}_{H^\mp G^\pm} = \sin \beta \cos \beta (\delta \mathcal{Z}_{h_d} - \delta \mathcal{Z}_{h_u}). \quad (4.24i)$$

Thus, the counterterm Lagrangian reads as follows:

$$\begin{aligned} \mathcal{L}_{\text{Higgs}}^{\text{CT}} &= \frac{1}{2} (h^0, H^0) [\delta \mathcal{Z}_{h^0 H^0} (p^2 - \mathcal{D}_{h^0 H^0}) - \delta \mathcal{D}_{h^0 H^0}] \begin{pmatrix} h^0 \\ H^0 \end{pmatrix} \\ &+ \frac{1}{2} (A^0, G^0) [\delta \mathcal{Z}_{A^0 G^0} (p^2 - \mathcal{D}_{A^0 G^0}) - \delta \mathcal{D}_{A^0 G^0}] \begin{pmatrix} A^0 \\ G^0 \end{pmatrix} \\ &+ (H^\pm, G^\pm) [\delta \mathcal{Z}_{H^\pm G^\pm} (p^2 - \mathcal{D}_{H^\pm G^\pm}) - \delta \mathcal{D}_{H^\pm G^\pm}] \begin{pmatrix} H^\pm \\ G^\pm \end{pmatrix}. \end{aligned} \quad (4.25)$$

Again, the renormalized self-energies are obtained by taking the sum of the unrenormalized self-energy and the derivatives of the counterterm Lagrangian (4.25) with respect to the

Higgs fields,

$$\hat{\Sigma}_{h^0 h^0}(p^2) = \Sigma_{h^0 h^0}(p^2) + \delta Z_{h^0 h^0}(p^2 - m_{h^0}^2) - \delta m_{h^0}^2, \quad (4.26a)$$

$$\hat{\Sigma}_{H^0 H^0}(p^2) = \Sigma_{H^0 H^0}(p^2) + \delta Z_{H^0 H^0}(p^2 - m_{H^0}^2) - \delta m_{H^0}^2, \quad (4.26b)$$

$$\hat{\Sigma}_{h^0 H^0}(p^2) = \Sigma_{h^0 H^0}(p^2) + \delta Z_{h^0 H^0} \left(p^2 - \frac{1}{2}(m_{h^0}^2 + m_{H^0}^2) \right) - \delta m_{h^0 H^0}^2, \quad (4.26c)$$

$$\hat{\Sigma}_{A^0 A^0}(p^2) = \Sigma_{A^0 A^0}(p^2) + \delta Z_{A^0 A^0}(p^2 - m_{A^0}^2) - \delta m_{A^0}^2, \quad (4.26d)$$

$$\hat{\Sigma}_{G^0 G^0}(p^2) = \Sigma_{G^0 G^0}(p^2) + \delta Z_{G^0 G^0}(p^2 - m_{G^0}^2) - \delta m_{G^0}^2, \quad (4.26e)$$

$$\hat{\Sigma}_{A^0 G^0}(p^2) = \Sigma_{A^0 G^0}(p^2) + \delta Z_{A^0 G^0} \left(p^2 - \frac{1}{2}m_{A^0}^2 \right) - \delta m_{A^0 G^0}^2. \quad (4.26f)$$

For the charged Higgs bosons the following renormalized self-energies are obtained,

$$\hat{\Sigma}_{H^+ H^-}(p^2) = \Sigma_{H^+ H^-}(p^2) + \delta Z_{H^+ H^-}(p^2 - m_{H^\pm}^2) - \delta m_{H^\pm}^2, \quad (4.26g)$$

$$\hat{\Sigma}_{G^+ G^-}(p^2) = \Sigma_{G^+ G^-}(p^2) + \delta Z_{G^+ G^-} p^2 - \delta m_{G^\pm}^2, \quad (4.26h)$$

$$\hat{\Sigma}_{H^- G^+}(p^2) = \Sigma_{H^- G^+}(p^2) + \delta Z_{H^- G^+} \left(p^2 - \frac{1}{2}m_{H^\pm}^2 \right) - \delta m_{H^- G^+}^2. \quad (4.26i)$$

The CP-odd Higgs-boson mass m_{A^0} and the tadpole parameters T_h and T_H are renormalized according to the OS scheme:

$$\widetilde{\text{Re}} \hat{\Sigma}_{A^0 A^0}(m_{A^0}^2) = 0, \quad T_h + \delta T_h = 0, \quad T_H + \delta T_H = 0. \quad (4.27a)$$

Thus, the renormalization constants are determined by

$$\delta m_{A^0}^2 = \widetilde{\text{Re}} \Sigma_{A^0 A^0}(m_{A^0}^2), \quad \delta T_h = -T_h^{(1)}, \quad \delta T_H = -T_H^{(1)}, \quad (4.27b)$$

where $T_h^{(1)}$ and $T_H^{(1)}$ denote the one-loop tadpole vertex-amplitudes. For the fields and $\tan \beta$ the $\overline{\text{DR}}$ scheme is adopted,

$$\delta Z_{h_d} = - \left[\widetilde{\text{Re}} \Sigma'_{H^0 H^0}(p^2) |_{\alpha=0} \right]^{\text{div}}, \quad \delta Z_{h_u} = - \left[\widetilde{\text{Re}} \Sigma'_{h^0 h^0}(p^2) |_{\alpha=0} \right]^{\text{div}}, \quad (4.28a)$$

$$\delta \tan \beta = \tan \beta \left[\frac{1}{2} (\delta Z_{h_u} - \delta Z_{h_d}) + \frac{\delta v_u}{v_u} - \frac{\delta v_d}{v_d} \right]^{\text{div}} = \frac{1}{2} \tan \beta (\delta Z_{h_u} - \delta Z_{h_d}), \quad (4.28b)$$

where ‘‘div’’ signifies that only the divergent parts proportional to Δ (c.f. Eq.(4.4)) are taken. The last equality is due to the identical divergent parts of $\delta v_u/v_u$ and $\delta v_d/v_d$ (c.f. [44, 45]). The $\overline{\text{DR}}$ renormalization of $\tan \beta$ has been shown to yield stable numerical results [46] and to be gauge-independent at the one-loop level within the R_ξ gauges [47].

The masses of the CP-even Higgs bosons m_{h^0} , m_{H^0} and m_{H^\pm} are no free parameters. They are determined by the tree-level relations (2.45). However, they get large corrections from higher-order contributions reaching up to 50%. In the Feynman-diagrammatic approach, these contributions are determined using the Higgs-propagator matrices [29, 45],

$$\Delta_{h^0 H^0} = i \begin{pmatrix} p^2 - m_{h^0}^2 + \hat{\Sigma}_{h^0 h^0}(p^2) & \hat{\Sigma}_{h^0 H^0}(p^2) \\ \hat{\Sigma}_{h^0 H^0}(p^2) & p^2 - m_{H^0}^2 + \hat{\Sigma}_{H^0 H^0}(p^2) \end{pmatrix}^{-1}. \quad (4.29)$$

The Higgs-boson masses M_{h^0} and M_{H^0} including higher-order contributions are given by the poles of this propagator matrix. Note that M_i denotes the corrected Higgs-boson masses, whereas m_i denotes their tree-level values, $i = h^0, H^0$.

In processes with external Higgs bosons beyond lowest order, their proper on-shell conditions have to be assured. According to the LSZ formula the amplitudes have to be multiplied with finite wave-function renormalization factors such that the S-matrix is properly normalized. This also gives rise to mixing effects between the two neutral CP-even Higgs bosons h^0 and H^0 . The one-particle irreducible Higgs amplitude \mathcal{M}_i , where $i = h^0, H^0$ denotes the external Higgs boson, then receives the correction

$$\mathcal{M}_i \rightarrow \sqrt{\hat{Z}_i} \left(\mathcal{M}_i + \hat{Z}_{ij} \mathcal{M}_j \right), \quad (i \neq j), \quad (4.30)$$

with the finite wave function factors \hat{Z}_i given by the residues of the (h^0, H^0) propagator matrix [45],

$$\hat{Z}_i = \left[1 + \widetilde{\text{Re}} \hat{\Sigma}'_{ii}(p^2) - \widetilde{\text{Re}} \left(\frac{(\hat{\Sigma}_{ij}(p^2))^2}{p^2 - m_j^2 + \hat{\Sigma}_{jj}(p^2)} \right) \right]_{p^2=M_i^2}^{-1}. \quad (4.31a)$$

Finally the mixing terms read

$$\hat{Z}_{ij} = - \frac{\hat{\Sigma}_{ij}(M_i^2)}{M_i^2 - m_j^2 + \hat{\Sigma}_{jj}(M_i^2)}. \quad (4.31b)$$

Quark sector

After symmetry breaking, the bilinear terms in the quark Lagrangian read

$$\mathcal{L}_q = \bar{q} (\not{p} - m_q) q, \quad (4.32)$$

where $q = u_i, d_i$ denotes the fermion fields ($i = 1, 2, 3$) and generation mixing is neglected. The renormalization conditions for the quark fields and masses are

$$P_L q \rightarrow P_L \left(1 + \frac{1}{2} \delta Z_q^L \right) q, \quad (4.33a)$$

$$P_R q \rightarrow P_R \left(1 + \frac{1}{2} \delta Z_q^R \right) q, \quad (4.33b)$$

$$m_q \rightarrow m_q + \delta m_q, \quad (4.33c)$$

with the left- and right-handed quark states $q_{L/R} = P_{L/R} q$ obtained with help of the projection operators

$$P_L \equiv \frac{1}{2} (1 - \gamma_5), \quad P_R \equiv \frac{1}{2} (1 + \gamma_5). \quad (4.34)$$

With these renormalization transformations we obtain the counterterm Lagrangian,

$$\begin{aligned} \mathcal{L}_q^{\text{CT}} = & \frac{1}{2} \bar{q}_L \not{p} (\delta Z_q^L + \delta Z_q^{L\dagger}) q_L + \frac{1}{2} \bar{q}_R \not{p} (\delta Z_q^R + \delta Z_q^{R\dagger}) q_R \\ & - \bar{q}_R \left(\frac{m_q}{2} (\delta Z_q^L + \delta Z_q^{R\dagger}) + \delta m_q \right) q_L - \bar{q}_L \left(\frac{m_q}{2} (\delta Z_q^R + \delta Z_q^{L\dagger}) + \delta m_q \right) q_R. \end{aligned} \quad (4.35)$$

Thus, the renormalized self-energy is given by

$$\hat{\Sigma}^L(p^2) = \Sigma^L(p^2) + \frac{1}{2} (\delta Z_q^L + \delta Z_q^{L\dagger}), \quad (4.36a)$$

$$\hat{\Sigma}^R(p^2) = \Sigma^R(p^2) + \frac{1}{2} (\delta Z_q^R + \delta Z_q^{R\dagger}), \quad (4.36b)$$

$$\hat{\Sigma}^{SL}(p^2) = \Sigma^{SL}(p^2) - \left(\frac{m}{2} (\delta Z_q^L + \delta Z_q^{R\dagger}) + \delta m_q \right), \quad (4.36c)$$

$$\hat{\Sigma}^{SR}(p^2) = \Sigma^{SR}(p^2) - \left(\frac{m}{2} (\delta Z_q^R + \delta Z_q^{L\dagger}) + \delta m_q \right), \quad (4.36d)$$

where the Lorentz decomposition of the fermion self-energy has been used,

$$\Sigma(p) = \not{p} P_L \Sigma^L(p^2) + \not{p} P_R \Sigma^R(p^2) + P_L \Sigma^{SL}(p^2) + P_R \Sigma^{SR}(p^2). \quad (4.37)$$

The field- and mass-renormalization constants are obtained by imposing the OS renormalization conditions,

$$\widetilde{\text{Re}} \left[\hat{\Sigma}_q(p) \right] q(p) \Big|_{p^2=m_q^2} = 0, \quad \lim_{p^2 \rightarrow m^2} \frac{1}{\not{p} - m_q} \widetilde{\text{Re}} \left[\hat{\Sigma}_q(p) \right] q(p) = 0. \quad (4.38)$$

Inserting the renormalized self-energies (4.36) into the OS conditions (4.38) yields

$$\delta m_q = \frac{1}{2} \left(m_q \widetilde{\text{Re}} \left[\Sigma_q^L(m_q^2) + \Sigma_q^R(m_q^2) \right] + \widetilde{\text{Re}} \left[\Sigma_q^{SL}(m_q^2) + \Sigma_q^{SR}(m_q^2) \right] \right), \quad (4.39a)$$

$$\begin{aligned} \delta Z_q^L = & -\widetilde{\text{Re}} \left[\Sigma_q^L(m_q^2) + m_q^2 \left(\Sigma_q^{L'}(m_q^2) + \Sigma_q^{R'}(m_q^2) \right) \right. \\ & \left. + m_q \left(\Sigma_q^{SL'}(m_q^2) + \Sigma_q^{SR'}(m_q^2) \right) \right], \end{aligned} \quad (4.39b)$$

$$\begin{aligned} \delta Z_q^R = & -\widetilde{\text{Re}} \left[\Sigma_q^R(m_q^2) + m_q^2 \left(\Sigma_q^{L'}(m_q^2) + \Sigma_q^{R'}(m_q^2) \right) \right. \\ & \left. + m_q \left(\Sigma_q^{SL'}(m_q^2) + \Sigma_q^{SR'}(m_q^2) \right) \right]. \end{aligned} \quad (4.39c)$$

Since the masses of the first two quark generations are not observable, they will be neglected everywhere but in collinear singular regions, where λ_q is introduced as mass regulator. This differs for third-generation quarks, especially the top quark. It has a width of $\Gamma_t \approx 1.5$ GeV, which implies that it decays before it can hadronize. The most current measured value is $m_t = 173.3 \pm 1.1$ GeV [48], which is obtained using kinematic reconstruction from the decay products, comparing them to results obtained from Monte-Carlo simulations. However, the interpretation of this reconstructed top-quark mass and

its relation to the pole mass is very challenging [49, 50]. In this work the top-quark mass is treated in the OS renormalization scheme.

The calculations in the following chapters involving the bottom-quark mass use the running $\overline{\text{DR}}$ definition. Following [51], the bottom-quark mass in the $\overline{\text{DR}}$ scheme $m_b^{\overline{\text{DR}}}(\mu_R)$ at the scale μ_R is related to the bottom-quark pole-mass, which can be expressed in terms of the $\overline{\text{MS}}$ mass at the M_Z scale $m_b^{\overline{\text{MS}}}(M_Z) = 2.94 \text{ GeV}$ [16]. With the bottom-quark mass counterterms in the OS and $\overline{\text{DR}}$ scheme,

$$\delta m_b^{\overline{\text{OS}}} = \frac{1}{2} \left(m_b \widetilde{\text{Re}} \left[\Sigma_q^L(m_b^2) + \Sigma_q^R(m_b^2) \right] + \widetilde{\text{Re}} \left[\Sigma_q^{SL}(m_b^2) + \Sigma_q^{SR}(m_b^2) \right] \right), \quad (4.40a)$$

$$\delta m_b^{\overline{\text{DR}}} = \frac{1}{2} \left(m_b \widetilde{\text{Re}} \left[\Sigma_q^L(m_b^2) + \Sigma_q^R(m_b^2) \right] + \widetilde{\text{Re}} \left[\Sigma_q^{SL}(m_b^2) + \Sigma_q^{SR}(m_b^2) \right] \right) \Big|_{\text{div}}, \quad (4.40b)$$

and the relation $m_b^{\overline{\text{DR}}} = m_b^{\overline{\text{OS}}} + \delta m_b^{\overline{\text{OS}}} - \delta m_b^{\overline{\text{DR}}}$ one finds

$$m_b^{\overline{\text{DR}}}(\mu_R) = m_b^{\overline{\text{OS}}} + \frac{m_b}{2} \left(\Sigma_L^{\text{fin}}(m_b) + \Sigma_R^{\text{fin}}(m_b) + 2\Sigma_S^{\text{fin}}(m_b) \right), \quad (4.41)$$

where $\Sigma^{\text{fin}} \equiv \Sigma - \Sigma^{\text{div}}$ denotes the UV-finite part of the self energy. The on-shell bottom-quark mass is related to the $\overline{\text{MS}}$ mass via

$$m_b^{\overline{\text{OS}}} = m_b^{\overline{\text{MS}}}(M_Z) b^{\text{shift}}, \quad b^{\text{shift}} = 1 + \frac{\alpha_s}{\pi} \left(\frac{4}{3} - \log \frac{\left(m_b^{\overline{\text{MS}}} \right)^2}{m_Z^2} \right). \quad (4.42)$$

It also gets potentially large $\tan \beta$ enhanced contributions. Thus, the computation of $m_b^{\overline{\text{DR}}}$ will be addressed in more detail in Subsection 4.1.4.

Light-flavor sfermion sector

The renormalization procedure for sfermions is based on [52]. For a sfermion $\tilde{f} = \tilde{u}, \tilde{d}, \tilde{c}, \tilde{s}, \tilde{\nu}, \tilde{e}$ the bilinear terms in the Lagrangian are given by

$$\mathcal{L}_{\tilde{f}} = \left(\tilde{f}_L^*, \tilde{f}_R^* \right) (p^2 - \mathcal{M}_{\tilde{f}}) \begin{pmatrix} \tilde{f}_L \\ \tilde{f}_R \end{pmatrix}, \quad (4.43)$$

with the mass matrix $\mathcal{M}_{\tilde{f}}$ from (2.49). For light-flavor sfermions mixing effects are neglected and the mass matrix reduces to

$$\begin{aligned} \mathcal{M}_{\tilde{f}} &= \begin{pmatrix} M_{\tilde{f}_L}^2 + (I_f^3 - Q_f s_W^2) \cos 2\beta M_Z^2 & 0 \\ 0 & M_{\tilde{f}_R}^2 + Q_f s_W^2 \cos 2\beta M_Z^2 \end{pmatrix} \\ &= \begin{pmatrix} m_{\tilde{f}_L}^2 & 0 \\ 0 & m_{\tilde{f}_R}^2 \end{pmatrix}. \end{aligned} \quad (4.44)$$

The left-handed sneutrino is described by the one-dimensional mass matrix

$$\mathcal{M}_{\tilde{\nu}} = M_{\tilde{l}_L}^2 + \frac{1}{2} \cos 2\beta M_Z^2. \quad (4.45)$$

Free parameters of the light-flavor squark sector are $M_{\tilde{f}_L}^2$, $M_{\tilde{u}_R}^2$, $M_{\tilde{d}_R}^2$ and $M_{\tilde{e}_R}^2$. Because of the $SU(2)$ symmetry the soft breaking parameters for the left-handed up- and down-type sfermions are the same: $M_{\tilde{u}_L} = M_{\tilde{d}_L} \equiv M_{\tilde{q}_L}$ and $M_{\tilde{\nu}} = M_{\tilde{e}_L} \equiv M_{\tilde{l}_L}$. Thus, the renormalization conditions for the sfermion mass-parameters and fields read

$$\begin{aligned} M_{\tilde{q}_L}^2 &\rightarrow M_{\tilde{q}_L}^2 + \delta M_{\tilde{q}_L}^2, & M_{\tilde{l}_L}^2 &\rightarrow M_{\tilde{l}_L}^2 + \delta M_{\tilde{l}_L}^2, \\ M_{\tilde{u}_R}^2 &\rightarrow M_{\tilde{u}_R}^2 + \delta M_{\tilde{u}_R}^2, & M_{\tilde{d}_R}^2 &\rightarrow M_{\tilde{d}_R}^2 + \delta M_{\tilde{d}_R}^2, \end{aligned} \quad (4.46a)$$

$$\begin{aligned} M_{\tilde{e}_R}^2 &\rightarrow M_{\tilde{e}_R}^2 + \delta M_{\tilde{e}_R}^2, \\ \begin{pmatrix} \tilde{f}_L \\ \tilde{f}_R \end{pmatrix} &\rightarrow \left(\mathbf{1} + \frac{1}{2} \delta \mathcal{Z}_{\tilde{f}} \right) \begin{pmatrix} \tilde{f}_L \\ \tilde{f}_R \end{pmatrix}, \quad \text{with} \quad \delta \mathcal{Z}_{\tilde{f}} = \begin{pmatrix} \delta Z_{\tilde{f}_L \tilde{f}_L} & \delta Z_{\tilde{f}_L \tilde{f}_R} \\ \delta Z_{\tilde{f}_R \tilde{f}_L} & \delta Z_{\tilde{f}_R \tilde{f}_R} \end{pmatrix}. \end{aligned} \quad (4.46b)$$

With the renormalization of the sfermion mass-parameters and the parameters from the electroweak sector (4.6), the renormalization condition for the sfermion mass-matrix can be written down,

$$\mathcal{M}_{\tilde{f}} \rightarrow \mathcal{M}_{\tilde{f}} + \delta \mathcal{M}_{\tilde{f}} = \begin{pmatrix} m_{\tilde{f}_L}^2 & 0 \\ 0 & m_{\tilde{f}_R}^2 \end{pmatrix} + \begin{pmatrix} \delta m_{\tilde{f}_L}^2 & 0 \\ 0 & \delta m_{\tilde{f}_R}^2 \end{pmatrix}, \quad \tilde{f} = \tilde{u}, \tilde{d}, \tilde{e}, \quad (4.47a)$$

$$m_{\tilde{\nu}}^2 \rightarrow m_{\tilde{\nu}}^2 + \delta m_{\tilde{\nu}}^2, \quad (4.47b)$$

where

$$\delta m_{\tilde{f}_L}^2 = \delta M_{\tilde{f}_L}^2 + (I^3 - Q_f s_W^2) (\delta \cos 2\beta M_Z^2 + \cos 2\beta \delta M_Z^2) - Q_f \delta s_W^2 \cos 2\beta M_Z^2, \quad (4.47c)$$

$$\delta m_{\tilde{f}_R}^2 = \delta M_{\tilde{f}_R}^2 + Q_f \delta s_W^2 \cos 2\beta M_Z^2 + Q_f s_W^2 \delta \cos 2\beta M_Z^2 + Q_f s_W^2 \cos 2\beta \delta M_Z^2. \quad (4.47d)$$

Hence, the counterterm Lagrangian for the light-flavor sfermions reads

$$\mathcal{L}_{\tilde{f}}^{\text{CT}} = \left(\tilde{f}_L^*, \tilde{f}_R^* \right) \left[\frac{1}{2} \left(\delta \mathcal{Z}_{\tilde{f}} + \delta \mathcal{Z}_{\tilde{f}}^\dagger \right) p^2 - \frac{1}{2} \left(\delta \mathcal{Z}_{\tilde{f}}^\dagger \mathcal{M}_{\tilde{f}} + \mathcal{M}_{\tilde{f}} \delta \mathcal{Z}_{\tilde{f}} \right) - \delta \mathcal{M}_{\tilde{f}} \right] \begin{pmatrix} \tilde{f}_L \\ \tilde{f}_R \end{pmatrix}, \quad (4.48)$$

which yields the renormalized squark self-energy

$$\hat{\Sigma}_{\tilde{f}_i \tilde{f}_j} (p^2) = \Sigma_{\tilde{f}_i \tilde{f}_j} (p^2) + \left[\frac{1}{2} \left(\delta \mathcal{Z}_{\tilde{f}} + \delta \mathcal{Z}_{\tilde{f}}^\dagger \right) p^2 - \frac{1}{2} \left(\delta \mathcal{Z}_{\tilde{f}}^\dagger \mathcal{M}_{\tilde{f}} + \mathcal{M}_{\tilde{f}} \delta \mathcal{Z}_{\tilde{f}} \right) - \delta \mathcal{M}_{\tilde{f}} \right]_{ij}, \quad (4.49)$$

where the subscript “ $\tilde{f}_i \tilde{f}_j$ ” refers to the transition $\tilde{f}_i \rightarrow \tilde{f}_j$ ($i, j \in \{L, R\}$) and the subscripts “ i, j ” to the corresponding matrix elements of $\mathcal{M}_{\tilde{f}}$, $\delta \mathcal{M}_{\tilde{f}}$ and $\delta \mathcal{Z}_{\tilde{f}}$.

Since there are only three (two) independent mass parameters in the squark (slepton) sector, only three (two) OS conditions can be imposed on the squark (slepton) masses.

The renormalization constant of one sfermion mass then will depend on the other renormalization constants. This will also be referred to as the “dependent sfermion mass”. In this work the left-handed down-type squark \tilde{d}_L and the left-handed selectron masses are chosen to be the dependent quantities. The renormalization constants then are

$$\widetilde{\text{Re}}\hat{\Sigma}_{\tilde{f}_i\tilde{f}_i} \left(m_{\tilde{f}_i}^2 \right) = 0, \quad \tilde{f}_i \neq \tilde{d}_L, e_L, \quad (4.50a)$$

$$\widetilde{\text{Re}}\hat{\Sigma}_{\tilde{f}_L\tilde{f}_R} \left(m_{\tilde{f}_L}^2 \right) + \widetilde{\text{Re}}\hat{\Sigma}_{\tilde{f}_L\tilde{f}_R} \left(m_{\tilde{f}_R}^2 \right) = 0, \quad (4.50b)$$

$$\widetilde{\text{Re}}\hat{\Sigma}'_{\tilde{f}_i\tilde{f}_i} \left(m_{\tilde{f}_i}^2 \right) = 0. \quad (4.50c)$$

(4.50a) fixes the mass renormalization constant, whereas (4.50b) and (4.50c) determine the diagonal and off-diagonal entries of the field renormalization matrix. Thus, the following values for the renormalization constants are obtained,

$$\delta m_{\tilde{f}_i} = \widetilde{\text{Re}}\Sigma_{\tilde{f}_i\tilde{f}_i} \left(m_{\tilde{f}_i}^2 \right), \quad \tilde{f}_i \neq \tilde{d}_L, e_L, \quad (4.51a)$$

$$\delta Z_{\tilde{f}_i\tilde{f}_i} = -\widetilde{\text{Re}}\Sigma'_{\tilde{f}_i\tilde{f}_i} \left(m_{\tilde{f}_i}^2 \right), \quad (4.51b)$$

$$\delta Z_{\tilde{f}_i\tilde{f}_j} = \frac{2}{m_{\tilde{f}_i}^2 - m_{\tilde{f}_j}^2} \widetilde{\text{Re}}\Sigma_{\tilde{f}_i\tilde{f}_j} \left(m_{\tilde{f}_j}^2 \right), \quad \tilde{f}_i \neq \tilde{f}_j. \quad (4.51c)$$

The renormalization constants for the soft-breaking sfermion mass-parameters $\delta M_{\tilde{f}_L}^2$, $\delta M_{\tilde{u}_R}^2$, $\delta M_{\tilde{d}_R}^2$ and $\delta M_{\tilde{e}_R}^2$ are obtained by inverting (4.47),

$$\delta M_{\tilde{q}_L}^2 = \delta m_{\tilde{u}_L}^2 - \left(\frac{1}{2} - \frac{2}{3}s_W^2 \right) (\delta \cos 2\beta M_Z^2 + \cos 2\beta \delta M_Z^2) + \frac{2}{3}\delta s_W^2 \cos 2\beta M_Z^2, \quad (4.52a)$$

$$\delta M_{\tilde{l}_L}^2 = \delta m_{\tilde{\nu}}^2 - \frac{1}{2} (\delta \cos 2\beta M_Z^2 + \cos 2\beta \delta M_Z^2), \quad (4.52b)$$

$$\delta M_{\tilde{u}_R}^2 = \delta m_{\tilde{u}_R}^2 - \frac{2}{3}\delta s_W^2 \cos 2\beta M_Z^2 - \frac{2}{3}s_W^2 \delta \cos 2\beta M_Z^2 - \frac{2}{3}s_W^2 \cos 2\beta \delta M_Z^2, \quad (4.52c)$$

$$\delta M_{\tilde{d}_R}^2 = \delta m_{\tilde{d}_R}^2 + \frac{1}{3}\delta s_W^2 \cos 2\beta M_Z^2 + \frac{1}{3}s_W^2 \delta \cos 2\beta M_Z^2 + \frac{1}{3}s_W^2 \cos 2\beta \delta M_Z^2, \quad (4.52d)$$

$$\delta M_{\tilde{e}_R}^2 = \delta m_{\tilde{e}_R}^2 + \delta s_W^2 \cos 2\beta M_Z^2 + s_W^2 \delta \cos 2\beta M_Z^2 + s_W^2 \cos 2\beta \delta M_Z^2. \quad (4.52e)$$

Since $\delta M_{\tilde{q}_L}^2$ has the same value for $\tilde{q}_L = \tilde{u}_L$ and $\tilde{q}_L = \tilde{d}_L$ (4.47c) can be used to express the renormalization constant of the dependent squark mass $\delta m_{\tilde{d}_L}$ in terms of the independent renormalization constants,

$$\delta m_{\tilde{d}_L}^2 = \delta m_{\tilde{u}_L}^2 + s_W^2 (\delta \cos 2\beta M_Z^2 + \cos 2\beta \delta M_Z^2) + \cos 2\beta M_Z^2 \delta s_W^2. \quad (4.53)$$

Analogously, the left-handed selectron mass renormalization constant can be described in terms of the independent quantities,

$$\delta m_{\tilde{e}_L}^2 = \delta m_{\tilde{\nu}}^2 - c_W^2 (\delta \cos 2\beta M_Z^2 + \cos 2\beta \delta M_Z^2) + \cos 2\beta M_Z^2 \delta s_W^2. \quad (4.54)$$

Thus, the tree-level mass of the left-handed down-type squark and selectron receive a finite shift to their on-shell value,

$$\left(m_{\tilde{f}_L}^{\text{OS}}\right)^2 = m_{\tilde{f}_L}^2 + \delta m_{\tilde{f}_L}^2 - \widetilde{\text{Re}}\Sigma_{\tilde{f}_L\tilde{f}_L}\left(m_{\tilde{f}_L}^2\right), \quad \tilde{f} = d, e. \quad (4.55)$$

Third-generation sfermion sector

As mentioned in for the sfermion sector, for third-generation sfermions mixing effects have to be taken into account. The mass matrix now also includes non-diagonal terms,

$$\mathcal{M}_{\tilde{f}} = \begin{pmatrix} M_{\tilde{f}_L}^2 + m_f^2 + (I_f^3 - Q_f s_W^2) \cos 2\beta M_Z^2 & m_f (A_f - \mu\kappa) \\ m_f (A_f - \mu\kappa) & M_{\tilde{f}_R}^2 + m_f^2 + Q_f s_W^2 \cos 2\beta M_Z^2 \end{pmatrix} \quad (4.56)$$

with $\kappa = \cot \beta$ for the top squark $\tilde{f} = \tilde{t}$ and $\kappa = \tan \beta$ for the bottom squark and stau $\tilde{f} = \tilde{b}, \tilde{\tau}$. For third-generation sneutrinos (4.45) stays valid. In this part, third-generation sneutrinos will be excluded, since it can be treated as in the light-flavor sfermion sector. In addition to the renormalization of the mass parameters (4.47) performed for light-flavor sfermions, the renormalization of parameters relevant for sfermion mixing has to be taken into account,

$$A_t \rightarrow A_t + \delta A_t, \quad A_b \rightarrow A_b + \delta A_b, \quad (4.57a)$$

$$A_\tau \rightarrow A_\tau + \delta A_\tau, \quad (4.57b)$$

$$\tan \beta \rightarrow \tan \beta + \delta \tan \beta, \quad \mu \rightarrow \mu + \delta \mu. \quad (4.57c)$$

For the mass matrices the following renormalization constants are obtained,

$$\delta \mathcal{M}_{\tilde{f}} = \begin{pmatrix} \delta M_{\tilde{f}_L\tilde{f}_L} & \delta M_{\tilde{f}_L\tilde{f}_R} \\ \delta M_{\tilde{f}_R\tilde{f}_L} & \delta M_{\tilde{f}_R\tilde{f}_R} \end{pmatrix}, \quad (4.58a)$$

$$\begin{aligned} \delta M_{\tilde{f}_L\tilde{f}_L} &= \delta M_{\tilde{f}_L}^2 + 2m_f \delta m_f + (I_f^3 - Q_f s_W^2) (\delta c_{2\beta} M_Z^2 + c_{2\beta} \delta M_Z^2) \\ &\quad - Q_f \delta s_W^2 c_{2\beta} M_Z^2, \end{aligned} \quad (4.58b)$$

$$\delta M_{\tilde{f}_R\tilde{f}_R} = \delta M_{\tilde{f}_R}^2 + 2m_f \delta m_f + Q_f \delta s_W^2 c_{2\beta} M_Z^2 + Q_f s_W^2 \delta c_{2\beta} M_Z^2 + Q_f s_W^2 c_{2\beta} \delta M_Z^2, \quad (4.58c)$$

$$\delta M_{\tilde{f}_L\tilde{f}_R} = \delta M_{\tilde{f}_R\tilde{f}_L} = \delta m_f (A_f - \mu\kappa) + m_f \delta A_f - m_f \kappa \delta \mu - m_f \mu \delta \kappa, \quad (4.58d)$$

where $\delta \kappa = \delta \cot \beta$ for top squarks and $\delta \kappa = \tan \beta$ for bottom squarks and staus. This yields the following renormalization transformations for the diagonal sfermion mass matrices,

$$\mathcal{D}_{\tilde{f}} \rightarrow \mathcal{D}_{\tilde{f}} + \delta \mathcal{D}_{\tilde{f}} \equiv \mathcal{D}_{\tilde{f}} + U_{\tilde{f}} \delta \mathcal{M}_{\tilde{f}} U_{\tilde{f}}^\dagger, \quad (4.59a)$$

$$\delta \mathcal{D}_{\tilde{f}} = \begin{pmatrix} \delta m_{\tilde{f}_1}^2 & \delta Y_{\tilde{f}} \\ \delta Y_{\tilde{f}} & \delta m_{\tilde{f}_2}^2 \end{pmatrix}. \quad (4.59b)$$

In the second line, the diagonal mass matrix renormalization constant has been expressed by the mass renormalization constants of the sfermions $\delta m_{\tilde{f}_{1,2}}^2$ and the renormalization constants for the non-diagonal mixing parameters $\delta Y_{\tilde{f}}$. Hence, the renormalization constants of soft-breaking parameters are related to the mass and mixing renormalization constants via (4.59a),

$$\delta M_{\tilde{f}_L \tilde{f}_L} = U_{\tilde{f}_{11}}^2 \delta m_{\tilde{f}_1}^2 + U_{\tilde{f}_{21}}^2 \delta m_{\tilde{f}_2}^2 + 2U_{\tilde{f}_{11}} U_{\tilde{f}_{21}} \delta Y_{\tilde{f}}, \quad (4.60a)$$

$$\delta M_{\tilde{f}_R \tilde{f}_R} = U_{\tilde{f}_{12}}^2 \delta m_{\tilde{f}_1}^2 + U_{\tilde{f}_{22}}^2 \delta m_{\tilde{f}_2}^2 + 2U_{\tilde{f}_{12}} U_{\tilde{f}_{22}} \delta Y_{\tilde{f}}, \quad (4.60b)$$

$$\delta M_{\tilde{f}_L \tilde{f}_R} = \delta M_{\tilde{f}_R \tilde{f}_L} = U_{\tilde{f}_{11}} U_{\tilde{f}_{12}} \left(\delta m_{\tilde{f}_1}^2 - \delta m_{\tilde{f}_2}^2 \right) + (U_{\tilde{f}_{11}} U_{\tilde{f}_{22}} + U_{\tilde{f}_{12}} U_{\tilde{f}_{21}}) \delta Y_{\tilde{f}}. \quad (4.60c)$$

Sfermion fields are renormalized in terms of the mass eigenstates [52],

$$\begin{pmatrix} \tilde{f}_1 \\ \tilde{f}_2 \end{pmatrix} \rightarrow \left(1 + \frac{1}{2} \delta \mathcal{Z}_{\tilde{f}} \right) \begin{pmatrix} \tilde{f}_1 \\ \tilde{f}_2 \end{pmatrix}, \quad \text{with} \quad \delta \mathcal{Z}_{\tilde{f}} = \begin{pmatrix} \delta Z_{\tilde{f}_1 \tilde{f}_1} & \delta Z_{\tilde{f}_1 \tilde{f}_2} \\ \delta Z_{\tilde{f}_2 \tilde{f}_1} & \delta Z_{\tilde{f}_2 \tilde{f}_2} \end{pmatrix}. \quad (4.61)$$

This leads to the following sfermion counterterm Lagrangian in the mass eigenstate basis,

$$\mathcal{L}_{\tilde{f}}^{\text{CT}} = \left(\tilde{f}_1^*, \tilde{f}_2^* \right) \left[\frac{1}{2} \left(\delta \mathcal{Z}_{\tilde{f}} + \delta \mathcal{Z}_{\tilde{f}}^\dagger \right) p^2 - \frac{1}{2} \left(\delta \mathcal{Z}_{\tilde{f}}^\dagger \mathcal{D}_{\tilde{f}} + \mathcal{D}_{\tilde{f}} \delta \mathcal{Z}_{\tilde{f}} \right) - \delta \mathcal{D}_{\tilde{f}} \right] \begin{pmatrix} \tilde{f}_1 \\ \tilde{f}_2 \end{pmatrix}, \quad (4.62)$$

as well as the renormalized self-energies

$$\hat{\Sigma}_{\tilde{f}_1 \tilde{f}_1}(p^2) = \Sigma_{\tilde{f}_1 \tilde{f}_1}(p^2) + \frac{1}{2} \left(p^2 - m_{\tilde{f}_1}^2 \right) \left[\delta Z_{\tilde{f}_1 \tilde{f}_1} + \delta Z_{\tilde{f}_1 \tilde{f}_1}^* \right] - \delta m_{\tilde{f}_1}^2, \quad (4.63a)$$

$$\hat{\Sigma}_{\tilde{f}_2 \tilde{f}_2}(p^2) = \Sigma_{\tilde{f}_2 \tilde{f}_2}(p^2) + \frac{1}{2} \left(p^2 - m_{\tilde{f}_2}^2 \right) \left[\delta Z_{\tilde{f}_2 \tilde{f}_2} + \delta Z_{\tilde{f}_2 \tilde{f}_2}^* \right] - \delta m_{\tilde{f}_2}^2, \quad (4.63b)$$

$$\hat{\Sigma}_{\tilde{f}_1 \tilde{f}_2}(p^2) = \Sigma_{\tilde{f}_1 \tilde{f}_2}(p^2) + \frac{1}{2} \left(p^2 - m_{\tilde{f}_1}^2 \right) \delta Z_{\tilde{f}_1 \tilde{f}_2} + \frac{1}{2} \left(p^2 - m_{\tilde{f}_2}^2 \right) \delta Z_{\tilde{f}_2 \tilde{f}_1}^* - \delta Y_f, \quad (4.63c)$$

$$\hat{\Sigma}_{\tilde{f}_2 \tilde{f}_1}(p^2) = \Sigma_{\tilde{f}_2 \tilde{f}_1}(p^2) + \frac{1}{2} \left(p^2 - m_{\tilde{f}_1}^2 \right) \delta Z_{\tilde{f}_1 \tilde{f}_2}^* + \frac{1}{2} \left(p^2 - m_{\tilde{f}_2}^2 \right) \delta Z_{\tilde{f}_2 \tilde{f}_1} - \delta Y_f. \quad (4.63d)$$

The third-generation squark (slepton) sector is described by five (three) squark mass parameters: $M_{\tilde{q}_L}$, $M_{\tilde{t}_R}$, $M_{\tilde{b}_R}$, A_t and A_b ($M_{\tilde{l}_L}$, $M_{\tilde{\tau}_R}$ and A_τ). Again, one sfermion mass renormalization-constant depends on the others. The dependent sfermion masses are chosen to be $m_{\tilde{b}_1}$ and $m_{\tilde{\tau}_1}$, respectively. Renormalizing the third-generation sfermion sector in the OS scheme is done by imposing conditions (4.50). This fixes the mass ($\delta m_{\tilde{f}_i}^2$) and mixing renormalization constants (δY_f),

$$\delta m_{\tilde{f}_i}^2 = \widetilde{\text{Re}} \Sigma_{\tilde{f}_i \tilde{f}_i} \left(m_{\tilde{f}_i}^2 \right), \quad \tilde{f}_i \neq \tilde{b}_1, \tilde{\tau}_1, \quad (4.64a)$$

$$\delta Y_{\tilde{f}} = \frac{\widetilde{\text{Re}} \Sigma_{\tilde{f}_1 \tilde{f}_2} \left(m_{\tilde{f}_1}^2 \right) + \widetilde{\text{Re}} \Sigma_{\tilde{f}_1 \tilde{f}_2} \left(m_{\tilde{f}_2}^2 \right)}{2}. \quad (4.64b)$$

For the mass-mixing renormalization constants $\delta Y_{\tilde{f}}$ additional conditions $\delta Z_{\tilde{f}_1 \tilde{f}_2} = \delta Z_{\tilde{f}_2 \tilde{f}_1}$ have to be imposed [52]. The renormalization constant for the dependent sfermion $\tilde{b}_1, \tilde{\tau}_1$ is then obtained by applying (4.60a) for up- and down-type sfermions,

$$\delta m_{\tilde{b}_1}^2 = \frac{1}{U_{\tilde{b}_{11}}^2} \left[U_{\tilde{t}_{11}}^2 \delta m_{\tilde{t}_1}^2 + U_{\tilde{t}_{21}}^2 \delta m_{\tilde{t}_2}^2 + 2U_{\tilde{t}_{11}} U_{\tilde{t}_{21}} \delta Y_{\tilde{t}} - U_{\tilde{b}_{21}}^2 \delta m_{\tilde{b}_2}^2 - 2U_{\tilde{b}_{11}} U_{\tilde{b}_{21}} \delta Y_{\tilde{b}} \right. \\ \left. - 2m_t \delta m_t + 2m_b \delta m_b - M_W^2 \delta c_{2\beta} - c_{2\beta} \delta M_W^2 \right], \quad (4.65a)$$

$$\delta m_{\tilde{\tau}_1}^2 = \frac{1}{U_{\tilde{\tau}_{11}}^2} \left[\delta m_{\tilde{\nu}}^2 - U_{\tilde{\tau}_{21}}^2 \delta m_{\tilde{\tau}_2}^2 - 2U_{\tilde{\tau}_{11}} U_{\tilde{\tau}_{21}} \delta Y_{\tilde{\tau}} \right. \\ \left. + 2m_\tau \delta m_\tau - M_W^2 \delta c_{2\beta} - c_{2\beta} \delta M_W^2 + \delta s_W c_{2\beta} M_Z^2 \right], \quad (4.65b)$$

where $\delta c_{2\beta} = -4t_\beta / (1 + t_\beta^2)^2 \delta t_\beta$. Applying (4.60), renormalization constants for the soft-breaking squark mass-parameters are obtained,

$$\delta M_{\tilde{q}_L}^2 = U_{\tilde{t}_{11}}^2 \delta m_{\tilde{t}_1}^2 + U_{\tilde{t}_{12}}^2 \delta m_{\tilde{t}_2}^2 + 2U_{\tilde{t}_{11}} U_{\tilde{t}_{12}} \delta Y_{\tilde{t}} \\ - 2m_t \delta m_t - \left(\frac{1}{2} - \frac{2}{3} s_W^2 \right) (\delta c_{2\beta} M_Z^2 + c_{2\beta} \delta M_Z^2) - \frac{2}{3} \delta s_W^2 c_{2\beta} M_Z^2, \quad (4.66a)$$

$$\delta M_{\tilde{t}_R}^2 = U_{\tilde{t}_{12}}^2 \delta m_{\tilde{t}_1}^2 + U_{\tilde{t}_{22}}^2 \delta m_{\tilde{t}_2}^2 + 2U_{\tilde{t}_{12}} U_{\tilde{t}_{22}} \delta Y_{\tilde{t}} \\ - 2m_t \delta m_t - \frac{2}{3} \delta s_W^2 c_{2\beta} M_Z^2 - \frac{2}{3} s_W^2 \delta c_{2\beta} M_Z^2 - \frac{2}{3} s_W^2 c_{2\beta} \delta M_Z^2, \quad (4.66b)$$

$$\delta M_{\tilde{b}_R}^2 = U_{\tilde{b}_{12}}^2 \delta m_{\tilde{b}_1}^2 + U_{\tilde{b}_{22}}^2 \delta m_{\tilde{b}_2}^2 + 2U_{\tilde{b}_{12}} U_{\tilde{b}_{22}} \delta Y_{\tilde{b}} \\ - 2m_b \delta m_b + \frac{1}{3} \delta s_W^2 c_{2\beta} M_Z^2 + \frac{1}{3} s_W^2 \delta c_{2\beta} M_Z^2 + \frac{1}{3} s_W^2 c_{2\beta} \delta M_Z^2. \quad (4.66c)$$

The renormalization constants of the trilinear couplings are given by

$$\delta A_t = \frac{1}{m_t} \left[U_{\tilde{t}_{11}} U_{\tilde{t}_{12}} (\delta m_{\tilde{t}_1}^2 - \delta m_{\tilde{t}_2}^2) + (U_{\tilde{t}_{11}} U_{\tilde{t}_{22}} + U_{\tilde{t}_{12}} U_{\tilde{t}_{21}}) \delta Y_{\tilde{t}} \right. \\ \left. - \delta m_t \left(A_t - \frac{\mu}{t_\beta} \right) + \frac{m_t \delta \mu}{t_\beta} - \frac{m_t \mu \delta t_\beta}{t_\beta^2} \right], \quad (4.66d)$$

$$\delta A_b = \frac{1}{m_b U_{\tilde{b}_{11}}} \left[-U_{\tilde{b}_{12}} \delta m_{\tilde{b}_2}^2 + U_{\tilde{b}_{22}} \delta Y_{\tilde{b}} - (U_{\tilde{b}_{11}} (A_b - \mu t_\beta) - 2U_{\tilde{b}_{12}} m_b) \delta m_b \right. \\ \left. + U_{\tilde{b}_{12}} (U_{\tilde{t}_{11}}^2 \delta m_{\tilde{t}_1}^2 + U_{\tilde{t}_{12}}^2 \delta m_{\tilde{t}_2}^2 + U_{\tilde{t}_{11}} U_{\tilde{t}_{21}} \delta Y_{\tilde{t}}) - 2U_{\tilde{b}_{12}} m_t \delta m_t - U_{\tilde{b}_{12}} c_{2\beta} \delta M_W^2 \right. \\ \left. + \left(4U_{\tilde{b}_{12}} M_W^2 \frac{t_\beta}{(1 + t_\beta^2)} + U_{\tilde{b}_{11}} m_b \mu \right) \delta t_\beta + U_{\tilde{b}_{11}} m_b t_\beta \delta \mu. \right] \quad (4.66e)$$

For third-generation slepton parameters the renormalization constants read

$$\delta M_{\tilde{l}_L}^2 = \delta m_{\tilde{\nu}}^2 - \frac{1}{2} (\delta c_{2\beta} M_Z^2 + c_{2\beta} \delta M_Z^2), \quad (4.67a)$$

$$\begin{aligned} \delta M_{\tilde{\tau}_R}^2 &= U_{\tilde{\tau}12}^2 \delta m_{\tilde{\tau}_1}^2 + U_{\tilde{\tau}22}^2 \delta m_{\tilde{\tau}_2}^2 + 2U_{\tilde{\tau}12} U_{\tilde{\tau}22} \delta Y_{\tilde{\tau}} \\ &\quad - 2m_{\tau} \delta m_{\tau} + \delta s_W^2 c_{2\beta} M_Z^2 + s_W^2 \delta c_{2\beta} M_Z^2 + s_W^2 c_{2\beta} \delta M_Z^2, \end{aligned} \quad (4.67b)$$

$$\begin{aligned} \delta A_{\tau} &= \frac{1}{m_{\tau} U_{\tilde{\tau}11}} \left[-U_{\tilde{\tau}12} \delta m_{\tilde{\tau}_2}^2 + U_{\tilde{\tau}22} \delta Y_{\tilde{\tau}} - (U_{\tilde{\tau}11} (A_{\tau} - \mu t_{\beta}) - 2U_{\tilde{\tau}12} m_{\tau}) \delta m_{\tau} \right. \\ &\quad \left. + U_{\tilde{\tau}12} \delta m_{\tilde{\nu}}^2 - U_{\tilde{\tau}12} c_{2\beta} \delta M_W^2 \right. \\ &\quad \left. + \left(4U_{\tilde{\tau}12} M_W^2 \frac{t_{\beta}}{(1+t_{\beta}^2)} + U_{\tilde{\tau}11} m_{\tau} \mu \right) \delta t_{\beta} + U_{\tilde{\tau}11} m_{\tau} t_{\beta} \delta \mu. \right. \end{aligned} \quad (4.67c)$$

However, the OS renormalization scheme in the bottom/sbottom sector is numerically unreliable. Since δA_b gets the contribution

$$\delta A_b = \frac{1}{m_b} [-(A_b - \mu \tan \beta) \delta m_b + \dots] \quad (4.68)$$

the OS renormalization scheme becomes unstable for large $\tan \beta$. In the parameter region where $\mu \tan \beta \gg A_b$, counterterm contributions receive a large finite shift through δA_b invalidating the perturbative expansion. In the top/stop sector this is not an issue where $\mu \tan \beta$ is replaced by $\mu \cot \beta$, which is strongly suppressed for large values of $\tan \beta$. According to [51, 53] this problem can be avoided by changing the renormalization scheme in the bottom/sbottom sector. We choose to renormalize m_b and A_b in the $\overline{\text{DR}}$ scheme. The problem is then not present anymore, since by definition, $\delta m_b^{\overline{\text{DR}}}$ and consequently $\delta A_b^{\overline{\text{DR}}}$ do not lead to finite contributions. The bottom-squark mass renormalization constant in the $\overline{\text{DR}}$ scheme is then given by

$$\begin{aligned} \delta m_b^{\overline{\text{DR}}} &= \frac{1}{2} \left(m_b \left(\widetilde{\text{Re}} [\Sigma_b^L (m_b^2)]^{\text{div}} + \widetilde{\text{Re}} [\Sigma_b^R (m_b^2)]^{\text{div}} \right) \right. \\ &\quad \left. + \widetilde{\text{Re}} [\Sigma_b^{SL} (m_b^2)]^{\text{div}} + \widetilde{\text{Re}} [\Sigma_b^{SR} (m_b^2)]^{\text{div}} \right). \end{aligned} \quad (4.69)$$

For the bottom trilinear coupling the renormalization constant in the $\overline{\text{DR}}$ scheme is obtained by taking the divergent parts of all renormalization constants appearing in (4.66e),

$$\begin{aligned} \delta A_b^{\overline{\text{DR}}} &= \frac{1}{m_b U_{\tilde{b}11}} \left[-U_{\tilde{b}12} \delta m_{b_2}^2 |_{\text{div}} + U_{\tilde{b}22} \delta Y_{\tilde{b}} |_{\text{div}} - (U_{\tilde{b}11} (A_b - \mu t_{\beta}) - 2U_{\tilde{b}12} m_b) \delta m_b |_{\text{div}} \right. \\ &\quad \left. + U_{\tilde{b}12} (U_{\tilde{t}11}^2 \delta m_{\tilde{t}_1}^2 |_{\text{div}} + U_{\tilde{t}12}^2 \delta m_{\tilde{t}_2}^2 |_{\text{div}} + U_{\tilde{t}11} U_{\tilde{t}21} \delta Y_{\tilde{t}} |_{\text{div}}) - 2U_{\tilde{b}12} m_t \delta m_t |_{\text{div}} \right. \\ &\quad \left. - U_{\tilde{b}12} c_{2\beta} \delta M_W^2 |_{\text{div}} + \left(4U_{\tilde{b}12} M_W^2 \frac{t_{\beta}}{(1+t_{\beta}^2)} + U_{\tilde{b}11} m_b \mu \right) \delta t_{\beta} \right. \\ &\quad \left. + U_{\tilde{b}11} m_b t_{\beta} \delta \mu |_{\text{div}}. \right. \end{aligned} \quad (4.70)$$

Using (4.60b) to replace $\delta Y_{\tilde{b}}$ with δA_b in (4.65) yields the dependent bottom-squark mass in terms of the $\overline{\text{DR}}$ renormalized parameters,

$$\begin{aligned} \delta m_{\tilde{b}_1}^2 = & \frac{1}{U_{\tilde{b}_{11}}^2} \left[(1 - 2U_{\tilde{b}_{12}}^2) (U_{\tilde{t}_{11}}^2 \delta m_{\tilde{t}_1}^2 + U_{\tilde{t}_{21}}^2 \delta m_{\tilde{t}_2}^2 + 2U_{\tilde{t}_{11}} U_{\tilde{t}_{21}} \delta Y_{\tilde{t}} \right. \\ & - 2m_t \delta m_t - c_{2\beta} \delta M_W^2 - M_W^2 \delta c_{2\beta}) + U_{\tilde{b}_{12}}^2 \delta m_{\tilde{b}_2}^2 \\ & + 2U_{\tilde{b}_{11}} U_{\tilde{b}_{12}} m_b (\delta A_b - \delta \mu t_\beta - \mu \delta t_\beta) \\ & \left. + \delta m_b (2U_{\tilde{b}_{11}} U_{\tilde{b}_{12}} (A_b - \mu t_\beta) + 2(1 - 2U_{\tilde{b}_{12}}^2) m_b) \right]. \end{aligned} \quad (4.71)$$

The relation between the tree-level mass and the on-shell mass of the dependent bottom squark \tilde{b}_1 is given by

$$(\delta m_{\tilde{b}_1}^{\text{OS}})^2 = m_{\tilde{b}_1}^2 + \delta m_{\tilde{b}_1}^2 - \widetilde{\text{Re}} \Sigma_{\tilde{b}_1 \tilde{b}_1} (m_{\tilde{b}_1}^2). \quad (4.72)$$

In processes with external \tilde{b}_1 bottom squarks its on-shell mass is used in the computation of the decay widths. However, in order not to spoil UV-finiteness, the on-shell mass cannot be used everywhere in the calculation. This will be addressed in Section 4.3.

As in the b/\tilde{b} sector the τ mass m_τ and its corresponding trilinear coupling A_τ are renormalized in the $\overline{\text{DR}}$ scheme. Analogously the renormalization constants read

$$\begin{aligned} \delta m_\tau^{\overline{\text{DR}}} = & \frac{1}{2} \left(m_\tau \left(\widetilde{\text{Re}} [\Sigma_\tau^L (m_\tau^2)]^{\text{div}} + \widetilde{\text{Re}} [\Sigma_\tau^R (m_\tau^2)]^{\text{div}} \right) \right. \\ & \left. + \widetilde{\text{Re}} [\Sigma_\tau^{SL} (m_\tau^2)]^{\text{div}} + \widetilde{\text{Re}} [\Sigma_\tau^{SR} (m_\tau^2)]^{\text{div}} \right), \end{aligned} \quad (4.73a)$$

$$\begin{aligned} \delta A_\tau^{\overline{\text{DR}}} = & \frac{1}{m_\tau U_{\tilde{\tau}_{11}}} \left[-U_{\tilde{\tau}_{12}} \delta m_{\tau_2}^2 |_{\text{div}} + U_{\tilde{\tau}_{22}} \delta Y_{\tilde{\tau}} |_{\text{div}} - (U_{\tilde{\tau}_{11}} (A_\tau - \mu t_\beta) - 2U_{\tilde{\tau}_{12}} m_\tau) \delta m_\tau |_{\text{div}} \right. \\ & + U_{\tilde{\tau}_{12}} \delta m_\nu^2 |_{\text{div}} - U_{\tilde{\tau}_{12}} c_{2\beta} \delta M_W^2 |_{\text{div}} + \left(4U_{\tilde{\tau}_{12}} M_W^2 \frac{t_\beta}{(1+t_\beta^2)} + U_{\tilde{\tau}_{11}} m_\tau \mu \right) \delta t_\beta \\ & \left. + U_{\tilde{\tau}_{11}} m_\tau t_\beta \delta \mu |_{\text{div}}, \right] \end{aligned} \quad (4.73b)$$

$$\begin{aligned} \delta m_{\tilde{\tau}_1}^2 = & \frac{1}{U_{\tilde{\tau}_{11}}^2} \left[(1 - 2U_{\tilde{\tau}_{12}}^2) (\delta m_\nu^2 - c_{2\beta} \delta M_W^2 - M_W^2 \delta c_{2\beta}) + U_{\tilde{\tau}_{12}}^2 \delta m_{\tilde{\tau}_2}^2 \right. \\ & + 2U_{\tilde{\tau}_{11}} U_{\tilde{\tau}_{12}} m_\tau (\delta A_\tau - \delta \mu t_\beta - \mu \delta t_\beta) \\ & \left. + \delta m_\tau (2U_{\tilde{\tau}_{11}} U_{\tilde{\tau}_{12}} (A_\tau - \mu t_\beta) + 2(1 - 2U_{\tilde{\tau}_{12}}^2) m_\tau) \right]. \end{aligned} \quad (4.73c)$$

The relation between the tree-level mass and the on-shell mass of the dependent stau $\tilde{\tau}_1$ is given by

$$(\delta m_{\tilde{\tau}_1}^{\text{OS}})^2 = m_{\tilde{\tau}_1}^2 + \delta m_{\tilde{\tau}_1}^2 - \widetilde{\text{Re}} \Sigma_{\tilde{\tau}_1 \tilde{\tau}_1} (m_{\tilde{\tau}_1}^2). \quad (4.74)$$

Chargino sector

For the renormalization of the chargino and neutralino sector we rely on [54]. The bilinear terms of the chargino Lagrangian in terms of the mass eigenstates are given by,

$$\mathcal{L}_{\chi^\pm} = \overline{\tilde{\chi}_i^\pm} \left[\not{p} \delta_{ij} - P_L (U^* \mathcal{M}_{\chi^\pm} V^\dagger)_{ij} - P_R (V \mathcal{M}_{\chi^\pm}^\dagger U^T)_{ij} \right] \tilde{\chi}_j^\pm. \quad (4.75)$$

The free parameters of the chargino sector are μ and M_2 . Their renormalization transformations are given by

$$\mu \rightarrow \mu + \delta\mu, \quad M_2 \rightarrow M_2 + \delta M_2. \quad (4.76)$$

This implies for the chargino mass matrix:

$$\mathcal{M}_{\tilde{\chi}^\pm} \rightarrow \mathcal{M}_{\tilde{\chi}^\pm} + \delta\mathcal{M}_{\tilde{\chi}^\pm}, \quad (4.77a)$$

$$\delta\mathcal{M}_{\tilde{\chi}^\pm} = \begin{pmatrix} \delta M_2 & \sqrt{2}\delta(M_W s_\beta) \\ \sqrt{2}\delta(M_W c_\beta) & \delta\mu \end{pmatrix}, \quad (4.77b)$$

$$\delta(M_W s_\beta) = s_\beta \delta M_W + M_W \delta s_\beta, \quad \delta(M_W c_\beta) = c_\beta \delta M_W + M_W \delta c_\beta. \quad (4.77c)$$

The chargino fields in the mass eigenstates are renormalized according to

$$P_L \tilde{\chi}_i^+ \rightarrow \left(\delta_{ij} + \frac{1}{2} [\delta \mathcal{Z}_{\tilde{\chi}^\pm}^L]_{ij} \right) P_L \tilde{\chi}_j^+, \quad (4.78a)$$

$$P_L \tilde{\chi}_i^- \rightarrow \left(\delta_{ij} + \frac{1}{2} [\delta \mathcal{Z}_{\tilde{\chi}^\pm}^R]_{ij}^* \right) P_L \tilde{\chi}_j^-, \quad (4.78b)$$

$$P_R \tilde{\chi}_i^+ \rightarrow \left(\delta_{ij} + \frac{1}{2} [\delta \mathcal{Z}_{\tilde{\chi}^\pm}^R]_{ij} \right) P_R \tilde{\chi}_j^+, \quad (4.78c)$$

$$P_R \tilde{\chi}_i^- \rightarrow \left(\delta_{ij} + \frac{1}{2} [\delta \mathcal{Z}_{\tilde{\chi}^\pm}^L]_{ij}^* \right) P_R \tilde{\chi}_j^-. \quad (4.78d)$$

For the diagonal chargino mass matrix we get

$$\mathcal{D}_{\tilde{\chi}^\pm} \rightarrow \mathcal{D}_{\tilde{\chi}^\pm} + \delta\mathcal{D}_{\tilde{\chi}^\pm} = \mathcal{D}_{\tilde{\chi}^\pm} + U^* \delta\mathcal{M}_{\tilde{\chi}^\pm} V^\dagger, \quad (4.79)$$

which relates the chargino mass parameters renormalization constants $\delta\mu$ and δM_2 to the diagonal terms of $(\delta\mathcal{D}_{\tilde{\chi}^\pm})_{ii} \equiv \delta m_{\tilde{\chi}_i^\pm}$,

$$\begin{aligned} \delta\mu = \frac{1}{\Delta} \left[U_{11} V_{11} \delta m_{\tilde{\chi}_2^\pm} - U_{21} V_{21} \delta m_{\tilde{\chi}_1^\pm} + \sqrt{2} U_{11} U_{21} (V_{12} V_{21} - V_{11} V_{22}) \delta(M_W s_\beta) \right. \\ \left. + \sqrt{2} V_{11} V_{21} (U_{12} U_{21} - U_{11} U_{22}) \delta(M_W c_\beta) \right], \end{aligned} \quad (4.80a)$$

$$\begin{aligned} \delta M_2 = \frac{1}{\Delta} \left[U_{22} V_{22} \delta m_{\tilde{\chi}_1^\pm} - U_{12} V_{12} \delta m_{\tilde{\chi}_2^\pm} + \sqrt{2} U_{12} U_{22} (V_{12} V_{21} - V_{11} V_{22}) \delta(M_W c_\beta) \right. \\ \left. + \sqrt{2} V_{12} V_{22} (U_{12} U_{21} - U_{11} U_{22}) \delta(M_W s_\beta) \right], \end{aligned} \quad (4.80b)$$

$$\Delta = U_{11} U_{22} V_{11} V_{22} - U_{12} U_{21} V_{12} V_{21}. \quad (4.80c)$$

With these transformation rules the following counterterm Lagrangian is obtained,

$$\begin{aligned} \mathcal{L}_{\tilde{\chi}^\pm}^{\text{CT}} = \overline{\tilde{\chi}_i^\pm} \left[\frac{1}{2} \not{p} \left([\delta \mathcal{Z}_{\tilde{\chi}^\pm}^L + \delta \mathcal{Z}_{\tilde{\chi}^\pm}^{L\dagger}] P_L + [\delta \mathcal{Z}_{\tilde{\chi}^\pm}^R + \delta \mathcal{Z}_{\tilde{\chi}^\pm}^{RT}] P_R \right) \right. \\ \left. - \left(\frac{1}{2} \mathcal{D}_{\tilde{\chi}^\pm} \delta \mathcal{Z}_{\tilde{\chi}^\pm}^L + \frac{1}{2} \delta \mathcal{Z}_{\tilde{\chi}^\pm}^{RT} \mathcal{D}_{\tilde{\chi}^\pm} + \delta \mathcal{D}_{\tilde{\chi}^\pm} \right) P_L \right. \\ \left. - \left(\frac{1}{2} \mathcal{D}_{\tilde{\chi}^\pm} \delta \mathcal{Z}_{\tilde{\chi}^\pm}^{R*} + \frac{1}{2} \delta \mathcal{Z}_{\tilde{\chi}^\pm}^{L\dagger} \mathcal{D}_{\tilde{\chi}^\pm} + \delta \mathcal{D}_{\tilde{\chi}^\pm}^\dagger \right) P_R \right]_{ij} \tilde{\chi}_j^\pm. \end{aligned} \quad (4.81)$$

Taking the derivative with respect to the fields $\overline{\tilde{\chi}_i^+}$ and $\tilde{\chi}_j^+$ yields the renormalized self-energies,

$$\hat{\Sigma}_{\tilde{\chi}_i^+ \tilde{\chi}_j^-}^L(p^2) = \Sigma_{\tilde{\chi}_i^+ \tilde{\chi}_j^-}^L(p^2) + \frac{1}{2} \left[\delta \mathcal{Z}_{\tilde{\chi}^\pm}^L + \delta \mathcal{Z}_{\tilde{\chi}^\pm}^{L\dagger} \right]_{ij}, \quad (4.82a)$$

$$\hat{\Sigma}_{\tilde{\chi}_i^+ \tilde{\chi}_j^-}^R(p^2) = \Sigma_{\tilde{\chi}_i^+ \tilde{\chi}_j^-}^R(p^2) + \frac{1}{2} \left[\delta \mathcal{Z}_{\tilde{\chi}^\pm}^{R*} + \delta \mathcal{Z}_{\tilde{\chi}^\pm}^{RT} \right]_{ij}, \quad (4.82b)$$

$$\hat{\Sigma}_{\tilde{\chi}_i^\pm \tilde{\chi}_j^\pm}^{SL}(p^2) = \Sigma_{\tilde{\chi}_i^\pm \tilde{\chi}_j^\pm}^{SL}(p^2) - \left[\frac{1}{2} \mathcal{D}_{\tilde{\chi}^\pm} \delta \mathcal{Z}_{\tilde{\chi}^\pm}^L + \frac{1}{2} \delta \mathcal{Z}_{\tilde{\chi}^\pm}^{RT} \mathcal{D}_{\tilde{\chi}^\pm} + \delta \mathcal{D}_{\tilde{\chi}^\pm} \right]_{ij}, \quad (4.82c)$$

$$\hat{\Sigma}_{\tilde{\chi}_i^\pm \tilde{\chi}_j^\pm}^{SR}(p^2) = \Sigma_{\tilde{\chi}_i^\pm \tilde{\chi}_j^\pm}^{SR}(p^2) - \left[\frac{1}{2} \mathcal{D}_{\tilde{\chi}^\pm} \delta \mathcal{Z}_{\tilde{\chi}^\pm}^{R*} + \frac{1}{2} \delta \mathcal{Z}_{\tilde{\chi}^\pm}^{L\dagger} \mathcal{D}_{\tilde{\chi}^\pm} + \delta \mathcal{D}_{\tilde{\chi}^\pm}^\dagger \right]_{ij}, \quad (4.82d)$$

where the self-energy is decomposed into the respective Lorentz covariant parts according to (4.37). The chargino sector consists of two free parameters μ and M_2 . They are fixed by OS renormalization conditions for the diagonal renormalized self energies ($i = j$ in (4.83)). The other renormalization conditions fix the field renormalization factors $\left[\delta \mathcal{Z}_{\tilde{\chi}^\pm}^{L/R} \right]_{ij}$,

$$m_{\tilde{\chi}_j^\pm} \widetilde{\text{Re}} \hat{\Sigma}_{\tilde{\chi}_i^+ \tilde{\chi}_j^-}^R(m_{\tilde{\chi}_j^\pm}^2) + \widetilde{\text{Re}} \hat{\Sigma}_{\tilde{\chi}_i^+ \tilde{\chi}_j^-}^{SL}(m_{\tilde{\chi}_j^\pm}^2) = 0, \quad (4.83a)$$

$$m_{\tilde{\chi}_j^\pm} \widetilde{\text{Re}} \hat{\Sigma}_{\tilde{\chi}_i^+ \tilde{\chi}_j^-}^L(m_{\tilde{\chi}_j^\pm}^2) + \widetilde{\text{Re}} \hat{\Sigma}_{\tilde{\chi}_i^+ \tilde{\chi}_j^-}^{SR}(m_{\tilde{\chi}_j^\pm}^2) = 0, \quad (4.83b)$$

$$\begin{aligned} & \widetilde{\text{Re}} \hat{\Sigma}_{\tilde{\chi}_i^+ \tilde{\chi}_i^-}^L(m_{\tilde{\chi}_i^\pm}^2) + 2m_{\tilde{\chi}_i^\pm} \widetilde{\text{Re}} \hat{\Sigma}_{\tilde{\chi}_i^+ \tilde{\chi}_i^-}^{SL'}(m_{\tilde{\chi}_i^\pm}^2) \\ & + m_{\tilde{\chi}_i^\pm}^2 \left(\widetilde{\text{Re}} \hat{\Sigma}_{\tilde{\chi}_i^+ \tilde{\chi}_i^-}^{L'}(m_{\tilde{\chi}_i^\pm}^2) + \widetilde{\text{Re}} \hat{\Sigma}_{\tilde{\chi}_i^+ \tilde{\chi}_i^-}^{R'}(m_{\tilde{\chi}_i^\pm}^2) \right) = 0. \end{aligned} \quad (4.83c)$$

Inserting the self-energies (4.82) into the renormalization conditions (4.83) yields the renormalization constants for chargino masses

$$\text{Re } \delta m_{\tilde{\chi}_i^\pm} = \frac{1}{2} m_{\tilde{\chi}_i^\pm} \left[\widetilde{\text{Re}} \hat{\Sigma}_{\tilde{\chi}_i^+ \tilde{\chi}_i^-}^L(m_{\tilde{\chi}_i^\pm}^2) + \widetilde{\text{Re}} \hat{\Sigma}_{\tilde{\chi}_i^+ \tilde{\chi}_i^-}^R(m_{\tilde{\chi}_i^\pm}^2) \right] + \widetilde{\text{Re}} \hat{\Sigma}_{\tilde{\chi}_i^+ \tilde{\chi}_i^-}^{SL}(m_{\tilde{\chi}_i^\pm}^2), \quad (4.84a)$$

diagonal field renormalization constants

$$\begin{aligned} \left[\delta \mathcal{Z}_{\tilde{\chi}^\pm}^{L/R} \right]_{ii} &= -\widetilde{\text{Re}} \hat{\Sigma}_{\tilde{\chi}_i^+ \tilde{\chi}_i^-}^{L/R}(m_{\tilde{\chi}_i^\pm}^2) - m_{\tilde{\chi}_i^\pm}^2 \left[\widetilde{\text{Re}} \hat{\Sigma}_{\tilde{\chi}_i^+ \tilde{\chi}_i^-}^{L'}(m_{\tilde{\chi}_i^\pm}^2) + \widetilde{\text{Re}} \hat{\Sigma}_{\tilde{\chi}_i^+ \tilde{\chi}_i^-}^{R'}(m_{\tilde{\chi}_i^\pm}^2) \right] \\ &\quad - 2m_{\tilde{\chi}_i^\pm} \widetilde{\text{Re}} \hat{\Sigma}_{\tilde{\chi}_i^+ \tilde{\chi}_i^-}^{SL'}(m_{\tilde{\chi}_i^\pm}^2), \end{aligned} \quad (4.84b)$$

and off-diagonal field renormalization constants

$$\begin{aligned}
[\delta \mathcal{Z}_{\tilde{\chi}^\pm}^L]_{ij} &= \frac{2}{m_{\tilde{\chi}_i^\pm}^2 - m_{\tilde{\chi}_j^\pm}^2} \left[m_{\tilde{\chi}_j^\pm}^2 \widetilde{\text{Re}}\Sigma_{\tilde{\chi}_i^\pm \tilde{\chi}_j^\pm}^L(m_{\tilde{\chi}_j^\pm}^2) + m_{\tilde{\chi}_i^\pm} m_{\tilde{\chi}_j^\pm} \widetilde{\text{Re}}\Sigma_{\tilde{\chi}_i^\pm \tilde{\chi}_j^\pm}^R(m_{\tilde{\chi}_j^\pm}^2) \right. \\
&\quad + m_{\tilde{\chi}_i^\pm} \widetilde{\text{Re}}\Sigma_{\tilde{\chi}_i^\pm \tilde{\chi}_j^\pm}^{SL}(m_{\tilde{\chi}_j^\pm}^2) + m_{\tilde{\chi}_j^\pm} \widetilde{\text{Re}}\Sigma_{\tilde{\chi}_i^\pm \tilde{\chi}_j^\pm}^{SR}(m_{\tilde{\chi}_j^\pm}^2) \\
&\quad \left. - m_{\tilde{\chi}_i^\pm} [\delta \mathcal{D}_{\tilde{\chi}^\pm}]_{ij} - m_{\tilde{\chi}_j^\pm} [\delta \mathcal{D}_{\tilde{\chi}^\pm}^\dagger]_{ij} \right], \tag{4.84c}
\end{aligned}$$

$$\begin{aligned}
[\delta \mathcal{Z}_{\tilde{\chi}^\pm}^R]_{ij} &= \frac{2}{m_{\tilde{\chi}_i^\pm}^2 - m_{\tilde{\chi}_j^\pm}^2} \left[m_{\tilde{\chi}_j^\pm}^2 \widetilde{\text{Re}}\Sigma_{\tilde{\chi}_i^\pm \tilde{\chi}_j^\pm}^R(m_{\tilde{\chi}_j^\pm}^2) + m_{\tilde{\chi}_i^\pm} m_{\tilde{\chi}_j^\pm} \widetilde{\text{Re}}\Sigma_{\tilde{\chi}_i^\pm \tilde{\chi}_j^\pm}^L(m_{\tilde{\chi}_j^\pm}^2) \right. \\
&\quad + m_{\tilde{\chi}_i^\pm} \widetilde{\text{Re}}\Sigma_{\tilde{\chi}_i^\pm \tilde{\chi}_j^\pm}^{SR}(m_{\tilde{\chi}_j^\pm}^2) + m_{\tilde{\chi}_j^\pm} \widetilde{\text{Re}}\Sigma_{\tilde{\chi}_i^\pm \tilde{\chi}_j^\pm}^{SL}(m_{\tilde{\chi}_j^\pm}^2) \\
&\quad \left. - m_{\tilde{\chi}_i^\pm} [\delta \mathcal{D}_{\tilde{\chi}^\pm}^\dagger]_{ij} - m_{\tilde{\chi}_j^\pm} [\delta \mathcal{D}_{\tilde{\chi}^\pm}]_{ij} \right], \tag{4.84d}
\end{aligned}$$

where $i \neq j$. Inserting the mass renormalization constants $\delta m_{\tilde{\chi}_i^\pm}$ into (4.80) yields the renormalization constants for the parameters μ and M_2 .

Neutralino sector

Using the four-component Majorana spinors from (2.67) the bilinear terms for the neutralinos read

$$\mathcal{L}_{\tilde{\chi}^0} = \frac{1}{2} \overline{\tilde{\chi}_i^0} \left[\not{p} \delta_{ij} - P_L (N^* \mathcal{M}_{\tilde{\chi}^0} N^\dagger)_{ij} - P_R (N \mathcal{M}_{\tilde{\chi}^0}^\dagger N^T)_{ij} \right] \tilde{\chi}_j^0. \tag{4.85}$$

The left-over neutralino mass parameter is given by M_1 . It transforms under renormalization as

$$M_1 \rightarrow M_1 + \delta M_1. \tag{4.86}$$

Together with the renormalization transformations of the parameters in the chargino sector (4.76), the renormalization of the neutralino mass matrix reads

$$\mathcal{M}_{\tilde{\chi}^0} \rightarrow \mathcal{M}_{\tilde{\chi}^0} + \delta \mathcal{M}_{\tilde{\chi}^0}, \tag{4.87}$$

$$\delta \mathcal{M}_{\tilde{\chi}^0} = \begin{pmatrix} \delta M_1 & 0 & -\delta (M_Z s_W c_\beta) & \delta (M_Z s_W s_\beta) \\ 0 & \delta M_2 & \delta (M_Z c_W c_\beta) & -\delta (M_Z c_W s_\beta) \\ -\delta (M_Z s_W c_\beta) & \delta (M_Z c_W c_\beta) & 0 & -\delta \mu \\ \delta (M_Z s_W s_\beta) & -\delta (M_Z c_W s_\beta) & -\delta \mu & 0 \end{pmatrix}. \tag{4.88}$$

For the diagonal neutralino mass matrix $\mathcal{D}_{\tilde{\chi}^0}$ this implies

$$\mathcal{D}_{\tilde{\chi}^0} \rightarrow \mathcal{D}_{\tilde{\chi}^0} + \delta \mathcal{D}_{\tilde{\chi}^0} = \mathcal{D}_{\tilde{\chi}^0} + N^* \delta \mathcal{M}_{\tilde{\chi}^0} N^\dagger. \tag{4.89}$$

Combining (4.87) and (4.89) yields the renormalization constant in terms of the renormalization constants of the electroweak, Higgs, and chargino sector,

$$\delta M_1 = \frac{1}{N_{11}^2} \left[\delta m_{\tilde{\chi}_1^0} - N_{12}^2 \delta M_2 + 2N_{13}N_{14} \delta \mu + 2N_{11}N_{13} \delta (M_Z s_W c_\beta) - 2N_{11}N_{14} \delta (M_Z s_W s_\beta) - 2N_{12}N_{13} \delta (M_Z c_W c_\beta) + 2N_{12}N_{14} \delta (M_Z c_W s_\beta) \right], \quad (4.90)$$

with $\delta m_{\tilde{\chi}_1^0} \equiv (\delta \mathcal{D}_{\tilde{\chi}^0})_{11}$. The neutralino fields transform as

$$P_L \tilde{\chi}_i^0 \rightarrow \left(\delta_{ij} + \frac{1}{2} [\delta \mathcal{Z}_{\tilde{\chi}^0}]_{ij} \right) P_L \tilde{\chi}_j^0, \quad (4.91a)$$

$$P_R \tilde{\chi}_i^0 \rightarrow \left(\delta_{ij} + \frac{1}{2} [\delta \mathcal{Z}_{\tilde{\chi}^0}^*]_{ij} \right) P_R \tilde{\chi}_j^0, \quad (4.91b)$$

yielding the counterterm Lagrangian of (4.85),

$$\begin{aligned} \mathcal{L}_{\tilde{\chi}^0}^{\text{CT}} = & \frac{1}{2} \overline{\tilde{\chi}_i^0} \left[\frac{1}{2} \not{p} \left([\delta \mathcal{Z}_{\tilde{\chi}^0} + \delta \mathcal{Z}_{\tilde{\chi}^0}^\dagger] P_L + [\delta \mathcal{Z}_{\tilde{\chi}^0}^* + \delta \mathcal{Z}_{\tilde{\chi}^0}^T] P_R \right) \right. \\ & - \left(\frac{1}{2} \mathcal{D}_{\tilde{\chi}^0} \delta \mathcal{Z}_{\tilde{\chi}^0} + \frac{1}{2} \delta \mathcal{Z}_{\tilde{\chi}^0}^T \mathcal{D}_{\tilde{\chi}^0} + \delta \mathcal{D}_{\tilde{\chi}^0} \right) P_L \\ & \left. - \left(\frac{1}{2} \mathcal{D}_{\tilde{\chi}^0} \delta \mathcal{Z}_{\tilde{\chi}^0}^* + \frac{1}{2} \delta \mathcal{Z}_{\tilde{\chi}^0}^\dagger \mathcal{D}_{\tilde{\chi}^0} + \delta \mathcal{D}_{\tilde{\chi}^0}^\dagger \right) P_L \right]_{ij} \tilde{\chi}_j^0. \end{aligned} \quad (4.92)$$

Hence, in terms of the Lorentz covariant decomposition (4.37) the renormalized neutralino self energies are given by

$$\hat{\Sigma}_{\tilde{\chi}_i^0 \tilde{\chi}_j^0}^L(p^2) = \Sigma_{\tilde{\chi}_i^0 \tilde{\chi}_j^0}^L(p^2) + \frac{1}{2} [\delta \mathcal{Z}_{\tilde{\chi}^0} + \delta \mathcal{Z}_{\tilde{\chi}^0}^\dagger]_{ij}, \quad (4.93a)$$

$$\hat{\Sigma}_{\tilde{\chi}_i^0 \tilde{\chi}_j^0}^R(p^2) = \Sigma_{\tilde{\chi}_i^0 \tilde{\chi}_j^0}^R(p^2) + \frac{1}{2} [\delta \mathcal{Z}_{\tilde{\chi}^0}^* + \delta \mathcal{Z}_{\tilde{\chi}^0}^T]_{ij}, \quad (4.93b)$$

$$\hat{\Sigma}_{\tilde{\chi}_i^0 \tilde{\chi}_j^0}^{SL}(p^2) = \Sigma_{\tilde{\chi}_i^0 \tilde{\chi}_j^0}^{SL}(p^2) - \left[\frac{1}{2} \mathcal{D}_{\tilde{\chi}^0} \delta \mathcal{Z}_{\tilde{\chi}^0} + \frac{1}{2} \delta \mathcal{Z}_{\tilde{\chi}^0}^T \mathcal{D}_{\tilde{\chi}^0} + \delta \mathcal{D}_{\tilde{\chi}^0} \right]_{ij}, \quad (4.93c)$$

$$\hat{\Sigma}_{\tilde{\chi}_i^0 \tilde{\chi}_j^0}^{SR}(p^2) = \Sigma_{\tilde{\chi}_i^0 \tilde{\chi}_j^0}^{SR}(p^2) - \left[\frac{1}{2} \mathcal{D}_{\tilde{\chi}^0} \delta \mathcal{Z}_{\tilde{\chi}^0}^* + \frac{1}{2} \delta \mathcal{Z}_{\tilde{\chi}^0}^\dagger \mathcal{D}_{\tilde{\chi}^0} + \delta \mathcal{D}_{\tilde{\chi}^0}^\dagger \right]_{ij}. \quad (4.93d)$$

The OS renormalization conditions in the neutralino sector read

$$m_{\tilde{\chi}_j^0} \widetilde{\text{Re}} \hat{\Sigma}_{\tilde{\chi}_i^0 \tilde{\chi}_j^0}^L(m_{\tilde{\chi}_j^0}^2) + \widetilde{\text{Re}} \hat{\Sigma}_{\tilde{\chi}_i^0 \tilde{\chi}_j^0}^{SL}(m_{\tilde{\chi}_j^0}^2) = 0, \quad \text{for } (i \neq j) \text{ and } (i = j = 1), \quad (4.94a)$$

$$\widetilde{\text{Re}} \hat{\Sigma}_{\tilde{\chi}_i^0 \tilde{\chi}_i^0}^L(m_{\tilde{\chi}_i^0}^2) + 2m_{\tilde{\chi}_i^0}^2 \widetilde{\text{Re}} \hat{\Sigma}_{\tilde{\chi}_i^0 \tilde{\chi}_i^0}^{L'}(m_{\tilde{\chi}_i^0}^2) + 2m_{\tilde{\chi}_i^0}^2 \widetilde{\text{Re}} \hat{\Sigma}_{\tilde{\chi}_i^0 \tilde{\chi}_j^0}^{SL'}(m_{\tilde{\chi}_i^0}^2) = 0, \quad (4.94b)$$

The only free parameter M_1 is fixed by the on-shell renormalization condition for the lightest neutralino mass $m_{\tilde{\chi}_1^0}$ (4.94a) ($i = j = 1$), whereas the other conditions fix the diagonal (4.94b) and non-diagonal (4.94a) ($i \neq j$) entries of $\delta \mathcal{Z}_{\tilde{\chi}^0}$. Hence, the renormalization

constants read,

$$\text{Re } \delta m_{\tilde{\chi}_1^0} = m_{\tilde{\chi}_1^0} \widetilde{\text{Re}} \Sigma_{\tilde{\chi}_1^0 \tilde{\chi}_1^0}^L (m_{\tilde{\chi}_1^0}^2) + \widetilde{\text{Re}} \Sigma_{\tilde{\chi}_1^0 \tilde{\chi}_1^0}^{SL} (m_{\tilde{\chi}_1^0}^2), \quad (4.95a)$$

$$[\delta \mathcal{Z}_{\tilde{\chi}^0}]_{ii} = -\widetilde{\text{Re}} \Sigma_{\tilde{\chi}_i^0 \tilde{\chi}_i^0}^L (m_{\tilde{\chi}_i^0}^2) - 2m_{\tilde{\chi}_i^0} \left[m_{\tilde{\chi}_i^0} \widetilde{\text{Re}} \Sigma_{\tilde{\chi}_i^0 \tilde{\chi}_i^0}^{L'} (m_{\tilde{\chi}_i^0}^2) + \widetilde{\text{Re}} \Sigma_{\tilde{\chi}_i^0 \tilde{\chi}_i^0}^{SL'} (m_{\tilde{\chi}_i^0}^2) \right], \quad (4.95b)$$

$$[\delta \mathcal{Z}_{\tilde{\chi}^0}]_{ij} = \frac{1}{m_{\tilde{\chi}_i^0}^2 - m_{\tilde{\chi}_j^0}^2} \left[2 \left(m_{\tilde{\chi}_j^0} \widetilde{\text{Re}} \Sigma_{\tilde{\chi}_i^0 \tilde{\chi}_j^0}^L (m_{\tilde{\chi}_j^0}^2) + \widetilde{\text{Re}} \Sigma_{\tilde{\chi}_i^0 \tilde{\chi}_j^0}^{SL} (m_{\tilde{\chi}_j^0}^2) - [\delta \mathcal{D}_{\tilde{\chi}^0}]_{ij} \right) \right]. \quad (4.95c)$$

With the mass renormalization constant of the lightest neutralino $\delta m_{\tilde{\chi}_1^0}$ from (4.95a) the neutralino mass-parameter renormalization constant (4.86) is obtained.

Since there is only one free parameter in the neutralino sector, the OS condition can be imposed for one neutralino only. In this work we choose the lightest neutralino $\tilde{\chi}_1^0$. The other neutralino masses $m_{\tilde{\chi}_{2,3,4}^0}$ get finite shifts to their on-shell values,

$$m_{\tilde{\chi}_i^0}^{\text{OS}} = m_{\tilde{\chi}_i^0} + \delta m_{\tilde{\chi}_i^0} - \left(m_{\tilde{\chi}_i^0} \widetilde{\text{Re}} \Sigma_{\tilde{\chi}_i^0 \tilde{\chi}_i^0}^L (m_{\tilde{\chi}_i^0}^2) + \widetilde{\text{Re}} \Sigma_{\tilde{\chi}_i^0 \tilde{\chi}_i^0}^{SL} (m_{\tilde{\chi}_i^0}^2) \right), \quad i = 2, 3, 4, \quad (4.96a)$$

$$\delta m_{\tilde{\chi}_i^0} = \delta \mathcal{D}_{ii}. \quad (4.96b)$$

In processes with external neutralinos, the on-shell masses are used. This will be described in more detail in Section 4.3.

Glino sector

The bilinear terms in the gluino Lagrangian are given by,

$$\mathcal{L}_{\tilde{g}} = \frac{1}{2} \bar{\Psi}_{\tilde{g}} (\not{p} - M_3) \Psi_{\tilde{g}}, \quad (4.97)$$

where $\Psi_{\tilde{g}} = (\tilde{g}, \bar{\tilde{g}})^T$ is the Majorana spinor built from the left-handed Weyl spinors \tilde{g} (2.69). By renormalizing the gluino mass-parameter and gluino field

$$M_3 \rightarrow M_3 + \delta M_3, \quad (4.98a)$$

$$\tilde{g} \rightarrow \left(1 + \frac{1}{2} \delta Z_{\tilde{g}} \right) \tilde{g}, \quad (4.98b)$$

the counterterm gluino Lagrangian (4.97) is obtained,

$$\mathcal{L}_{\tilde{g}}^{\text{CT}} = \bar{\Psi}_{\tilde{g}} \not{p} \delta Z_{\tilde{g}} \Psi_{\tilde{g}} - (M_3 \delta Z_{\tilde{g}} + \delta M_3) \bar{\Psi}_{\tilde{g}} \Psi_{\tilde{g}}. \quad (4.99)$$

Here we used that in the CP-conserving case, there is no difference between left- and right-handed renormalization constants, i.e. $\delta Z_{\tilde{g}}^* = \delta Z_{\tilde{g}}$ for Majorana spinors. Thus, the gluino self-energy can be decomposed into its Lorentz-covariant parts,

$$\Sigma_{\tilde{g}}(p^2) = \not{p} \Sigma_{\tilde{g}}(p^2) + M_3 \Sigma_{\tilde{g}}^S(p^2). \quad (4.100)$$

The coefficients of the renormalized self-energy are then obtained from Eq.(4.99),

$$\hat{\Sigma}_{\tilde{g}}^L(p^2) = \Sigma_{\tilde{g}}^L(p^2) + \delta Z_{\tilde{g}}, \quad \hat{\Sigma}_{\tilde{g}}^S(p^2) = \Sigma_{\tilde{g}}^S(p^2) - \delta Z_{\tilde{g}} - \frac{\delta M_3}{M_3}. \quad (4.101)$$

For the gluino mass M_3 and gluino field the OS conditions are imposed analogously to the quark case (c.f. (4.38)) yielding the renormalization constants

$$\delta M_3 = M_3 \widetilde{\text{Re}}\Sigma_{\tilde{g}}^L(M_3^2) + \widetilde{\text{Re}}\Sigma_{\tilde{g}}^{SL}(M_3^2), \quad (4.102a)$$

$$\delta Z_{\tilde{g}} = -\widetilde{\text{Re}}\Sigma_{\tilde{g}}^L(M_3^2) + 2M_3^2 \widetilde{\text{Re}}\Sigma_{\tilde{g}}^{L'}(M_3^2) + 2M_3^2 \widetilde{\text{Re}}\Sigma_{\tilde{g}}^{SL'}(M_3^2). \quad (4.102b)$$

Strong coupling constant

Neglecting the gauge fixing terms, the bilinear part of the gluon-field Lagrangian is given by

$$\mathcal{L}_G = -\frac{1}{2} G_\mu^a [p^2 g^{\mu\nu} - p^\mu p^\nu] G_\nu^a. \quad (4.103)$$

The renormalization transformations for the gluon field and strong coupling-constant read

$$G_\mu^a \rightarrow \left(1 + \frac{1}{2} \delta Z_G\right) G_\mu^a, \quad (4.104)$$

$$g_s \rightarrow (1 + \delta Z_{g_s}) g_s. \quad (4.105)$$

Since the strong coupling-constant g_s becomes large at small energy scales, OS renormalization at zero-momentum transfer is not well defined. Hence, the strong coupling constants are treated in the $\overline{\text{DR}}$ scheme. They are given by the gluonic self-energy and triple gluon vertex. In this scheme, δZ_G and δZ_{g_s} then read,

$$\delta Z_G = -\frac{\alpha_s}{4\pi} \beta_0 \Delta, \quad \delta Z_{g_s} = -\frac{\alpha_s}{4\pi} \frac{\beta_0}{2} \Delta, \quad (4.106)$$

$$\beta_0 = \left(\frac{11}{3}N - \frac{2}{3}n_f\right) + \left(-\frac{2}{3}N - \frac{1}{3}(n_f + 1) - \frac{2}{3}\right) = 3, \quad (4.107)$$

with $N = 3$ and $n_f = 5$. β_0 is the one-loop coefficient of the running coupling $\alpha_s(\mu) = g_s^2(\mu)/4\pi$. In the following computations, the strong coupling will be evaluated at the mass scale of the decaying squarks and gluinos. The β_0 coefficient therefore receives contributions from light quarks and gluons as well as from top quarks, squarks, and gluinos.

Since at scales comparable to the masses of heavy particles, their contribution to the strong coupling have to be taken into account. The value of α_s at the Z mass scale M_Z including contributions from squarks and gluinos is given by [55],

$$\alpha_s^{\overline{\text{DR}}}(M_Z) = \frac{\alpha_s^{\overline{\text{MS}}}(M_Z)}{1 - \Delta\alpha_s}, \quad (4.108)$$

$$\Delta\alpha_s = \frac{\alpha_s^{\overline{\text{MS}}}(M_Z)}{2\pi} \left[\frac{1}{2} - \frac{2}{3} \log \frac{m_t}{M_Z} - 2 \log \frac{m_{\tilde{g}}}{M_Z} - \frac{1}{6} \sum_{\tilde{q}} \sum_{i=1}^2 \log \frac{m_{\tilde{q}_i}}{M_Z} \right], \quad (4.109)$$

where the first sum runs over the six different squark species \tilde{q} and the second sum over the two mass eigenstate i . The value of $\alpha_s^{\overline{\text{DR}}}$ at a given scale μ is then given by

$$\alpha_s^{\overline{\text{DR}}}(\mu) = \frac{\alpha_s^{\overline{\text{DR}}}(M_Z)}{1 - \frac{3}{4\pi}\alpha_s^{\overline{\text{DR}}}(M_Z)\log\frac{M_Z^2}{\mu^2}}. \quad (4.110)$$

4.1.4 Resummation in the b / \tilde{b} sector

Following [51], at tree-level, the mass of the bottom quark is given by its Yukawa coupling to the down-type Higgs field $\lambda_b h_d b \bar{b}$ via the relation $m_b = \lambda_b v_d$. Through higher-order corrections, the bottom quark couples to the up-type Higgs field $\Delta\lambda_b h_u b \bar{b}$ altering the relation between the corresponding Yukawa coupling and mass to

$$m_b = \lambda_b v_d \rightarrow m_b = v_d (\lambda_b + \Delta\lambda_b \tan\beta) = \lambda_b v_d (1 + \Delta m_b). \quad (4.111)$$

An explicit calculation of the gluino-sbottom and higgsino-stop loop yields

$$\Delta m_b = \frac{2\alpha_s}{3\pi} M_3 \mu \tan\beta I(m_{\tilde{b}_1}, m_{\tilde{b}_2}, M_3) + \frac{\lambda_t^2}{16\pi^2} \mu A_t \tan\beta I(m_{\tilde{t}_1}, m_{\tilde{t}_2}, \mu), \quad (4.112)$$

which depends on the gluino mass-parameter M_3 , the higgsino mass-parameter μ , the ratio of the Higgs vevs $\tan\beta$, the sbottom masses $m_{\tilde{b}_{1,2}}$, the trilinear coupling A_t and the stop masses $m_{\tilde{t}_{1,2}}$. The loop function $I(a, b, c)$ is given by

$$I(a, b, c) = \frac{1}{(a^2 - b^2)(b^2 - c^2)(a^2 - c^2)} \left[a^2 b^2 \log \frac{a^2}{b^2} + b^2 c^2 \log \frac{b^2}{c^2} + c^2 a^2 \log \frac{c^2}{a^2} \right]. \quad (4.113)$$

These contributions are enhanced by $\tan\beta$ and can change the tree-level relation significantly. As shown in [51], the leading $\tan\beta$ -enhanced terms can be resummed by using an effective bottom Yukawa coupling. Following [51] we use a $\overline{\text{DR}}$ definition of the bottom quark mass. The effective Yukawa coupling is then defined as

$$\lambda_b^{\text{eff}} = \frac{1}{v_d} \frac{m_b^{\overline{\text{DR}}}(\mu_R) + m_b \Delta m_b}{1 + \Delta m_b} \equiv \frac{m_b^{\overline{\text{DR,eff}}}}{v_d}. \quad (4.114)$$

The second term in the numerator avoids double-counting of the resummed terms.

4.2 Infrared singularities

We have seen in the previous subsection that virtual correction exhibit UV singularities which arise due to infinite loop momenta and are treated by means of renormalization. However, there are also singularities related to finite or vanishing momenta – the infrared (IR) and collinear singularities. Kinoshita has shown [56] that these singularities arise from two different configurations. On the one hand are soft singularities, which occur

when a particle emits or absorbs a massless particle. On the other hand are the collinear divergencies, which appear when a massless particles splits into two massless particles. Also, both conditions can overlap at the same time. IR singularities arise in real and virtual diagrams. Their physical origin is the presence of degenerate initial or final states. For example, in QED final states with an arbitrary number of soft photons are indistinguishable due to the finite energy resolution of the detector. Or two collinear radiated particles are indistinguishable due to its finite angular resolution. In order to cancel these singularities, sufficiently inclusive observables have to be considered including these degenerate states.

For QED Bloch and Nordsieck [57] have shown that it is sufficient to sum over all degenerate final states (i.e. all states with an arbitrary number of soft photons in the final state). Kinoshita, Lee and Nauenberg [58] generalized this statement. Thus, the sum of soft and collinear divergencies cancel in the sum of virtual and real corrections.

There are different methods to deal with the cancellation of the IR singularities. The most prominent methods are phase-space slicing [59] which is applied in this work and the dipole subtraction method [60–62]. In the phase-space slicing method the soft and collinear divergent regions in the phase-space of real radiation diagrams are split off by introducing phase-space cut parameters. The remaining real hard, non-singular phase-space region can be integrated numerically. The soft and collinear singular regions can be integrated analytically under the assumption that the cut parameters are small enough. They are then added to the virtual contribution. Thus, after removing the singular regions from the real contribution and adding them to the virtual part, both are IR finite. The sum of soft, collinear and hard contributions then has to be independent of the cut parameters.

For two-body decays the complete bremsstrahlung processes including soft and hard radiation can be integrated analytically [30]. The corresponding integrals are given in Appendix A. The total decay width for the two-body decay including soft and hard radiation can be expressed in terms of these bremsstrahlung integrals. This method has the downside that only total decay widths and cross sections can be computed, i.e. it is not possible to compute differential distributions with this method. In this work, this method has been applied for the processes $\tilde{t}_2 \rightarrow \tilde{t}_1 h^0$ and $\tilde{t}_2 \rightarrow \tilde{t}_1 Z$ and yields the same results as the phase-space slicing method.

4.2.1 Soft bremsstrahlung

Soft singularities in bremsstrahlung processes are parameterized by the cutoff parameter ΔE . The momentum of the radiated gluon or photon k has to fulfill the condition $k < \Delta E$. The infrared singularity is regularized by a photon mass λ . Hence, the amplitude for soft photon emission factorizes from the Born matrix element \mathcal{M}_0 ,

$$\mathcal{M}_1^{\text{soft,EW}} = -e\mathcal{M}_0 \sum_i (\pm q_i) \frac{\epsilon p_i}{k p_i}, \quad (4.115)$$

where p_i, q_i are the momentum and charge of the i -th external particle, k is the outgoing photon momentum and ϵ the polarization vector of the photon (following the notation of [30]). The plus sign originates from initial state radiation, the minus sign from final

state radiation. The soft photon decay width is obtained by squaring the soft photon matrix element (4.115), summing over the photon polarizations and integrating over the soft photon phase space ($|k| \leq \Delta E$),

$$\begin{aligned}\Gamma_1^{\text{soft,EW}} &= -\Gamma_0 \frac{\alpha}{2\pi^2} \int_{|k| \leq \Delta E} \frac{d^3|k|}{2E_k} \sum_{ij} \frac{\pm p_i p_j R_{ij}}{p_i k p_j k} \\ &= -\Gamma_0 \frac{\alpha}{2\pi^2} \sum_{ij} (\pm) R_{ij} I_{ij} \equiv \delta_{\text{soft}} \Gamma_0,\end{aligned}\quad (4.116)$$

where $E_k = \sqrt{\mathbf{k}^2 + \lambda^2}$ and (\pm) refers to the relative sign of the emitters i and j . R_{ij} denotes the charge factors for the emitting particles i and j and δ_{soft} is called the soft-photon factor. For photon radiation the charge factors are simply given by $R_{ij} = q_i q_j$. For QCD corrections, the electroweak coupling constant has to be replaced by the strong coupling constant $\alpha \rightarrow \alpha_s$ and color algebra has to be taken into account. However, for decays mediated by the electroweak coupling (i.e. all squark decays except squark into quark plus gluino) one can simply take $q_i = 2/\sqrt{3}$ for quarks and squarks and $q_i = 0$ for all other particles. The color factor for the strong decay $\tilde{q}_a \rightarrow q \tilde{g}$ will be addressed in Subsection 6.2.4.

The basic integrals have been worked out by 't Hooft and Veltman [30, 63]. They are given by

$$\begin{aligned}I_{ij} &= 4\pi \frac{r p_i p_j}{(r p_i)^2 - p_j^2} \left\{ \frac{1}{2} \log \frac{4\Delta E^2}{\lambda^2} \right. \\ &\quad \left. + \left[\frac{1}{4} \log^2 \frac{u_0 - |\mathbf{u}|}{u_0 + |\mathbf{u}|} + \text{Li}_2 \left(1 - \frac{u_0 + |\mathbf{u}|}{v} \right) + \text{Li}_2 \left(1 - \frac{u_0 - |\mathbf{u}|}{v} \right) \right]_{u=p_j}^{u=r p_i} \right\},\end{aligned}\quad (4.117)$$

where Li_2 is the dilogarithm or Spence function

$$\text{Li}_2 = - \int_0^1 \frac{dt}{t} \log(1 - xt), \quad |\arg(1 - x)| < \pi \quad (4.118)$$

and r and v are defined as

$$r^2 p_i^2 - 2r p_i p_j + p_j^2 = 0, \quad \frac{r p_{i,0} - p_{j,0}}{p_{j,0}} > 0, \quad v = \frac{(r p_i)^2 - p_j^2}{2(r p_{i,0} - p_{j,0})}. \quad (4.119)$$

4.2.2 Collinear bremsstrahlung

Collinear singularities occur, when the angle θ between the emitting and radiated particle, in the rest frame of the decaying particle, vanishes, i.e. $1 > \cos \theta > 1 - \delta_c$, for sufficiently small δ_c . Since the soft radiation already has been taken care of by (4.115) only the hard-collinear radiation ($E_k > \Delta E$) has to be integrated over. The expression for the collinear singularities using a finite mass regulator m_e for the emitting particle have been worked

out in [64]. Since we only have to deal with final-state collinear radiation the collinear singularity factorizes into the Born decay width

$$\begin{aligned}\Gamma_1^{\text{real,coll}} &= \Gamma_0 \frac{\alpha}{2\pi} q_e^2 \left\{ \left(\left[\frac{3}{2} + 2 \log \left(\frac{\Delta E}{E_e} \right) \right] \left[1 - \log \left(\frac{2E_e^2 \delta_c}{m_e^2} \right) \right] + 3 - \frac{2\pi^2}{3} \right) \right. \\ &\equiv \delta_{\text{coll}} \Gamma_0,\end{aligned}\tag{4.120}$$

where q_e , m_e and E_e denote the charge, mass, and energy of the emitting particle. δ_{coll} denotes the collinear photon/gluon factor. Again, for gluon radiation one has to replace $\alpha \rightarrow \alpha_s$ and take $q_e = 2/\sqrt{3}$.

4.3 Dependent masses in higher order calculations

As we have seen in Subsection 4.1.3, there is a finite shift between the tree-level and on-shell masses for the left-handed down-type squark, selectron (respectively \tilde{b}_1 quark and $\tilde{\tau}_1$ slepton) and the three heavier neutralinos ($\tilde{\chi}_i$, $i = 2, 3, 4$). In order to account for the on-shell property of the external dependent particles their on-shell masses have to be used for the phase-space integration. However, for real-radiation processes (e.g. $\tilde{b}_1 \rightarrow \tilde{\chi}_1^0 b \gamma$) infrared-singular terms proportional to $\ln(\lambda^2/(m_{\tilde{b}_1}^{\text{OS}} m_b))$ arise, where λ is the photon mass regulator and $m_{\tilde{b}_1}^{\text{OS}}$ denotes the on-shell mass. In order to cancel these infrared singularities, the on-shell mass also has to be used in the infrared-singular terms in the virtual corrections. Since tree-level relations between the squark masses have to be fulfilled in order to cancel the UV singularities, the on-shell mass is only introduced in the purely infrared-singular terms [65]. These are obtained by separating the virtual diagrams with photon exchange and performing the Passarino-Veltman decomposition [31]. The only IR divergent loop integral which is a function of the dependent masses, is the scalar 3-point function C_0 . Hence in the appearing terms proportional to $m^2 C_0(\{m^2\})$ and $C_0(\{m^2\})$, with m being the mass of the dependent particle, m is replaced with the according on-shell mass m^{OS} . In summary, the following approach is used:

- For the phase space integration in $1 \rightarrow 2$ and $1 \rightarrow 3$ processes the on-shell masses are used. Furthermore, in amplitudes of diagrams where a photon is emitted of a dependent particle the on-shell mass is inserted into the propagator.
- In one-loop diagrams, the contributions originating from photon/gluon exchange are separated. After applying the Passarino-Veltman decomposition to the corresponding amplitude, the tree-level mass m in expressions $m^2 C_0(\{m^2\})$ and $C_0(\{m^2\})$ is replaced with the on-shell value m^{OS} .

4.4 Computation methods

First, Feynman diagrams for particular processes were generated with FeynArts 3.4 [66]. The tree-level Feynman rules are implemented in the MSSM model file [67]. For the

counterterm Feynman rules the renormalization transformations introduced in Chapter 4 are inserted into the MSSM Lagrangian as described in Chapters 6 and 9. After separating the contributions to the counterterm Lagrangian, the counterterm Feynman rules (Appendix C) can be deduced. With these Feynman rules, analytical expressions for the genuine 1-loop and counterterm amplitudes are generated. These amplitudes are passed to FormCalc 6.0 [32], where analytical simplifications are performed and a Fortran 77 code is generated. This code is evaluated using LoopTools 2.5 [32, 68] to compute the scalar and tensor one-loop functions and the Cuba library [69] for the numerical phase space integration. The input parameters are read in the SUSY Les Houches Accord (SLHA) format [70], a unique set of conventions for SUSY extensions of the SM specifying model parameters and decay tables. This is done with the help of SLHALib 2.2 [71], a library of routines to read and write files in SLHA format.

Chapter 5

Squark decays: introduction

After having discussed the theoretical framework of the MSSM in Chapter 2, decay observables in Chapter 3, and methods for NLO calculations in Chapter 4 we turn to the phenomenological implications on collider physics. In Section 5.1 we discuss how sparticles, in particular squarks, appear at the large hadron collider (LHC). This is followed by a survey over squark decays in Section 5.2 and a discussion of the different computations performed so far in Section 5.3.

5.1 Squarks at the LHC

There are two different kinds of SUSY signals at experimental facilities. On the one hand, there are virtual sparticle effects on SM processes. For example, electroweak precision observables such as Z-pole observables, the W-boson mass, and the anomalous magnetic moment of the muon get altered by virtual SUSY effects. Sparticle loops also contribute to processes which are rare in the SM such as $b \rightarrow s \gamma$. However, it would be impossible to ascribe deviations from the SM predictions to supersymmetry in an unambiguous way. On the other hand, there is the direct production of SUSY particles at colliders. In order to identify SUSY and determine its parameters it will be crucial to detect sparticles directly, identify their quantum numbers and measure their masses and coupling constants. Therefore it is important to have a profound knowledge of the sparticle decays and the associated radiative corrections.

Up to now no evidence for supersymmetric particles has been found. However, if supersymmetry is realized at the TeV scale, the large hadron collider at CERN has good prospects of detecting new supersymmetric particles. The LHC is a proton-proton collider with a center of mass energy of 7 TeV which is planned to be upgraded to 14 TeV. The two multi-purpose experiments ATLAS [72] and CMS [73] are designed for searches of new particles. Furthermore, there are the LHCb [74] experiment investigating the CP properties in the B meson system and the ALICE [75] experiment designed for detection of heavy-ion collisions.

If SUSY is realized at the TeV scale, production of colored supersymmetric particles

(squarks and gluinos) mediated by the strong interaction will dominate. In R-parity conserving supersymmetric theories these sparticles will be produced in pairs and subsequently decay into SM particles and an even number of lightest supersymmetric particles (LSP). For an adequate analysis it is necessary to go beyond Born approximations [76,77]. In a number of publications, radiative corrections to squark production and decays have been studied. For the squark and gluino production processes the computations of next-to-leading order (NLO) QCD [78], as well as the NLO electroweak contributions¹ [79] are available. These are complemented with next-to-leading-logarithmic (NLL) [81–83], next-to-next-to-leading-logarithmic (NNLL) [84], and next-to-next-to-leading-order QCD corrections [85]. The subsequent decays will be the subject of the next section.

5.2 Squark decays: phenomenological overview

In the following analysis we will distinguish between the first two generations (light-flavor squarks) and the third-generation squarks. Because of their negligible Yukawa couplings the light-flavor squarks are often considered as degenerate in mass and the squark mass eigenstates are the SUSY partners of the left- and right-handed quarks. For the third-generation squarks however, the large Yukawa coupling can account for a considerable mass difference for top and bottom squarks and a large mixing between left- and right-handed chiral eigenstates. Therefore, it will be important for our analysis to distinguish between light-flavor and third-generation squarks.

For adequate sparticle masses, light-flavor squarks can decay into quark plus gluino, quark plus neutralino, and quark plus chargino,

$$\tilde{q}_{L/R} \rightarrow q \tilde{g}, \quad (5.1a)$$

$$\tilde{q}_{L/R} \rightarrow q \tilde{\chi}_i^0, \quad i = 1, \dots, 4, \quad (5.1b)$$

$$\tilde{q}_{L/R} \rightarrow q' \tilde{\chi}_i^\pm \quad i = 1, 2, \quad q \neq q'. \quad (5.1c)$$

The decay into quark plus gluino mediated by the strong coupling α_s is only available when the gluino mass is smaller than the squark mass, i.e. $m_{\tilde{g}} < m_{\tilde{q}}$. However, when this decay is possible it is the dominating decay mode. Hence, the gluino mass in relation to the squark mass is an important quantity concerning squark decays.

Since the right-handed squarks only couple to the bino component of the neutralinos and the left-handed squarks couple to winos they decay differently [23]. If

$$m_Z \ll |\mu \pm M_1|, |\mu \pm M_2|, \quad (5.2)$$

the neutralino mass eigenstates are very nearly bino-like ($\tilde{\chi}_1^0 \approx \tilde{B}$), wino-like ($\tilde{\chi}_2^0 \approx \tilde{W}^3$) and higgsino-like ($\tilde{\chi}_{3,4}^0 \approx (h_u^0 \pm h_d^0)$). In this limit the chargino mass eigenstates consist of a wino-like $\tilde{\chi}_1^\pm \approx \tilde{W}^\pm = 1/\sqrt{2}(\tilde{W}^1 \pm \tilde{W}^2)$ and a higgsino-like eigenstate $\tilde{\chi}_2^\pm$. Thus, in

¹The only missing NLO electroweak contribution is the non-diagonal squark–anti-squark production, i.e. $\tilde{q}_\alpha \tilde{q}_\beta^*$ production for $\alpha \neq \beta$ and $\tilde{q}_\alpha q_\beta^*$ production for $\tilde{q} \neq \tilde{q}'$.

this parameter region, the right-handed squarks will mostly decay as $\tilde{q}_R \rightarrow q \tilde{\chi}_1^0$ where the lightest neutralino $\tilde{\chi}_1^0$ is the LSP and escapes the detector contributing to the missing transverse energy. The left-handed squarks decay differently, namely $\tilde{q}_L \rightarrow q \tilde{\chi}_2^0$ and $\tilde{q}_L \rightarrow q' \tilde{\chi}_1^\pm$ if the phase space is open for these decays. The heavier neutralinos and chargino then subsequently decay with a LSP in the final state. Often, the two-body decays for $\tilde{\chi}_2^0$ and $\tilde{\chi}_1^\pm$ are kinematically forbidden resulting in the three-body decays $\tilde{\chi}_2^0 \rightarrow \bar{f} f \tilde{\chi}_1^0$ and $\tilde{\chi}_1^\pm \rightarrow \bar{f} f' \tilde{\chi}_1^0$, where f and f' denote a lepton or quark belonging to the same $SU(2)_L$ multiplet. The decays into the higgsino-like neutralinos and chargino are negligible because of the vanishing Yukawa couplings. The consequential signatures with missing transverse energy and several jets constitute the typical signal for squark production at the LHC. With additional requirement of leptons (originating from heavier neutralinos/chargino decays) the SM background can be considerably reduced whereas most of the SUSY signal is retained.

The Yukawa couplings of the third generation cannot be neglected anymore. Since the off-diagonal entries of the squark mass matrix (2.49) are proportional to the quark mass, i.e. $m_q(A_q - \mu\kappa)$ ($\kappa = \cot\beta$ for top and $\kappa = \tan\beta$ for bottom squarks), differences between the two mass eigenstates $\tilde{t}_2 - \tilde{t}_1$ and $\tilde{b}_2 - \tilde{b}_1$ are considerable. Mixing between the top squarks is strongly enhanced because of the large top-quark mass, whereas the mixing between the bottom squarks grows for large values of $\tan\beta$. Hence, the squarks cannot be categorized into left- and right-handed eigenstates and the simplified analysis applied to the light-flavor squarks does not apply. Additionally, the decays into the higgsino-like neutralinos and charginos become relevant. Due to the possibly large mass-splitting further decay modes for the top and bottom squarks have to be considered,

$$\tilde{t}_2 \rightarrow \tilde{t}_1 Z, \quad \tilde{t}_2 \rightarrow \tilde{t}_1 h^0, \quad (5.3a)$$

$$\tilde{t}_2 \rightarrow \tilde{t}_1 H^0, \quad \tilde{t}_2 \rightarrow \tilde{t}_1 A^0, \quad (5.3b)$$

$$\tilde{t}_2 \rightarrow \tilde{b}_i W^+, \quad \tilde{t}_2 \rightarrow \tilde{b}_i H^+, \quad i = 1, 2, \quad (5.3c)$$

$$\tilde{b}_2 \rightarrow \tilde{b}_1 Z, \quad \tilde{b}_2 \rightarrow \tilde{b}_1 h^0, \quad (5.3d)$$

$$\tilde{b}_2 \rightarrow \tilde{b}_1 H^0, \quad \tilde{b}_2 \rightarrow \tilde{b}_1 A^0, \quad (5.3e)$$

$$\tilde{b}_2 \rightarrow \tilde{t}_i W^-, \quad \tilde{b}_2 \rightarrow \tilde{t}_i H^-, \quad i = 1, 2. \quad (5.3f)$$

The decay of the heavier top squark into the lighter top squark and the lightest Higgs boson can be relevant for the associated production of the lightest Higgs boson with a top squark pair, i.e. $\tilde{t}_1 \tilde{t}_1^* h^0$ [86]. For large top squark mixing the $\tilde{t}_1 \tilde{t}_1^* h^0$ cross section can be larger than its SM counterpart $t\bar{t}h^0$. For top squark masses suitably larger than the top quark mass the decay $\tilde{t}_1 \rightarrow t \tilde{\chi}_1^0$ can occur with a large branching ratio. The final outcome would have a similar signature as the one emerging from $t\bar{t}h^0$ production. Due to the two neutralinos in the final state escaping detection there is more missing transverse energy allowing for an additional handle for background rejection. In the appropriate parameter region the $\tilde{t}_1 \tilde{t}_1^* h^0$ channel has the potential to be an interesting channel for Higgs discovery. Further the $\tilde{t}_1 \tilde{t}_1^* h^0$ cross section could give insights into the SUSY-breaking scenario and its parameters. Therefore precise theoretical predictions on top-squark production and its

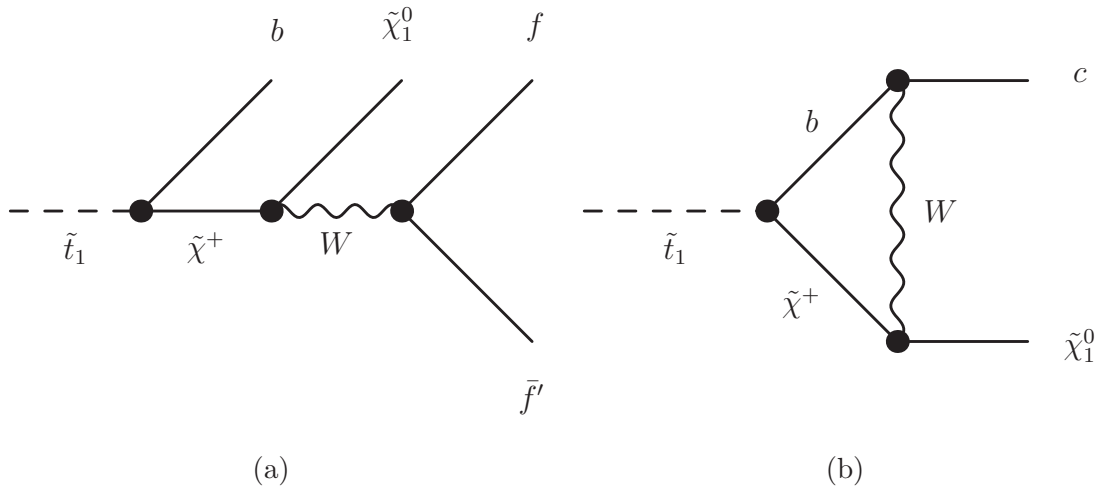


Figure 5.1: Typical diagrams contributing to the four-body decay $\tilde{t}_1 \rightarrow b f \bar{f}' \tilde{\chi}_1^0$ (a) and to the loop-suppressed decay $\tilde{t}_1 \rightarrow c \tilde{\chi}_1^0$ (b).

decay into Higgs bosons could become important.

In certain regions of the MSSM parameter space the decay channels mentioned above for the lighter top squark \tilde{t}_1 are kinematically forbidden. In that case the flavor-changing decay

$$\tilde{t}_1 \rightarrow c \tilde{\chi}_1^0 \quad (5.4)$$

and the four body decay

$$\tilde{t}_1 \rightarrow b f \bar{f}' \tilde{\chi}_1^0 \quad (5.5)$$

become relevant. In Fig. 5.1 two typical Feynman diagrams contributing to these processes are shown. However, these decays are not further examined in this work.

5.3 Squark decays: calculations

Early analyses of squark production with their subsequent decays at leading order assumed that the squark-decay into photino and quark dominates [87]. In subsequent publications it was shown that this hypothesis is generally not justified for higher masses of the gluino and the squarks ($m_{\tilde{g},\tilde{q}} > 50$ GeV) and different decay modes of light-flavor squarks must be taken into account [88–92]. Third-generation squark decays incorporating the Yukawa coupling and all mass terms of the top quark have been computed at tree level in [93].

The QCD NLO calculations to squark decays have first been performed for the decays of third-generation squarks into neutralinos and charginos ($\tilde{q} \rightarrow q \tilde{\chi}_i^0$ and $\tilde{q} \rightarrow q' \tilde{\chi}_j^\pm$ where $q, q' = t, b, i = 1, \dots, 4, j = 1, 2$) [94]. The authors found corrections of about 10% except for decays with higgsino-like neutralinos or chargino where they can amount to 40%. This

computation has been generalized for decays of light-flavor squarks with massless quarks as decay products [95]. In this case the corrections to light-flavor squark decays did not exceed 10%. The first electroweak (EW) NLO computations have been performed in [96] for bottom squark decays in the Yukawa coupling approximation. Finally, complete EW corrections to squark decays into neutralinos and charginos for third-generation and light-flavor squarks have been presented in [97]. The authors identified universal corrections but also found non-decoupling terms that make it necessary to take into account the whole MSSM spectrum. The QCD corrections were improved by using an effective bottom quark Yukawa coupling and were combined with the electroweak corrections which can be of the same order of magnitude as the QCD ones. A computation using an effective description of squark interactions with neutralinos and charginos has been done in [98].

At the same time as the corrections to squark decays into neutralinos and charginos the NLO QCD corrections to light-flavor squark decays into quark plus gluino have been calculated in [99]. Subsequently, the corrections to top-squark decays into top quark plus gluino have been computed [100]. The corrections were found to be ranging between thirty and fifty percent. The electroweak corrections in the Yukawa coupling approximation amounting up to ten percent have been computed in [101]. The complete electroweak and QCD one-loop corrections were recently implemented in the SFold package [102].

In [103] the decays of third-generation squarks into W/Z-bosons and into Higgs bosons plus squarks have been discussed at tree-level. The analysis revealed that these decays can be dominant in a wide range of the MSSM parameter space owing to the large Yukawa couplings and mixing angles of \tilde{t} and \tilde{b} . The NLO QCD corrections for squark decays into W and Z bosons have been presented in [104]. It has been found that the corrections are typically negative and range from minus five to minus ten percent. In [105] the electroweak corrections were combined with the QCD correction, both being of the same order of magnitude.

For the squark decays into Higgs bosons, the one-loop QCD corrections have been calculated in [106] for the decay $\tilde{t}_2 \rightarrow \tilde{t}_1 (h^0, A^0)$ and generalized to all possible squark decays to Higgs bosons in [107]. The corrections are mostly negative and are of the order of a -10% to -20% . In [108] the electroweak corrections in the Yukawa coupling approximation were computed and the strict one-loop EW corrections have been calculated in [109].

The decays of the lighter top squark when the two-body decays (5.1) are kinematically forbidden, have first been studied in [110, 111] and more recently in [112, 113]. The full one-loop computation to the flavor changing neutral current decay $\tilde{t}_1 \rightarrow c\tilde{\chi}_1^0$ was recently done in [114].

QCD corrections to sparticle decays including squark decays have been implemented into the Fortran code SDECAY [115] which calculates the decay widths and branching ratios of all supersymmetric particles in the MSSM. It is a part of the SUSY-HIT package [116] which combines the SUSY particle spectrum generator SuSpect [117] with the program HDECAY [118] computing the decays of the MSSM Higgs boson.

The aim of the following chapters is to collect all electroweak and QCD corrections to all different squark decays (5.1) and (5.3) in a common approach for renormalization including higher-order contributions in the Higgs and bottom sector. Special care is taken

for the consistent treatment of the external on-shell particles, especially in the case of the dependent squarks and neutralinos masses. The Higgs sector has been treated according to the renormalization scheme used in FeynHiggs [29] which is also used to compute the two-loop corrections to the Higgs-boson masses. FeynHiggs is a Fortran code for the diagrammatic calculation of masses, mixing factors of Higgs bosons in the MSSM at the two-loop level. Furthermore production cross sections, decay widths, and branching ratios of Higgs bosons are computed up to the one-loop level. For the renormalization of the other parameters we have chosen the on-shell scheme, such that physical quantities, i.e. on-shell masses, can be used as input parameters. Only the bottom-quark mass and the according trilinear coupling are renormalized in the $\overline{\text{DR}}$ scheme in order to avoid instabilities in the perturbative expansion.

Chapter 6

Squark decays: process-specific calculations

In this chapter, process-specific calculations of NLO corrections to squark decays are presented. Explicitly, these are the derivation of the counterterm Lagrangians and counterterm Feynman rules, which are listed in Appendix C. Furthermore, all Feynman diagrams contributing to these processes are shown, treatment of the on-shell masses for the dependent particles is specified, and characteristic features of the calculations in the Higgs sector are discussed. Decays discussed in the following are the decays of squarks into quarks plus neutralinos/charginos, squarks into quarks plus gluino, squarks into squarks plus W/Z-bosons, and squark decays into squarks plus the various Higgs bosons.

6.1 $\tilde{q}_a \rightarrow q' \tilde{\chi}_i^\pm$ and $\tilde{q}_a \rightarrow q \tilde{\chi}_i^0$

6.1.1 Counterterm Lagrangian

The Lagrangian for squark-quark-chargino interactions in terms of the mass eigenstates is given by [22]

$$\mathcal{L}_{q\tilde{q}'\chi^\pm} = \overline{\tilde{\chi}_k^+} (C_{sk}^{L*} P_L + F_{sk}^R P_R) \tilde{d}_s^\dagger u + \overline{\tilde{\chi}_k^-} (D_{sk}^{L*} P_L + E_{sk}^R P_R) \tilde{u}_s^\dagger d + \text{hc}. \quad (6.1a)$$

For interactions of squarks with quarks and neutralinos the Lagrangian reads

$$\mathcal{L}_{q\tilde{q}\tilde{\chi}^0} = \overline{\tilde{\chi}_k^0} \left[(G_{sk}^{uL} P_L + G_{sk}^{uR} P_R) \tilde{u}_s^\dagger u + (G_{sk}^{dL} P_L + G_{sk}^{dR} P_R) \tilde{d}_s^\dagger d \right] + \text{hc}, \quad (6.1b)$$

where “hc” denotes the hermitian conjugate of the preceding terms. $\tilde{\chi}_k^\pm$ and $\tilde{\chi}_k^0$ denote the fields of the chargino and neutralino mass eigenstates (2.60) and (2.67), u and d the quark

spinors, and \tilde{u}_s and \tilde{d}_s the squark fields. The couplings in (6.1a) and (6.1b) are given by

$$C_{sk}^L = -g_2 U_{k1} U_{s1}^{\tilde{d}} + \frac{g_2 U_{k2}}{\sqrt{2} M_W c_\beta} m_d U_{s2}^{\tilde{d}}, \quad (6.2a)$$

$$D_{sk}^L = -g_2 V_{k1} U_{s1}^{\tilde{u}} + \frac{g_2 V_{k2}}{\sqrt{2} M_W c_\beta} m_u U_{s2}^{\tilde{u}}, \quad (6.2b)$$

$$E_{sk}^R = \frac{g_2 U_{k2} m_d}{\sqrt{2} M_W c_\beta} U_{s1}^{\tilde{u}}, \quad (6.2c)$$

$$F_{sk}^R = \frac{g_2 V_{k2} m_u}{\sqrt{2} M_W s_\beta} U_{s1}^{\tilde{d}}, \quad (6.2d)$$

$$G_{sk}^{uL} = G_k^{uL} U_{s1}^{\tilde{u}} - \frac{g_2}{\sqrt{2} M_W s_\beta} m_u N_{k4}^* U_{s2}^{\tilde{u}}, \quad (6.2e)$$

$$G_{sk}^{uR} = G_k^{uR} U_{s2}^{\tilde{u}} - \frac{g_2}{\sqrt{2} M_W s_\beta} m_u N_{k4} U_{s1}^{\tilde{u}}, \quad (6.2f)$$

$$G_{sk}^{dL} = G_k^{dL} U_{s1}^{\tilde{d}} - \frac{g_2}{\sqrt{2} M_W c_\beta} m_d N_{k3}^* U_{s2}^{\tilde{d}}, \quad (6.2g)$$

$$G_{sk}^{dR} = G_k^{dR} U_{s2}^{\tilde{d}} - \frac{g_2}{\sqrt{2} M_W c_\beta} m_u N_{k3} U_{s1}^{\tilde{d}}, \quad (6.2h)$$

$$G_k^{qL} = -\sqrt{2} g_2 [T_{3L}^q N_{k2}^* + t_W (Q_q - T_{3L}^q) N_{k1}^*], \quad (6.2i)$$

$$G_k^{qR} = \sqrt{2} g_2 t_W Q_q N_{k1}, \quad (6.2j)$$

where the parameters for the charginos, neutralinos, squarks, and quarks have been introduced in Chapter 2. The mixing matrices for the squarks $U_{ij}^{\tilde{q}}$, the charginos U_{ij}/V_{ij} , and neutralinos N_{ij} (Subsection 2.2.3) rotate the gauge eigenstates into mass eigenstates. The subscript s denotes the squark mass eigenstates and k the chargino / neutralino mass eigenstate. Indices in generation space are omitted throughout this work, since flavor-changing interactions are neglected.

The counterterms $\delta\mathcal{L}$ are obtained inserting the renormalization transformations for the chargino- (4.78), neutralino- (4.91), squark-, and quark-fields (4.33). Furthermore, the couplings (6.2) transform as

$$C_{sk}^L \rightarrow C_{sk}^L + \delta C_{sk}^L, \quad D_{sk}^L \rightarrow D_{sk}^L + \delta D_{sk}^L, \quad (6.3a)$$

$$E_{sk}^R \rightarrow E_{sk}^R + \delta E_{sk}^R, \quad F_{sk}^R \rightarrow F_{sk}^R + \delta F_{sk}^R, \quad (6.3b)$$

$$G_{sk}^{uL} \rightarrow G_{sk}^{uL} + \delta G_{sk}^{uL}, \quad G_{sk}^{uR} \rightarrow G_{sk}^{uR} + \delta G_{sk}^{uR}, \quad (6.3c)$$

$$G_{sk}^{dL} \rightarrow G_{sk}^{dL} + \delta G_{sk}^{dL}, \quad G_{sk}^{dR} \rightarrow G_{sk}^{dR} + \delta G_{sk}^{dR}. \quad (6.3d)$$

These renormalization constants are listed in Appendix B.1. This gives us the following

counterterm Lagrangian for charginos,

$$\begin{aligned} \delta\mathcal{L}_{q\tilde{q}'\chi^\pm} = & \overline{\tilde{\chi}_k^+} \left[P_L \left(\frac{1}{2} [\delta\mathcal{Z}_{\tilde{\chi}^+}]_{lk}^* C_{sl}^{L*} + \frac{1}{2} \delta Z_u^L C_{sk}^{L*} + \frac{1}{2} [\delta\mathcal{Z}_{\tilde{d}}]_{ts}^* C_{tk}^{L*} + \delta C_{tk}^{L*} \right) \right. \\ & \left. + P_R \left(\frac{1}{2} [\delta\mathcal{Z}_{\tilde{\chi}^+}]_{lk}^* F_{sl}^R + \frac{1}{2} \delta Z_u^R F_{sk}^R + \frac{1}{2} [\delta\mathcal{Z}_{\tilde{d}}]_{ts}^* F_{tk}^R + \delta F_{tk}^R \right) \right] \tilde{d}_t^* u \\ & + \overline{\tilde{\chi}_k^-} \left[P_L \left(\frac{1}{2} [\delta\mathcal{Z}_{\tilde{\chi}^\pm}]_{lk}^* D_{sl}^{L*} + \frac{1}{2} \delta Z_d^L D_{sk}^{L*} + \frac{1}{2} [\delta\mathcal{Z}_{\tilde{u}}]_{ts}^* D_{tk}^{L*} + \delta D_{sk}^{L*} \right) \right. \\ & \left. + P_R \left(\frac{1}{2} [\delta\mathcal{Z}_{\tilde{\chi}^\pm}]_{lk}^* E_{sl}^R + \frac{1}{2} \delta Z_d^R E_{sk}^R + \frac{1}{2} [\delta\mathcal{Z}_{\tilde{u}}]_{ts}^* E_{tk}^R + \delta E_{sk}^R \right) \right] \tilde{u}_t^* d + \text{hc}, \quad (6.4a) \end{aligned}$$

and neutralinos,

$$\begin{aligned} \delta\mathcal{L}_{q\tilde{q}\tilde{\chi}^0} = & \overline{\tilde{\chi}_l^0} \left[P_L \left(\frac{1}{2} [\delta\mathcal{Z}_{\tilde{\chi}^0}]_{lk} G_{sl}^{uL} + \frac{1}{2} [\delta\mathcal{Z}_{\tilde{u}}]_{ts}^* G_{tk}^{uL} + \frac{1}{2} \delta Z_u^L G_{sk}^{uL} + \delta G_{sk}^{uL} \right) \right. \\ & \left. + P_R \left(\frac{1}{2} [\delta\mathcal{Z}_{\tilde{\chi}^0}]_{lk}^* G_{sl}^{uR} + \frac{1}{2} [\delta\mathcal{Z}_{\tilde{u}}]_{ts}^* G_{tk}^{uR} + \frac{1}{2} \delta Z_u^R G_{sk}^{uR} + \delta G_{sk}^{uR} \right) \right] \tilde{u}_s^* u \\ & + \overline{\tilde{\chi}_l^0} \left[P_L \left(\frac{1}{2} [\delta\mathcal{Z}_{\tilde{\chi}^0}]_{lk} G_{sl}^{dL} + \frac{1}{2} [\delta\mathcal{Z}_{\tilde{d}}]_{ts}^* G_{tk}^{dL} + \frac{1}{2} \delta Z_d^L G_{sk}^{dL} + \delta G_{sk}^{dL} \right) \right. \\ & \left. + P_R \left(\frac{1}{2} [\delta\mathcal{Z}_{\tilde{\chi}^0}]_{lk}^* G_{sl}^{dR} + \frac{1}{2} [\delta\mathcal{Z}_{\tilde{d}}]_{ts}^* G_{tk}^{dR} + \frac{1}{2} \delta Z_d^R G_{sk}^{dR} + \delta G_{sk}^{dR} \right) \right] \tilde{d}_s^* d + \text{hc}. \quad (6.4b) \end{aligned}$$

The corresponding Feynman rules are listed in Appendix C.

6.1.2 Feynman diagrams

The QCD one-loop amplitude $\mathcal{M}_1^{1L,\text{QCD}}$ consist of diagrams (Fig. 6.1) with gluino- (a) and gluon-exchange (b). Furthermore, the counterterm contributions to $\mathcal{M}_1^{\text{CT},\text{QCD}}$ are depicted in (c), and diagrams with real gluon radiation contributing to the amplitude $\mathcal{M}_1^{\text{real},\text{QCD}}$ are given in (d)-(e). For the electroweak corrections (Fig. 6.2), triangle diagrams with a gaugino (a)-(b), Higgs boson (c)-(d), and gauge boson (e)-(g) contribute to $\mathcal{M}_1^{1L,\text{EW}}$, whereas diagram (h) contributes to the counterterm amplitude $\mathcal{M}^{\text{CT},\text{EW}}$. Real radiation accounting for $\mathcal{M}_1^{\text{real},\text{EW}}$ consist of diagrams, where a photon is radiated of a electrically charged particle (i)-(k), whereas diagram (i) only appears in processes with external charginos.

6.1.3 Partial decay widths and branching ratios

In these processes, some subtleties have to be taken care of. First, renormalization of the bottom quark mass and inclusion of $\tan\beta$ enhanced corrections, which is addressed in Subsection 4.1.4, have to be considered. Second, one has to pay attention to the treatment of the dependent masses for the particles \tilde{d}_L , \tilde{b}_1 and $\tilde{\chi}_i^0$, ($i = 2, 3, 4$). This concerns

all processes (at least those with particles with a dependent mass in the final state) and is highlighted in Section 4.3. Finally, when computing real corrections for the first generation squark decays, collinear divergencies occur due to the massless outgoing quark (Subsection 4.2.2).

Computation of partial decay widths and branching ratios is explained in Chapter 3. The tree-level partial decay widths for the decays into quarks and neutralinos/charginos is given by

$$\Gamma_0(\tilde{q}_a \rightarrow q' \tilde{\chi}_i) = \frac{(2\pi)^4}{m_{\tilde{q}_a}} \int d\text{PS}_2 |\mathcal{M}_0|^2, \quad (6.5)$$

where $\tilde{\chi}_i$ denotes a neutralino or chargino, $d\text{PS}_2$ the two-body phase space element, and \mathcal{M}_0 the tree-level amplitude for the corresponding decay. The decay widths at NLO are obtained with the amplitudes computed from the Feynman diagrams listed in Subsection 6.1.2,

$$\Gamma_1^{\text{virt,EW/QCD}}(\tilde{q}_a \rightarrow q' \tilde{\chi}_i) = \frac{(2\pi)^4}{m_{\tilde{q}_a}} \int d\text{PS}_2 2\text{Re} \left(\mathcal{M}_0 \mathcal{M}_1^{\text{EW/QCD}} \right) + \delta_{\text{soft}} \Gamma_0 + \delta_{\text{coll}} \Gamma_0, \quad (6.6a)$$

$$\Gamma_1^{\text{real,EW/QCD}}(\tilde{q}_a \rightarrow q' \tilde{\chi}_i) = \frac{(2\pi)^4}{m_{\tilde{q}_a}} \int d\text{PS}_3 |\mathcal{M}_1^{\text{real,EW/QCD}}|^2, \quad (6.6b)$$

where $\mathcal{M}_1^{\text{EW/QCD}} = \mathcal{M}_1^{\text{IL,EW/QCD}} + \mathcal{M}_1^{\text{CT,EW/QCD}}$. δ_{soft} and δ_{coll} denote the soft-photon/gluon and collinear-photon/gluon factors (4.116) and (4.120). The partial decay widths at EW/QCD NLO are then given by

$$\Gamma_1^{\text{EW/QCD}}(\tilde{q}_a \rightarrow q' \tilde{\chi}_i) = \Gamma_1^{\text{virt,EW/QCD}}(\tilde{q}_a \rightarrow q' \tilde{\chi}_i) + \Gamma_1^{\text{real,EW/QCD}}(\tilde{q}_a \rightarrow q' \tilde{\chi}_i). \quad (6.7)$$

Finally, the branching ratios are calculated according to (3.14).

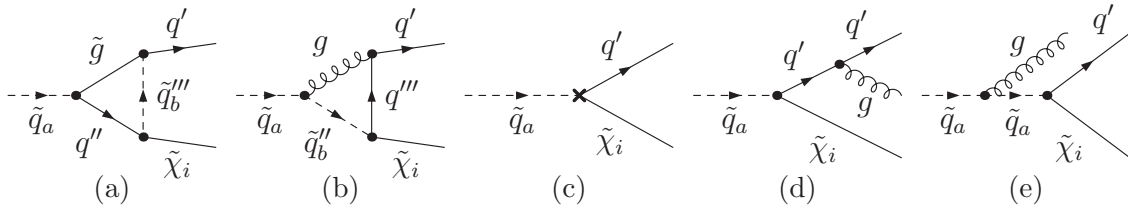


Figure 6.1: Generic Feynman diagrams contributing to QCD corrections to the process $\tilde{q}_a \rightarrow q' \tilde{\chi}_i$: (a), (b) virtual corrections, (c) counterterm diagram and (d), (e) real radiation diagrams. Notation as in Fig. 6.2.

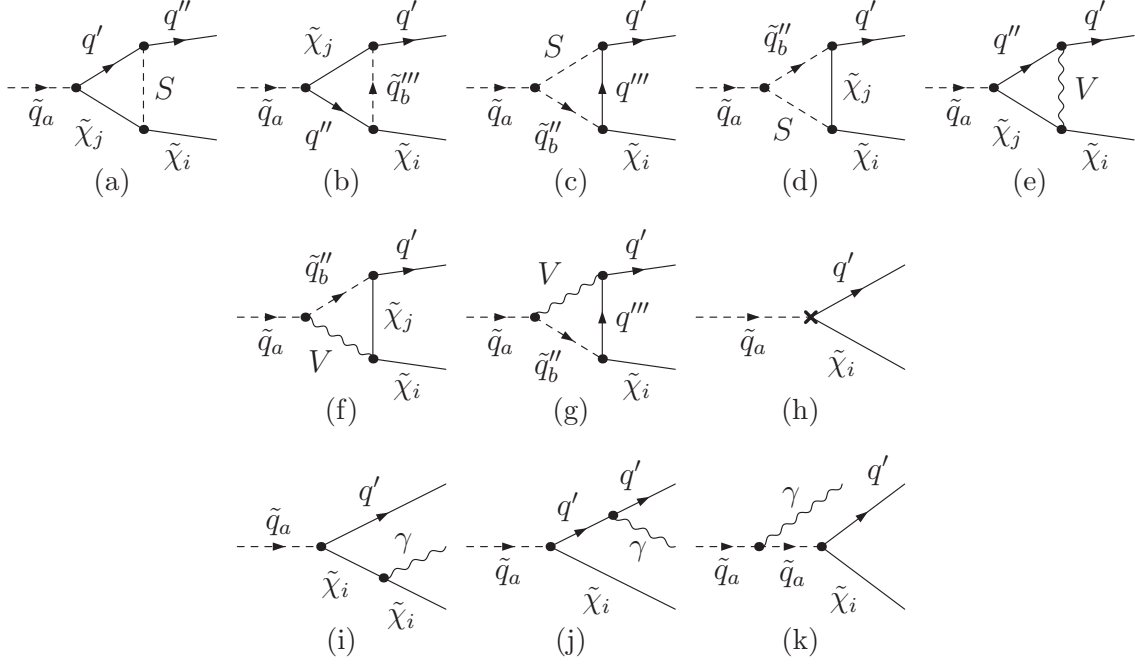


Figure 6.2: Generic Feynman diagrams contributing to electroweak corrections to the process $\tilde{q}_a \rightarrow q' \tilde{\chi}_i$: (a)-(g) virtual corrections, (h) counterterm diagram, (i)-(k) real radiation diagrams. The common label V denotes the gauge bosons γ , Z or W . S refers to the Higgs bosons h^0 , H^0 , A^0 and H^\pm , for internal particles it also stands for the Goldstone bosons G^0 and G^\pm . $\tilde{\chi}_i$ labels neutralinos and charginos, respectively. Insertions of the specific particles have to be combined such that the $U(1)$ and $SU(2)$ charges are conserved at each vertex.

6.2 $\tilde{q}_a \rightarrow q\tilde{g}$

6.2.1 Counterterm Lagrangian

The Lagrangian for squark-quark-gluino interactions is given by [22]

$$\mathcal{L}_{\tilde{q}_s q \tilde{g}^a} = -\sqrt{2} g_s T^a \sum_{q=u,d} \bar{q} \left(U_{1s}^{\tilde{q}} P_R - U_{2s}^{\tilde{q}} P_L \right) \tilde{g}^a \tilde{q}_s + \text{hc.} \quad (6.8)$$

The renormalization transformations introduced for the squark, quark, and gluino fields (4.61, 4.33, 4.98b) and for the strong coupling constant (4.105), yield the counterterm

Lagrangian

$$\begin{aligned} \delta\mathcal{L}_{\tilde{q}_s q \tilde{g}^a} = & \sqrt{2}T^a \sum_{q=u,d} \bar{q} \left[P_L \left(\delta Z_{g_s} g_s U_{2s}^{\tilde{q}} + \frac{1}{2} [\delta \mathcal{Z}_{\tilde{q}}]_{ts} g_s U_{2t}^{\tilde{q}} + \frac{1}{2} \delta Z_q^{R*} g_s U_{2s}^{\tilde{q}} \right) \right. \\ & \left. - P_R \left(\delta Z_{g_s} g_s U_{1s}^{\tilde{q}} + \frac{1}{2} [\delta \mathcal{Z}_{\tilde{q}}]_{ts} g_s U_{1t}^{\tilde{q}} + \frac{1}{2} \delta Z_q^{L*} g_s U_{1s}^{\tilde{q}} \right) \right] \tilde{g}^a \tilde{q}_s + \text{hc}. \end{aligned} \quad (6.9)$$

From this counterterm Lagrangian the counterterm Feynman rules can be deduced. They are listed in in Appendix C.

6.2.2 Feynman diagrams

Genuine 1-loop QCD diagrams contributing to the amplitude $\mathcal{M}_1^{1\text{L},\text{QCD}}$ (Fig. 6.3) consist of gluon and gluino exchange (a)-(d). Diagram (e) contributes to the QCD counterterm amplitude $\mathcal{M}_1^{\text{CT},\text{QCD}}$ and diagrams (f)-(h) account for $\mathcal{M}_1^{\text{real},\text{QCD}}$. The genuine 1-loop EW corrections (Fig. 6.4) are built up of triangle diagrams with quark–squark–gauge-boson (a), quark–squark–neutralino (b) and quark–squark–Higgs-boson loops (c) and the corresponding amplitude is denoted as $\mathcal{M}_1^{1\text{L},\text{EW}}$. The counterterm diagram (d) contributes to $\mathcal{M}_1^{\text{CT},\text{EW}}$. Finally, the real EW corrections consist of photon radiation of external particles with electrical charge (Fig. 6.4 (e) and (f)). The corresponding amplitude reads $\mathcal{M}_1^{\text{EW},\text{real}}$.

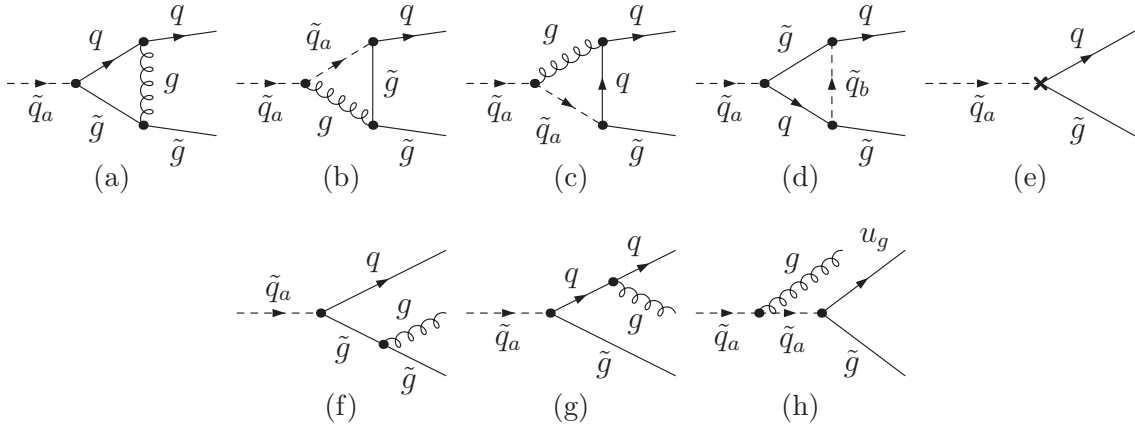


Figure 6.3: Feynman diagrams contributing to QCD corrections to $\tilde{q}_a \rightarrow q \tilde{g}$: (a)-(d) virtual diagrams, (e) counterterm, (f)-(h) real radiation diagrams. Notation as in Fig. 6.2.

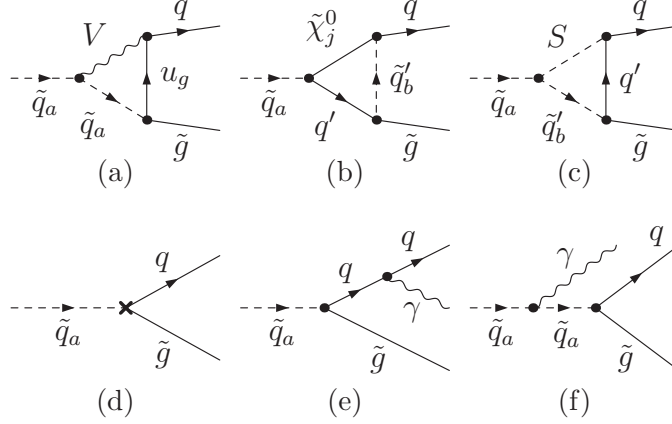


Figure 6.4: Generic Feynman diagrams contributing to electroweak corrections to the process $\tilde{q}_a \rightarrow q\tilde{g}$: (a)-(c) virtual corrections, (d) counterterm diagrams and (e)-(f) real radiation diagrams. Notation as in Fig. 6.2.

6.2.3 Partial decay width and branching ratios

As described in Chapter 3, the tree-level decay width is given by

$$\Gamma_0(\tilde{q}_a \rightarrow q\tilde{g}) = \frac{(2\pi)^4}{m_{\tilde{q}_a}} \int d\text{PS}_2 |\mathcal{M}_0|^2, \quad (6.10)$$

where \mathcal{M}_0 is the tree-level amplitude for the corresponding decay. The decay widths at NLO are obtained with the amplitudes computed from the Feynman diagrams in Subsection 6.2.2,

$$\Gamma_1^{\text{virt,EW/QCD}}(\tilde{q}_a \rightarrow q\tilde{g}) = \frac{(2\pi)^4}{m_{\tilde{q}_a}} \int d\text{PS}_2 2\text{Re} \left(\mathcal{M}_0 \mathcal{M}_1^{\text{EW/QCD}} \right) + \delta_{\text{soft}} \Gamma_0 + \delta_{\text{coll}} \Gamma_0, \quad (6.11a)$$

$$\Gamma_1^{\text{real,EW/QCD}}(\tilde{q}_a \rightarrow q\tilde{g}) = \frac{(2\pi)^4}{m_{\tilde{q}_a}} \int d\text{PS}_3 |\mathcal{M}_1^{\text{real,EW/QCD}}|^2, \quad (6.11b)$$

where $\mathcal{M}_1^{\text{EW/QCD}} = \mathcal{M}_1^{\text{1L,EW/QCD}} + \mathcal{M}_1^{\text{CT,EW/QCD}}$. δ_{soft} and δ_{coll} denote the soft-photon/gluon and collinear-photon/gluon factors (4.116) and (4.120). Because of the external gluino, the QCD soft color factors involve a non-trivial color factor matrix R_{ij} (c.f. (4.116)). Its calculation is shown in Subsection 6.2.4. The partial decay widths at EW/QCD NLO are given by

$$\Gamma_1^{\text{EW/QCD}}(\tilde{q}_a \rightarrow q\tilde{g}) = \Gamma_1^{\text{virt,EW/QCD}}(\tilde{q}_a \rightarrow q\tilde{g}) + \Gamma_1^{\text{real,EW/QCD}}(\tilde{q}_a \rightarrow q\tilde{g}). \quad (6.12)$$

Finally, the branching ratios are calculated with (3.14).

6.2.4 Color factors

Since gluon-radiation of a gluino introduces different color factors than gluon-radiation of squarks and quarks, the color factor matrix R (cf. (4.116)) for the real QCD corrections of squark decays into quark plus gluino is not trivial anymore. Gluon radiation of quarks and squarks yields the following charge factors:

$$(T^a)_{ij} = \begin{cases} t_{ij}^a & \text{for ingoing (s)quark or outgoing anti-(s)quark} \\ -t_{ij}^a & \text{for ingoing anti-(s)quark or outgoing (s)quark} \end{cases} \quad (6.13)$$

Furthermore, the gluino emitting a gluon yields the factor

$$(T_G^a)_{bc} = if_{abc}. \quad (6.14)$$

The amplitudes in the soft-gluon approximation for gluon radiation are denoted in Tab. 6.1.

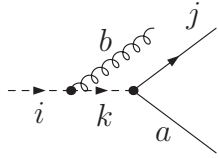
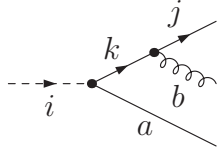
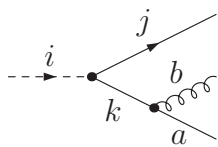
	$= -t_{jk}^a t_{ki}^b g_s \mathcal{M}_0 \frac{p_0 \epsilon}{p_0 k},$
	$= t_{ki}^a t_{jk}^b g_s \mathcal{M}_0 \frac{p_1 \epsilon}{p_1 k},$
	$= if_{bka} t_{ji}^k g_s \mathcal{M}_0 \frac{p_2 \epsilon}{p_2 k} = (t_{jk}^a t_{ki}^b - t_{ki}^a t_{jk}^b) g_s \mathcal{M}_0 \frac{p_2 \epsilon}{p_2 k}.$

Table 6.1: Gluon radiation matrix elements in the soft-gluon approximation for the processes $\tilde{q}_a \rightarrow \tilde{g}q$. a, b, i, j and k denote the color charges of the particles. p_0 denotes the momentum of the particle with color charge i , p_1 belongs to particle j and p_2 to particle with index a .

Squaring the real gluon radiation amplitude yields products $t_{jk}^a t_{ki}^b t_{li}^a t_{lj}^b$. Color algebra and the Fierz identity yield the color factor matrix (c.f. (4.116))

$$R = \begin{pmatrix} 16/3 & -2/3 & 6 \\ -2/3 & 16/3 & -6 \\ 6 & -6 & 12 \end{pmatrix}. \quad (6.15)$$

6.3 $\tilde{q}_a \rightarrow \tilde{q}_b Z$ and $\tilde{q}_a \rightarrow \tilde{q}'_b W^\pm$

In the basis of mass eigenstates, the Lagrangians for electroweak squark–squark–W/Z-boson interactions read as follows,

$$\mathcal{L}_{\tilde{q}_s^* \tilde{q}_t A} = -i Q_{\tilde{q}} e A_\mu \left(U_{s1}^{\tilde{q}} U_{t1}^{\tilde{q}} + U_{s2}^{\tilde{q}} U_{t2}^{\tilde{q}} \right) \tilde{q}_s^* \overleftrightarrow{\partial}^\mu \tilde{q}_t \equiv -i C(A, \tilde{q}_s^*, \tilde{q}_t) A_\mu \tilde{q}_s^* \overleftrightarrow{\partial}^\mu \tilde{q}_t, \quad (6.16)$$

$$\begin{aligned} \mathcal{L}_{\tilde{q}_s^* \tilde{q}_t Z} &= -\frac{ie}{s_W c_W} Z_\mu \left[T_{3L}^{\tilde{q}} \left(1 - 4 T_{3L}^{\tilde{q}} Q_{\tilde{q}} s_W^2 \right) U_{s1}^{\tilde{q}} U_{t1}^{\tilde{q}} - s_W^2 Q_{\tilde{q}} U_{s2}^{\tilde{q}} U_{t2}^{\tilde{q}} \right] \tilde{q}_s^* \overleftrightarrow{\partial}^\mu \tilde{q}_t \\ &\equiv -i C(Z, \tilde{q}_s^*, \tilde{q}_t) Z_\mu \tilde{q}_s^* \overleftrightarrow{\partial}^\mu \tilde{q}_t, \end{aligned} \quad (6.17)$$

$$\begin{aligned} \mathcal{L}_{\tilde{q}_s^* \tilde{q}'_t W} &= -\frac{ie}{\sqrt{2} s_W} \left(W_\mu^+ U_{s1}^{\tilde{u}} U_{t1}^{\tilde{d}} \tilde{u}_s^* \overleftrightarrow{\partial}^\mu \tilde{d}_t + \text{hc} \right) \\ &\equiv -i C(W^+, \tilde{u}_s^*, \tilde{d}_t) W_\mu^+ \tilde{u}_s^* \overleftrightarrow{\partial}^\mu \tilde{d}_t + \text{hc}, \end{aligned} \quad (6.18)$$

$$C(W^+, \tilde{u}_s^*, \tilde{d}_t) = C(W^-, \tilde{d}_s^*, \tilde{u}_t). \quad (6.19)$$

Via the renormalization transformations for the squark-fields (4.61), vector-fields (4.9), the electric charge (4.14), and the weak mixing angle (4.7) constituting the counterterm couplings $\delta C(\dots)$ given in Appendix B.2, the counterterm Lagrangian is obtained. It is given by

$$\begin{aligned} \delta \mathcal{L}_{\tilde{q}_s^* \tilde{q}_t Z} &= -i \left[\delta C(Z, \tilde{q}_s^*, \tilde{q}_t) + \frac{1}{2} \delta Z_{11}^{ZA} C(Z, \tilde{q}_s^*, \tilde{q}_t) + \frac{1}{2} \delta Z_{21}^{ZA} C(A, \tilde{q}_s^*, \tilde{q}_t) \right. \\ &\quad \left. + \frac{1}{2} [\delta \mathcal{Z}_{\tilde{q}_s}]_{us}^* C(Z, \tilde{q}_s^*, \tilde{q}_t) + \frac{1}{2} [\delta \mathcal{Z}_{\tilde{q}}]_{vt} C(Z, \tilde{q}_s^*, \tilde{q}_v) \right] Z_\mu \tilde{q}_s^* \overleftrightarrow{\partial}^\mu \tilde{q}_t, \end{aligned} \quad (6.20a)$$

$$\begin{aligned} \delta \mathcal{L}_{\tilde{q}_s^* \tilde{q}'_t W} &= -i \left[\delta C(W^+, \tilde{u}_s^*, \tilde{d}_t) + \frac{1}{2} \delta Z_W C(W^+, \tilde{u}_s^*, \tilde{d}_t) + \frac{1}{2} [\delta \mathcal{Z}_{\tilde{u}}]_{su}^* C(W^+, \tilde{u}_s^*, \tilde{d}_t) \right. \\ &\quad \left. + \frac{1}{2} [\delta \mathcal{Z}_{\tilde{v}}]_{vt} C(W^+, \tilde{u}_s^*, \tilde{d}_v) \right] W_\mu^+ \tilde{u}_s^* \overleftrightarrow{\partial}^\mu \tilde{d}_t + \text{hc}. \end{aligned} \quad (6.20b)$$

From this counterterm Lagrangian the counterterm Feynman rules listed in Appendix C are deduced.

6.3.1 Feynman diagrams

The 1-loop QCD diagrams contributing to $\mathcal{M}_1^{\text{LL, QCD}}$ (Fig. 6.5) include triangle diagrams with gluino (a) and gluon exchange (b). Furthermore, two-point corrections of squark–gluon (c)-(d) and squark–squark (e) loops have to be included. The counterterm amplitude $\mathcal{M}_1^{\text{CT, QCD}}$ is represented by diagram (f). Real radiation diagrams accounting for $\mathcal{M}_1^{\text{real, QCD}}$ consist of gluon radiation of the external squarks (h)-(i) and the four-point interaction between squark–squark–gluon–W/Z-boson (g). The electroweak diagrams (Fig. 6.6) used for the calculation of $\mathcal{M}_1^{\text{LL, EW}}$ include triangle diagrams with quarks–neutralino/chargino

(a)-(c), squarks–Higgs-boson (d)-(e), squark–Higgs-boson–gauge-boson (f)-(g), squarks–gauge-bosons (h)-(i). There are also diagrams with two-point functions of squark–gauge-bosons (j)-(k), Higgs-boson–Higgs-boson (l), sfermion–sfermion (m), and gauge-boson–gauge-boson (n). For the counterterm amplitude $\mathcal{M}_1^{\text{CT,EW}}$, diagram (o) has to be evaluated. In addition to photon radiation of external squarks (s)-(t) the four-point interaction between squark–squark–gauge-boson–photon (p) contribute to $\mathcal{M}_1^{\text{real,EW}}$. Furthermore, when the external W-boson radiates a photon (r), the diagram with a Goldstone-boson propagator (q) has to be included.

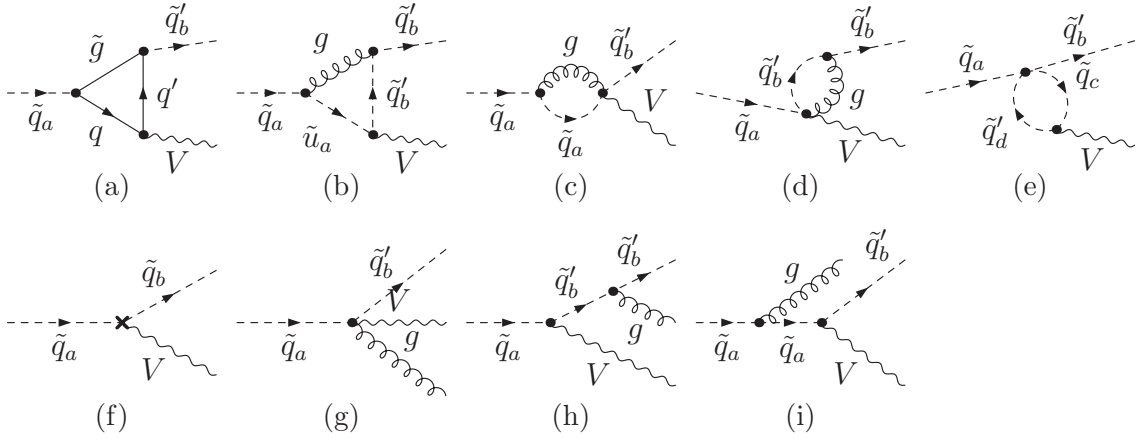


Figure 6.5: Generic Feynman diagrams contributing to QCD corrections to the process $\tilde{q}_a \rightarrow V \tilde{q}_b$: (a)-(e) virtual corrections, (f) counterterm diagrams and (g)-(i) real radiation diagrams. Notation as in Fig. 6.2.

6.3.2 Partial decay width and branching ratios

Referring to Chapter 3, the tree-level decay width is given by

$$\Gamma_0(\tilde{q}_a \rightarrow \tilde{q}_b V) = \frac{(2\pi)^4}{m_{\tilde{q}_a}} \int d\text{PS}_2 |\mathcal{M}_0|^2, \quad (6.21)$$

where V denotes the Z/W-boson and \mathcal{M}_0 the tree-level amplitude for the corresponding decay. The decay widths at NLO are obtained with the amplitudes computed from the Feynman diagrams in Subsection 6.3.1,

$$\Gamma_1^{\text{virt,EW/QCD}}(\tilde{q}_a \rightarrow \tilde{q}_b V) = \frac{(2\pi)^4}{m_{\tilde{q}_a}} \int d\text{PS}_2 2\text{Re} \left(\mathcal{M}_0 \mathcal{M}_1^{\text{EW/QCD}} \right) + \delta_{\text{soft}} \Gamma_0, \quad (6.22a)$$

$$\Gamma_1^{\text{real,EW/QCD}}(\tilde{q}_a \rightarrow \tilde{q}_b V) = \frac{(2\pi)^4}{m_{\tilde{q}_a}} \int d\text{PS}_3 |\mathcal{M}_1^{\text{real,EW/QCD}}|^2, \quad (6.22b)$$

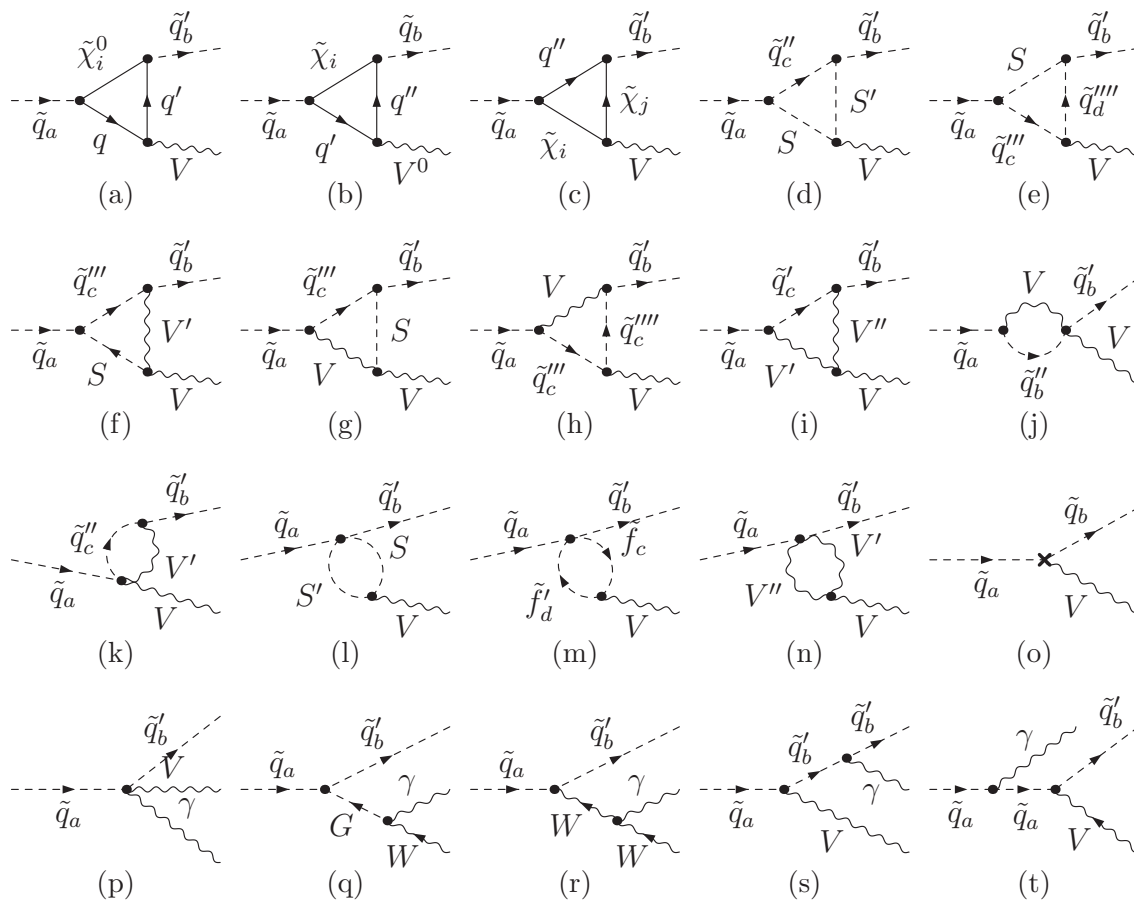


Figure 6.6: Generic Feynman diagrams contributing to electroweak corrections to the process $\tilde{q}_a \rightarrow V \tilde{q}'_b$: (a)-(n) virtual corrections, (o) counterterm diagrams and (p)-(t) real radiation diagrams. Notation as in Fig. 6.2.

where $\mathcal{M}_1^{\text{EW/QCD}} = \mathcal{M}_1^{1\text{L,EW/QCD}} + \mathcal{M}_1^{\text{CT,EW/QCD}}$. δ_{soft} denotes the soft-photon/gluon factor (4.116). Since there is no external massless particle, there are no collinear singularities and the collinear-photon/gluon factor does not appear. As we have seen in Subsection 4.1.3, there is a finite shift between the tree-level and on-shell masses of the left-handed down-type sfermions. In order not to spoil UV-finiteness, the on-shell masses only have to be inserted into terms of one-loop amplitudes $\mathcal{M}_1^{1\text{L,EW}}$ including the IR divergent loop-integrals C_0 . These terms involve the coupling between $\tilde{t}_2 \tilde{b}_1^* G^-$. In order to maintain IR-finiteness, the procedure described in Section 6.3.3 has to be applied. Finally, the EW/QCD NLO partial decay widths are given by

$$\Gamma_1^{\text{EW/QCD}}(\tilde{q}_a \rightarrow \tilde{q}'_b V) = \Gamma_1^{\text{virt,EW/QCD}}(\tilde{q}_a \rightarrow \tilde{q}'_b V) + \Gamma_1^{\text{real,EW/QCD}}(\tilde{q}_a \rightarrow \tilde{q}'_b V). \quad (6.23)$$

and the branching ratios are calculated with (3.14).

Real radiation

Alternatively, real radiation for the decay $\tilde{q}_a \rightarrow \tilde{q}_b Z$ has also been computed by integrating the 3-body phase space analytically. The decay width including real photon emission $\tilde{q}_a \rightarrow \tilde{q}_b Z \gamma$ (including soft and hard photons) in terms of the bremsstrahlung integrals given in Appendix A reads

$$\Gamma_1^{\text{real+soft,EW}} = \frac{4\pi\alpha m_{\tilde{q}_a}^2}{\pi\kappa} Q_{\tilde{q}}^2 \left(\frac{3M_Z^2}{\kappa^2} I - (I_0 + I_1 + m_{\tilde{q}_a}^2 I_{00} + m_{\tilde{q}_b}^2 I_{11} + (m_{\tilde{q}_a}^2 + m_{\tilde{q}_b}^2 - M_Z^2) I_{01}) \right) \Gamma_0, \quad (6.24)$$

where the charges of the squarks are given by $Q_{\tilde{q}}$ and their masses are denoted as $m_{\tilde{q}_a}, m_{\tilde{q}_b}$. Furthermore, the abbreviation $\kappa \equiv \kappa(m_{\tilde{q}_a}^2, m_{\tilde{q}_b}^2, M_Z^2)$ for the Källén function (3.2) is used. The decay width for real gluon radiation $\Gamma_1^{\text{real,QCD}}$ is obtained by replacing $Q_{\tilde{q}} \rightarrow 4/3$ and $\alpha \rightarrow \alpha_s$. The NLO decay width then is given by

$$\Gamma_1^{\text{EW/QCD}}(\tilde{q}_a \rightarrow \tilde{q}_b Z) = \frac{(2\pi)^4}{m_{\tilde{q}_a}} \int \text{dPS}_2 \, 2\text{Re} \left(\mathcal{M}_0 \mathcal{M}_1^{\text{EW/QCD}} \right) + \Gamma_1^{\text{real+soft,EW/QCD}}. \quad (6.25)$$

This yields exactly the same numerical results as the phase-space slicing method in the preceding subsection. However, in this approach it is not possible to extract kinematical distributions, since the phase space is integrated analytically. Therefore, in general we apply the phase space slicing method for all processes.

6.3.3 Dependent masses in squark–squark–Goldstone vertices

When computing the decay $\tilde{t}_2 \rightarrow \tilde{b}_1 W$ one has to take special care while inserting the on-shell mass of \tilde{b}_1 (cf. Section 4.3). In several one-loop diagrams in Fig. 6.6, the vertex

$\tilde{t}_2 \tilde{b}_1^* G^-$ appears. The Feynman rule for this vertex reads

$$\begin{aligned}
-iC(G^-, \tilde{t}_2, \tilde{b}_1^*) &= -\frac{ie}{\sqrt{2} M_W s_W t_\beta} \left(-t_\beta U_{2,2}^{\tilde{t}} U_{1,1}^{\tilde{b}} \underbrace{m_t \left(A_u - \frac{\mu}{t_\beta} \right)}_X \right. \\
&\quad \left. + t_\beta U_{2,1}^{\tilde{t}} \left(U_{1,2}^{\tilde{b}} \underbrace{m_b (A^b - \mu t_\beta)}_Y + U_{1,1}^{\tilde{b}} \underbrace{(m_b^2 - m_t^2 - c_{2\beta} M_W^2)}_Z \right) \right). \quad (6.26)
\end{aligned}$$

The expressions X , Y and Z can be written in terms of the squark masses. In order to maintain IR-finiteness, the tree-level value $m_{\tilde{b}_1}$ has to be replaced by the on-shell value $m_{\tilde{b}_1}^{\text{OS}}$. Terms X and Y can be replaced through linear combinations of the squark masses, using the relation

$$[\mathcal{D}_{\tilde{q}}]_{12} = [U^{\tilde{q}\dagger} \mathcal{M}_{\tilde{q}} U^{\tilde{q}}]_{12}, \quad \tilde{q} = \tilde{t}, \tilde{b}. \quad (6.27)$$

Expression Z , on the other hand, can be written in terms of the squark masses using

$$\tilde{M}_{11}^{\tilde{b}} - \tilde{M}_{11}^{\tilde{t}} = [U^{\tilde{b}\dagger} M^{\tilde{b}} U^{\tilde{b}}]_{11} - [U^{\tilde{t}\dagger} M^{\tilde{t}} U^{\tilde{t}}]_{11}. \quad (6.28)$$

Using these relations and inserting the on-shell value $m_{\tilde{b}_1}^{\text{OS}}$ one gets

$$X = |U_{11}^{\tilde{b}}|^2 m_{\tilde{b}_1}^{\text{OS}2} + |U_{21}^{\tilde{b}}|^2 m_{\tilde{b}_2}^2 - |U_{11}^{\tilde{t}}|^2 m_{\tilde{t}_1}^2 - |U_{21}^{\tilde{t}}|^2 m_{\tilde{t}_2}^2, \quad (6.29a)$$

$$Y = U_{11}^{\tilde{b}} U_{12}^{\tilde{b}} m_{\tilde{b}_1}^{\text{OS}2} + U_{21}^{\tilde{b}} U_{22}^{\tilde{b}} m_{\tilde{b}_2}^2, \quad (6.29b)$$

$$Z = U_{11}^{\tilde{t}} U_{12}^{\tilde{t}} m_{\tilde{t}_1}^2 + U_{21}^{\tilde{t}} U_{22}^{\tilde{t}} m_{\tilde{t}_2}^2. \quad (6.29c)$$

6.4 $\tilde{q}_a \rightarrow \tilde{q}_b h^0, H^0, A^0$ and $\tilde{q}_a \rightarrow \tilde{q}'_b H^\pm$

6.4.1 Counterterm Lagrangian

The cubic Higgs-boson-squark-squark interactions can be written in terms of the Lagrangian [22, 119]

$$\mathcal{L}_{S \tilde{q}_s^* \tilde{q}'_t} = \sum_{S, \tilde{q}_s, \tilde{q}'_t} C(S, \tilde{q}_s^*, \tilde{q}'_t) S \tilde{q}_s^* \tilde{q}'_t, \quad (6.30)$$

where S stands for any Higgs field of the MSSM. The cubic interaction terms $C(S, \tilde{q}_s^*, \tilde{q}'_t)$ are given by

$$\begin{aligned} C(H^+, \tilde{u}_s^*, \tilde{d}_t) &= \frac{g_2}{\sqrt{2} M_W} \left[U_{s1}^{\tilde{u}} U_{t1}^{\tilde{d}} \left(m_u^2 \frac{c_{\beta_c}}{s_\beta} + m_d^2 \frac{s_{\beta_c}}{c_\beta} - M_W^2 (s_\beta c_{\beta_c} + c_\beta s_{\beta_c}) \right) \right. \\ &\quad - U_{s1}^{\tilde{u}} U_{t2}^{\tilde{d}} m_d \left(\mu \frac{c_{\beta_c}}{c_\beta} - A_d \frac{s_{\beta_c}}{c_\beta} \right) - U_{s2}^{\tilde{u}} U_{t1}^{\tilde{d}} m_u \left(\mu \frac{s_{\beta_c}}{s_\beta} - A_u \frac{c_{\beta_c}}{s_\beta} \right) \\ &\quad \left. + U_{2s}^{\tilde{u}} U_{2t}^{\tilde{d}} \left(\frac{s_{\beta_c}}{c_\beta} + \frac{c_{\beta_c}}{s_\beta} \right) m_u m_d \right], \end{aligned} \quad (6.31a)$$

$$\begin{aligned} C(G^+, \tilde{u}_s^*, \tilde{d}_t) &= \frac{g_2}{\sqrt{2} M_W} \left[U_{s1}^{\tilde{u}} U_{t1}^{\tilde{d}} \left(m_u^2 \frac{s_{\beta_c}}{s_\beta} - m_d^2 \frac{c_{\beta_c}}{c_\beta} - M_W^2 (s_\beta s_{\beta_c} - c_\beta c_{\beta_c}) \right) \right. \\ &\quad - U_{s1}^{\tilde{u}} U_{t2}^{\tilde{d}} m_d \left(\mu \frac{s_{\beta_c}}{c_\beta} + A_d \frac{c_{\beta_c}}{c_\beta} \right) + U_{s2}^{\tilde{u}} U_{t1}^{\tilde{d}} m_u \left(\mu \frac{c_{\beta_c}}{s_\beta} + A_u \frac{s_{\beta_c}}{s_\beta} \right) \\ &\quad \left. + U_{2s}^{\tilde{u}} U_{2t}^{\tilde{d}} \left(\frac{s_{\beta_c}}{s_\beta} - \frac{c_{\beta_c}}{c_\beta} \right) m_u m_d \right], \end{aligned} \quad (6.31b)$$

$$C(H^0, \tilde{u}_s^*, \tilde{u}_t) = C_A(\tilde{u}_s^*, \tilde{u}_t) s_\alpha + C_\mu(\tilde{u}_s^*, \tilde{u}_t) c_\alpha - C_g(\tilde{u}_s^*, \tilde{u}_t) c_{\alpha+\beta}, \quad (6.31c)$$

$$C(h^0, \tilde{u}_s^*, \tilde{u}_t) = C_A(\tilde{u}_s^*, \tilde{u}_t) c_\alpha - C_\mu(\tilde{u}_s^*, \tilde{u}_t) s_\alpha + C_g(\tilde{u}_s^*, \tilde{u}_t) s_{\alpha+\beta}, \quad (6.31d)$$

$$C(H^0, \tilde{d}_s^*, \tilde{d}_t) = C_A(\tilde{d}_s^*, \tilde{d}_t) c_\alpha + C_\mu(\tilde{d}_s^*, \tilde{d}_t) s_\alpha - C_g(\tilde{d}_s^*, \tilde{d}_t) c_{\alpha+\beta}, \quad (6.31e)$$

$$C(h^0, \tilde{d}_s^*, \tilde{d}_t) = -C_A(\tilde{d}_s^*, \tilde{d}_t) s_\alpha + C_\mu(\tilde{d}_s^*, \tilde{d}_t) c_\alpha + C_g(\tilde{d}_s^*, \tilde{d}_t) s_{\alpha+\beta}, \quad (6.31f)$$

$$C(A^0, \tilde{u}_s^*, \tilde{u}_t) = \frac{i g_2 m_u s_{\beta_n}}{2 M_W s_\beta} \left(U_{s1}^{\tilde{u}} U_{t2}^{\tilde{u}} \left(\mu - \frac{A_u}{t_{\beta_n}} \right) - U_{s2}^{\tilde{u}} U_{t1}^{\tilde{u}} \left(\mu - \frac{A_u}{t_{\beta_n}} \right) \right), \quad (6.31g)$$

$$C(A^0, \tilde{d}_s^*, \tilde{d}_t) = \frac{i g_2 m_d c_{\beta_n}}{2 M_W c_\beta} \left(U_{s1}^{\tilde{d}} U_{t2}^{\tilde{d}} (\mu - A_d t_{\beta_n}) - U_{s2}^{\tilde{d}} U_{t1}^{\tilde{d}} (\mu - A_d t_{\beta_n}) \right), \quad (6.31h)$$

$$C(G^0, \tilde{u}_s^*, \tilde{u}_t) = \frac{i g_2 m_u c_{\beta_n}}{2 M_W s_\beta} \left(-U_{s1}^{\tilde{u}} U_{t2}^{\tilde{u}} (\mu + A_u t_{\beta_n}) + U_{s2}^{\tilde{u}} U_{t1}^{\tilde{u}} (\mu + A_u t_{\beta_n}) \right), \quad (6.31i)$$

$$C(G^0, \tilde{d}_s^*, \tilde{d}_t) = \frac{i g_2 m_d s_{\beta_n}}{2 M_W c_\beta} \left(U_{s1}^{\tilde{d}} U_{t2}^{\tilde{d}} \left(\mu + \frac{A_d}{t_{\beta_n}} \right) - U_{s2}^{\tilde{d}} U_{t1}^{\tilde{d}} \left(\mu + \frac{A_d}{t_{\beta_n}} \right) \right), \quad (6.31j)$$

with the abbreviations for the contributions via the trilinear couplings $A_{u,d}$,

$$C_A(\tilde{u}_s^*, \tilde{u}_t) \equiv \frac{g_2}{M_W s_\beta} \left[\frac{m_u A_u}{2} (U_{s1}^{\tilde{u}} U_{t2}^{\tilde{u}} + U_{s2}^{\tilde{u}} U_{t1}^{\tilde{u}}) - m_u^2 (U_{s1}^{\tilde{u}} U_{t1}^{\tilde{u}} + U_{s2}^{\tilde{u}} U_{t2}^{\tilde{u}}) \right], \quad (6.32a)$$

$$C_A(\tilde{d}_s^*, \tilde{d}_t) \equiv \frac{g_2}{M_W c_\beta} \left[\frac{m_d A_d}{2} (U_{s1}^{\tilde{d}} U_{t2}^{\tilde{d}} + U_{s2}^{\tilde{d}} U_{t1}^{\tilde{d}}) - m_d^2 (U_{s1}^{\tilde{d}} U_{t1}^{\tilde{d}} + U_{s2}^{\tilde{d}} U_{t2}^{\tilde{d}}) \right], \quad (6.32b)$$

the higgsino mass parameter μ ,

$$C_\mu(\tilde{u}_s^*, \tilde{u}_t) \equiv \frac{g_2 m_u \mu}{2 M_W s_\beta} (U_{s1}^{\tilde{u}} U_{t2}^{\tilde{u}} + U_{s2}^{\tilde{u}} U_{t1}^{\tilde{u}}), \quad (6.32c)$$

$$C_\mu(\tilde{d}_s^*, \tilde{d}_t) \equiv \frac{g_2 m_d \mu}{2 M_W c_\beta} (U_{s1}^{\tilde{d}} U_{t2}^{\tilde{d}} + U_{s2}^{\tilde{d}} U_{t1}^{\tilde{d}}), \quad (6.32d)$$

and the gauge coupling g_2 ,

$$C_g(\tilde{u}_s^*, \tilde{u}_t) \equiv \frac{g_2 M_W}{2} [U_{s1}^{\tilde{u}} U_{t1}^{\tilde{u}} (1 + (1 - 2Q_u)t_W^2) + 2Q_u U_{s2}^{\tilde{u}} U_{t2}^{\tilde{u}} t_W^2], \quad (6.32e)$$

$$C_g(\tilde{d}_s^*, \tilde{d}_t) \equiv -\frac{g_2 M_W}{2} [U_{s1}^{\tilde{d}} U_{t1}^{\tilde{d}} (1 + (1 + 2Q_d)t_W^2) - 2Q_d U_{s2}^{\tilde{d}} U_{t2}^{\tilde{d}} t_W^2]. \quad (6.32f)$$

We distinguish between β_n, β_c and β , since the parameter β has to be renormalized whereas the mixing angles α, β_n and β_c need not to as already explained in Subsection 4.1.3. This distinction becomes important when computing the counterterms below.

Again, the counterterm Lagrangian is obtained inserting the transformations for the squark fields, the Higgs fields (4.23), and for the couplings (6.31),

$$C(\dots) \rightarrow C(\dots) + \delta C(\dots). \quad (6.33)$$

This results in the following counterterm Lagrangian,

$$\begin{aligned} \delta \mathcal{L}_{S \tilde{q}_s^* \tilde{q}'_t} = & \sum_{S, \tilde{q}_s^*, \tilde{q}'_t} \left[\delta C(S, \tilde{q}_s^*, \tilde{q}'_t) + \frac{1}{2} [\delta \mathcal{Z}_{\tilde{q}}]_{su}^* C(S, \tilde{q}_s^*, q'_t) + \frac{1}{2} [\delta \mathcal{Z}_{\tilde{q}}]_{tv} C(S, \tilde{q}_u^*, q'_v) \right] S \tilde{q}_s^* \tilde{q}'_t \\ & + \sum_{\tilde{q}} \left[\left(\frac{1}{2} \delta Z_{h^0 h^0} C(h^0, \tilde{q}_s^*, \tilde{q}_t) + \frac{1}{2} \delta Z_{h^0 H^0} C(H^0, \tilde{q}_s^*, \tilde{q}_t) \right) h^0 \tilde{q}_s^* \tilde{q}_t \right. \\ & + \left(\frac{1}{2} \delta Z_{H^0 H^0} C(H^0, \tilde{q}_s^*, \tilde{q}_t) + \frac{1}{2} \delta Z_{h^0 H^0} C(h^0, \tilde{q}_s^*, \tilde{q}_t) \right) H^0 \tilde{q}_s^* \tilde{q}_t \\ & + \left(\frac{1}{2} \delta Z_{A^0 A^0} C(A^0, \tilde{q}_s^*, \tilde{q}_t) + \frac{1}{2} \delta Z_{A^0 G^0} C(G^0, \tilde{q}_s^*, \tilde{q}_t) \right) A^0 \tilde{q}_s^* \tilde{q}_t \\ & + \left. \left(\frac{1}{2} \delta Z_{G^0 G^0} C(G^0, \tilde{q}_s^*, \tilde{q}_t) + \frac{1}{2} \delta Z_{A^0 G^0} C(A^0, \tilde{q}_s^*, \tilde{q}_t) \right) G^0 \tilde{q}_s^* \tilde{q}_t \right] \\ & + \sum_{\tilde{q}, \tilde{q}'} \left[\left(\frac{1}{2} \delta Z_{H^\pm H^\mp} C(H^\pm, \tilde{q}_s^*, \tilde{q}'_t) + \frac{1}{2} \delta Z_{H^\pm G^\mp} C(G^\pm, \tilde{q}_s^*, \tilde{q}'_t) \right) H^\pm \tilde{q}_s^* \tilde{q}'_t \right. \\ & + \left. \left(\frac{1}{2} \delta Z_{G^\pm G^\mp} C(G^\pm, \tilde{q}_s^*, \tilde{q}'_t) + \frac{1}{2} \delta Z_{H^\mp G^\pm} C(H^\pm, \tilde{q}_s^*, \tilde{q}'_t) \right) G^\pm \tilde{q}_s^* \tilde{q}'_t \right]. \quad (6.34) \end{aligned}$$

The coupling renormalization constants $\delta C(S, \tilde{q}_s^*, \tilde{q}'_t)$ are given in Appendix B.3 and the resulting counterterm Feynman rules are listed in Appendix C.

Furthermore, we need the counterterms for $W^\pm - H^\pm$ and $Z - A^0$ mixing depicted in Fig. 6.9. They stem from the kinetic terms of the Higgs fields

$$(D_\mu H_1)^\dagger (D^\mu H_1) + (D_\mu H_2)^\dagger (D^\mu H_2). \quad (6.35)$$

Renormalizing the parameters and fields respectively, the counterterm Lagrangian for the $A^0 - Z$ and $H^\pm - W^\pm$ interactions reads

$$\delta \mathcal{L} = -M_Z \left(c_\beta^2 \delta t_\beta + \frac{1}{2} \delta Z_{A^0 G^0} \right) Z_\mu \partial^\mu A^0 \pm \left(c_\beta^2 \delta t_\beta + \frac{1}{2} \delta Z_{G^\pm H^\mp} \right) W_\mu^\pm \partial^\mu H^\mp. \quad (6.36)$$

6.4.2 Feynman diagrams

The genuine 1-loop QCD amplitudes $\mathcal{M}_1^{1L,QCD}$ are computed via triangle diagrams (Fig. 6.7) with gluino (a) and gluon exchange (b). Furthermore, the α_s -dependent part of the four-squark vertex is present in diagram (c). The counterterm amplitude $\mathcal{M}_1^{CT,QCD}$ is given in terms of the counterterm diagram (d). Real radiation consists of diagrams, where the in- and outgoing squarks radiate a gluon (e)-(f) and contribute to $\mathcal{M}_1^{\text{real},QCD}$.

For the virtual EW amplitudes $\mathcal{M}_1^{1L,EW}$, triangle diagrams (Fig. 6.8) with quarks–neutralinos or quark–charginos (a)-(c), squarks–Higgs-bosons (d)-(f), squark–Higgs-boson–gauge-boson (g)-(h), and squarks–gauge-bosons (i)-(j) have to be computed. Further corrections including two-point functions with squark–Higgs-boson (k)-(l), Higgs-boson–Higgs-boson (m), and sfermion–sfermion (n) are present. Note, that the diagrams (b), (f) and (j) only appear for the decays into neutral Higgs-bosons. The counterterm amplitude $\mathcal{M}_1^{CT,EW}$ consists of diagrams (o). The real radiation amplitude $\mathcal{M}_1^{\text{real},EW}$ is computed with diagrams (p)-(r), where (p) only appears in processes with external charged Higgs bosons. When the squark decays into the CP-odd or charged Higgs boson, the mixing between the Higgs and the Z/W boson has to be taken into account. These diagrams are drawn in Fig. 6.9. The 1-loop amplitude $\mathcal{M}_1^{1L,EW}$ then also consists of diagrams with SM fermions (a,f), neutralinos/charginos (b,g), Higgs boson (c,h), sfermion (d,i), and sfermion–gauge-boson (e,j) bubble diagrams. In this case, also the counterterm amplitude $\mathcal{M}_1^{CT,EW}$ has to include counterterm diagram (k,l).

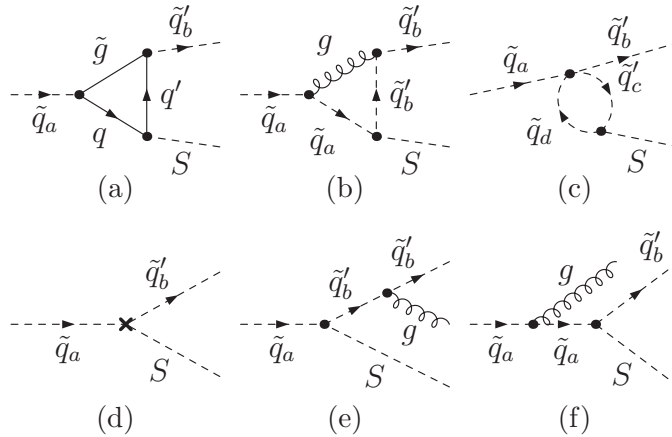


Figure 6.7: Generic Feynman diagrams contributing to QCD corrections to the process $\tilde{q}_a \rightarrow H \tilde{q}'_b$: (a)-(c) virtual corrections, (d) counterterm diagrams and (e)-(f) real radiation diagrams. Notation as in Fig. 6.2.

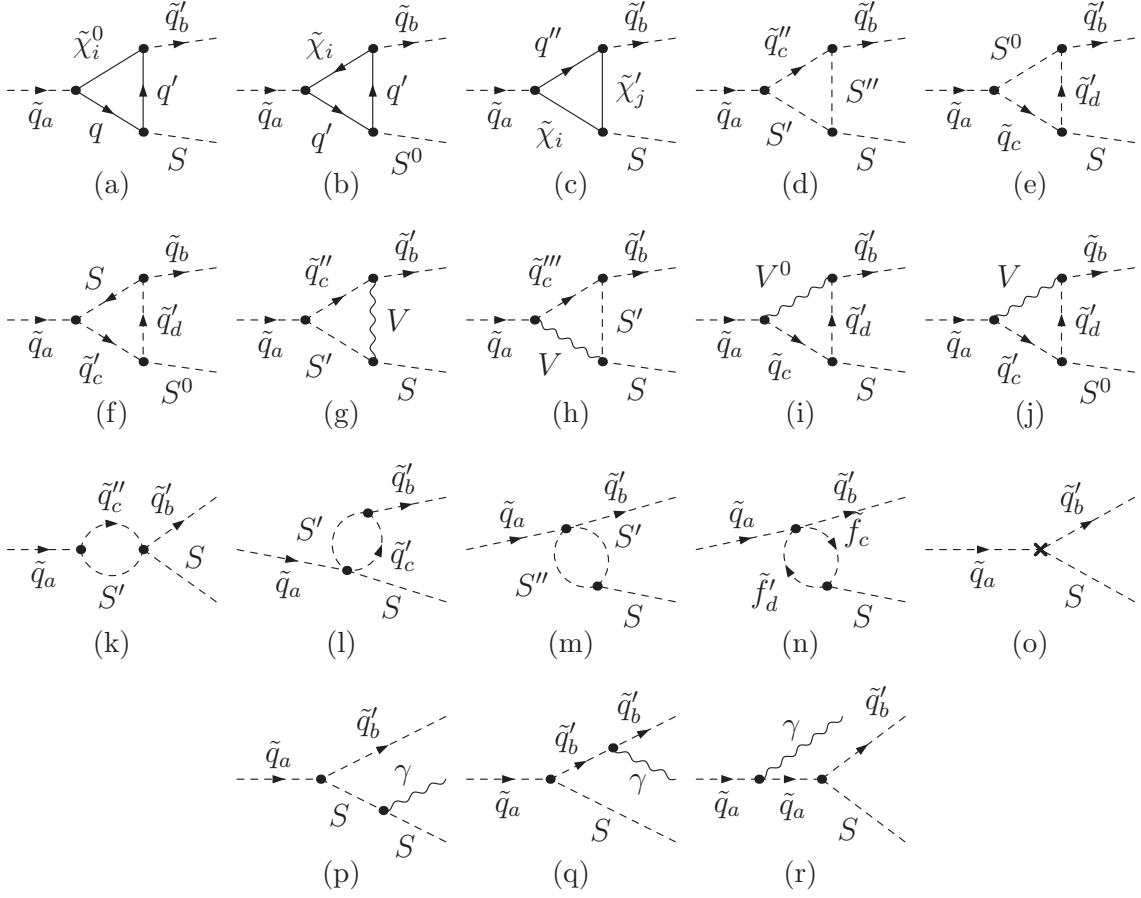


Figure 6.8: Generic Feynman diagrams contributing to electroweak corrections to the process $\tilde{q}_a \rightarrow H \tilde{q}'_b$: (a)-(n) virtual corrections, (o) counterterm diagrams, (p)-(r) real radiation diagrams. Notation as in Fig. 6.2.

6.4.3 Partial decay widths and branching ratios

Referring to Chapter 3, the partial tree-level decay width for the decay of a squark into squark plus Higgs boson reads

$$\Gamma_0(\tilde{q}_a \rightarrow \tilde{q}'_b S) = \frac{(2\pi)^4}{m_{\tilde{q}_a}} \int d\text{PS}_2 |\mathcal{M}_0|^2, \quad (6.37)$$

where S denotes any of the five physical Higgs bosons and \mathcal{M}_0 the corresponding tree-level amplitude. The computations of the partial decay widths beyond leading order will be divided between the decays $\tilde{q}_a \rightarrow \tilde{q}_b (h^0, H^0)$ (Subsection 6.4.4) and $\tilde{q}_a \rightarrow \tilde{q}'_b (A^0, H^\pm)$ (Subsection 6.4.6).

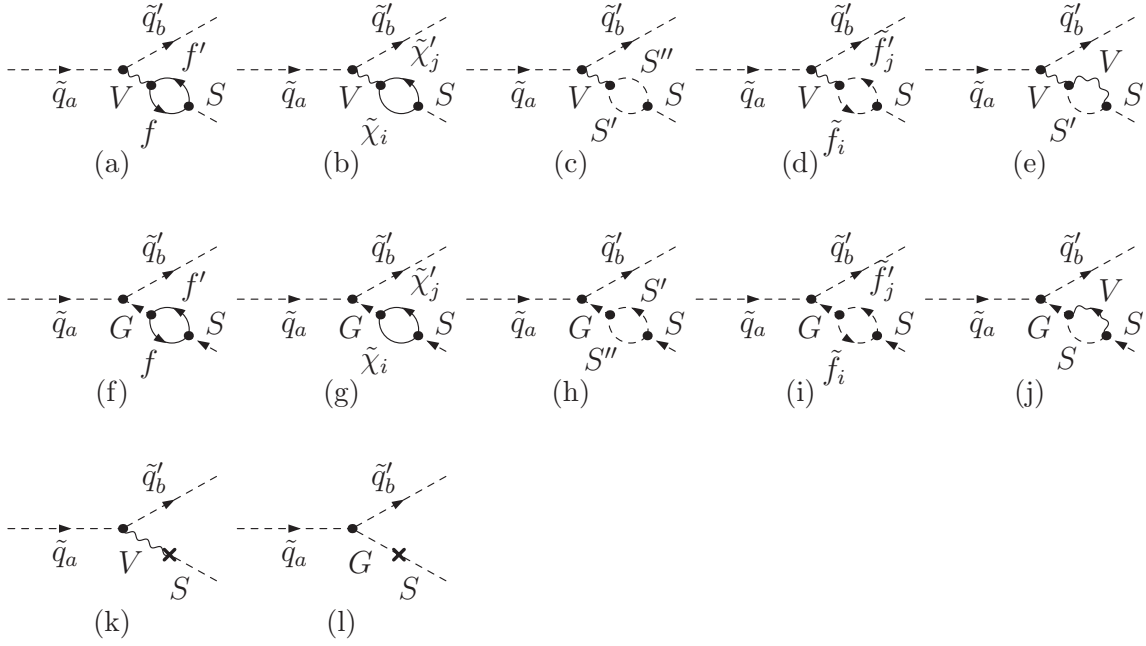


Figure 6.9: Generic Feynman diagrams contributing to Higgs–gauge-boson mixing for the process $\tilde{q}_a \rightarrow H \tilde{q}'_b$. In this case (V, S) stands for (Z, A^0) or (W, S) . Otherwise, the notation is as in Fig. 6.2.

6.4.4 $\tilde{q}_a \rightarrow \tilde{q}_b (h^0, H^0)$

When computing squark decays into (on-shell) Higgs bosons beyond leading order, the finite wave-function normalization factors Z_i (4.31a) and Z_{ij} (4.31b) have to be included. For decays into the neutral CP-even Higgs bosons this implies a mixing between amplitudes with external h and H . This is worked out in detail in Subsection 4.1.3.

Improved Born approximation

It has been shown in [45] that in large MSSM parameter regions the improved Born approximation [45, 120] containing the Yukawa contributions of $\mathcal{O}(G_F m_t^4 / M_W^2)$ deviates from the complete one-loop calculation only by a few percent. The improved Born approximation includes the effects from the Higgs propagator corrections using the finite Z -factors (4.31a, 4.31b). The improved amplitude \mathcal{M}_0^Z is obtained by summing over the tree-level amplitudes $\mathcal{M}_{0,\{h^0, H^0\}}$, weighted by the appropriate Z -factors¹,

$$\mathcal{M}_0^Z(\tilde{q}_2 \rightarrow \tilde{q}_1 h^0) = \sqrt{Z_{h^0}} (\mathcal{M}_{0,h^0} + Z_{h^0 H^0} \mathcal{M}_{0,H^0}), \quad (6.38a)$$

$$\mathcal{M}_0^Z(\tilde{q}_2 \rightarrow \tilde{q}_1 H^0) = \sqrt{Z_{H^0}} (\mathcal{M}_{0,H^0} + Z_{H^0 h^0} \mathcal{M}_{0,h^0}). \quad (6.38b)$$

¹The subscripts h^0 and H^0 denote the amplitudes for the processes $\tilde{q}_2 \rightarrow \tilde{q}_1 h^0$ and $\tilde{q}_2 \rightarrow \tilde{q}_1 H^0$, respectively.

The partial decay widths improved by Z -factors then read

$$\Gamma_0^Z(\tilde{q}_2 \rightarrow \tilde{q}_1 h^0) = \frac{(2\pi)^4}{m_{\tilde{q}_2}} \int \text{dPS}_2 |\mathcal{M}_0^Z(\tilde{q}_2 \rightarrow \tilde{q}_1 h^0)|^2, \quad (6.39a)$$

$$\Gamma_0^Z(\tilde{q}_2 \rightarrow \tilde{q}_1 H^0) = \frac{(2\pi)^4}{m_{\tilde{q}_2}} \int \text{dPS}_2 |\mathcal{M}_0^Z(\tilde{q}_2 \rightarrow \tilde{q}_1 H^0)|^2. \quad (6.39b)$$

One-loop corrections

In order to have the right on-shell properties for the external h^0 and H^0 bosons, the one-loop amplitudes and decay widths have to be multiplied with the field renormalization factors Z . The amplitudes for virtual EW/QCD corrections then read

$$\mathcal{M}_1^{\text{EW/QCD}}(\tilde{q}_2 \rightarrow \tilde{q}_1 h^0) = \sqrt{Z_{h^0}} \left(\mathcal{M}_{1,h^0}^{\text{EW/QCD}} + Z_{h^0 H^0} \mathcal{M}_{1,H^0}^{\text{EW/QCD}} \right), \quad (6.40a)$$

$$\mathcal{M}_1^{\text{EW/QCD}}(\tilde{q}_2 \rightarrow \tilde{q}_1 H^0) = \sqrt{Z_{H^0}} \left(\mathcal{M}_{1,H^0}^{\text{EW/QCD}} + Z_{H^0 h^0} \mathcal{M}_{1,h^0}^{\text{EW/QCD}} \right), \quad (6.40b)$$

where $\mathcal{M}_{1,\{h^0, H^0\}}^{\text{EW/QCD}} = \mathcal{M}_{1,\{h^0, H^0\}}^{\text{1L,EW/QCD}} + \mathcal{M}_{1,\{h^0, H^0\}}^{\text{CT,EW/QCD}}$ are the amplitudes with external h^0/H^0 boson listed in Subsection 6.4.2. Similarly, for the real corrections we get

$$\mathcal{M}_1^{\text{real,EW/QCD}}(\tilde{q}_2 \rightarrow \tilde{q}_1 h^0) = \sqrt{Z_{h^0}} \left(\mathcal{M}_{1,h^0}^{\text{real,EW/QCD}} + Z_{h^0 H^0} \mathcal{M}_{1,H^0}^{\text{real,EW/QCD}} \right), \quad (6.41a)$$

$$\mathcal{M}_1^{\text{real,EW/QCD}}(\tilde{q}_2 \rightarrow \tilde{q}_1 H^0) = \sqrt{Z_{H^0}} \left(\mathcal{M}_{1,H^0}^{\text{real,EW/QCD}} + Z_{H^0 h^0} \mathcal{M}_{1,h^0}^{\text{real,EW/QCD}} \right), \quad (6.41b)$$

where $\mathcal{M}_{1,\{h^0, H^0\}}^{\text{real,EW/QCD}}$ denote the amplitudes for real photon/gluon radiation with external Higgs boson h^0/H^0 . The partial decay widths for the virtual and real corrections, using this amplitudes, then are

$$\Gamma_1^{\text{virt,EW/QCD}}(\tilde{q}_2 \rightarrow \tilde{q}_1 h^0/H^0) = \frac{(2\pi)^4}{m_{\tilde{q}_2}} \int \text{dPS}_2 2\text{Re} \left[\mathcal{M}_1^{Z*} \mathcal{M}_1^{\text{EW/QCD}} \right] + \delta_{\text{soft}} \Gamma_0^Z, \quad (6.42a)$$

$$\Gamma_1^{\text{real,EW/QCD}}(\tilde{q}_2 \rightarrow \tilde{q}_1 h^0/H^0) = \frac{(2\pi)^4}{m_{\tilde{q}_2}} \int \text{dPS}_3 |\mathcal{M}_1^{\text{real,EW/QCD}}|^2, \quad (6.42b)$$

where dPS_3 denotes the 3-body phase-space element (c.f. Chapter 3) and δ_{soft} the soft-photon/gluon factor. Hence, the partial decay width at NLO is given by

$$\begin{aligned} \Gamma_1^{\text{EW/QCD}}(\tilde{q}_2 \rightarrow \tilde{q}_1 h^0/H^0) &= \Gamma_1^{\text{virt,EW/QCD}}(\tilde{q}_2 \rightarrow \tilde{q}_1 h^0/H^0) \\ &\quad + \Gamma_1^{\text{real,EW/QCD}}(\tilde{q}_2 \rightarrow \tilde{q}_1 h^0/H^0). \end{aligned} \quad (6.43)$$

6.4.5 Real radiation

In addition to the phase-space slicing method of the preceding subsection, the real radiation was computed integrating the 3-body phase space analytically. In terms of the

bremsstrahlung integrals including soft and hard photon radiation given in Appendix A, the decay width for the real radiation process $\tilde{q}_2 \rightarrow \tilde{q}_1 h^0/H^0 \gamma$ can be written as

$$\Gamma_1^{\text{real+soft,EW}} = -\frac{4\alpha m_{\tilde{q}_2}^2}{\pi\kappa\left(m_{\tilde{q}_2}^2, m_{\tilde{q}_1}^2, M_{h^0/H^0}^2\right)} \left(m_{\tilde{q}_2}^2 Q_{\tilde{q}}^2 I_{00} + m_{\tilde{q}_1}^2 Q_{\tilde{q}}^2 I_{11} + Q_{\tilde{q}}^2 (I_0 + I_1 + (m_{\tilde{q}_2}^2 + m_{\tilde{q}_1}^2 - M_{h^0, H^0}^2) I_{01})\right) \Gamma_0^Z, \quad (6.44)$$

where Q_i, m_i denote the charge and mass of the particle i and κ the Källén function (3.2). The decay width for real gluon radiation is obtained by setting $Q_0^2 = Q_1^2 = Q_0 Q_1 = 4/3$, $Q_2 = 0$ and replacing $\alpha \rightarrow \alpha_s$.

Thus, the partial decay width at NLO is then given by

$$\Gamma_1^{\text{EW/QCD}}(\tilde{q}_2 \rightarrow \tilde{q}_1 h^0/H^0) = \frac{(2\pi)^4}{m_{\tilde{q}_2}} \int \text{dPS}_2 2\text{Re} \left[\mathcal{M}_1^{Z*} \mathcal{M}_1^{\text{EW/QCD}} \right] + \Gamma_1^{\text{real+soft,EW/QCD}}. \quad (6.45)$$

Numerically, the decay widths obtained with the analytical bremsstrahlung integrals yield the same result as the phase-space slicing result described in the preceding subsection.

6.4.6 $\tilde{q}_a \rightarrow \tilde{q}'_b (A^0, H^\pm)$

The decay widths at NLO are obtained with the amplitudes computed from the Feynman diagrams in Subsection 6.4.2,

$$\Gamma_1^{\text{virt,EW/QCD}}(\tilde{q}_a \rightarrow \tilde{q}'_b (A^0, H^\pm)) = \frac{(2\pi)^4}{m_{\tilde{q}_a}} \int \text{dPS}_2 2\text{Re} \left(\mathcal{M}_0 \mathcal{M}_1^{\text{EW/QCD}} \right) + \delta_{\text{soft}} \Gamma_0, \quad (6.46a)$$

$$\Gamma_1^{\text{real,EW/QCD}}(\tilde{q}_a \rightarrow \tilde{q}'_b (A^0, H^\pm)) = \frac{(2\pi)^4}{m_{\tilde{q}_a}} \int \text{dPS}_3 |\mathcal{M}_1^{\text{real,EW/QCD}}|^2, \quad (6.46b)$$

Since the A^0 and H^\pm fields are renormalized according to the $\overline{\text{DR}}$ scheme, the EW one-loop amplitudes have to include the finite factors

$$\sqrt{\hat{Z}_{A^0}} \simeq 1 - \frac{1}{2} \delta \hat{Z}_{A^0} \equiv 1 - \frac{1}{2} \text{Re} \frac{\partial}{\partial p^2} \hat{\Sigma}_{A^0} \Big|_{p^2=m_{A^0}^2}, \quad (6.47a)$$

$$\sqrt{\hat{Z}_{H^\pm}} \simeq 1 - \frac{1}{2} \delta \hat{Z}_{H^\pm} \equiv 1 - \frac{1}{2} \text{Re} \frac{\partial}{\partial p^2} \hat{\Sigma}_{H-H^\pm} \Big|_{p^2=m_{H^\pm}^2}, \quad (6.47b)$$

with the $\overline{\text{DR}}$ renormalized self energies $\hat{\Sigma}$ (4.26). The infrared divergence contained in δZ^{H^\pm} is canceled with the one from soft radiation (explicitly the soft divergent part in the square of the diagrams Fig. 6.8 (p)). Hence, the amplitudes $\mathcal{M}_1^{\text{EW}}$ for squark decays into A^0 and H^\pm are given by

$$\mathcal{M}_1^{\text{EW}}(\tilde{q}_a \rightarrow \tilde{q}_b A^0) = \mathcal{M}_1^{\text{1L,EW}} + \mathcal{M}_1^{\text{CT,EW}} - \frac{1}{2} \mathcal{M}_0 \delta \hat{Z}_{A^0}, \quad (6.48a)$$

$$\mathcal{M}_1^{\text{EW}}(\tilde{q}_a \rightarrow \tilde{q}'_b H^\pm) = \mathcal{M}_1^{\text{1L,EW}} + \mathcal{M}_1^{\text{CT,EW}} - \frac{1}{2} \mathcal{M}_0 \delta Z_{H^\pm}. \quad (6.48b)$$

Finally, the decay widths at NLO are given by

$$\Gamma_1^{\text{EW/QCD}}(\tilde{q}_a \rightarrow \tilde{q}_b A^0) = \Gamma_1^{\text{virt,EW/QCD}}(\tilde{q}_a \rightarrow \tilde{q}_b A^0) + \Gamma_1^{\text{real,EW/QCD}}(\tilde{q}_a \rightarrow \tilde{q}_b A^0), \quad (6.49a)$$

$$\Gamma_1^{\text{EW/QCD}}(\tilde{q}_a \rightarrow \tilde{q}'_b H^\pm) = \Gamma_1^{\text{virt,EW/QCD}}(\tilde{q}_a \rightarrow \tilde{q}'_b H^\pm) + \Gamma_1^{\text{real,EW/QCD}}(\tilde{q}_a \rightarrow \tilde{q}'_b H^\pm). \quad (6.49b)$$

Chapter 7

Squark decays: numerical evaluation

In the previous chapter the computation of NLO corrections to squark decays was discussed. In this chapter the decay widths including the computed NLO corrections are numerically evaluated. First, in Section 7.1 the input parameters are given and the decay widths and branching ratios are subsequently evaluated in Section 7.2. Following, the numerical impact of using the correct on-shell values for the dependent particles is discussed in Subsection 7.2.1. In Section 7.3 different parameter dependence studies with respect to the relevant parameters, $\tan\beta$, the CP-odd Higgs-boson mass m_{A^0} , and the trilinear couplings A_t , A_b are performed. Also, a two-dimensional parameter scan varying squark (M_{SUSY}) and gluino (M_3) masses is presented. In Section 7.4 the impact of NLO corrections to differential kinematic distributions of quark jets in the decays of squarks into quark and neutralino are discussed. Finally, in Section 7.5 our results are compared with the results obtained with SFOLD [102].

7.1 Input parameters

The SM parameters are chosen in correspondence with [16],

$$\begin{aligned} M_Z &= 91.1876 \text{ GeV}, & M_W &= 80.399 \text{ GeV}, \\ \alpha^{-1} &= 137.036, & \alpha_S(M_Z) &= 0.118, \\ m_t &= 172.0 \text{ GeV}, & m_b^{\overline{\text{MS}}}(M_Z) &= 2.94 \text{ GeV}. \end{aligned} \tag{7.1}$$

The MSSM with real parameters in minimal flavor violation (MFV) counts 30 parameters in addition to the aforementioned SM parameters. In order to simplify numerical studies and to be able to interpret them, it is necessary to reduce the number of parameters. This is usually done by assuming specific models of SUSY breaking or classes of simplified models [121]. The following numerical studies will be performed in benchmark scenarios based on the minimal supergravity breaking mechanism mSUGRA [122]. Because of the natural link of SUSY models to grand unified theories (GUTs), the boundary conditions imposed by mSUGRA and parameters describing the model are given at the GUT scale.

For the following analyses we chose benchmark scenarios where the gluino is heavier than the squarks. Otherwise, the decays of the squarks into gluinos would predominate over all other decay channels. The decay of squarks into gluinos is then part of the study in the parameter scan in Subsection 7.3.5. Hence, the numerical evaluation is performed at the Snowmass Points SPS1a' [55, 123]

$$\begin{aligned} M_0 = 70 \text{ GeV}, \quad M_{1/2} = 150 \text{ GeV}, \quad A_0 = -300 \text{ GeV}, \\ \tan \beta = 10, \quad \text{sgn } \mu > 0, \end{aligned} \quad (7.2)$$

and SPS4

$$\begin{aligned} M_0 = 400 \text{ GeV}, \quad M_{1/2} = 300 \text{ GeV}, \quad A_0 = 0 \text{ GeV}, \\ \tan \beta = 50, \quad \text{sgn } \mu > 0. \end{aligned} \quad (7.3)$$

The Snowmass Points are already under pressure [124] from ATLAS [125] and CMS SUSY searches [126]. Since these analyses have been made under simplifying assumptions (e.g. simplified SUSY models, global K-factors for production processes, and no higher-order corrections for sparticle decays), numerical examinations in these challenged regions are important to study the quality of the used approximations in the experimental analyses. In order to adapt to the recent SUSY limits, updated benchmark scenarios have been proposed in [127]. From these benchmark scenarios we chose Point 10.1.1 with the GUT-scale parameters,

$$\begin{aligned} M_0 = 125 \text{ GeV}, \quad M_{1/2} = 550 \text{ GeV}, \quad A_0 = 0 \text{ GeV}, \\ \tan \beta = 10, \quad \text{sgn } \mu > 0. \end{aligned} \quad (7.4)$$

With the spectrum calculator Softsusy 3.1.7 [128] the SUSY parameters in the $\overline{\text{DR}}$ scheme at the scale $Q_{\text{SUSY}} = 1 \text{ TeV}$ are obtained, which is in accordance with the SPA convention [55]. However, in our calculation, the SUSY parameters are defined in the on-shell (OS) scheme. Hence, the $\overline{\text{DR}}$ SUSY parameters are converted into the OS scheme according to the procedure described in Appendix D. The only exception is given by the trilinear couplings in the b and τ sector which are renormalized according to the $\overline{\text{DR}}$ scheme as described in Section 4.1.2. In general, tree-level Higgs-boson masses get large radiative corrections. Since especially third-generation squarks can also decay into their lighter partners plus Higgs bosons, it is important that these corrections are incorporated. This is done with the help of FeynHiggs 2.7.4 [29] where one- and leading two-loop corrections to the Higgs-boson masses are computed. These corrected masses are used as OS masses for the external particles and for Higgs bosons propagating in loops. The OS SUSY parameters and mass spectra of the relevant particles (squarks, gauginos and Higgs bosons) are summarized in Tabs. 7.1, 7.2 for SPS1a', in Tabs. 7.3, 7.4 for SPS4, and in Tabs. 7.5, 7.6 for the Point 10.1.1. Note, that the input parameters and results are given in a precision much higher than the uncertainties from missing higher-order contributions would allow for. This is done to provide for comparison with our results.

These parameter points are also used as a starting point to study parameter dependences in Subsection 7.3.

$M_{A^0} = 418.51 \text{ GeV}$	$\tan \beta = 9.65$	$\mu = 386.96 \text{ GeV}$
$M_1 = 100.50 \text{ GeV}$	$M_2 = 197.48 \text{ GeV}$	$M_3 = 608.17 \text{ GeV}$
$M_{\tilde{t}_L^{(1,2)}} = 181.07 \text{ GeV}$	$M_{\tilde{e}_R^{(1,2)}} = 115.67 \text{ GeV}$	
$M_{\tilde{t}_L^{(3)}} = 179.41 \text{ GeV}$	$M_{\tilde{\tau}_R} = 110.34 \text{ GeV}$	
$M_{\tilde{q}_L^{(1,2)}} = 559.79 \text{ GeV}$	$M_{\tilde{u}_R^{(1,2)}} = 540.91 \text{ GeV}$	$M_{\tilde{d}_R^{(1,2)}} = 539.03 \text{ GeV}$
$M_{\tilde{q}_L^{(3)}} = 493.93 \text{ GeV}$	$M_{\tilde{t}_R} = 404.02 \text{ GeV}$	$M_{\tilde{b}_R} = 526.65 \text{ GeV}$
$A_\tau = -445.80 \text{ GeV}$	$A_t = -514.37 \text{ GeV}$	$A_b = -938.42 \text{ GeV}$

Table 7.1: SUSY-breaking on-shell parameters for the parameter point SPS1a' [55, 123].

$m_{h^0} = 112.18 \text{ GeV}$	$m_{H^0} = 418.73 \text{ GeV}$	$m_{A^0} = 418.51 \text{ GeV}$	$m_{H^\pm} = 426.44 \text{ GeV}$
$m_{\tilde{\chi}_1^0} = 97.95 \text{ GeV}$	$m_{\tilde{\chi}_2^0} = 183.44 \text{ GeV}$	$m_{\tilde{\chi}_3^0} = 395.15 \text{ GeV}$	$m_{\tilde{\chi}_4^0} = 408.66 \text{ GeV}$
$m_{\tilde{\chi}_1^\pm} = 183.14 \text{ GeV}$	$m_{\tilde{\chi}_2^\pm} = 410.02 \text{ GeV}$		$m_{\tilde{g}} = 608.17 \text{ GeV}$
$m_{\tilde{u}_L} = 557.23 \text{ GeV}$	$m_{\tilde{u}_R} = 539.79 \text{ GeV}$	$m_{\tilde{d}_L} = 562.69 \text{ GeV}$	$m_{\tilde{d}_R} = 539.59 \text{ GeV}$
$m_{\tilde{t}_1} = 357.64 \text{ GeV}$	$m_{\tilde{t}_2} = 578.26 \text{ GeV}$	$m_{\tilde{b}_1} = 497.84 \text{ GeV}$	$m_{\tilde{b}_2} = 530.51 \text{ GeV}$

Table 7.2: On-shell masses of Higgs bosons, gauginos and squarks for the parameter point SPS1a' [55, 123]. Masses of the Higgs bosons include 1- and 2-loop corrections obtained with FeynHiggs 2.6.5.

$M_{A^0} = 177.24 \text{ GeV}$	$\tan \beta = 49.35$	$\mu = 368.94 \text{ GeV}$
$M_1 = 122.81 \text{ GeV}$	$M_2 = 240.95 \text{ GeV}$	$M_3 = 731.20 \text{ GeV}$
$M_{\tilde{t}_L^{(1,2)}} = 446.57 \text{ GeV}$	$M_{\tilde{e}_R^{(1,2)}} = 414.98 \text{ GeV}$	
$M_{\tilde{t}_L^{(3)}} = 392.57 \text{ GeV}$	$M_{\tilde{\tau}_R} = 407.59 \text{ GeV}$	
$M_{\tilde{q}_L^{(1,2)}} = 764.36 \text{ GeV}$	$M_{\tilde{u}_R^{(1,2)}} = 745.73 \text{ GeV}$	$M_{\tilde{d}_R^{(1,2)}} = 743.76 \text{ GeV}$
$M_{\tilde{q}_L^{(3)}} = 555.85 \text{ GeV}$	$M_{\tilde{t}_R} = 625.03 \text{ GeV}$	$M_{\tilde{b}_R} = 601.61 \text{ GeV}$
$A_\tau = -445.80 \text{ GeV}$	$A_t = 444.73 \text{ GeV}$	$A_b = -636.24 \text{ GeV}$

Table 7.3: SUSY-breaking on-shell parameters for the parameter point SPS4 [123].

$m_{h^0} = 112.36 \text{ GeV}$	$m_{H^0} = 176.77 \text{ GeV}$	$m_{A^0} = 177.25 \text{ GeV}$	$m_{H^\pm} = 164.22 \text{ GeV}$
$m_{\tilde{\chi}_1^0} = 120.61 \text{ GeV}$	$m_{\tilde{\chi}_2^0} = 223.87 \text{ GeV}$	$m_{\tilde{\chi}_3^0} = 375.82 \text{ GeV}$	$m_{\tilde{\chi}_4^0} = 395.10 \text{ GeV}$
$m_{\tilde{\chi}_1^\pm} = 223.63 \text{ GeV}$	$m_{\tilde{\chi}_2^\pm} = 396.35 \text{ GeV}$		$m_{\tilde{g}} = 731.20 \text{ GeV}$
$m_{\tilde{u}_L} = 762.45 \text{ GeV}$	$m_{\tilde{u}_R} = 744.90 \text{ GeV}$	$m_{\tilde{d}_L} = 766.67 \text{ GeV}$	$m_{\tilde{d}_R} = 744.17 \text{ GeV}$
$m_{\tilde{t}_1} = 539.75 \text{ GeV}$	$m_{\tilde{t}_2} = 680.67 \text{ GeV}$	$m_{\tilde{b}_1} = 544.86 \text{ GeV}$	$m_{\tilde{b}_2} = 614.97 \text{ GeV}$

Table 7.4: On-shell masses of Higgs bosons, gauginos and squarks for the parameter point SPS4 [123]. The masses of the Higgs bosons include 1- and 2-loop corrections obtained with FeynHiggs 2.6.5.

$M_{A^0} = 713.63 \text{ GeV}$	$\tan \beta = 9.66$	$\mu = 623.99 \text{ GeV}$
$M_1 = 206.48 \text{ GeV}$	$M_2 = 399.33 \text{ GeV}$	$M_3 = 1146.89; \text{ GeV}$
$M_{\tilde{t}_L^{(1,2)}} = 353.74 \text{ GeV}$	$M_{\tilde{e}_R^{(1,2)}} = 221.90 \text{ GeV}$	
$M_{\tilde{t}_L^{(3)}} = 352.74 \text{ GeV}$	$M_{\tilde{\tau}_R} = 218.64 \text{ GeV}$	
$M_{\tilde{q}_L^{(1,2)}} = 1052.77; \text{ GeV}$	$M_{\tilde{u}_R^{(1,2)}} = 1013.42 \text{ GeV}$	$M_{\tilde{d}_R^{(1,2)}} = 1009.15 \text{ GeV}$
$M_{\tilde{q}_L^{(3)}} = 960.94 \text{ GeV}$	$M_{\tilde{t}_R} = 825.29 \text{ GeV}$	$M_{\tilde{b}_R} = 997.12 \text{ GeV}$
$A_\tau = -297.01 \text{ GeV}$	$A_t = -778.14 \text{ GeV}$	$A_b = -1294.84 \text{ GeV}$

Table 7.5: SUSY-breaking on-shell parameters for Point 10.1.1 [127].

$m_{h^0} = 115.01 \text{ GeV}$	$m_{H^0} = 713.63 \text{ GeV}$	$m_{A^0} = 713.36 \text{ GeV}$	$m_{H^\pm} = 718.17 \text{ GeV}$
$m_{\tilde{\chi}_1^0} = 204.64 \text{ GeV}$	$m_{\tilde{\chi}_2^0} = 385.68 \text{ GeV}$	$m_{\tilde{\chi}_3^0} = 628.67 \text{ GeV}$	$m_{\tilde{\chi}_4^0} = 642.30 \text{ GeV}$
$m_{\tilde{\chi}_1^\pm} = 385.67 \text{ GeV}$	$m_{\tilde{\chi}_2^\pm} = 642.66 \text{ GeV}$		$m_{\tilde{g}} = 1146.89 \text{ GeV}$
$m_{\tilde{u}_L} = 1051.41 \text{ GeV}$	$m_{\tilde{u}_R} = 1012.83 \text{ GeV}$	$m_{\tilde{d}_L} = 1054.41 \text{ GeV}$	$m_{\tilde{d}_R} = 1009.45 \text{ GeV}$
$m_{\tilde{t}_1} = 800.88 \text{ GeV}$	$m_{\tilde{t}_2} = 1009.05 \text{ GeV}$	$m_{\tilde{b}_1} = 960.75 \text{ GeV}$	$m_{\tilde{b}_2} = 999.34 \text{ GeV}$

Table 7.6: On-shell masses of Higgs bosons, gauginos and squarks for the benchmark point 10.1.1 [127]. The masses of the Higgs bosons include 1- and 2-loop corrections obtained with FeynHiggs 2.6.5.

7.1.1 Soft and collinear cuts

The first and second generation quarks (light-flavor quarks) are treated as massless in general. Hence, in decays of squarks into light-flavor quarks and neutralinos, the one-loop amplitudes are collinear divergent (cf. Chapter 4.2). These collinear divergencies are regulated with $\lambda_q = 10^{-3}$ GeV. The cutoff parameters for the soft and collinear regions are fixed at $\Delta E/\sqrt{s} = 10^{-3}$ and $\delta_c = 10^{-2}$. It has been verified numerically that these values are small enough to justify the eikonal approximation. In Fig. 7.1, the dependence on the cut parameters in benchmark scenario SPS1a' is exemplary shown for the decay $\tilde{u}_R \rightarrow u \tilde{\chi}_1^0$. We compare the decay widths

$$\Gamma_1^{\text{virt,EW}} = \Gamma_1^{\text{1L,EW}} + \Gamma_1^{\text{CT,EW}} + \Gamma_1^{\text{soft,EW}} + \Gamma_1^{\text{coll,EW}}, \quad (7.5a)$$

$$\Gamma_1^{\text{real,EW}} \quad (7.5b)$$

$$\Gamma_1^{\text{sum,EW}} = \Gamma_1^{\text{virt,EW}} + \Gamma_1^{\text{real,EW}} \quad (7.5c)$$

The left plot shows the dependence on the variation of $\Delta E/\sqrt{s}$ where $\delta_c = 10^{-2}$ is fixed and the right plot vice versa. Both, the 1-loop corrections including contributions from the soft and collinear regions $\Gamma_1^{\text{virt,EW}}$ and the real hard non-collinear contribution $\Gamma_1^{\text{real,EW}}$ depend on the cutoff parameters but their sum $\Gamma_1^{\text{sum,EW}}$ remains constant. For small cutoff parameters large cancellations occur whereas for larger values of the soft cutoff parameter the sum shows a small deviation, indicating that the eikonal approximation is not valid anymore.

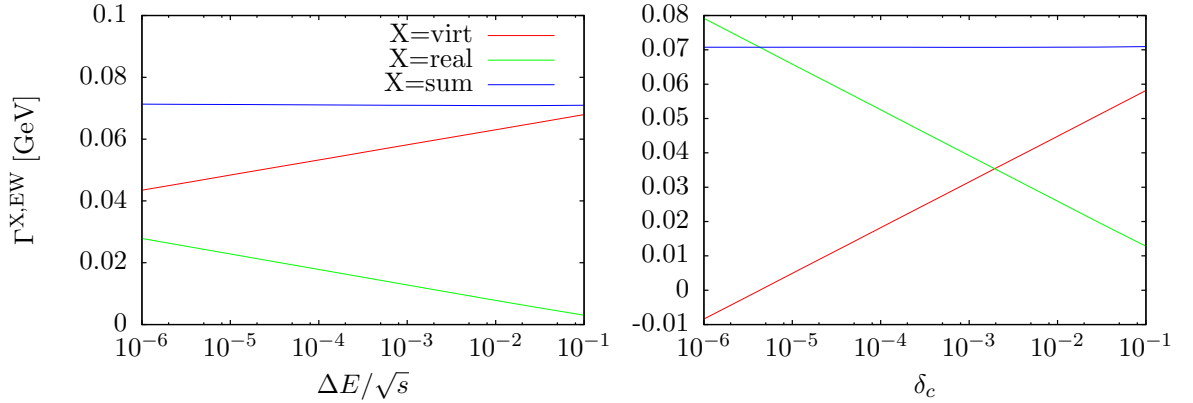


Figure 7.1: Dependence of Γ_1^{EW} on the cut parameters $\Delta E/\sqrt{s}$ (left) and δ_c (right) for the decay $\tilde{u}_R \rightarrow u \tilde{\chi}_1^0$ at the benchmark point SPS1a'.

7.2 Numerical evaluation

In this analyses, we are interested in the different squark decays into neutralinos, charginos, W/Z-bosons, and Higgs bosons. Since the decay into gluinos would dominate over all these mentioned decay channels, we choose parameter points, where the gluino is heavier than the squarks. Therefore, we evaluate the (improved) tree-level decay widths Γ_0 and branching ratios BR_0 , as well as the NLO quantities Γ_1 and BR_1 including EW and QCD corrections in the SPS1a' scenario (Tabs. 7.7, 7.8) and benchmark Point 10.1.1 (Tabs. 7.9, 7.10). For the decay into Higgs bosons (i.e. $\tilde{t}_2 \rightarrow \tilde{t}_1 h^0$) Γ_0 includes higher-order improvements from Higgs-propagator effects using finite Z-factors (cf. Chapter 6.4.4). Likewise, for decays involving the bottom-quark Yukawa coupling (i.e. $\tilde{t}_i \rightarrow b \tilde{\chi}_j^+$, $\tilde{b}_i \rightarrow b \tilde{\chi}_k^0$, and $\tilde{b}_i \rightarrow t \tilde{\chi}_j^-$), the partial decay width Γ_0 includes higher-order effects from the effective bottom quark mass m_b^{eff} .

In both scenarios the bino-like neutralino is the $\tilde{\chi}_1^0$, where $\tilde{\chi}_2^0/\tilde{\chi}_1^\pm$ are wino-like and $\tilde{\chi}_{3,4}^0/\tilde{\chi}_2^\pm$ are higgsino-like. Therefore, the right-handed light-flavor squarks decay dominantly into $\tilde{\chi}_1^0$, whereas the left-handed light-flavor squarks decay into $\tilde{\chi}_2^0$ and $\tilde{\chi}_1^\pm$. For third-generation squarks decays into lighter squarks plus W/Z-bosons or Higgs bosons become relevant. At SPS1a' decays into W/Z-bosons have branching ratios up to 40%, whereas at Point 10.1.1 branching ratios for decays into W/Z-bosons reach 13%. The only possible decay into Higgs bosons is $\tilde{t}_2 \rightarrow \tilde{t}_1 h^0$ with branching ratios around 5% in both scenarios.

For both of the two benchmark points, relative QCD corrections $(\Gamma_1^{\text{QCD}} - \Gamma_0)/\Gamma_0$ have a negative value and lie in the range between -2% and -10% . Only for decays into top quarks, where the available phase space for real radiation is restricted, relative QCD corrections can have a positive sign and value up to 25%. Relative EW corrections $(\Gamma_1^{\text{EW}} - \Gamma_0)/\Gamma_0$ can be positive or negative, depending on the decay channel. Thus, there can be significant cancellations between QCD and EW corrections. The absolute value of the relative EW corrections is of the order of the QCD corrections. Therefore, a consistent treatment of squark decays beyond leading order demands to include QCD and EW contributions.

Decay channel	Γ_0 [GeV]	BR ₀	Γ_1 [GeV]	BR ₁
$\tilde{u}_L \rightarrow u \tilde{\chi}_1^0$	0.036	0.68 %	0.037	0.69 %
$\tilde{u}_L \rightarrow u \tilde{\chi}_2^0$	1.700	32.14 %	1.695	32.21 %
$\tilde{u}_L \rightarrow u \tilde{\chi}_3^0$	0.003	0.06 %	0.002	0.05 %
$\tilde{u}_L \rightarrow u \tilde{\chi}_4^0$	0.035	0.66 %	0.033	0.62 %
$\tilde{u}_L \rightarrow d \tilde{\chi}_1^+$	3.476	65.72 %	3.456	65.66 %
$\tilde{u}_L \rightarrow d \tilde{\chi}_2^+$	0.040	0.75 %	0.040	0.76 %
$\sum_{\{a,b\}} \tilde{u}_L \rightarrow a b$	5.290		5.263	
$\tilde{u}_R \rightarrow u \tilde{\chi}_1^0$	1.031	99.09 %	1.086	99.03 %
$\tilde{u}_R \rightarrow u \tilde{\chi}_2^0$	0.006	0.62 %	0.007	0.65 %
$\tilde{u}_R \rightarrow u \tilde{\chi}_3^0$	0.001	0.07 %	0.001	0.07 %
$\tilde{u}_R \rightarrow u \tilde{\chi}_4^0$	0.002	0.22 %	0.002	0.24 %
$\sum_{\{a,b\}} \tilde{u}_R \rightarrow a b$	1.040		1.096	
$\tilde{d}_L \rightarrow d \tilde{\chi}_1^0$	0.108	2.13 %	0.113	2.22 %
$\tilde{d}_L \rightarrow d \tilde{\chi}_2^0$	1.617	31.73 %	1.603	31.50 %
$\tilde{d}_L \rightarrow d \tilde{\chi}_3^0$	0.005	0.11 %	0.006	0.12 %
$\tilde{d}_L \rightarrow d \tilde{\chi}_4^0$	0.048	0.93 %	0.048	0.94 %
$\tilde{d}_L \rightarrow u \tilde{\chi}_1^-$	3.181	62.40 %	3.185	62.58 %
$\tilde{d}_L \rightarrow u \tilde{\chi}_2^-$	0.137	2.69 %	0.134	2.63 %
$\sum_{\{a,b\}} \tilde{d}_L \rightarrow a b$	5.096		5.089	
$\tilde{d}_R \rightarrow d \tilde{\chi}_1^0$	0.258	99.09 %	0.272	99.02 %
$\tilde{d}_R \rightarrow d \tilde{\chi}_2^0$	0.002	0.62 %	0.002	0.66 %
$\tilde{d}_R \rightarrow d \tilde{\chi}_3^0$	0.000	0.07 %	0.000	0.07 %
$\tilde{d}_R \rightarrow d \tilde{\chi}_4^0$	0.001	0.22 %	0.001	0.24 %
$\sum_{\{a,b\}} \tilde{d}_R \rightarrow a b$	0.261		0.275	

Table 7.7: Decay widths of light-flavor squarks at the benchmark point SPS1a'. Listed are values at tree-level (Γ_0 , BR₀) and including both, electroweak and QCD corrections (Γ_1 , BR₁).

Decay channel	Γ_0 [GeV]	BR ₀	Γ_1 [GeV]	BR ₁
$\tilde{t}_1 \rightarrow t \tilde{\chi}_1^0$	0.265	19.98 %	0.289	21.98 %
$\tilde{t}_1 \rightarrow t \tilde{\chi}_2^0$	0.037	2.81 %	0.039	3.00 %
$\tilde{t}_1 \rightarrow b \tilde{\chi}_1^+$	1.025	77.21 %	0.985	75.02 %
$\sum_{\{a,b\}} \tilde{t}_1 \rightarrow a b$	1.327		1.313	
$\tilde{t}_2 \rightarrow t \tilde{\chi}_1^0$	0.204	3.20 %	0.219	3.56 %
$\tilde{t}_2 \rightarrow t \tilde{\chi}_2^0$	0.611	9.57 %	0.613	9.95 %
$\tilde{t}_2 \rightarrow t \tilde{\chi}_3^0$	0.072	1.13 %	0.055	0.89 %
$\tilde{t}_2 \rightarrow b \tilde{\chi}_1^+$	1.593	24.96 %	1.683	27.32 %
$\tilde{t}_2 \rightarrow b \tilde{\chi}_2^+$	1.199	18.78 %	0.942	15.30 %
$\tilde{t}_2 \rightarrow \tilde{t}_1 Z$	2.288	35.85 %	2.228	36.95%
$\tilde{t}_2 \rightarrow \tilde{b}_1 W^+$	0.003	0.04 %	0.003	0.05%
$\tilde{t}_2 \rightarrow \tilde{t}_1 h^0$	0.413	6.47 %	0.368	5.98%
$\sum_{\{a,b\}} \tilde{t}_2 \rightarrow a b$	6.383		6.111	
$\tilde{b}_1 \rightarrow b \tilde{\chi}_1^0$	0.138	3.23 %	0.140	3.15 %
$\tilde{b}_1 \rightarrow b \tilde{\chi}_2^0$	1.270	29.68 %	1.327	29.79 %
$\tilde{b}_1 \rightarrow b \tilde{\chi}_3^0$	0.011	0.25 %	0.010	0.23 %
$\tilde{b}_1 \rightarrow b \tilde{\chi}_4^0$	0.018	0.42 %	0.016	0.36 %
$\tilde{b}_1 \rightarrow t \tilde{\chi}_1^-$	1.536	35.90 %	1.620	36.36 %
$\tilde{b}_1 \rightarrow \tilde{t}_1 W^+$	1.305	30.52 %	1.342	30.11%
$\sum_{\{a,b\}} \tilde{b}_1 \rightarrow a b$	4.278		4.455	
$\tilde{b}_2 \rightarrow b \tilde{\chi}_1^0$	0.212	25.61 %	0.220	25.65 %
$\tilde{b}_2 \rightarrow b \tilde{\chi}_2^0$	0.094	11.32 %	0.099	11.55 %
$\tilde{b}_2 \rightarrow b \tilde{\chi}_3^0$	0.026	3.18 %	0.028	3.30 %
$\tilde{b}_2 \rightarrow b \tilde{\chi}_4^0$	0.034	4.10 %	0.034	3.94 %
$\tilde{b}_2 \rightarrow t \tilde{\chi}_1^-$	0.120	14.47 %	0.125	14.59 %
$\tilde{b}_2 \rightarrow \tilde{t}_1 W^+$	0.342	41.32 %	0.352	40.98%
$\sum_{\{a,b\}} \tilde{b}_2 \rightarrow a b$	0.828		0.858	

Table 7.8: Decay widths of third-generation squarks at the benchmark point SPS1a'. Listed are the values at tree-level (Γ_0 , BR₀) and including both, electroweak and QCD corrections (Γ_1 , BR₁).

Decay channel	Γ_0 [GeV]	BR ₀	Γ_1 [GeV]	BR ₁
$\tilde{u}_L \rightarrow u \tilde{\chi}_1^0$	0.102	1.06 %	0.106	1.14 %
$\tilde{u}_L \rightarrow u \tilde{\chi}_2^0$	3.057	31.92 %	2.951	31.93 %
$\tilde{u}_L \rightarrow u \tilde{\chi}_3^0$	0.003	0.04 %	0.002	0.02 %
$\tilde{u}_L \rightarrow u \tilde{\chi}_4^0$	0.095	0.99 %	0.084	0.91 %
$\tilde{u}_L \rightarrow d \tilde{\chi}_1^+$	6.182	64.54 %	5.970	64.62 %
$\tilde{u}_L \rightarrow d \tilde{\chi}_2^+$	0.139	1.45 %	0.127	1.38 %
$\sum_{\{a,b\}} \tilde{u}_L \rightarrow a b$	9.578		9.240	
$\tilde{u}_R \rightarrow u \tilde{\chi}_1^0$	1.929	99.62 %	2.032	99.59 %
$\tilde{u}_R \rightarrow u \tilde{\chi}_2^0$	0.002	0.12 %	0.003	0.12 %
$\tilde{u}_R \rightarrow u \tilde{\chi}_3^0$	0.001	0.04 %	0.001	0.04 %
$\tilde{u}_R \rightarrow u \tilde{\chi}_4^0$	0.004	0.22 %	0.005	0.24 %
$\sum_{\{a,b\}} \tilde{u}_R \rightarrow a b$	1.936		2.041	
$\tilde{d}_L \rightarrow d \tilde{\chi}_1^0$	0.152	1.61 %	0.156	1.70 %
$\tilde{d}_L \rightarrow d \tilde{\chi}_2^0$	2.983	31.53 %	2.870	31.35 %
$\tilde{d}_L \rightarrow d \tilde{\chi}_3^0$	0.005	0.06 %	0.007	0.07 %
$\tilde{d}_L \rightarrow d \tilde{\chi}_4^0$	0.118	1.25 %	0.111	1.22 %
$\tilde{d}_L \rightarrow u \tilde{\chi}_1^-$	5.899	62.35 %	5.733	62.62 %
$\tilde{d}_L \rightarrow u \tilde{\chi}_2^-$	0.303	3.20 %	0.279	3.05 %
$\sum_{\{a,b\}} \tilde{d}_L \rightarrow a b$	9.460		9.156	
$\tilde{d}_R \rightarrow d \tilde{\chi}_1^0$	0.480	99.62 %	0.507	99.59 %
$\tilde{d}_R \rightarrow d \tilde{\chi}_2^0$	0.001	0.12 %	0.001	0.12 %
$\tilde{d}_R \rightarrow d \tilde{\chi}_3^0$	0.000	0.04 %	0.000	0.05 %
$\tilde{d}_R \rightarrow d \tilde{\chi}_4^0$	0.001	0.22 %	0.001	0.24 %
$\sum_{\{a,b\}} \tilde{d}_R \rightarrow a b$	0.482		0.509	

Table 7.9: Decay widths of light-flavor squarks at benchmark Point 10.1.1. Listed are the values at tree-level (Γ_0 , BR₀) and including both, electroweak and QCD corrections (Γ_1 , BR₁).

Decay channel	Γ_0 [GeV]	BR ₀	Γ_1 [GeV]	BR ₁
$\tilde{t}_1 \rightarrow t \tilde{\chi}_1^0$	1.171	22.54 %	1.257	26.48 %
$\tilde{t}_1 \rightarrow t \tilde{\chi}_2^0$	0.729	14.04 %	0.664	13.99 %
$\tilde{t}_1 \rightarrow t \tilde{\chi}_3^0$	0.093	1.80 %	0.076	1.61 %
$\tilde{t}_1 \rightarrow b \tilde{\chi}_1^+$	1.872	36.05 %	1.715	36.13 %
$\tilde{t}_1 \rightarrow b \tilde{\chi}_2^+$	1.328	25.56 %	1.034	21.79 %
$\sum_{\{a,b\}} \tilde{t}_1 \rightarrow a b$	5.193		4.746	
$\tilde{t}_2 \rightarrow t \tilde{\chi}_1^0$	0.287	1.75 %	0.314	2.10 %
$\tilde{t}_2 \rightarrow t \tilde{\chi}_2^0$	1.609	9.83 %	1.637	10.95 %
$\tilde{t}_2 \rightarrow t \tilde{\chi}_3^0$	2.139	13.07 %	1.643	10.99 %
$\tilde{t}_2 \rightarrow t \tilde{\chi}_4^0$	4.241	25.91 %	3.314	22.17 %
$\tilde{t}_2 \rightarrow b \tilde{\chi}_1^+$	3.455	21.11 %	3.705	24.78 %
$\tilde{t}_2 \rightarrow b \tilde{\chi}_2^+$	2.044	12.49 %	1.698	11.35 %
$\tilde{t}_2 \rightarrow \tilde{t}_1 Z$	1.766	10.79 %	1.790	11.97%
$\tilde{t}_2 \rightarrow \tilde{t}_1 h^0$	0.824	5.04 %	0.849	5.68%
$\sum_{\{a,b\}} \tilde{t}_2 \rightarrow a b$	16.365		14.950	

Table 7.10: Decay widths of top squarks at benchmark Point 10.1.1. Listed are the values at tree-level (Γ_0 , BR₀) and including both, electroweak and QCD corrections (Γ_1 , BR₁).

7.2.1 Dependent masses

In Chapter 4.1, we have seen, that the following masses are dependent quantities at the one-loop level:

$$m_{\tilde{d}_L}, m_{\tilde{b}_1}, m_{\tilde{\chi}_2^0}, m_{\tilde{\chi}_3^0}, m_{\tilde{\chi}_4^0}.$$

Therefore, finite shifts have to be introduced for these masses, such that the right on-shell values are obtained. In General, these mass-shifts are of the order of 1%. Exemplary, the aforementioned masses are shown in Tab. 7.12 at the benchmark point SPS1a'.

In decays involving particles with dependant masses, the mass-shifts enter the decay widths through the phase-space integration. Unsurprisingly, effects are largest for decays of the lighter bottom squark \tilde{b}_1 , which is the squark with the largest shift between tree-level and on-shell value. The corrected decay widths for these decays in GeV with and without usage of the right on-shell masses for the dependent particles are given in Tab. 7.13 and can differ by up to 9%. Therefore it is important, that these effects are included.

Decay channel	Γ_0 [GeV]	BR ₀	Γ_1 [GeV]	BR ₁
$\tilde{b}_1 \rightarrow b \tilde{\chi}_1^0$	0.179	1.30 %	0.175	1.36 %
$\tilde{b}_1 \rightarrow b \tilde{\chi}_2^0$	2.497	18.09 %	2.592	20.10 %
$\tilde{b}_1 \rightarrow b \tilde{\chi}_3^0$	0.051	0.37 %	0.052	0.40 %
$\tilde{b}_1 \rightarrow b \tilde{\chi}_4^0$	0.095	0.69 %	0.089	0.69 %
$\tilde{b}_1 \rightarrow t \tilde{\chi}_1^-$	4.432	32.11 %	4.468	34.64 %
$\tilde{b}_1 \rightarrow t \tilde{\chi}_2^-$	4.723	34.22 %	3.667	28.43 %
$\tilde{b}_1 \rightarrow \tilde{t}_1 W^+$	1.824	13.22 %	1.854	14.38%
$\sum_{\{a,b\}} \tilde{b}_1 \rightarrow a b$	13.801		12.897	
$\tilde{b}_2 \rightarrow b \tilde{\chi}_1^0$	0.435	25.34 %	0.458	27.27 %
$\tilde{b}_2 \rightarrow b \tilde{\chi}_2^0$	0.088	5.11 %	0.093	5.52 %
$\tilde{b}_2 \rightarrow b \tilde{\chi}_3^0$	0.074	4.29 %	0.082	4.87 %
$\tilde{b}_2 \rightarrow b \tilde{\chi}_4^0$	0.100	5.81 %	0.104	6.19 %
$\tilde{b}_2 \rightarrow t \tilde{\chi}_1^-$	0.161	9.40 %	0.162	9.63 %
$\tilde{b}_2 \rightarrow t \tilde{\chi}_2^-$	0.631	36.75 %	0.549	32.68 %
$\tilde{b}_2 \rightarrow \tilde{t}_1 W^+$	0.228	13.30 %	0.232	13.83%
$\sum_{\{a,b\}} \tilde{b}_2 \rightarrow a b$	1.717		1.980	

Table 7.11: Decay widths of bottom squarks at benchmark Point 10.1.1. Listed are the values at tree-level (Γ_0 , BR₀) and including both, electroweak and QCD corrections (Γ_1 , BR₁).

	$m_{\tilde{d}_L}$ [GeV]	$m_{\tilde{b}_1}$ [GeV]	$m_{\tilde{\chi}_2^0}$ [GeV]	$m_{\tilde{\chi}_3^0}$ [GeV]	$m_{\tilde{\chi}_4^0}$ [GeV]
tree-level	562.879	493.328	183.547	392.867	409.355
on-shell	562.686	498.169	183.440	395.155	408.663
$\Delta m/m$	-0.03%	0.98%	-0.06%	0.58%	-0.17%

Table 7.12: Tree-level, on-shell masses, and the relative difference in benchmark scenario SPS1a'.

decay products	$b \tilde{\chi}_1^0$	$b \tilde{\chi}_2^0$	$b \tilde{\chi}_3^0$	$b \tilde{\chi}_4^0$	$t \tilde{\chi}_1^-$	$\tilde{t}_1 W^-$
Γ_1 in GeV using tree-level masses	0.1409	1.3301	0.0106	0.0153	1.5899	1.1779
Γ_1 in GeV using on-shell masses	0.1422	1.3477	0.0108	0.0167	1.6209	1.1325

Table 7.13: NLO corrected decay width Γ_1 for decays of the lighter bottom squark \tilde{b}_1 using tree-level and on-shell dependant masses.

7.3 Parameter dependences

7.3.1 Scale dependence

The renormalization scale μ_R enters via the $\overline{\text{DR}}$ renormalization of the Higgs field (4.28b), the finite Z-factors (4.31a, 4.31b), the trilinear coupling A_b (4.70), and the strong coupling constant $\alpha_s^{\overline{\text{DR}}}(\mu_R)$ in the decay amplitude. Hence, the improved and NLO decay widths including these parameters depend on μ_R .

In order to show the dependence on μ_R via Higgs field-renormalization and Z-factors, in the left panel of Fig. 7.2 we show the decay widths for $\tilde{t}_2 \rightarrow \tilde{t}_1 h^0$ as function of $\tan \beta$. The renormalization scale is varied between $m/2 \leq \mu_R \leq 2m$, where m denotes the mass of the decaying particle. The red curve shows the improved tree-level decay width Γ_Z (9.8) and the red light area its spreading when μ_R is varied. The blue curve shows the NLO decay width Γ_1 (6.43) including EW and QCD contributions. The variation then is drastically reduced, such that it is not visible anymore. Hence, as expected, the NLO contributions reduce the scale uncertainty of the improved Born approximation.

In the right panel of Fig. 7.2, the decay widths for $\tilde{b}_1 \rightarrow b \tilde{\chi}_1^0$ are shown. Here, μ_R enters via A_b , and α_s . The red curve represents the tree-level decay width Γ_0 including the effective bottom quark mass m_b^{eff} . It does not depend on the renormalization scale. At one-loop order including EW and QCD corrections, the variation of μ_R is clearly visible. It is mainly due to the μ_R -dependence of the $\overline{\text{DR}}$ renormalization constant δA_b .

7.3.2 Dependence on $\tan \beta$

For the variation of $\tan \beta$ the SPS4 benchmark scenario (Tab. 7.3) is taken as a starting point. This parameter point is characterized by having a large value for $\tan \beta$. As mentioned in Chapter 4 the b/\tilde{b} sector strongly depends on $\tan \beta$. Hence, in Fig. 7.3 the branching ratio for the decays of the heavier bottom squark \tilde{b}_2 are presented. An important contribution to the radiative corrections for large $\tan \beta$ originates from the effective bottom mass m_b^{eff} . In order to show the $\tan \beta$ dependence of the effective bottom quark mass m_b^{eff} , the relative corrections

$$\delta_0 = \frac{\Gamma_b^X - \Gamma_0}{\Gamma_0}, \quad X \in \{\text{tree, EW, QCD, EW+QCD}\}, \quad (7.6)$$

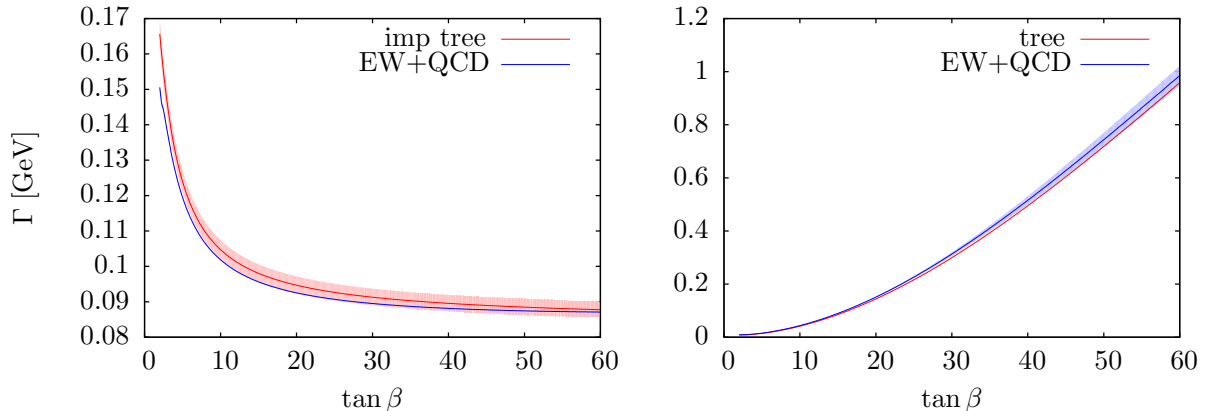


Figure 7.2: Scale dependence for $\tilde{t}_2 \rightarrow \tilde{t}_1 h^0$ (left) and $\tilde{b}_1 \rightarrow b \tilde{\chi}_1^0$ (right) as a function of $\tan\beta$ in benchmark scenario SPS1a'.

are considered. The subscript b denotes the decay width, where the effective bottom quark mass is used to compute the corresponding amplitude. These relative corrections are plotted in the left plot of Fig. 7.4, whereas the right plot shows the relative corrections with respect to the m_b^{eff} -improved tree-level decay width Γ_b^{tree}

$$\delta_b = \frac{\Gamma_b^X - \Gamma_b^{\text{tree}}}{\Gamma_b^{\text{tree}}}, \quad X \in \{\text{EW}, \text{QCD}, \text{EW+QCD}\}. \quad (7.7)$$

There is a strong dependence of the improved tree-level decay width on $\tan\beta$. For large values of $\tan\beta$ it gives a correction of up to -8% . Furthermore, EW, QCD, and EW+QCD corrected decay widths show the same $\tan\beta$ dependence. Thus, their relative corrections with respect to Γ_b^{eff} only show a mild variation with $\tan\beta$ and the total corrections amount up to 2% leading to an overall correction of -4% . Hence, the major $\tan\beta$ dependence is absorbed into the effective bottom quark mass.

For the other decays, the relative NLO corrections do not depend strongly on $\tan\beta$. As an example, the branching ratios including NLO corrections for the heavier top squark \tilde{t}_2 are plotted in Fig. 7.5. The most important decay channels are the ones into the neutralinos with large higgsino components. The decays into the Z (W^+) gauge bosons and lighter top (bottom) squarks do also have a considerable branching ratio – depending on $\tan\beta$ – reaching 14% . For small $\tan\beta$ the branching ratio into a W^+ boson is very small, since now the lighter bottom squark essentially is right-handed. For larger $\tan\beta$ the bottom squark \tilde{b}_1 has a larger left-handed component, enabling the decay $\tilde{t}_2 \rightarrow \tilde{b}_1 W^+$. The same characteristic can be seen for the wino-like chargino $\tilde{\chi}_1^+$.

In contrast, for decay widths not including the bottom Yukawa coupling at the tree level, the relative corrections do not depend on $\tan\beta$ strongly. Hence, in Fig. 7.6 the relative corrections

$$\delta = \frac{\Gamma_1^X - \Gamma_0}{\Gamma_0}, \quad X \in \{\text{tree}, \text{EW}, \text{QCD}, \text{EW+QCD}\}, \quad (7.8)$$

are plotted for the decays $\tilde{t}_2 \rightarrow t \tilde{\chi}_4$ (left plot) and $\tilde{t}_2 \rightarrow \tilde{b}_1 W^+$ (right plot). The tree-level decay widths for both processes do not depend on the bottom mass and their relative corrections show no strong dependence on $\tan\beta$.

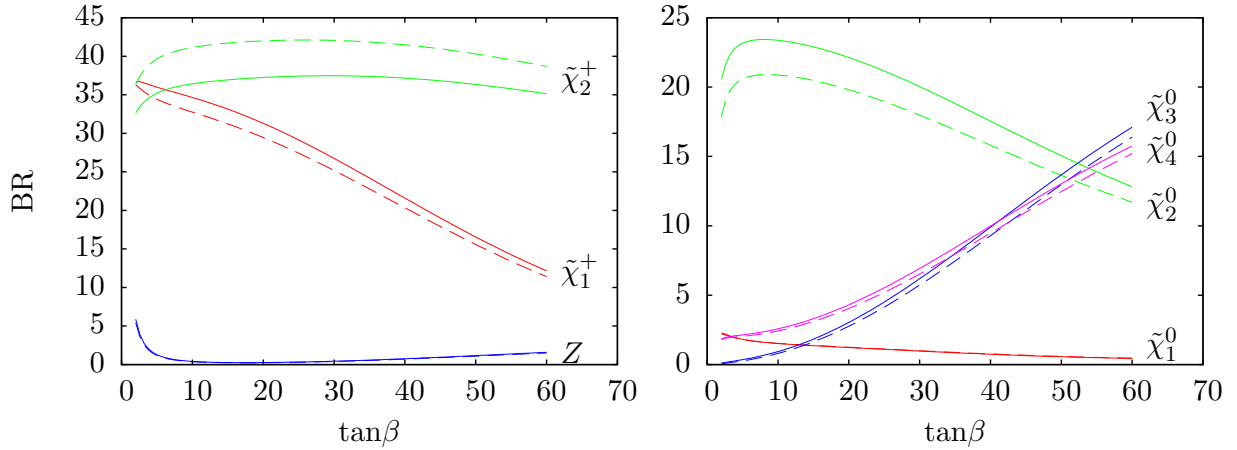


Figure 7.3: Branching ratios in % for the decays of the heavier bottom squark \tilde{b}_2 as function of $\tan\beta$. The other parameters are taken from the SPS4 parameter point. The branching ratio for the decay $\tilde{b}_2 \rightarrow \tilde{t}_1 W^+$ is not displayed since its value is far below one percent. The dashed lines represent the tree-level and the full line the branching ratios including the m_b^{eff} -improvement and additional the EW and QCD corrections.

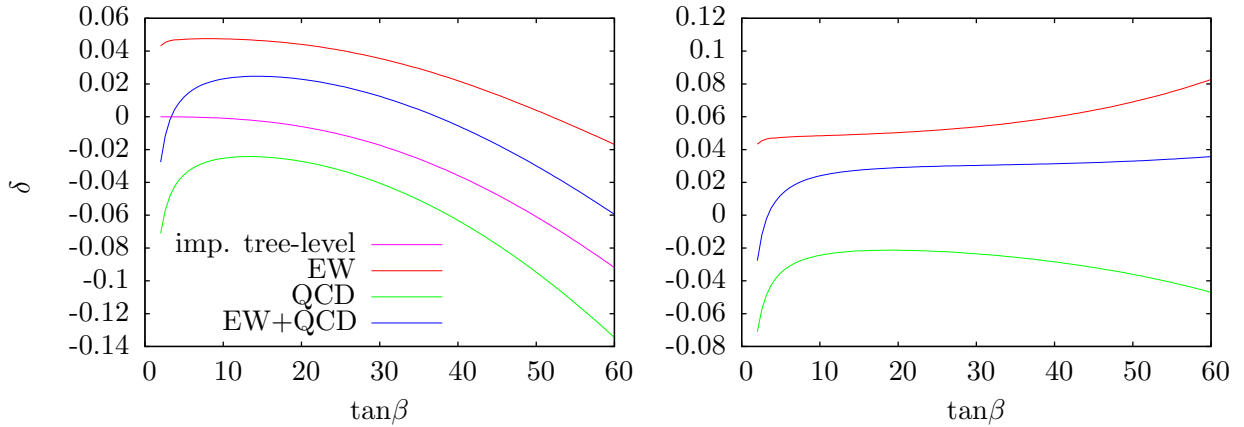


Figure 7.4: Relative corrections with respect to the tree-level decay width (7.8) (left) and with respect to the improved tree-level decay width (7.7) (right) for the decay $\tilde{b}_2 \rightarrow t \tilde{\chi}_1^-$. Both plots show the variation as function of $\tan\beta$ whereas the other parameters are fixed according to the SPS4 parameter point.

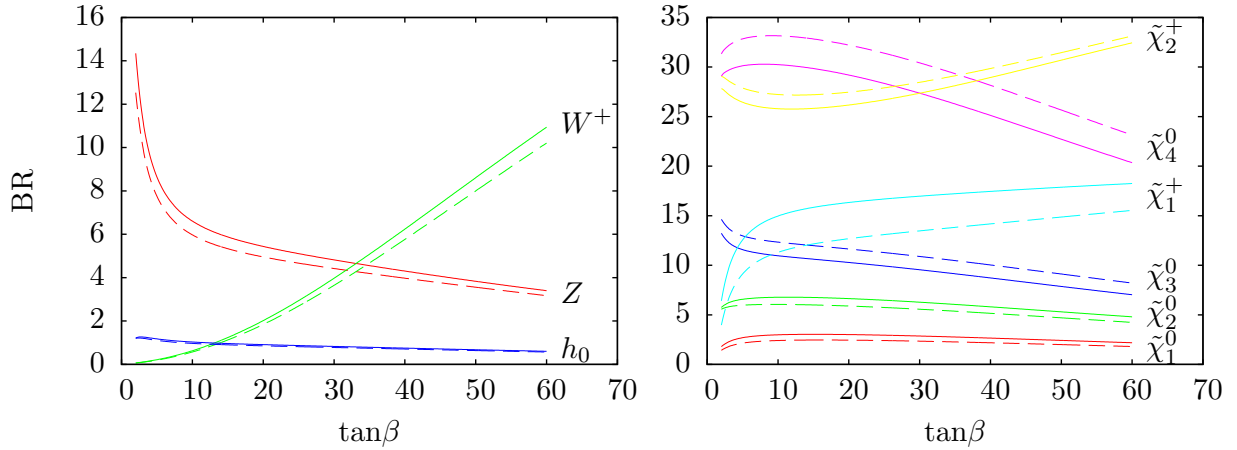


Figure 7.5: Branching ratios in % for the decays of the heavier top squark \tilde{t}_2 as function of $\tan\beta$. The other parameters are fixed according to the SPS4 parameter point. The dashed line represent the tree-level and the full line the NLO branching ratios including EW and QCD corrections.

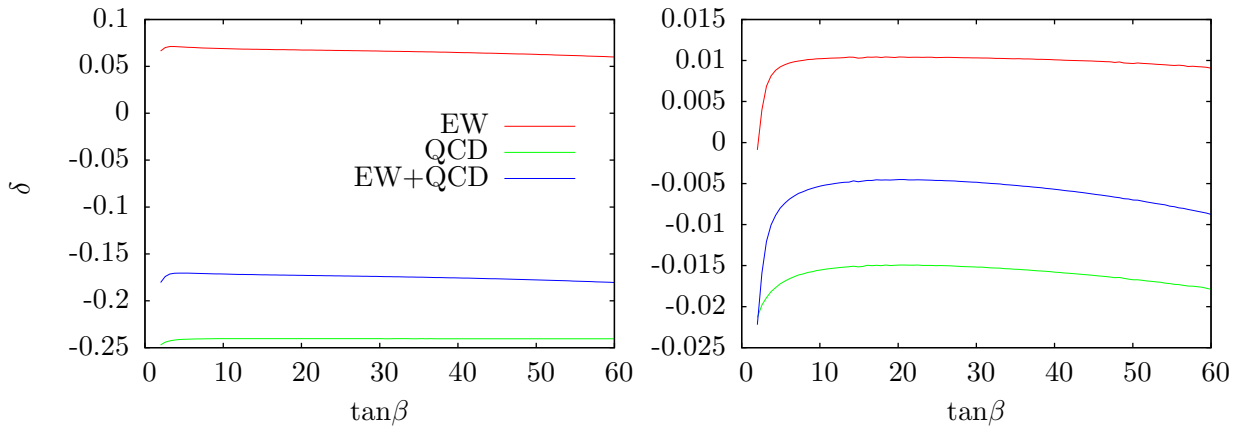


Figure 7.6: Relative corrections for the decays $\tilde{t}_2 \rightarrow t \tilde{\chi}_4^0$ (left) and $\tilde{t}_2 \rightarrow \tilde{b}_1 W^+$ as function of $\tan\beta$. The other parameters are fixed according to the SPS4 parameter point.

7.3.3 Dependence on m_{A^0}

The dependence on the mass of the CP-odd Higgs boson m_{A^0} is examined for the decays of third-generation squarks, which couple to Higgs bosons via their large Yukawa couplings. As a starting point the benchmark scenario SPS1a' (cf. 7.1, 7.2) is taken and m_{A^0} is varied. In particular, squark decays into Higgs bosons are affected by the variation of m_{A^0} . Therefore the decay of the heavier top squark \tilde{t}_2 is inspected, where the decay channels into the

Higgs bosons and the lighter top squark \tilde{t}_1 are opened for (Fig. 7.7). Here, tree-level values do not include Z -factors for the external Higgs bosons, whereas they are included for all corrected decay widths. For small values of m_{A^0} the decay $\tilde{t}_2 \rightarrow \tilde{t}_1 A^0$ has a BR of about 10%. One can also see that there are large corrections for the decays into Higgs bosons for small m_{A^0} , especially for the decay $\tilde{t}_2 \rightarrow \tilde{t}_1 A^0$ and $\tilde{t}_2 \rightarrow \tilde{t}_1 h^0$.

In order to study the various contributions for decays into Higgs bosons, the relative corrections

$$\delta_0 = \frac{\Gamma_Z^X - \Gamma_0}{\Gamma_0}, \quad X \in \{\text{tree, EW, QCD, EW+QCD}\}, \quad (7.9)$$

for the process $\tilde{t}_2 \rightarrow \tilde{t}_1 h^0$ are plotted. The subscript Z denotes the decay width improved by the appropriate Z -factors for the external Higgs bosons (Subsection 4.1.3). In the left plot of Fig. 7.8 the four different values for (7.9) are plotted. For small values of m_{A^0} the largest effects originate from the Z -factors in the improved tree-level decay width. For larger m_{A^0} the corrections from the Z -factors in the improved tree-level decay width nearly vanish. The effects of the one-loop EW and QCD corrections are better visible in the relative corrections with respect to the improved decay width

$$\delta_Z = \frac{\Gamma_Z^X - \Gamma_Z^{\text{tree}}}{\Gamma_Z^{\text{tree}}}, \quad X \in \{\text{EW, QCD, EW+QCD}\}. \quad (7.10)$$

They are depicted in the right plot of Fig. 7.8. These corrections reaching from -25% for smaller values of m_{A^0} to -10% for larger m_{A^0} are added to the improved tree-level decay width.

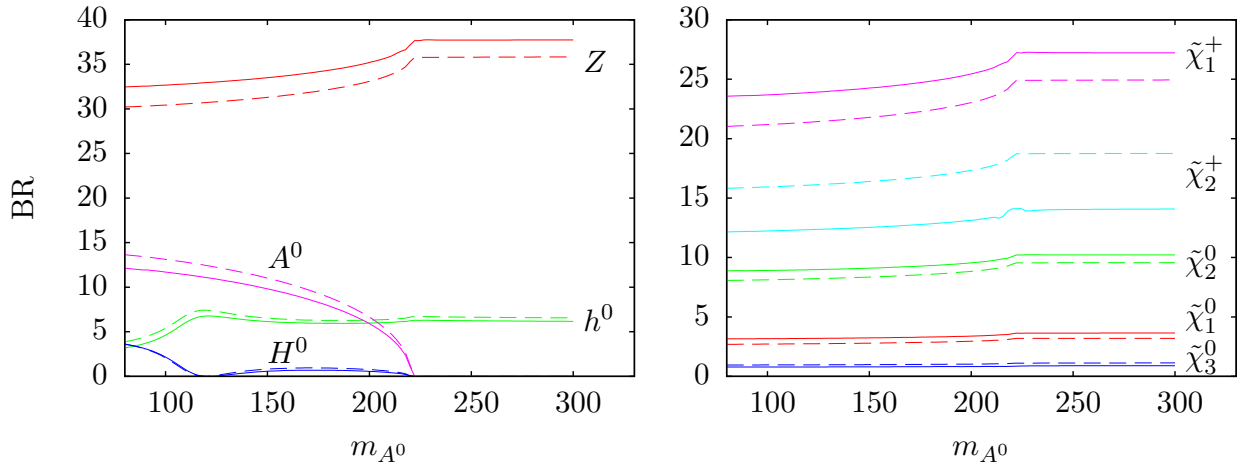


Figure 7.7: Branching ratios in % for the decays of the heavier bottom squark \tilde{t}_2 as function of m_{A^0} . The other parameters are fixed according to the SPS1a' parameter point. The dashed lines represent the tree-level and the full lines the NLO branching ratios including EW and QCD contributions.

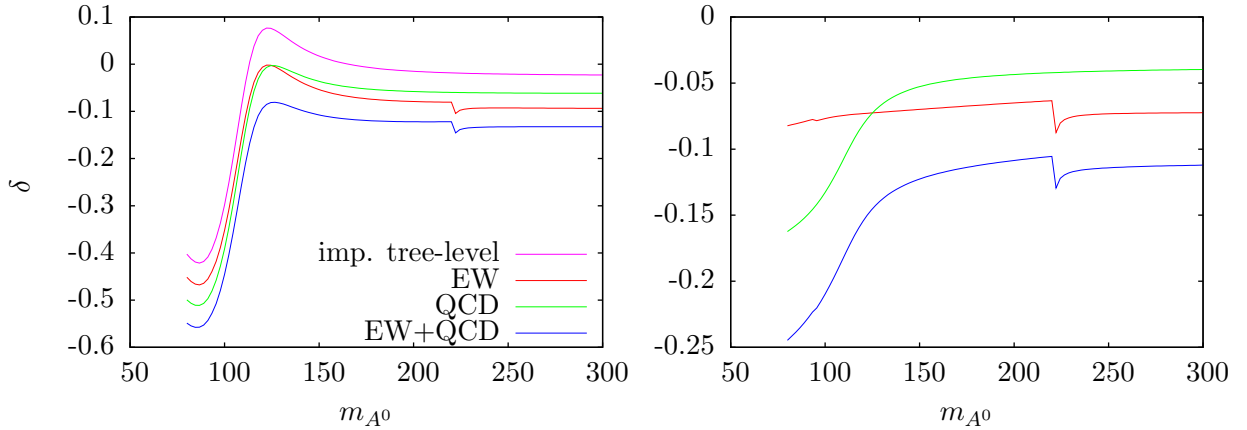


Figure 7.8: Relative corrections for the decay $\tilde{t}_2 \rightarrow \tilde{t}_1 h^0$ with respect to the tree-level decay width (left) and to the improved tree-level decay width (right) as function of m_{A^0} . The other parameters are fixed according to the SPS1a' parameter point.

7.3.4 Dependence on A_t and A_b

It was mentioned in the previous chapters that for third-generation squarks mixing effects have to be taken into account. The off-diagonal entries of the third-generation squark matrices are given by $m_q(A_q - \mu\kappa)$ with $\kappa = \cot\beta$ for $q = t$ and $\kappa = \tan\beta$ for $q = b$. Therefore the trilinear couplings have a strong effect on the decay of third-generation squarks. In order to examine the dependence on A_t and A_b , in Fig. 7.9 the trilinear couplings are varied, $A_t = A_b \in [-1000, 1000]$ GeV. The other parameters are fixed according to SPS1a' parameter point.

For $A_t \in [-150, 150]$ GeV the mass difference between the heavier and lighter top squark is too small to allow the decays $\tilde{t}_2 \rightarrow \tilde{t}_1 h^0/Z$. In this parameter region the most important decays are $\tilde{t}_2 \rightarrow t \tilde{\chi}_2^0$ and $\tilde{t}_2 \rightarrow \tilde{b} \tilde{\chi}_1^+$ since the off-diagonal entries in the squark mass matrix become small and \tilde{t}_2 is mostly left-handed. For larger values of A_t the mixing between left- and right-handed squarks becomes important and the top squark mass eigenstates cannot be regarded as left- and right-handed chiral states. In this region, phase space also allows for the decays into h^0 and Z . The latter becoming important for large values of $|A_t|$ with a branching ratio reaching 50%. The branching ratio for the decay into the lightest Higgs boson reaches up to 6%.

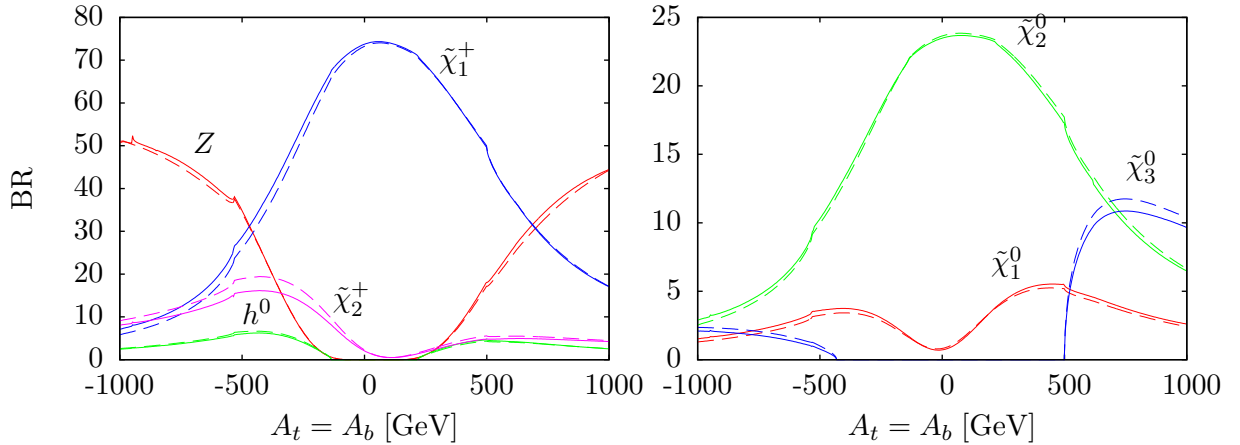


Figure 7.9: Branching ratios in % for the decays of the heavier bottom squark \tilde{t}_2 as function of $A_t = A_b$. The other parameters are fixed according to the SPS1a' parameter point. The dashed line represent the tree-level and the full line the NLO branching ratios including EW and QCD contributions.

7.3.5 Parameter scan over M_{SUSY} and M_3

Here, the decays of light-flavor squarks are considered with respect to squark and gluino masses. In order to identify the parameter regions where big corrections arise in light-generation squark decays, the following parameter scan is performed. The parameters varied are $M_{\text{SUSY}} \in [400, 2000]$ GeV and $M_3 = m_{\tilde{g}} \in [400, 2000]$ GeV. The gaugino parameters M_1 and M_2 obey the GUT relation $M_1 = \frac{5}{3} \tan^2 \theta_w M_2 = \frac{5\alpha}{(3\alpha_s \cos^2 \theta_w)} M_3$. The other relevant parameters for light-flavor squark decays are $\tan \beta = 10$, $M_{A^0} = 500$ GeV, $\mu = 500$ GeV, $M_{\tilde{f}_L} = M_{\tilde{f}_R} = M_{\text{SUSY}}$.

For $M_3 > M_{\text{SUSY}}$ the squark decay into quark and gluino dominates. This is clearly visible in Fig. 7.10(a), where the branching ratio for the process $\tilde{u}_L \rightarrow u \tilde{g}$ is plotted. In the lower right half of the parameter space the branching ratio reaches over 90 %. In the upper left corner the white space indicates that the decay into gluino is kinematically not available.

When squarks are lighter than the gluino, left- and right-handed squarks decay differently and their decays have to be analyzed separately. In Fig. 7.11(a) and 7.11(b) the branching ratios for the decays $\tilde{u}_L \rightarrow u \tilde{\chi}_2^0$ and $\tilde{u}_L \rightarrow d \tilde{\chi}_1^+$ are drawn. The green area in both plots indicate the region where this two decays dominate since in this region $\tilde{\chi}_2^0$ and $\tilde{\chi}_1^+$ are wino-like. In the upper region, these decays are much less important, since the wino-like neutralino and chargino then are $\tilde{\chi}_4^0$ and $\tilde{\chi}_2^+$.

The branching ratio for the decay of the right-handed squark is studied in Fig. 7.10(b). Here the branching ratio for the decay $\tilde{u}_R \rightarrow u \tilde{\chi}_1^0$ is plotted. Since $\tilde{\chi}_1^0$ is mostly bino-like, the right-handed squark dominantly decays via this channel for $M_3 > M_{\text{SUSY}}$.

In Fig. 7.13(a) the relative correction of the NLO decay width including EW and QCD

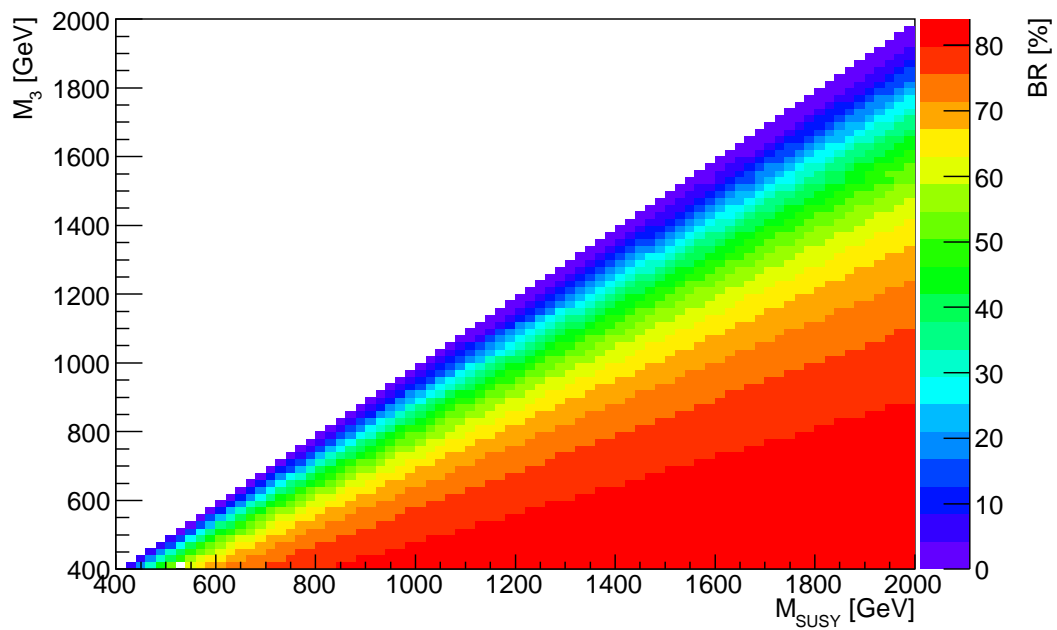
contributions to the total decay width of the left-handed up-type squark

$$\delta_{\text{tot}} = \frac{\Gamma_1^{\text{EW+QCD}}(\tilde{u}_L) - \Gamma_0(\tilde{u}_L)}{\Gamma_0(\tilde{u}_L)} \quad (7.11)$$

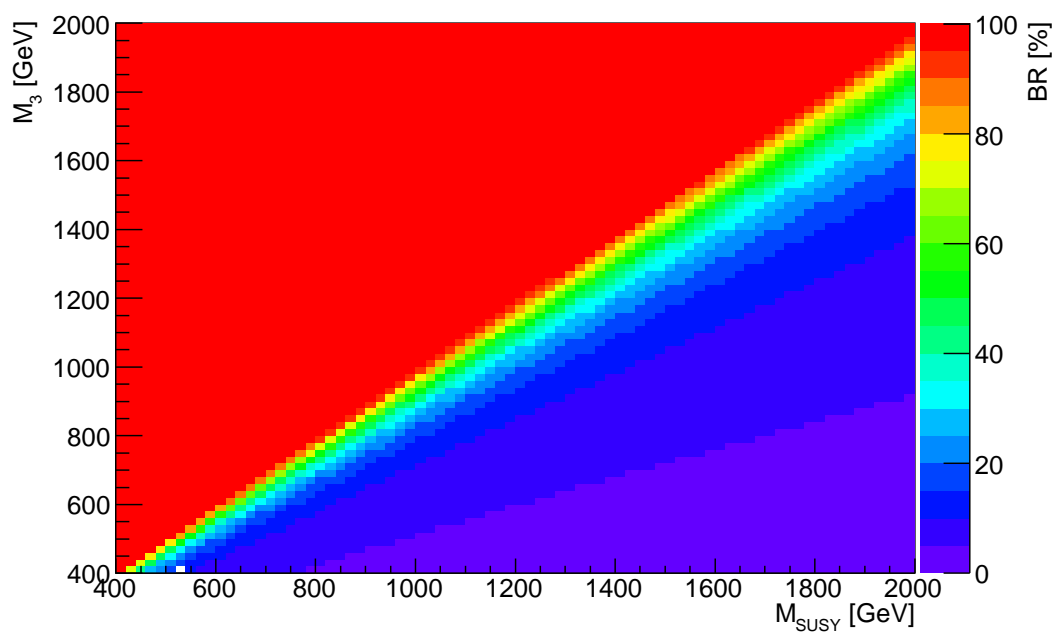
is plotted. $\Gamma(\tilde{u}_L)$ denotes the total decay width (3.13b) of the left-handed up-type squark. Since the denominator of δM_2 and $\delta\mu$ can be written as $\Delta = M_2^2 - \mu^2$ [129], the renormalization constants δM_2 and $\delta\mu$ diverge for $M_3 \approx 1500$ GeV, $M_2 \approx \mu \approx 500$ GeV. Since our renormalization scheme is not valid in this case, relative corrections in this region are manually set to zero (which is also visible in Fig. 7.11(a), 7.11(b), 7.12(b)) since they would predominate the corrections in the valid parameter space. This pole in the renormalization constants when $M_2 \approx \mu$ can be avoided by choosing different neutralinos for the on-shell renormalization conditions. However, these different renormalization schemes can lead to instabilities in other regions of parameter space [130].

The biggest relative corrections occur for $M_3 < M_{\text{SUSY}}$. In that region the squark dominantly decays into a quark and a gluino and the QCD corrections to this decay dominate, which is visible in Fig. 7.12(a) where only the relative QCD corrections are shown. The relative electroweak corrections to the total decay width of the left-handed up-type squark are shown in Fig. 7.12(b). They are mostly negative when the squark decays predominantly into a quark and a gluino, and positive when it decays into quark and neutralino / chargino. In the latter case, they are of the same order as the QCD corrections.

The total relative corrections (7.11) for the decay width of the right-handed up-type squark are depicted in Fig. 7.13(b). The biggest corrections again occur in the region, where QCD corrections to the decay $\tilde{u}_R \rightarrow u \tilde{g}$ are predominant (Fig. 7.14(a)). Apart from the decay of \tilde{u}_L , electroweak corrections (Fig. 7.14(b)) in this parameter region are negligible. Whereas in the region where the decay $\tilde{u}_R \rightarrow u \tilde{\chi}_1^0$ is most important, corrections reach up to 9%.

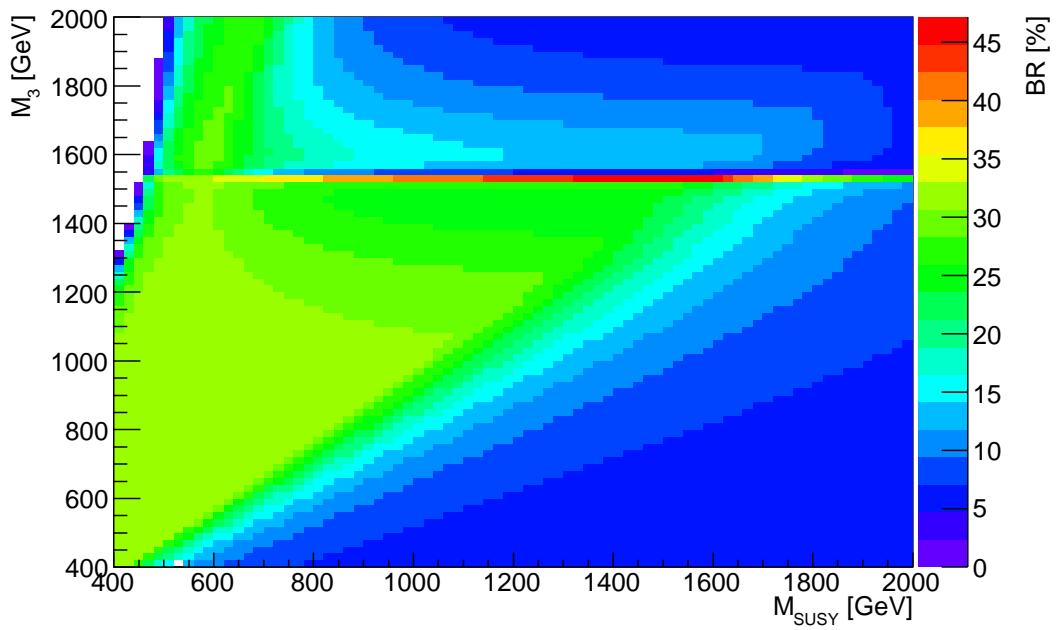


(a)

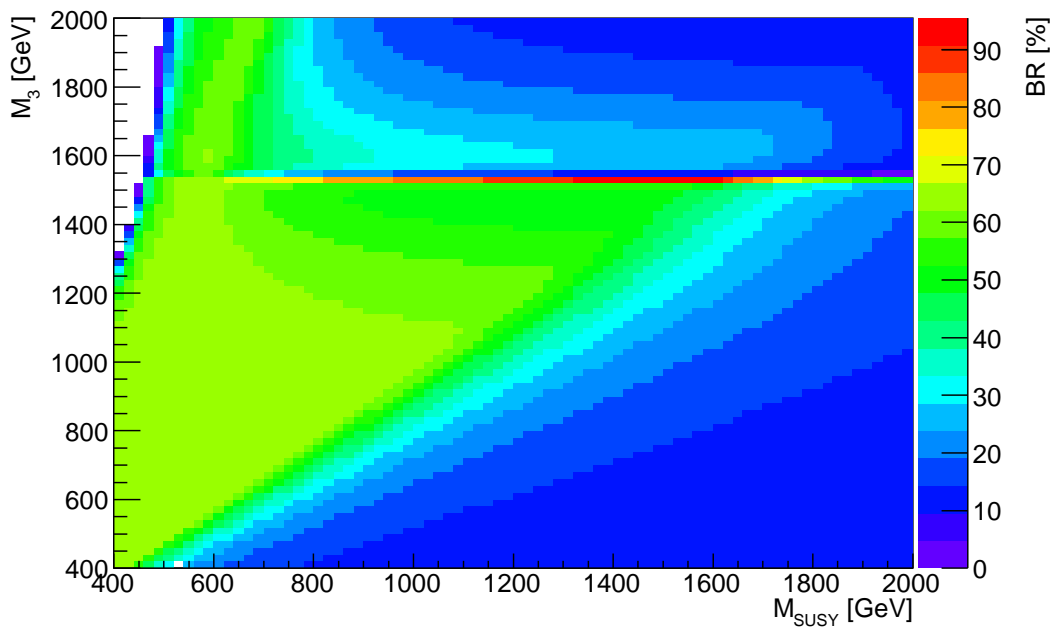


(b)

Figure 7.10: Branching ratio in % for the decay $\tilde{u}_L \rightarrow u \tilde{g}$ (a) and $\tilde{u}_R \rightarrow u \tilde{\chi}_1^0$ (b). Parameters are chosen as described in the first paragraph of Subsection 7.3.5.

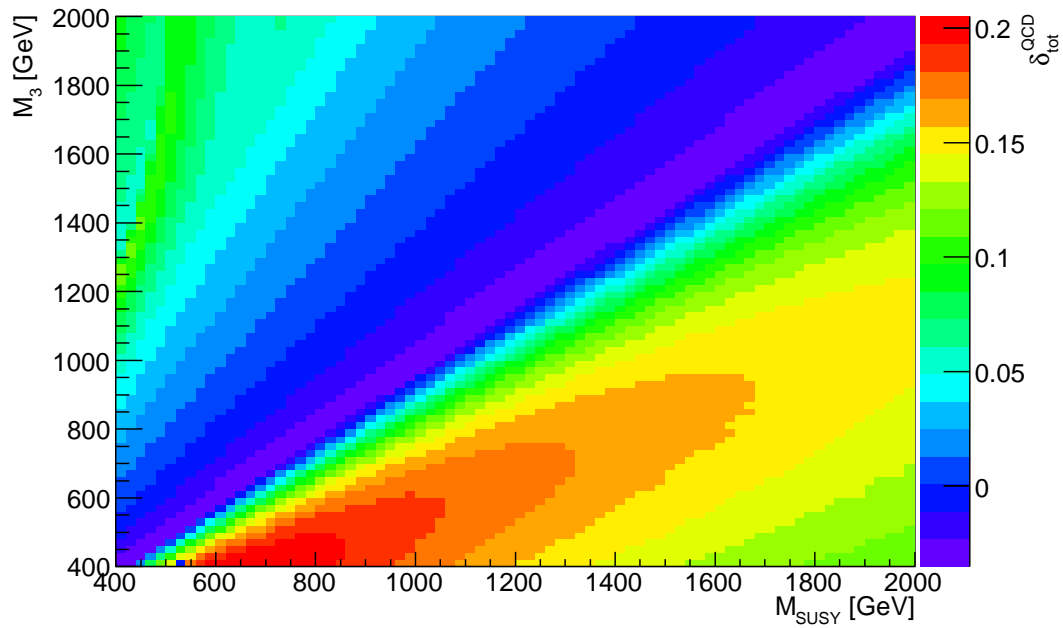


(a)

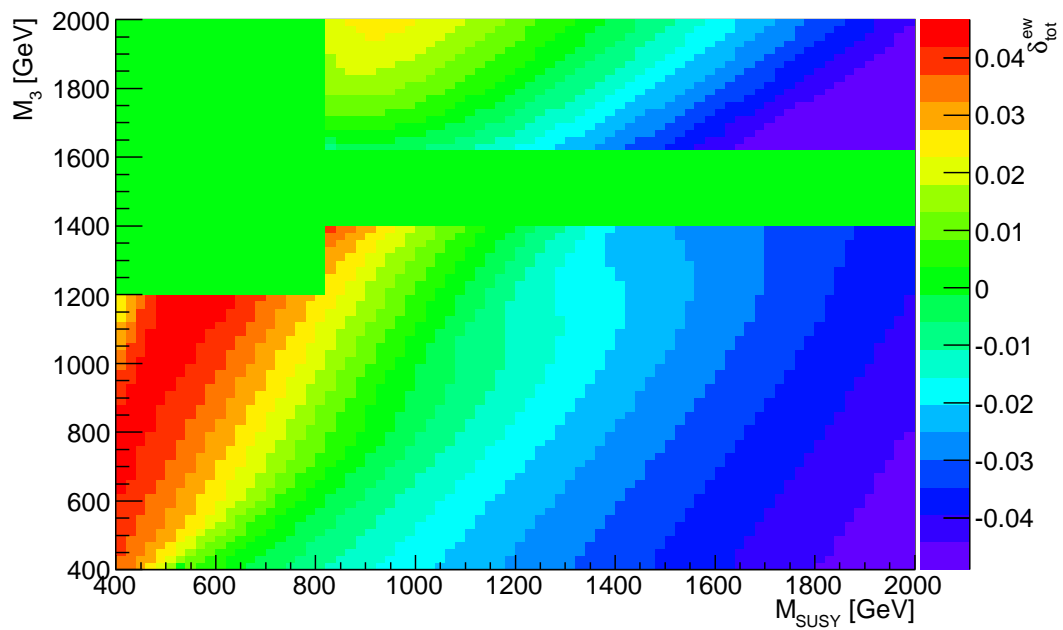


(b)

Figure 7.11: Branching ratio in % for the decay $\tilde{u}_L \rightarrow u \tilde{\chi}_2^0$ (a) and $\tilde{u}_L \rightarrow d \tilde{\chi}_1^+$ (b). Parameters are chosen as described in the first paragraph of Subsection 7.3.5.

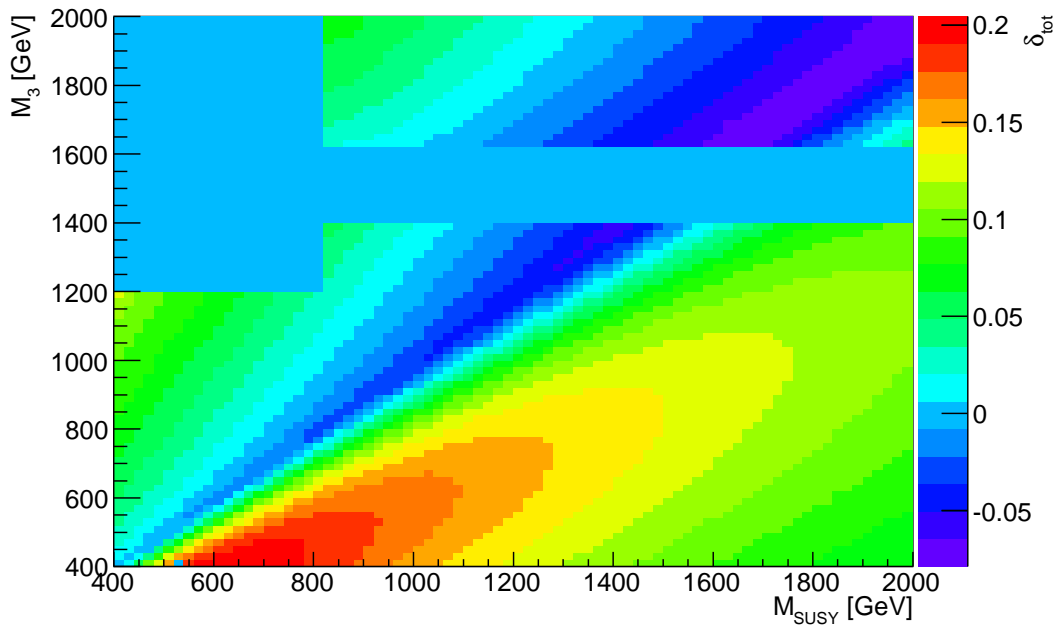


(a)

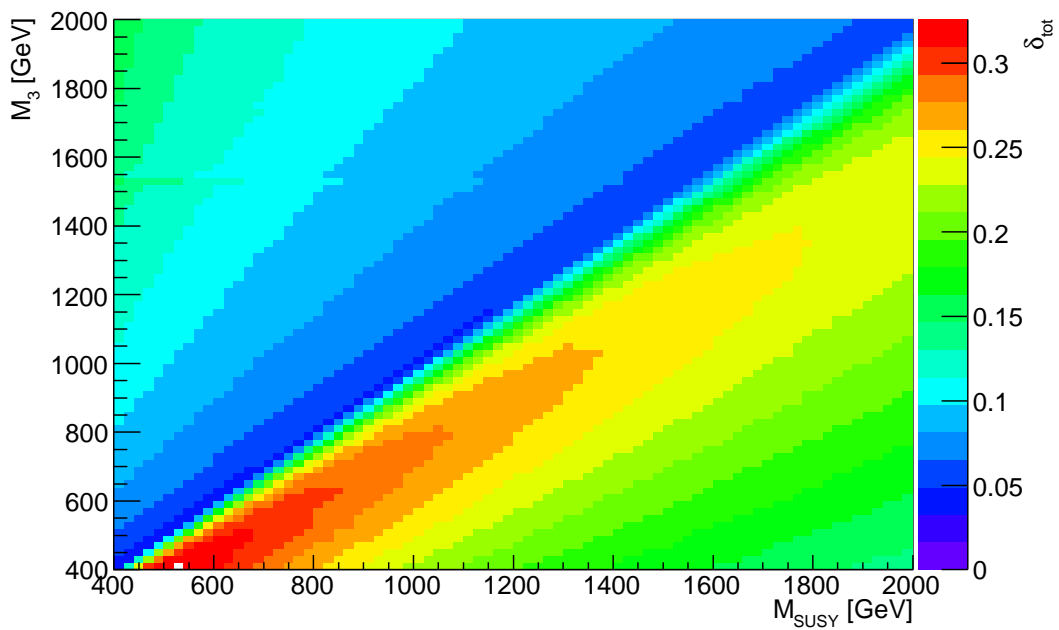


(b)

Figure 7.12: Relative QCD (a) and electroweak (b) corrections to the total decay width of \tilde{u}_L . Parameters are chosen as described in the first paragraph of Subsection 7.3.5.

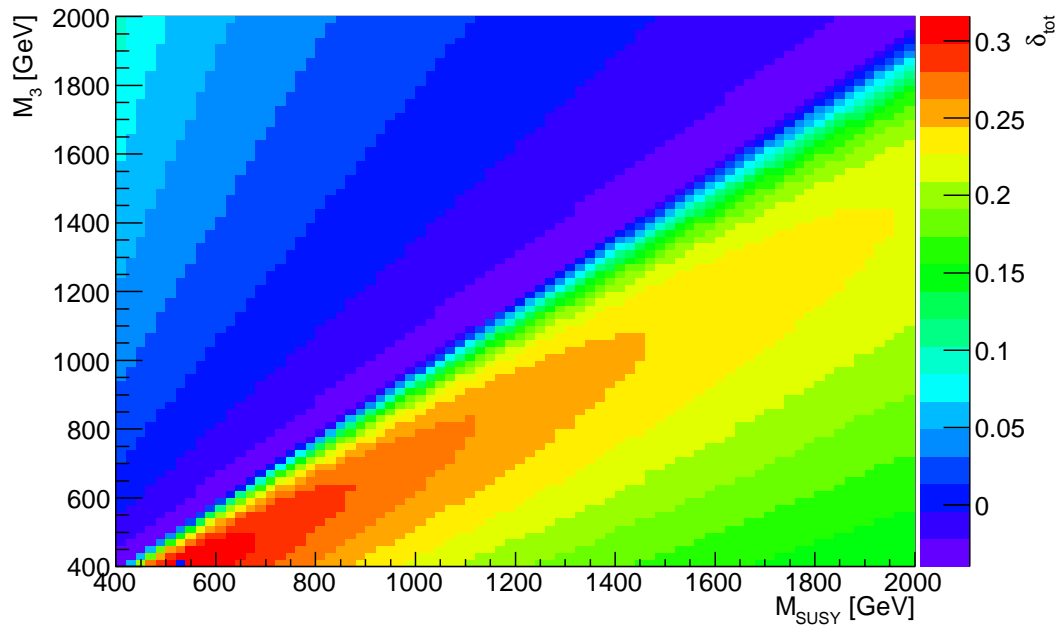


(a)

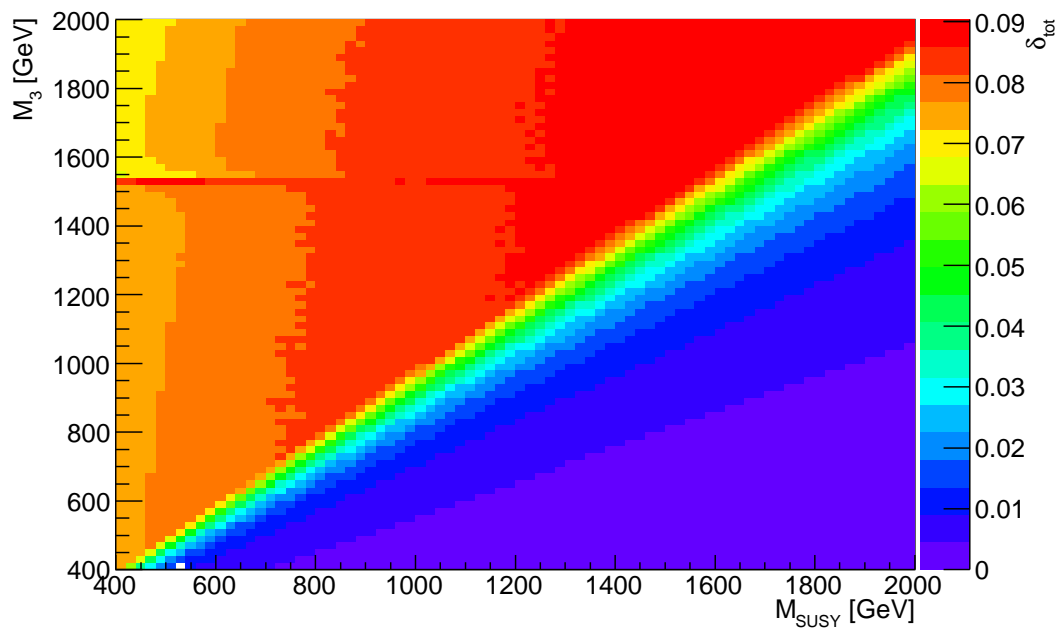


(b)

Figure 7.13: Relative total corrections to the total decay width of \tilde{u}_L (a) and \tilde{u}_R (b). Parameters are chosen as described in the first paragraph of Subsection 7.3.5.



(a)



(b)

Figure 7.14: Relative QCD (a) and electroweak (b) corrections to the total decay width of \tilde{u}_R . Parameters are chosen as described in the first paragraph of Subsection 7.3.5.

7.4 Quark jet p_T distribution

The electroweak and QCD corrections also have a substantial effect on differential distributions. These are of particular interest when production and decay of squarks are combined. In order to get observable distributions events of the decaying squarks would have to be combined with the events of squark production, i.e. the momenta of the decay products would have to be boosted with the distribution originating from the squark production. In this analysis we focus on the p_T distribution of the quark in the decay of a squark into quark plus neutralino. This shows whether big effects can arise due to corrections only in the squark decay.

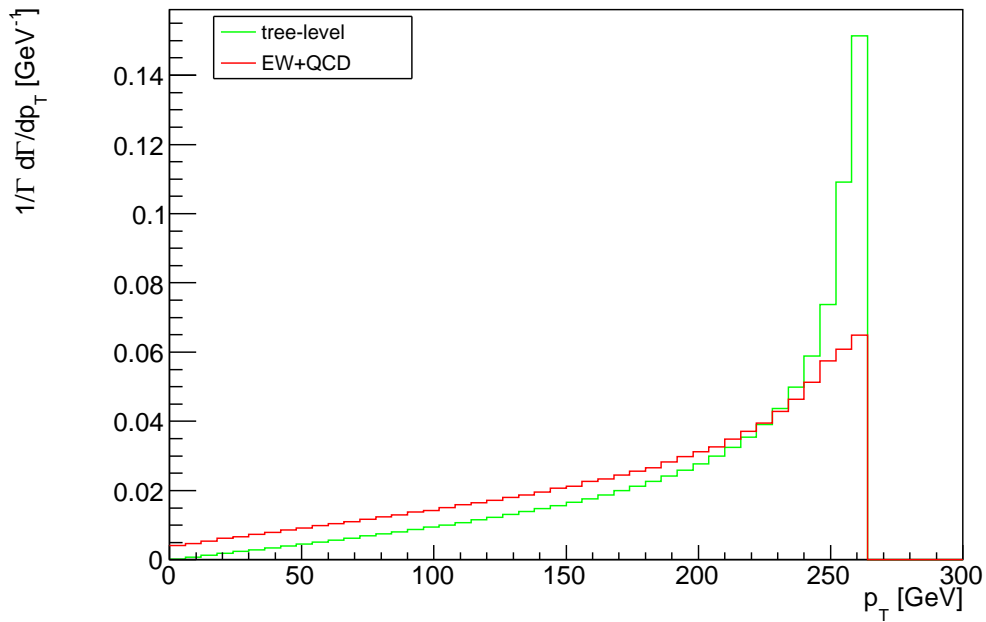
The effects of NLO contributions to p_T distributions of squark decays into neutralinos or charginos are very similar for the different light-flavor squark decay channels. As an example we show the p_T distribution of the quark jet of the decay $\tilde{u}_R \rightarrow u \tilde{\chi}_1^0$ in the SPS1a' benchmark scenario. In Fig. 7.15(a) the tree-level and corrected p_T distributions of the u quark in the decay $\tilde{u}_R \rightarrow u \tilde{\chi}_1^0$ at the SPS1a' parameter point are plotted ¹. The different relative corrections are defined as

$$\delta = \frac{d \Delta \Gamma^X / d p_T}{d \Gamma_0 / d p_T}, \quad X \in \{\text{EW, QCD, (real,QCD), (virt,QCD)}\}, \quad (7.12)$$

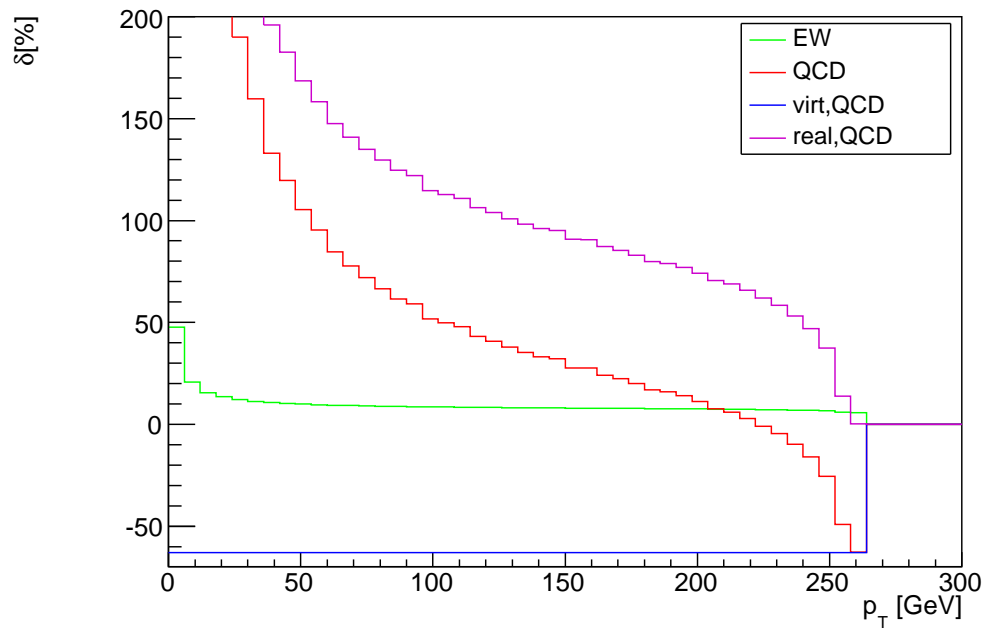
where p_T is the transverse momentum of the quark in the rest frame of the squark and the different contributions to the decay widths are defined in Chapter 3. This distribution is plotted in Fig. 7.15(b). Since for p_T distributions, QCD corrections are largest, real and virtual corrections are shown separately. The virtual contributions to the p_T distribution do not change its shape, i.e. the contribution of the relative virtual corrections (7.12) is flat. Noticeable is the finite value of the decay width for zero p_T . At tree-level the distribution reaches zero, whereas the corrected distribution reaches a finite, non-zero value.

The same distributions are plotted for the decay $\tilde{t}_1 \rightarrow t \tilde{\chi}_1^0$ in Fig. 7.16(a) and 7.16(b). Here, the effect of the real corrections on the distribution is much weaker. This can be explained by the presence of the massive top quark. Hence, the available phase space for the gluon radiation is much smaller and therefore influences the p_T distribution much less.

¹ p_T distribution in the center of mass system of the decaying particle denotes the distribution of the transverse component of the momentum in relation to a chosen direction rest frame of the decaying particle.

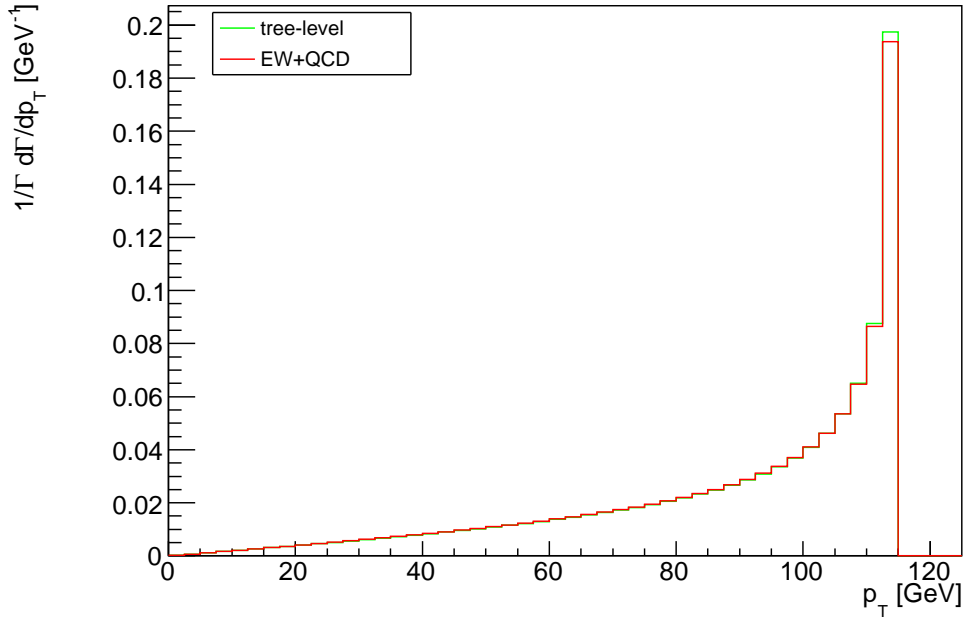


(a)

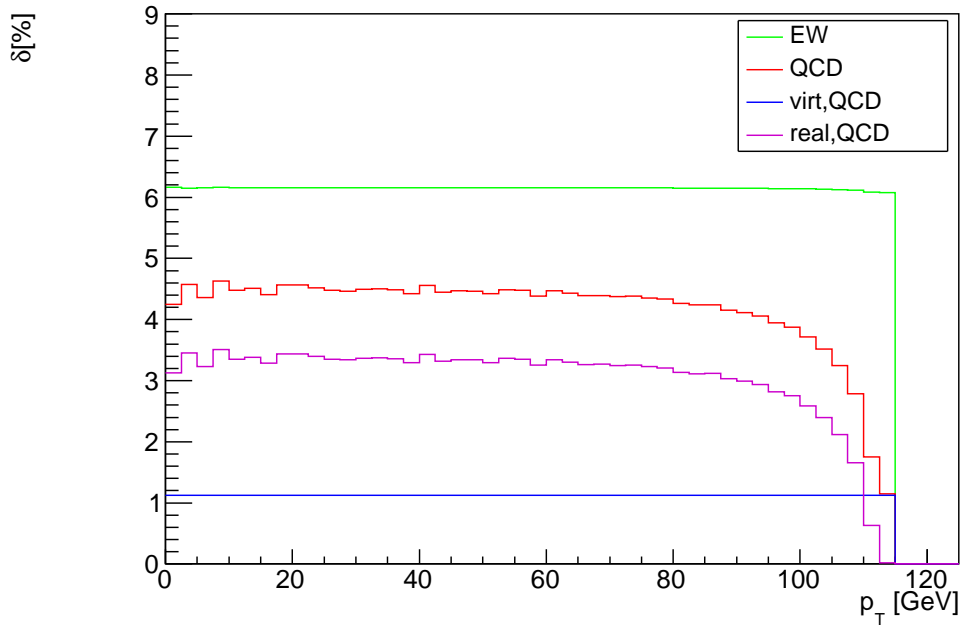


(b)

Figure 7.15: p_T distribution of the quark for the decay $\tilde{u}_R \rightarrow u \tilde{\chi}_1^0$ in the benchmark scenario SPS1a'. (a) shows the tree-level and the total corrected distribution, (b) the relative distributions (7.12).



(a)



(b)

Figure 7.16: p_T distribution of the quark for the decay $\tilde{t}_1 \rightarrow t \tilde{\chi}_1^0$ in the benchmark scenario SPS1a'. (a) shows the tree-level and the total corrected distribution, (b) the relative distributions (7.12).

7.5 Comparison with SFOLD

In the computer program SFOLD [102], strict one-loop QCD and EW corrections to two-body decays of sfermions are computed. The calculation at the one-loop level is performed in the $\overline{\text{DR}}$ scheme, whereas for the kinematics and one-loop functions on-shell masses are used. These input parameters are given in the SLHA [70] format. In order to compare the results of our calculations with the results of SFOLD we use the on-shell masses and mixing angles used by SFOLD to calculate the soft-breaking parameters. For the light-flavor squarks we choose the on-shell masses $m_{\tilde{u}_1}$, $m_{\tilde{u}_2}$, and $m_{\tilde{d}_2}$ to compute the on-shell soft-breaking parameters $M_{\tilde{q}_L}$, $M_{\tilde{u}_R}$, and $M_{\tilde{d}_R}$. Since the trilinear coupling in the bottom/sbottom sector is renormalized in the $\overline{\text{DR}}$ scheme we take the $\overline{\text{DR}}$ value of A_b as input parameter. For the remaining parameters for third-generation squarks we choose the masses and mixing angles $m_{\tilde{t}_1}$, $m_{\tilde{t}_2}$, $m_{\tilde{b}_2}$, and $\theta_{\tilde{t}}$ to compute $M_{\tilde{q}_L^3}$, $M_{\tilde{t}_R}$, $M_{\tilde{b}_R}$, and A_t . Similarly, in the slepton sector the on-shell masses $m_{\tilde{\nu}_\tau}$, $m_{\tilde{\tau}_2}$ are used to calculate $M_{\tilde{l}_L^3}$, $M_{\tilde{\tau}_2}$ and A_τ is taken in the $\overline{\text{DR}}$ scheme. In the neutralino/chargino sector we use the on-shell masses of $m_{\tilde{\chi}_1^0}$, $m_{\tilde{\chi}_1^\pm}$, and $m_{\tilde{\chi}_2^\pm}$ to compute the parameters M_1 , M_2 , and μ in the on-shell scheme. For the gluino we take the on-shell mass $m_{\tilde{g}}$ as input for the soft-breaking parameter M_3 . Finally we take the $\overline{\text{DR}}$ value of $\tan\beta$. According to the SPA convention [55], parameters in the $\overline{\text{DR}}$ scheme are given at the scale $Q_{\text{SUSY}} = 1 \text{ TeV}$.

The decay widths and branching ratios are compared at the [55, 123] benchmark point SPS1a' with the SM parameters used by SFOLD

$$\begin{aligned}
 M_Z &= 91.1876 \text{ GeV}, & M_W &= 80.3183 \text{ GeV}, \\
 \alpha^{\overline{\text{DR}}}(1 \text{ TeV}) &= 124.9736^{-1}, & \alpha_S(M_Z) &= 0.1176, \\
 m_t &= 171.2 \text{ GeV}, & m_b(m_b) &= 4.2 \text{ GeV}.
 \end{aligned}
 \tag{7.13}$$

Since in our computation, the electric charge e is renormalized in the on-shell scheme, we take the fine-structure constant $\alpha = 137.036^{-1}$ as input. The soft-breaking parameters in the $\overline{\text{DR}}$ scheme used by the SFOLD code and in an on-shell/ $\overline{\text{DR}}$ scheme used by our squark decay code (SDC) are listed in Tab. 7.15. The on-shell masses in Tab. 7.14 are used by SFOLD for the kinematics and one-loop functions. Furthermore, we use these on-shell masses to calculate the soft-breaking parameters in the on-shell scheme listed in Tab. 7.15.

Since SFOLD uses the input parameters in the $\overline{\text{DR}}$ scheme and we choose the input parameters in the on-shell scheme (only the trilinear coupling A_b and the bottom quark mass are renormalized in the $\overline{\text{DR}}$ scheme) it only makes sense to compare the results including EW and QCD corrections. SFOLD also includes higher-order contributions from the bottom-quark resummation which is also included in our result. Furthermore, in our computation the decay widths for squark decays into Higgs boson also include higher-order contributions from the finite field renormalization factors (4.31a) and (4.31b).

For the light-flavor squark decays, the relative NLO corrections obtained with SFOLD are about 30%, where the largest part of the NLO corrections stem from the QCD corrections. As discussed in Section 7.2 in our computation there are large cancellations between QCD and EW corrections and the relative corrections to the decay widths of light-flavor

$m_{h^0} = 110.70 \text{ GeV}$	$m_{H^0} = 421.15 \text{ GeV}$	$m_{A^0} = \mathbf{421.00 \text{ GeV}}$	$m_{H^\pm} = 428.96 \text{ GeV}$
$m_{\tilde{\chi}_1^0} = \mathbf{97.97 \text{ GeV}}$	$m_{\tilde{\chi}_2^0} = 183.87 \text{ GeV}$	$m_{\tilde{\chi}_3^0} = 396.74 \text{ GeV}$	$m_{\tilde{\chi}_4^0} = 410.51 \text{ GeV}$
$m_{\tilde{\chi}_1^\pm} = \mathbf{183.63 \text{ GeV}}$	$m_{\tilde{\chi}_2^\pm} = \mathbf{411.94 \text{ GeV}}$		$m_{\tilde{g}} = \mathbf{611.46 \text{ GeV}}$
$m_{\tilde{\nu}} = \mathbf{172.31 \text{ GeV}}$		$m_{\tilde{e}_L} = 189.66 \text{ GeV}$	$m_{\tilde{e}_R} = \mathbf{125.25 \text{ GeV}}$
$m_{\tilde{\nu}_\tau} = \mathbf{170.26 \text{ GeV}}$		$m_{\tilde{\tau}_1} = 108.00 \text{ GeV}$	$m_{\tilde{\tau}_2} = \mathbf{194.65 \text{ GeV}}$
$m_{\tilde{u}_L} = \mathbf{560.76 \text{ GeV}}$	$m_{\tilde{u}_R} = \mathbf{543.18 \text{ GeV}}$	$m_{\tilde{d}_L} = 566.24 \text{ GeV}$	$m_{\tilde{d}_R} = \mathbf{542.87 \text{ GeV}}$
$m_{\tilde{t}_1} = \mathbf{361.08 \text{ GeV}}$	$m_{\tilde{t}_2} = \mathbf{583.10 \text{ GeV}}$	$m_{\tilde{b}_1} = 502.67 \text{ GeV}$	$m_{\tilde{b}_2} = \mathbf{541.71 \text{ GeV}}$
$\theta_{\tilde{\tau}} = 1.2430$	$\theta_{\tilde{t}} = \mathbf{0.9714}$	$\theta_{\tilde{b}} = 0.3675$	

Table 7.14: On-shell masses for the Higgs bosons, gauginos and sfermions at the SPS1a' parameter point [55, 123] given by SFOLD. The mixing angles for $\tilde{\tau}$, \tilde{t} , and \tilde{b} mixing are given in radian. The quantities in bold letters are used to compute the soft-breaking parameters.

squarks are generally smaller than 10%. Furthermore, the decay widths computed with SFOLD and the ones from our computation deviate by around 30%. Because of this large discrepancy, we will not compare the results for light-flavor squarks in more detail.

In Tab. 7.16 the decay widths and branching ratios for third-generation squark decays obtained with SFOLD and our squark decay code denoted as SDC are shown. As described before, the decay widths and branching ratios include the complete EW and QCD one-loop corrections, as well as higher-order corrections from the resummed bottom Yukawa coupling. Furthermore, our code also includes higher-order contributions from the finite Higgs field renormalization factors (4.31a) and (4.31b). For most decay channels the relative difference between the partial decay widths obtained with SFOLD and the ones obtained with our computation is less than 10%. Only for the decays $\tilde{t}_2 \rightarrow \tilde{t}_1 h^0$, $\tilde{b}_2 \rightarrow b \tilde{\chi}_2^0$, $\tilde{b}_2 \rightarrow t \tilde{\chi}_1^-$, and $\tilde{b}_2 \rightarrow \tilde{t}_1 W^-$ the differences are considerably larger and amount up to 30%. So far, the reason for this discrepancy between the two computations has not been identified and needs further examination. The large difference between the decay widths for decays into Higgs bosons could originate from the different renormalization scheme used in the Higgs sector, whereas the deviations in the decay widths of the bottom squarks could stem from the discrepancies in the effective bottom quark mass.

	SFOLD ($\overline{\text{DR}}$)	SDC (on-shell/ $\overline{\text{DR}}$)
$\tan \beta$	10	10
μ	392.131 GeV	389.158 GeV
M_1	103.584 GeV	100.468 GeV
M_2	193.495 GeV	197.662 GeV
M_3	568.374 GeV	611.459 GeV
m_{A^0}	368.483 GeV	420.996 GeV
$M_{\tilde{t}_L}$	180.821 GeV	183.758 GeV
$M_{\tilde{e}_R}$	115.633 GeV	117.733 GeV
$M_{\tilde{t}_L^3}$	179.061 GeV	181.832 GeV
$M_{\tilde{\tau}_R}$	109.940 GeV	114.096 GeV
$M_{\tilde{q}_L}$	522.286 GeV	563.305 GeV
$M_{\tilde{u}_R}$	503.613 GeV	544.298 GeV
$M_{\tilde{d}_R}$	501.409 GeV	542.312 GeV
$M_{\tilde{t}_L^3}$	468.257 GeV	496.836 GeV
$M_{\tilde{t}_R}$	384.891 GeV	411.090 GeV
$M_{\tilde{b}_R}$	497.188 GeV	538.390 GeV
A_τ	-444.550 GeV	-444.550 GeV
A_t	-565.875 GeV	-531.406 GeV
A_b	-937.430 GeV	-937.430 GeV

Table 7.15: Soft-breaking parameters in the $\overline{\text{DR}}$ scheme used as input by the SFOLD code (left column). In the right column the soft-breaking parameters used as input in our calculation are listed. The parameters $\tan \beta$, A_τ , and A_b are given in the $\overline{\text{DR}}$ scheme.

Process	SFOLD		SDC	
	Γ_1 [GeV]	BR ₁	Γ_1 [GeV]	BR ₁
$\tilde{t}_1 \rightarrow t \tilde{\chi}_1^0$	0.290	21.9%	0.298	23.1%
$\tilde{t}_1 \rightarrow t \tilde{\chi}_2^0$	0.066	4.9%	0.067	5.2%
$\tilde{t}_1 \rightarrow b \tilde{\chi}_1^+$	0.971	73.2%	0.925	71.7%
$\tilde{t}_2 \rightarrow t \tilde{\chi}_1^0$	0.223	3.4%	0.243	3.6%
$\tilde{t}_2 \rightarrow t \tilde{\chi}_2^0$	0.633	9.7%	0.642	9.6%
$\tilde{t}_2 \rightarrow t \tilde{\chi}_3^0$	0.073	1.1%	0.071	1.1%
$\tilde{t}_2 \rightarrow t \tilde{\chi}_4^0$	0.267	4.1%	0.288	4.3%
$\tilde{t}_2 \rightarrow b \tilde{\chi}_1^+$	1.699	25.9%	1.699	25.4%
$\tilde{t}_2 \rightarrow b \tilde{\chi}_2^+$	0.967	14.8%	0.929	13.9%
$\tilde{t}_2 \rightarrow \tilde{t}_1 Z$	2.387	36.5%	2.467	36.8%
$\tilde{t}_2 \rightarrow \tilde{t}_1 h^0$	0.299	4.5%	0.355	5.3%
$\tilde{b}_1 \rightarrow b \tilde{\chi}_1^0$	0.132	2.9%	0.123	2.6%
$\tilde{b}_1 \rightarrow b \tilde{\chi}_2^0$	1.335	29.0%	1.332	28.3%
$\tilde{b}_1 \rightarrow b \tilde{\chi}_3^0$	0.011	0.2%	0.010	0.2%
$\tilde{b}_1 \rightarrow t \tilde{\chi}_4^0$	0.019	0.4%	0.016	0.3%
$\tilde{b}_1 \rightarrow t \tilde{\chi}_1^-$	1.667	36.2%	1.719	36.6%
$\tilde{b}_1 \rightarrow \tilde{t}_1 W^-$	1.437	31.2%	1.499	31.9%
$\tilde{b}_2 \rightarrow b \tilde{\chi}_1^0$	0.222	27.3%	0.232	34.8%
$\tilde{b}_2 \rightarrow b \tilde{\chi}_2^0$	0.081	9.9%	0.054	8.0%
$\tilde{b}_2 \rightarrow b \tilde{\chi}_3^0$	0.030	3.7%	0.025	3.8%
$\tilde{b}_2 \rightarrow b \tilde{\chi}_4^0$	0.037	4.5%	0.028	4.3%
$\tilde{b}_2 \rightarrow t \tilde{\chi}_1^-$	0.104	12.8%	0.070	10.5%
$\tilde{b}_2 \rightarrow \tilde{t}_1 W^-$	0.340	41.8%	0.258	38.7%

Table 7.16: Comparison of decay widths and branching ratios between SFOLD and our code denoted as SDC. The decay widths are given including EW and QCD corrections.

Chapter 8

Gluino decays

In this chapter, gluino decays into quark plus squark are discussed. This process is obtained by crossing the squark decay into a quark and a gluino. Therefore, the framework of Section 6.2 can be reapplied. Section 8.1 introduces the decay channels considered in this work and in Section 8.2 the computation of the decay width is briefly discussed. Lastly, in Section 8.3 the numerical evaluation is presented.

8.1 Overview

The characteristics of gluino decays strongly depends on the relation between gluino and squark masses. If the gluino is heavier than the squarks, the two-body decays $\tilde{g} \rightarrow \bar{q} \tilde{q}_i$ (Fig. 8.1 (a)) are dominant because of the QCD strength of the squark-quark-gluino coupling. Since the top and bottom squarks can be considerably lighter than the other squarks, it is possible that only the decays $\tilde{g} \rightarrow t \tilde{t}_1$ and $\tilde{g} \rightarrow b \tilde{b}_1$ are relevant. However, if all of the squarks are heavier than the gluino, it will either decay through off-shell squarks, i.e. via the three-body decays $\tilde{g} \rightarrow q \bar{q} \tilde{\chi}_i^0$ and $\tilde{g} \rightarrow q q' \tilde{\chi}_i^\pm$ (Fig. 8.1 (b)) or via the loop-suppressed decay $\tilde{g} \rightarrow g \tilde{\chi}_i^0$ [88–90, 93, 131, 132]. In this work we only consider the two-body decays $\tilde{g} \rightarrow \bar{q} \tilde{q}_i$ for the case $m_{\tilde{g}} > m_{\tilde{q}}$.

The QCD corrections to gluino decays into quark and squark have been studied in [99, 100]. They amount to up to 10%. In [101], corresponding EW corrections in the Yukawa approximation have been worked out. They also reach up to 10%.

The aim of our work in this chapter is to compute all QCD and EW NLO corrections to the two-body decays of gluinos into squarks plus quarks, $\tilde{g} \rightarrow \bar{q} \tilde{q}_a + \text{cc}$. This calculation is performed within a general renormalization scheme also used for computing squark decays in the preceding chapters (cf. Chapter 4).

8.2 Decay width

The amplitudes for the decay $\tilde{g} \rightarrow \bar{q} \tilde{q}_a$ are obtained by crossing the diagrams in Figs. 6.3, 6.4. The tree-level amplitude is denoted as \mathcal{M}_0 , the NLO amplitudes including one-loop and

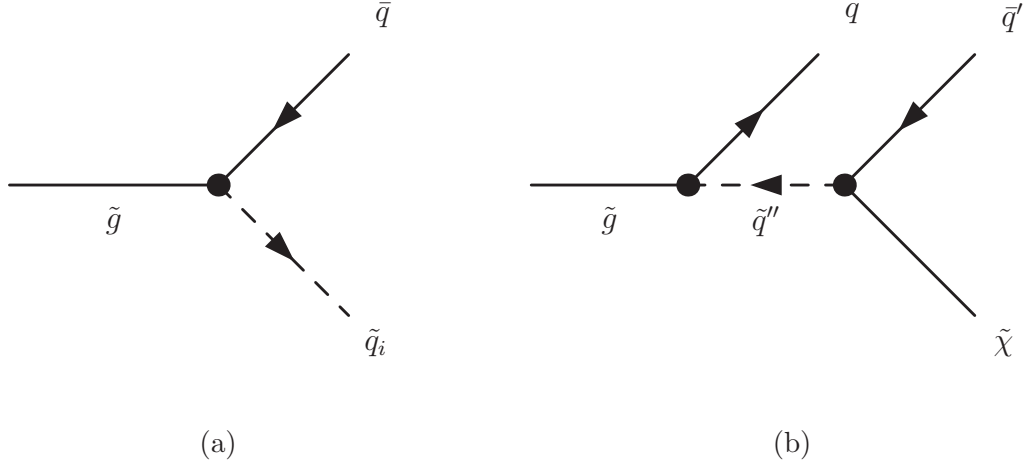


Figure 8.1: Feynman diagrams for gluino decays in the case $m_{\tilde{g}} > m_{\tilde{q}}$ (a) and $m_{\tilde{g}} < m_{\tilde{q}}$ (b).

counterterm contributions are given by $\mathcal{M}_1^{\text{EW/QCD}} = \mathcal{M}_1^{\text{1L,EW/QCD}} + \mathcal{M}_1^{\text{CT,EW/QCD}}$, and the amplitudes for real photon/gluon radiation are denoted as $\mathcal{M}_1^{\text{real,EW/QCD}}$.

The tree-level decay widths are given by

$$\Gamma_0(\tilde{g} \rightarrow \bar{q}\tilde{q}_a) = \frac{(2\pi)^4}{m_{\tilde{g}}} \int d\text{PS}_2 |\mathcal{M}_0|^2, \quad (8.1)$$

and the decay widths at NLO for virtual and real contributions read

$$\Gamma_1^{\text{virt,EW/QCD}}(\tilde{g} \rightarrow \bar{q}\tilde{q}_a) = \frac{(2\pi)^4}{m_{\tilde{g}}} \int d\text{PS}_2 2\text{Re} \left(\mathcal{M}_0 \mathcal{M}_1^{\text{EW/QCD}} \right) + \delta_{\text{soft}} \Gamma_0 + \delta_{\text{coll}} \Gamma_0, \quad (8.2a)$$

$$\Gamma_1^{\text{real,EW/QCD}}(\tilde{g} \rightarrow \bar{q}\tilde{q}_a) = \frac{(2\pi)^4}{m_{\tilde{g}}} \int d\text{PS}_3 |\mathcal{M}_1^{\text{real,EW/QCD}}|^2, \quad (8.2b)$$

where δ_{soft} and δ_{coll} denote the soft-photon/gluon and collinear-photon/gluon factors (4.116) and (4.120). An analogous calculation as in Subsection 6.2.4 yields the color factor matrix R_{ij} (cf. (4.116)),

$$R = \begin{pmatrix} 12 & 6 & 6 \\ 6 & 16/3 & 2/3 \\ 6 & 2/3 & 16/3 \end{pmatrix}. \quad (8.3)$$

Finally, the NLO decay width including real and virtual contributions is given by

$$\Gamma_1^{\text{EW/QCD}}(\tilde{g} \rightarrow \bar{q}\tilde{q}_a) = \Gamma_1^{\text{virt,EW/QCD}}(\tilde{g} \rightarrow \bar{q}\tilde{q}_a) + \Gamma_1^{\text{real,EW/QCD}}(\tilde{g} \rightarrow \bar{q}\tilde{q}_a) \quad (8.4)$$

In the numerical analyses, we consider MSSM parameters, where first and second generation squarks have the same masses and couplings. Therefore, for gluino decays into

light-flavor squarks, the decay widths will include the identical decays into the two light-flavor generations. Since the gluino also decays into the charge conjugated final state $\tilde{g} \rightarrow q \tilde{q}_i^*$, decays related by charge conjugation are combined into the same decay widths,

$$\Gamma(\tilde{g} \rightarrow \bar{q} \tilde{q}_a + \text{cc}) = \sum_{j=1,2} [\Gamma(\tilde{g} \rightarrow \bar{q}^j \tilde{q}_a^j) + \Gamma(\tilde{g} \rightarrow q^j \tilde{q}_a^{j*})], \quad (8.5a)$$

$$\Gamma(\tilde{g} \rightarrow \bar{t} \tilde{t}_a + \text{cc}) = \Gamma(\tilde{g} \rightarrow \bar{t} \tilde{t}_a) + \Gamma(\tilde{g} \rightarrow t \tilde{t}_a^*), \quad (8.5b)$$

$$\Gamma(\tilde{g} \rightarrow \bar{b} \tilde{b}_a + \text{cc}) = \Gamma(\tilde{g} \rightarrow \bar{b} \tilde{b}_a) + \Gamma(\tilde{g} \rightarrow b \tilde{b}_a^*), \quad (8.5c)$$

where the superscript g denotes the generation index and “cc” the charge-conjugate final state. Hence, for gluino decays into light-flavor squarks, the decay width is multiplied by a factor of 4 and for decays into third-generation squarks with a factor of 2.

8.3 Numerical evaluation

As SM input parameters we use the ones given in Section 7.1. Since we are interested in decays of gluinos into quarks plus squarks, for the numerical evaluation we choose parameter points where the squarks (or at least some of them) are lighter than the gluino. For the first analysis, we choose the benchmark Point 10.1.1 (Tab. 7.5, 7.6), which was already used for the analyses of squark decays. Here, the gluino is heavier than almost all squarks, allowing for gluino decays into quarks and squarks. Only the decay $\tilde{g} \rightarrow t \tilde{t}_2$ is kinematically forbidden due to the mass of the heavier top squark. In Tab. 8.1 the decay widths and branching ratios are listed at the tree level and at the one-loop level. The relative EW/QCD corrections are defined by

$$\delta^{\text{EW/QCD}} = \frac{\Gamma_1^{\text{EW/QCD}} - \Gamma_0}{\Gamma_0}. \quad (8.6)$$

For all decay channels, the relative QCD corrections are always negative and lie around -11% . Only for the decay of the gluino into bottom squarks their absolute values are slightly larger and the relative corrections amount to -13% . The relative EW corrections, however, all are positive. Their value differ for the different decay channels. For gluino decays into left-handed light-flavor squarks and quarks the relative EW corrections are given by $\delta^{\text{EW}} \approx 5\%$, whereas for the decay into light-flavor right-handed squarks and quarks the relative corrections only amount to 1% . Taking into account the cancellation between EW and QCD corrections, the total corrections for gluino decays into light-flavor left-handed squarks and quarks lie around -6% and for decays into light-flavor right-handed squarks and quarks they amount to -10% . For the gluino decays into top and bottom squarks, the overall corrections lie between 8% and 13% . The differences in the relative corrections for the different decay channels explain that the branching ratios at tree-level and at NLO change up to 5% .

A particular interesting case occurs when the light-flavor squarks are heavier and only the third-generation squarks are lighter than the gluino. This is the case for benchmark

Decay channel	Γ_0 [GeV]	BR ₀	Γ_1 [GeV]	BR ₁
$\tilde{g} \rightarrow u \tilde{u}_L$	1.293	8.82 %	1.223	9.23 %
$\tilde{g} \rightarrow u \tilde{u}_R$	2.460	16.79 %	2.194	16.56 %
$\tilde{g} \rightarrow d \tilde{d}_L$	1.221	8.33 %	1.154	8.71 %
$\tilde{g} \rightarrow d \tilde{d}_R$	2.577	17.59 %	2.278	17.19 %
$\tilde{g} \rightarrow t \tilde{t}_1$	3.417	23.33 %	3.101	23.41 %
$\tilde{g} \rightarrow b \tilde{b}_1$	2.205	15.05 %	2.014	15.20 %
$\tilde{g} \rightarrow b \tilde{b}_2$	1.478	10.09 %	1.283	9.69 %

Table 8.1: Decay widths of the gluino at the benchmark point 10.1.1. Listed are values at tree-level (Γ_0 , BR₀) and including both, electroweak and QCD one-loop corrections (Γ_1 , BR₁).

point 40.2.1 [127]. In terms of the mSUGRA parameters at the GUT scale (cf. Section 7.1) it is given by

$$\begin{aligned}
 M_0 = 550 \text{ GeV}, \quad M_{1/2} = 450 \text{ GeV}, \quad A_0 = -500 \text{ GeV}, \\
 \tan \beta = 40, \quad \text{sgn } \mu > 0.
 \end{aligned}
 \tag{8.7}$$

The soft-breaking parameters and relevant sparticle masses for this benchmark point are given in Tabs. 8.3 and 8.2, respectively. Since only third-generation squarks are lighter than the gluino, only the decays $\tilde{g} \rightarrow t \tilde{t}_1$ and $\tilde{g} \rightarrow b \tilde{b}_{1/2}$ are kinematically accessible. For these three possible two-body decay channels, the branching ratios are listed in Tab. 8.4 including NLO EW and QCD corrections. The relative EW corrections (8.6) are all positive and range from 0.2% to 3% whereas the relative QCD corrections are negative and lie between -8% and -11% . Considering the cancellation between EW and QCD NLO corrections, the relative corrections of both EW and QCD contributions are approximately 8% for all decay channels. Therefore, the branching ratios at tree-level and at NLO do not change significantly.

$m_{\tilde{g}} = 1146.89 \text{ GeV}$			
$m_{\tilde{u}_L} = 1092.45 \text{ GeV}$	$m_{\tilde{u}_R} = 1063.79 \text{ GeV}$	$m_{\tilde{d}_L} = 1095.40 \text{ GeV}$	$m_{\tilde{d}_R} = 1061.48 \text{ GeV}$
$m_{\tilde{t}_1} = 745.03 \text{ GeV}$	$m_{\tilde{t}_2} = 948.94 \text{ GeV}$	$m_{\tilde{b}_1} = 853.09 \text{ GeV}$	$m_{\tilde{b}_2} = 914.58 \text{ GeV}$

Table 8.2: On-shell masses for the gluino and squarks at the benchmark point 40.2.1.

$M_{A^0} = 632.32 \text{ GeV}$	$\tan \beta = 39.19$	$\mu = 627.26 \text{ GeV}$
$M_1 = 187.74 \text{ GeV}$	$M_2 = 364.54 \text{ GeV}$	$M_3 = 1063.29; \text{ GeV}$
$M_{\tilde{t}_L^{(1,2)}} = 623.44 \text{ GeV}$	$M_{\tilde{e}_R^{(1,2)}} = 573.31 \text{ GeV}$	
$M_{\tilde{t}_L^{(3)}} = 567.99 \text{ GeV}$	$M_{\tilde{\tau}_R} = 441.74 \text{ GeV}$	
$M_{\tilde{q}_L^{(1,2)}} = 1093.79; \text{ GeV}$	$M_{\tilde{u}_R^{(1,2)}} = 1064.37 \text{ GeV}$	$M_{\tilde{d}_R^{(1,2)}} = 1061.19 \text{ GeV}$
$M_{\tilde{q}_L^{(3)}} = 893.65 \text{ GeV}$	$M_{\tilde{t}_R} = 775.83 \text{ GeV}$	$M_{\tilde{b}_R} = 872.61 \text{ GeV}$
$A_\tau = -507.78 \text{ GeV}$	$A_t = -812.79 \text{ GeV}$	$A_b = -1338.17 \text{ GeV}$

Table 8.3: Soft SUSY-breaking on-shell parameters for the benchmark point 40.2.1. Since the bottom quark/squark sector is treated in the $\overline{\text{DR}}$ scheme, the trilinear coupling of the bottom quark A_b remains $\overline{\text{DR}}$.

Decay channel	Γ_0 [GeV]	BR ₀	Γ_1 [GeV]	BR ₁
$\tilde{g} \rightarrow t \tilde{t}_1$	2.705	36.61 %	2.495	36.80 %
$\tilde{g} \rightarrow b \tilde{b}_1$	3.200	43.32 %	2.920	43.07 %
$\tilde{g} \rightarrow b \tilde{b}_2$	1.483	20.07 %	1.364	20.12 %

Table 8.4: Decay widths of the gluino at the benchmark point 40.2.1. Listed are the values at tree-level (Γ_0 , BR₀) and including both, electroweak and QCD one-loop corrections (Γ_1 , BR₁).

8.4 Dependence on the squark masses

The squark-mass dependence of gluino decays into squarks plus quarks is analyzed starting from the benchmark Point 10.1.1 (c.f. Tab. 7.5), where the on-shell squark mass parameters are set to

$$M_{\tilde{q}_L^{(1,2,3)}} = M_{\tilde{u}_R^{(1,2)}} = M_{\tilde{d}_R^{(1,2)}} = M_{\tilde{b}_R} = M_{\text{SUSY}}, \quad (8.8a)$$

$$M_{\tilde{t}_R} = M_{\text{SUSY}} - 150 \text{ GeV}, \quad (8.8b)$$

and the parameter M_{SUSY} is varied between 800 GeV and 1150 GeV. Condition (8.8b) results in a top squark considerably lighter than the other squarks, which is a common feature of supersymmetric models due to the running of the SUSY parameters from the GUT scale.

The variation of the branching ratios with respect to M_{SUSY} are displayed in Fig. 8.2. In the left panel the branching ratios including QCD and EW corrections for the different decay channels are plotted. The red curve shows the branching ratio for the gluino

decaying into light-flavor quarks and squarks, where “cc” denotes the charge conjugated decay processes. For $M_{\text{SUSY}} < 900 \text{ GeV}$ the partial decay widths for the different decay channels have more or less the same value. This results in a branching ratio of approximately 64% for gluino decays into light-flavor quarks and squarks (red curve), $\text{BR} \approx 24\%$ for the decay into the heavier top squark and bottom squarks (blue curve), and $\text{BR} \approx 8\%$ for the decay into the lighter top squark (green curve). The kink in the curves at $M_{\text{SUSY}} \approx 930 \text{ GeV}$ appears since, the decay channel $\tilde{g} \rightarrow \bar{t}\tilde{t}_2 + cc$ is kinematically not accessible anymore. In the right panel of Fig. 8.2 the branching ratio is enlarged for the range $1100 \text{ GeV} \leq M_{\text{SUSY}} \leq 1150 \text{ GeV}$. For $M_{\text{SUSY}} \approx 1135 \text{ GeV}$ the branching ratio for a gluino decaying into the lighter top squark grows considerably reaching upto 55%. This is due to the smaller value of the lighter top squark mass $m_{\tilde{t}_1} \approx 972 \text{ GeV}$ compared to the other squark masses $m_{\tilde{q}} \approx 1135 \text{ GeV}$, resulting in a larger available phase space for the decay $\tilde{g} \rightarrow \bar{t}\tilde{t}_1 + cc$. For $1140 \text{ GeV} \leq M_{\text{SUSY}} \leq m_{\tilde{g}} \approx 1147 \text{ GeV}$ the gluino decay into the lighter top squark is kinematically forbidden and the BR for the decays into light-flavor squarks and the bottom squarks increase. When M_{SUSY} approaches the gluino mass $m_{\tilde{g}}$, the decay to bottom and lighter sbottom remains the only possible decay channel visible in the steep increase of the blue curve.

In order to study the dependence of the NLO corrections on M_{SUSY} , the relative corrections

$$\delta = \frac{\Gamma_1^X - \Gamma_0}{\Gamma_0}, \quad X \in \{\text{EW}, \text{QCD}, \text{EW+QCD}\} \quad (8.9)$$

are displayed in Fig. 8.3. The expressions for the decay widths are given in Section 8.2. We have seen in the preceding section, that the relative corrections, especially the EW corrections, depend on the different decay channels. Therefore, the relative corrections are displayed exemplary for the decay channels $\tilde{g} \rightarrow \bar{u}\tilde{u}_L + cc$ (left panel) and $\tilde{g} \rightarrow \bar{t}\tilde{t}_1 + cc$ (right panel). The relative EW corrections to the decay $\tilde{g} \rightarrow \bar{u}\tilde{u}_L + cc$ are positive and do not strongly depend on M_{SUSY} staying at a value of $\delta \approx 0.04$. For M_{SUSY} considerably smaller than $m_{\tilde{g}}$, the relative QCD corrections range between $-0.08 \geq \delta \geq -0.13$ resulting in relative EW and QCD corrections around -0.5 . For M_{SUSY} approaching the gluino mass, the relative QCD corrections grow positive resulting in an positive overall relative correction. The kink at $M_{\text{SUSY}} \approx 930 \text{ GeV}$ corresponds to the threshold $m_{\tilde{g}} = m_t + m_{\tilde{t}_2}$ and the kink at $M_{\text{SUSY}} \approx 1140 \text{ GeV}$ indicates the threshold $m_{\tilde{g}} = m_t + m_{\tilde{t}_1}$ in the field renormalization factor of the gluino. For the gluino decaying to the lighter top squark, the relative corrections are positive ranging between $0 < \delta \leq 0.03$ and strongly increase when M_{SUSY} approaches the gluino mass. The kinks at $M_{\text{SUSY}} \approx 975 \text{ GeV}$ and 985 GeV are due to the threshold $m_{\tilde{t}_1} = m_t + m_{\tilde{\chi}_{3,4}^0}$ in the field renormalization factor of the top squark \tilde{t}_1 . The relative QCD corrections range from $-0.05 \geq \delta \geq -0.13$ for M_{SUSY} considerably smaller than $m_{\tilde{g}}$. Unlike the relative QCD corrections to the gluino decaying into light-flavor squarks, the relative QCD corrections to the decay $\tilde{g} \rightarrow \bar{t}\tilde{t}_1$ become negative when M_{SUSY} approaches $m_{\tilde{g}}$. The kink at $M_{\text{SUSY}} \approx 930 \text{ GeV}$ again corresponds to the threshold $m_{\tilde{g}} = m_t + m_{\tilde{t}_2}$.

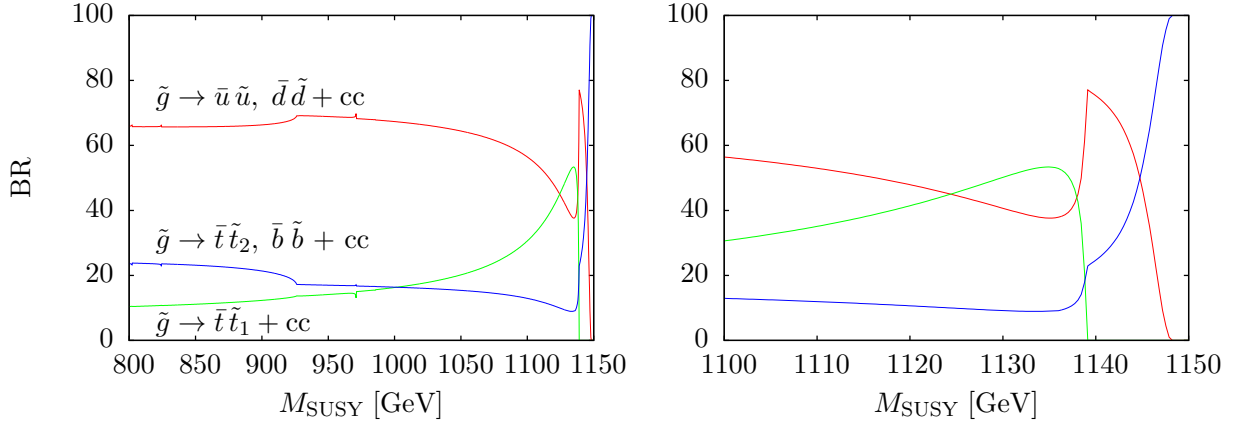


Figure 8.2: Branching ratios for the different gluino decay channels in function of M_{SUSY} including QCD and EW corrections. The other parameters are chosen according to benchmark point 10.1.1 as described in the first paragraph of Section 8.4. In the right panel the region $1100 \text{ GeV} \leq M_{\text{SUSY}} \leq 1150 \text{ GeV}$ is enlarged.

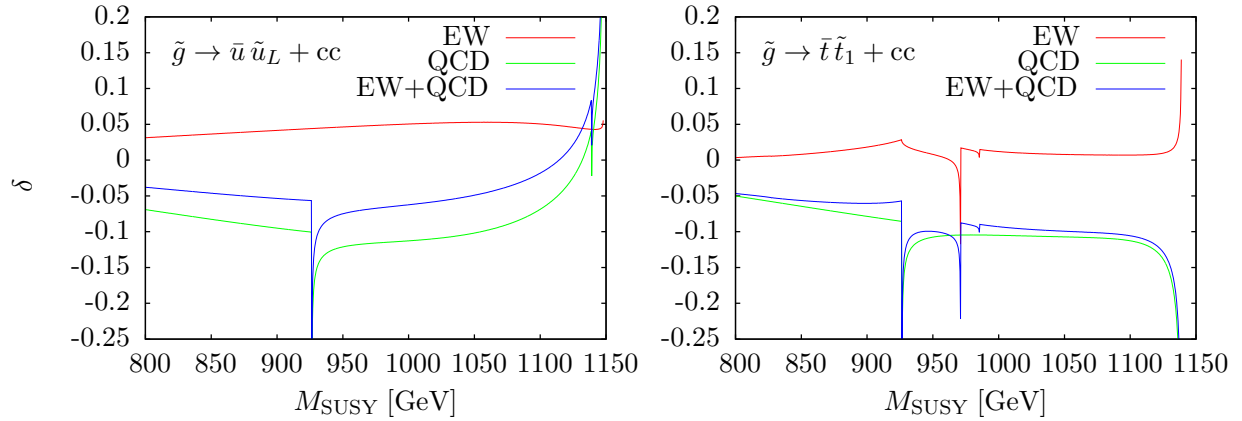


Figure 8.3: Relative corrections to the partial decay widths for the processes $\tilde{g} \rightarrow \bar{u} \tilde{u}_L + cc$ (left) and $\tilde{g} \rightarrow \bar{t} \tilde{t}_1 + cc$ (right) in function of M_{SUSY} . The other parameters are chosen according to benchmark point 10.1.1 as described in the first paragraph of Section 8.4.

Chapter 9

Higgs-boson decays into sfermions, neutralinos and charginos

In this chapter, NLO corrections to Higgs-boson decays into squarks, sleptons, neutralinos, and charginos are discussed. Section 9.1 introduces the different Higgs-boson decay channels and lists different publications where these decays have been computed. The following Section 9.2 discusses the calculation framework used in this work. In Section 9.3 the relevant decay widths and branching ratios are introduced and in Section 9.4 numerical results are presented. Finally, in Section 9.5 our results are compared with the results obtained with HFOLD [133].

9.1 Overview

A substantial difference between phenomenology of Higgs bosons in the SM and MSSM is the possibility of decays not only into SM particles but also into sparticles such as neutralinos, charginos and possibly sleptons and third-generation squarks. In the MSSM the lightest Higgs boson might decay invisibly into a pair of the lightest neutralinos $h^0 \rightarrow \tilde{\chi}_1^0 \tilde{\chi}_1^0$ with a branching ratio exceeding 10% [134]. This is particularly true when the universality condition $M_1 = \frac{5}{3} \tan^2 \theta_W M_2 \approx 2M_2$ is relaxed leading to light $\tilde{\chi}_1^0$ and still respecting the LEP bound on $m_{\tilde{\chi}_1^\pm}$. Decays of the lightest Higgs boson h^0 into other sparticles than possibly $\tilde{\chi}_1^0$ are kinematically forbidden. Overall, we consider here the following decays:

$$\begin{aligned} (H^0, A^0) &\rightarrow \tilde{\chi}_i^0 \tilde{\chi}_j^0, & h^0 &\rightarrow \tilde{\chi}_1^0 \tilde{\chi}_1^0, \\ (H^0, A^0) &\rightarrow \tilde{\chi}_k^+ \tilde{\chi}_l^- + \text{cc}, & H^- &\rightarrow \tilde{\chi}_k^- \tilde{\chi}_l^0, \\ (H^0, A^0) &\rightarrow \tilde{q}_m \tilde{q}_n^* + \text{cc}, & H^- &\rightarrow \tilde{u}_m^* \tilde{d}_n, \\ (H^0, A^0) &\rightarrow \tilde{l}_m \tilde{l}_n^* + \text{cc}, & H^- &\rightarrow \tilde{\nu} \tilde{e}_m, \end{aligned}$$

where the indices (i, j) number the four neutralinos, (k, l) the two charginos and (m, n) label the left- and right-handed sfermions, respectively their two mixed states for third-

generation sfermions. Generation indices for the sfermions have been omitted. Due to its CP property the only decays of the A^0 Higgs boson into sfermions are the diagonal decays $A^0 \rightarrow \tilde{t}_1^* \tilde{t}_2 + cc$, $A^0 \rightarrow \tilde{b}_1^* \tilde{b}_2 + cc$ and $A^0 \rightarrow \tilde{\tau}_1^* \tilde{\tau}_2 + cc$. Since the tree-level amplitudes are proportional to the Yukawa couplings, decays into light-generation squarks and sleptons are negligible. Similarly, the coupling of the charged Higgs boson H^\pm to right-handed sfermions is proportional to the corresponding Yukawa coupling. Thus, H^\pm does not decay into right-handed light-generation sfermions.

As for the squark decays into Higgs bosons, QCD corrections to the crossed processes, Higgs-boson decays into squarks, have been calculated in [106, 107, 135]. The EW corrections to these processes are given in [108, 109]. Decays of Higgs bosons into neutralinos and charginos have been analyzed in [136, 137] at tree level. For the decays of the charged Higgs boson $H^- \rightarrow \tilde{\chi}_i^0 \tilde{\chi}_j^-$ the EW corrections have been computed in [138]. The corrections to the invisible decays $(h^0, H^0, A^0) \rightarrow \tilde{\chi}_1^0 \tilde{\chi}_1^0$ have first been calculated in the higgsino limit ($\mu \ll M_1, M_2$) [139] and in the gaugino limit ($\mu \gg M_1, M_2$) [140] and the full one-loop corrections can be found in [141].

The aim of our work in this chapter is to compute all EW and QCD NLO corrections to the Higgs boson decays (9.1). This calculation is done in a common renormalization framework in accordance with FeynHiggs [29] and includes higher-order contributions from the Higgs field-renormalization factors and effective bottom Yukawa coupling.

9.2 Amplitudes

9.2.1 $H \rightarrow \tilde{q}_i^* \tilde{q}'_j$

Feynman diagrams for Higgs-boson decays into squarks are obtained by crossing the Feynman diagrams for $\tilde{q}_i \rightarrow \tilde{q}'_j S$ ($S = h^0, H^0, A^0, H^\pm$) (Section 6.4). These Feynman diagrams yield the tree-level amplitudes \mathcal{M}_0 , amplitudes for 1-loop EW and QCD contributions $\mathcal{M}_1^{\text{1L,EW/QCD}}$, for counterterm contributions $\mathcal{M}_1^{\text{CT,EW/QCD}}$, and the amplitudes including real contributions $\mathcal{M}_1^{\text{real,EW/QCD}}$.

9.2.2 $H \rightarrow \tilde{l}_i \tilde{l}'_j$

The Lagrangian and Feynman rules for Higgs-boson–slepton–slepton interactions are obtained from the Higgs-boson–squark–squark interactions by replacing $\tilde{u} \rightarrow \tilde{\nu}$ and $\tilde{d} \rightarrow \tilde{e}$ whereas all rules with $\tilde{\nu}_R$ are omitted. The amplitudes contributing to the EW corrections to Higgs-boson decays into sleptons are then computed analogously as the Higgs-boson decays into squarks in the preceding subsection. In Fig. 9.1 the generic Feynman diagrams contributing to the EW NLO corrections of the process $S \rightarrow \tilde{l}_i \tilde{l}'_j$ are displayed (S denotes any of the five physical Higgs bosons). For decays of A^0 and H^\pm the mixing between the Higgs bosons, the Goldstone bosons, and W/Z bosons have to be taken into account. These diagrams can be obtained by crossing the diagrams in Fig. 6.9 and replacing the external squarks by sleptons.

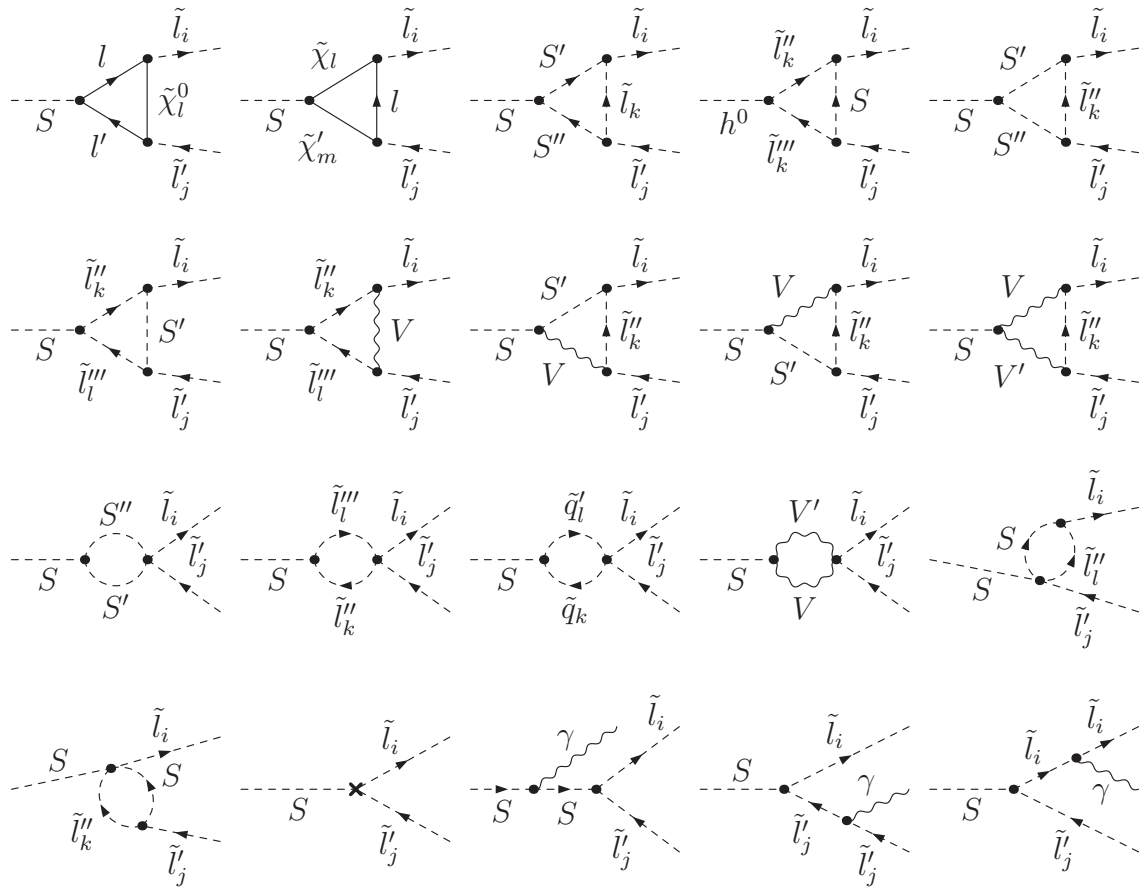


Figure 9.1: Generic virtual, counterterm and real Feynman diagrams contributing to electroweak corrections to the process $S \rightarrow \tilde{l}_i \tilde{l}'_j$. S denotes any of the five physical Higgs-bosons, \tilde{l}_i the sleptons, $\tilde{\chi}_l$ the neutralinos/charginos, V the electroweak gauge bosons, and γ the photon.

9.2.3 $H \rightarrow \tilde{\chi} \tilde{\chi}$

Adapting the notation of [22] the Lagrangians for Higgs-boson–neutralino and Higgs-boson–chargino interactions are given by

$$\mathcal{L}_{S^0 \tilde{\chi}_n^0 \tilde{\chi}_l^0} = \sum_{n,l=1}^4 \sum_{S^0} \frac{1}{2} \tilde{\chi}_n^0 (P_R C_{nl}^R(S^0) + P_L C_{nl}^L(S^0)) \tilde{\chi}_l^0 S^0, \quad (9.2a)$$

$$\mathcal{L}_{S^0 \tilde{\chi}_k^+ \tilde{\chi}_m^+} = \sum_{k,m=1}^2 \sum_{S^0} \tilde{\chi}_k^+ (P_R D_{km}^R(S^0) + P_L D_{km}^L(S^0)) \tilde{\chi}_m^+ S^0, \quad (9.2b)$$

$$\mathcal{L}_{S^- \tilde{\chi}_l^0 \tilde{\chi}_k^+} = \sum_{l=1}^4 \sum_{k=1}^2 \sum_{S^-} \tilde{\chi}_l^0 (P_R E_{lk}^R(S^-) + P_L E_{lk}^L(S^-)) \tilde{\chi}_k^+ S^- + \text{hc}, \quad (9.2c)$$

with $S^0 = h^0, H^0, A^0, G^0$ and $S^\pm = H^\pm, G^\pm$. The couplings are given by

$$C_{nl}^R(h^0) = C_{ln}^L(h^0)^* = g_2 (\sin \alpha Q_{nl}'' + \cos \alpha S_{nl}''), \quad (9.3a)$$

$$C_{nl}^R(H^0) = C_{ln}^L(H^0)^* = -g_2 (\cos \alpha Q_{nl}'' - \sin \alpha S_{nl}''), \quad (9.3b)$$

$$C_{nl}^R(A^0) = C_{ln}^L(A^0)^* = -ig_2 (\sin \beta Q_{nl}'' - \cos \beta S_{nl}''), \quad (9.3c)$$

$$C_{nl}^R(G^0) = C_{ln}^L(G^0)^* = ig_2 (\cos \beta Q_{nl}'' + \sin \beta S_{nl}''), \quad (9.3d)$$

$$D_{km}^R(h^0) = D_{mk}^L(h^0)^* = g_2 (\sin \alpha Q_{km} - \cos \alpha S_{km}), \quad (9.3e)$$

$$D_{km}^R(H^0) = D_{mk}^L(H^0)^* = -g_2 (\cos \alpha Q_{km} + \sin \alpha S_{km}), \quad (9.3f)$$

$$D_{km}^R(A^0) = D_{mk}^L(A^0)^* = -ig_2 (\sin \beta Q_{km} + \cos \beta S_{km}), \quad (9.3g)$$

$$D_{km}^R(G^0) = D_{mk}^L(G^0)^* = ig_2 (\cos \beta Q_{km} - \sin \beta S_{km}), \quad (9.3h)$$

$$E_{lk}^R(H^-) = -g_2 \sin \beta Q_{lk}'^R, \quad E_{lk}^L(H^-) = -g_2 \cos \beta Q_{lk}'^L, \quad (9.3i)$$

$$E_{lk}^R(G^-) = g_2 \cos \beta Q_{lk}'^R, \quad E_{lk}^L(G^-) = -g_2 \sin \beta Q_{lk}'^L, \quad (9.3j)$$

in terms of

$$Q_{km} = \frac{1}{\sqrt{2}} V_{k1} U_{m2}, \quad S_{km} = \frac{1}{\sqrt{2}} V_{k2} U_{m1}, \quad (9.3k)$$

$$Q_{lk}'^R = N_{l3} U_{k1} - \frac{1}{\sqrt{2}} U_{k2} (N_{l2} + \tan \theta_W N_{l1}), \quad (9.3l)$$

$$Q_{lk}'^L = N_{l4}^* V_{k1}^* + \frac{1}{\sqrt{2}} V_{k2}^* (N_{l2}^* + \tan \theta_W N_{l1}^*), \quad (9.3m)$$

$$Q_{nl}'' = \frac{1}{2} [N_{n3} (N_{l2} - \tan \theta_W N_{l1}) + N_{l3} (N_{n2} - \tan \theta_W N_{n1})], \quad (9.3n)$$

$$S_{nl}'' = \frac{1}{2} [N_{n4} (N_{l2} - \tan \theta_W N_{l1}) + N_{l4} (N_{n2} - \tan \theta_W N_{n1})]. \quad (9.3o)$$

Inserting the renormalization transformations for the Higgs fields (4.20), the neutralinos (4.91), and charginos (4.78) and the couplings

$$C_{nl}^{L/R}(S) \rightarrow C_{nl}^{L/R}(S) + \delta C_{nl}^{L/R}(S), \quad (9.4)$$

the counterterm Lagrangians are obtained. The explicit expressions for these renormalization constants are given in Appendix B.4. For the interactions between neutral Higgs bosons and neutralinos the counterterm Lagrangian then reads

$$\begin{aligned}
\delta\mathcal{L}_{S^0\tilde{\chi}_n^0\tilde{\chi}_l^0} &= \frac{1}{2} \sum_{n,l=1}^4 \sum_{S^0} \tilde{\chi}_n^0 \left[P_L \left(\frac{1}{2} [\delta Z_{\tilde{\chi}^0}]_{mn} C_{ml}^L(S^0) + \frac{1}{2} [\delta Z_{\tilde{\chi}^0}]_{kl} C_{nk}^L(S^0) + \delta C_{nl}^L(S^0) \right) \right. \\
&\quad \left. + P_R \left(\frac{1}{2} [\delta Z_{\tilde{\chi}^0}^*]_{mn} C_{ml}^R(S^0) + \frac{1}{2} [\delta Z_{\tilde{\chi}^0}^*]_{kl} C_{nk}^R(S^0) + \delta C_{nl}^R(S^0) \right) \right] \tilde{\chi}_l^0 S^0 \\
&\quad + \frac{1}{4} \sum_{n,l=1}^4 \tilde{\chi}_n^0 \left[\left\{ P_L (\delta Z_{h^0 h^0} C_{nl}^L(h^0) + \delta Z_{h^0 H^0} C_{nl}^L(H^0)) \right. \right. \\
&\quad \left. \left. + P_R (\delta Z_{h^0 h^0} C_{nl}^R(h^0) + \delta Z_{h^0 H^0} C_{nl}^R(H^0)) \right\} h^0 \right. \\
&\quad \left. + \left\{ P_L (\delta Z_{H^0 H^0} C_{nl}^L(H^0) + \delta Z_{h^0 H^0} C_{nl}^L(h^0)) \right. \right. \\
&\quad \left. \left. + P_R (\delta Z_{H^0 H^0} C_{nl}^R(H^0) + \delta Z_{h^0 H^0} C_{nl}^R(h^0)) \right\} H^0 \right. \\
&\quad \left. + \left\{ P_L (\delta Z_{A^0 A^0} C_{nl}^L(A^0) + \delta Z_{A^0 G^0} C_{nl}^L(G^0)) \right. \right. \\
&\quad \left. \left. + P_R (\delta Z_{A^0 A^0} C_{nl}^R(A^0) + \delta Z_{A^0 G^0} C_{nl}^R(G^0)) \right\} A^0 \right] \tilde{\chi}_l^0. \tag{9.5a}
\end{aligned}$$

The counterterm Lagrangian for the interaction between neutral Higgs fields and charginos is given by

$$\begin{aligned}
\delta\mathcal{L}_{S^0\tilde{\chi}_k^+ \tilde{\chi}_m^+} &= \sum_{k,m=1}^2 \sum_{S^0} \tilde{\chi}_k^+ \left[P_L \left(\frac{1}{2} [\delta Z_{\tilde{\chi}^\pm}^R]_{lk}^* D_{lm}^L(S^0) + \frac{1}{2} [\delta Z_{\tilde{\chi}^\pm}^L]_{nm} D_{kn}^L(S^0) + \delta D_{km}^L(S^0) \right) \right. \\
&\quad \left. + P_R \left(\frac{1}{2} [\delta Z_{\tilde{\chi}^\pm}^L]_{lk}^* D_{lm}^R(S^0) + \frac{1}{2} [\delta Z_{\tilde{\chi}^\pm}^R]_{nm} D_{kn}^R(S^0) + \delta D_{km}^R(S^0) \right) \right] \tilde{\chi}_m^+ S^0 \\
&\quad + \frac{1}{2} \sum_{k,m=1}^2 \tilde{\chi}_k^+ \left[\left\{ P_L (\delta Z_{h^0 h^0} D_{km}^L(h^0) + \delta Z_{h^0 H^0} D_{km}^L(H^0)) \right. \right. \\
&\quad \left. \left. + P_R (\delta Z_{h^0 h^0} D_{km}^R(h^0) + \delta Z_{h^0 H^0} D_{km}^R(H^0)) \right\} h^0 \right. \\
&\quad \left. + \left\{ P_L (\delta Z_{H^0 H^0} D_{km}^L(H^0) + \delta Z_{h^0 H^0} D_{km}^L(h^0)) \right. \right. \\
&\quad \left. \left. + P_R (\delta Z_{H^0 H^0} D_{km}^R(H^0) + \delta Z_{h^0 H^0} D_{km}^R(h^0)) \right\} H^0 \right. \\
&\quad \left. + \left\{ P_L (\delta Z_{A^0 A^0} D_{km}^L(A^0) + \delta Z_{A^0 G^0} D_{km}^L(G^0)) \right. \right. \\
&\quad \left. \left. + P_R (\delta Z_{A^0 A^0} D_{km}^R(A^0) + \delta Z_{A^0 G^0} D_{km}^R(G^0)) \right\} A^0 \right] \tilde{\chi}_m^+. \tag{9.5b}
\end{aligned}$$

Finally, the counterterm Lagrangian for interactions between charged Higgs bosons, neutralinos and charginos reads

$$\begin{aligned}
\delta\mathcal{L}_{S^-\tilde{\chi}_l^0\tilde{\chi}_k^+} = & \sum_{l=1}^4 \sum_{k=1}^2 \sum_{S^-} \tilde{\chi}_l^0 \left[P_L \left(\frac{1}{2} [\delta Z_{\tilde{\chi}^0}]_{ml} E_{mk}^L(S^-) + \frac{1}{2} [\delta Z_{\tilde{\chi}^\pm}^L]_{nk} E_{ln}^L(S^-) + \delta E_{lk}^L(S^-) \right) \right. \\
& + P_R \left(\frac{1}{2} [\delta Z_{\tilde{\chi}^0}]_{ml}^* E_{mk}^R(S^-) + \frac{1}{2} [\delta Z_{\tilde{\chi}^\pm}^R]_{nk} E_{ln}^R(S^-) + \delta E_{lk}^R(S^-) \right) \left. \right] \tilde{\chi}_k^+ S^- \\
& + \frac{1}{2} \sum_{l=1}^4 \sum_{k=1}^2 \tilde{\chi}_l^0 \left[\left\{ P_L (\delta Z_{H^+H^-} E_{lk}^L(H^-) + \delta Z_{H^+G^-} E_{lk}^L(G^-)) \right. \right. \\
& \left. \left. + P_R (\delta Z_{H^+H^-} E_{lk}^R(H^-) + \delta Z_{H^+G^-} E_{lk}^R(G^-)) \right\} H^- \right] \tilde{\chi}_k^+ + \text{hc} . \quad (9.5c)
\end{aligned}$$

From these counterterm Lagrangians the counterterm Feynman rules can be deduced. They are given in Appendix C.

Feynman diagrams

Feynman diagrams contributing to the amplitudes at NLO for neutral Higgs boson decays into neutralinos are depicted in Fig. 9.2. For neutral Higgs-boson decays into charginos, the Feynman diagrams are given in Fig. 9.3 and for charged Higgs-boson decays into a chargino and a neutralino the diagrams are shown in Fig. 9.4. The corrections due to the Higgs-field renormalization factors are computed as in Section 6.4. For decays of the CP-odd and charged Higgs bosons, Feynman diagrams with mixtures between the Higgs bosons, Goldstone bosons, and W/Z bosons contribute to the NLO amplitude $\mathcal{M}_1^{\text{EW}}$. They can be obtained by crossing the Feynman diagrams in Fig. 6.9 and replacing the squarks by neutralinos/charginos. The 1-loop amplitudes are then denoted as $\mathcal{M}_1^{\text{1L,EW}}$, amplitudes including counterterm corrections are given by $\mathcal{M}_1^{\text{CT,EW}}$, and real radiation contributes to the amplitudes $\mathcal{M}_1^{\text{real,EW}}$.

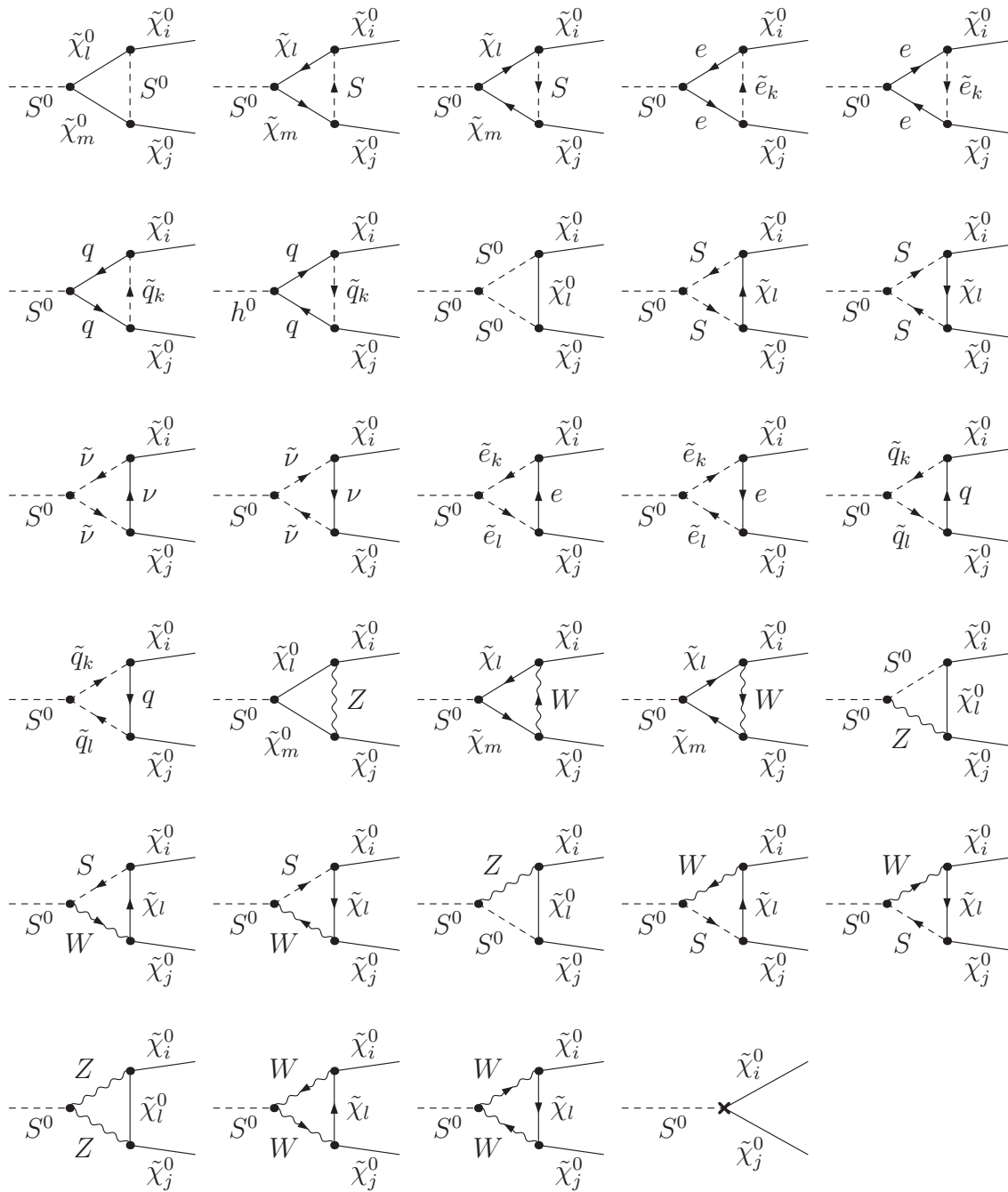


Figure 9.2: Generic virtual and counterterm Feynman diagrams contributing to electroweak corrections to the process $S^0 \rightarrow \tilde{\chi}_i^0 \tilde{\chi}_j^0$. Notation as in Fig. 9.1.

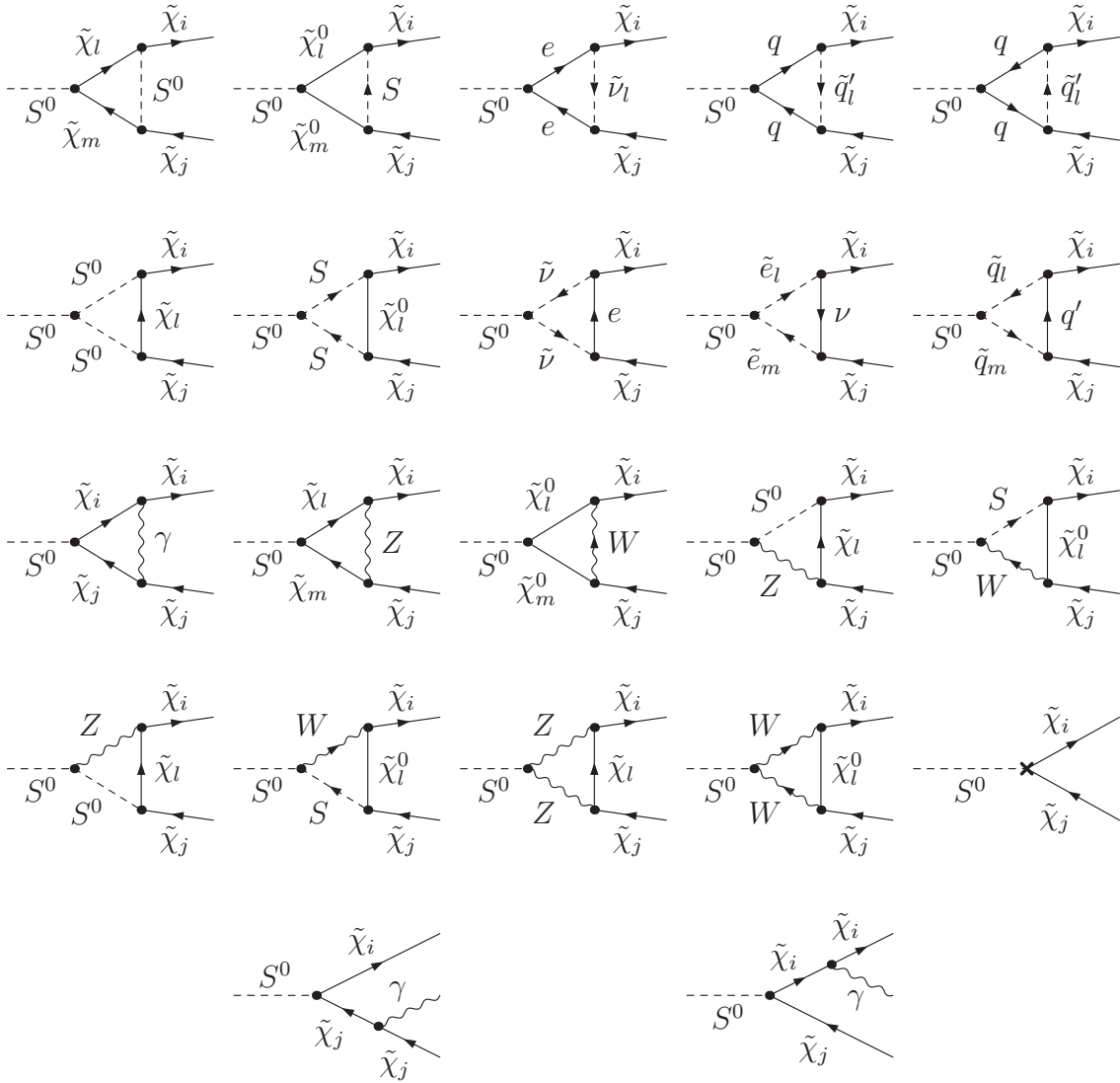


Figure 9.3: Generic virtual, counterterm and real Feynman diagrams contributing to electroweak corrections to the process $S^0 \rightarrow \tilde{\chi}_i^+ \tilde{\chi}_j^-$. Notation as in Fig. 9.1.

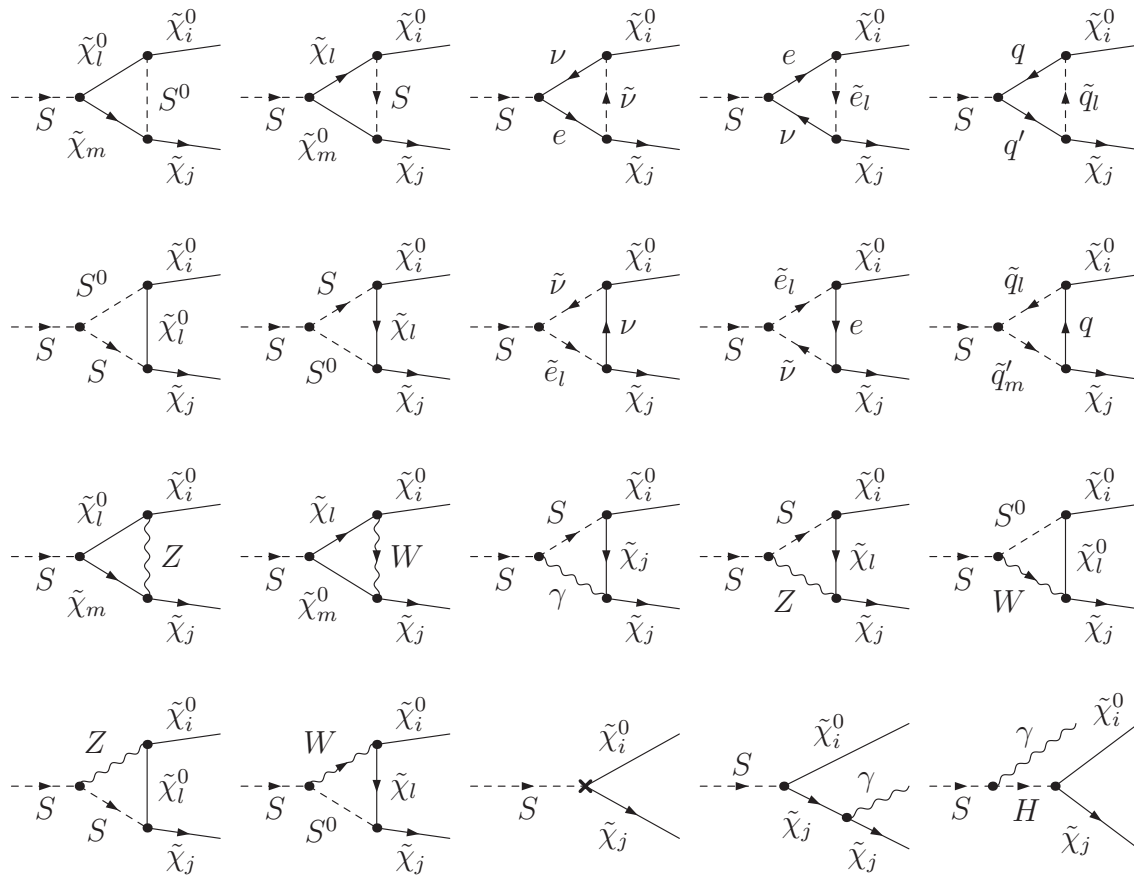


Figure 9.4: Generic virtual, counterterm and real Feynman diagrams contributing to electroweak corrections to the process $S^- \rightarrow \tilde{\chi}_i^0 \tilde{\chi}_j^-$. Notation as in Fig. 9.1.

9.3 Decay widths

For the decay $S \rightarrow ab$ the tree-level decay width is given by

$$\Gamma_0(S \rightarrow ab) = \frac{(2\pi)^4}{m_S} \int d\text{PS}_2 |\mathcal{M}_0|^2, \quad (9.6)$$

where S denotes any of the five physical Higgs bosons and a, b any of the possible decay products.

9.3.1 $h^0/H^0 \rightarrow ab$

As in Subsection 6.4.4, for decays of h^0 and H^0 we define the improved Born decay width which includes contributions of $\mathcal{O}(G_F m_t^4/M_W^2)$. The improved Born amplitude \mathcal{M}_0^Z is obtained by summing over the tree-level amplitudes with external h^0/H^0 bosons $\mathcal{M}_{0,h^0/H^0}$ and weighting them with the appropriate Z factors,

$$\mathcal{M}_0^Z(h^0 \rightarrow ab) = \sqrt{Z_{h^0}} (\mathcal{M}_{0,h^0} + Z_{h^0 H^0} \mathcal{M}_{0,H^0}), \quad (9.7a)$$

$$\mathcal{M}_0^Z(H^0 \rightarrow ab) = \sqrt{Z_{H^0}} (\mathcal{M}_{0,H^0} + Z_{H^0 h^0} \mathcal{M}_{0,h^0}). \quad (9.7b)$$

The partial decay widths improved by Z -factors then read

$$\Gamma_0^Z(h^0 \rightarrow ab) = \frac{(2\pi)^4}{m_{h^0}} \int d\text{PS}_2 |\mathcal{M}_0^Z(h^0 \rightarrow ab)|^2, \quad (9.8a)$$

$$\Gamma_0^Z(H^0 \rightarrow ab) = \frac{(2\pi)^4}{m_{H^0}} \int d\text{PS}_2 |\mathcal{M}_0^Z(H^0 \rightarrow ab)|^2. \quad (9.8b)$$

For decays of h^0/H^0 , the EW/QCD NLO amplitudes are given by

$$\mathcal{M}_1^{\text{EW/QCD}}(h^0 \rightarrow ab) = \sqrt{Z_{h^0}} \left(\mathcal{M}_{1,h^0}^{\text{EW/QCD}} + Z_{h^0 H^0} \mathcal{M}_{1,H^0}^{\text{EW/QCD}} \right), \quad (9.9a)$$

$$\mathcal{M}_1^{\text{EW/QCD}}(H^0 \rightarrow ab) = \sqrt{Z_{H^0}} \left(\mathcal{M}_{1,H^0}^{\text{EW/QCD}} + Z_{H^0 h^0} \mathcal{M}_{1,h^0}^{\text{EW/QCD}} \right), \quad (9.9b)$$

where $\mathcal{M}_{1,\{h^0,H^0\}}^{\text{EW/QCD}} = \mathcal{M}_{1,\{h^0,H^0\}}^{\text{1L,EW/QCD}} + \mathcal{M}_{1,\{h^0,H^0\}}^{\text{CT,EW/QCD}}$ are the amplitudes with external h^0/H^0 boson. Similarly, for the real corrections we get

$$\mathcal{M}_1^{\text{real,EW/QCD}}(h^0 \rightarrow ab) = \sqrt{Z_{h^0}} \left(\mathcal{M}_{1,h^0}^{\text{real,EW/QCD}} + Z_{h^0 H^0} \mathcal{M}_{1,H^0}^{\text{real,EW/QCD}} \right), \quad (9.10a)$$

$$\mathcal{M}_1^{\text{real,EW/QCD}}(H^0 \rightarrow ab) = \sqrt{Z_{H^0}} \left(\mathcal{M}_{1,H^0}^{\text{real,EW/QCD}} + Z_{H^0 h^0} \mathcal{M}_{1,h^0}^{\text{real,EW/QCD}} \right), \quad (9.10b)$$

where $\mathcal{M}_{1,\{h^0,H^0\}}^{\text{real,EW/QCD}}$ denote the amplitudes for real photon/gluon radiation with an external h^0/H^0 Higgs boson. The partial decay widths for the virtual and real corrections, using these amplitudes, then are

$$\Gamma_1^{\text{virt,EW/QCD}}(h^0 \rightarrow ab) = \frac{(2\pi)^4}{m_{h^0}} \int d\text{PS}_2 2\text{Re} \left[\mathcal{M}_1^{Z*} \mathcal{M}_1^{\text{EW/QCD}} \right] + \delta_{\text{soft}} \Gamma_0^Z, \quad (9.11a)$$

$$\Gamma_1^{\text{real,EW/QCD}}(H^0 \rightarrow ab) = \frac{(2\pi)^4}{m_{H^0}} \int d\text{PS}_3 |\mathcal{M}_1^{\text{real,EW/QCD}}|^2, \quad (9.11b)$$

where $d\text{PS}_3$ denotes the 3-body phase-space element (c.f. Chapter 3). Hence, the partial decay width at NLO is given by

$$\begin{aligned} \Gamma_1^{\text{EW/QCD}}(h^0/H^0 \rightarrow ab) &= \Gamma_1^{\text{virt,EW/QCD}}(h^0/H^0 \rightarrow ab) \\ &+ \Gamma_1^{\text{real,EW/QCD}}(h^0/H^0 \rightarrow ab). \end{aligned} \quad (9.12)$$

9.3.2 $A^0/H^\pm \rightarrow ab$

At NLO, the decay widths for decays of A^0/H^\pm into squarks are given by

$$\Gamma_1^{\text{virt,EW/QCD}}(A^0/H^\pm \rightarrow ab) = \frac{(2\pi)^4}{m_{A^0/H^\pm}} \int d\text{PS}_2 2\text{Re} \left(\mathcal{M}_0 \mathcal{M}_1^{\text{EW/QCD}} \right) + \delta_{\text{soft}} \Gamma_0, \quad (9.13a)$$

$$\Gamma_1^{\text{real,EW/QCD}}(A^0/H^\pm \rightarrow ab) = \frac{(2\pi)^4}{m_{A^0/H^\pm}} \int d\text{PS}_3 |\mathcal{M}_1^{\text{real,EW/QCD}}|^2, \quad (9.13b)$$

Since the A^0 and H^\pm fields are renormalized according to the $\overline{\text{DR}}$ scheme, the EW one-loop amplitudes have to include the finite factors

$$\sqrt{\hat{Z}_{A^0}} \simeq 1 - \frac{1}{2} \delta \hat{Z}_{A^0} \equiv 1 - \frac{1}{2} \text{Re} \frac{\partial}{\partial p^2} \hat{\Sigma}_{A^0} \Big|_{p^2=m_{A^0}^2}, \quad (9.14a)$$

$$\sqrt{\hat{Z}_{H^\pm}} \simeq 1 - \frac{1}{2} \delta \hat{Z}_{H^\pm} \equiv 1 - \frac{1}{2} \text{Re} \frac{\partial}{\partial p^2} \hat{\Sigma}_{H^-H^+} \Big|_{p^2=m_{H^\pm}^2}, \quad (9.14b)$$

with the $\overline{\text{DR}}$ renormalized self energies $\hat{\Sigma}$ (4.26). Hence, the amplitudes $\mathcal{M}_1^{\text{EW}}$ for squark decays into A^0 and H^\pm are given by

$$\mathcal{M}_1^{\text{EW}}(A^0 \rightarrow ab) = \mathcal{M}_1^{\text{1L,EW}} + \mathcal{M}_1^{\text{CT,EW}} - \frac{1}{2} \mathcal{M}_0 \delta \hat{Z}_{A^0}, \quad (9.15a)$$

$$\mathcal{M}_1^{\text{EW}}(H^\pm \rightarrow ab) = \mathcal{M}_1^{\text{1L,EW}} + \mathcal{M}_1^{\text{CT,EW}} - \frac{1}{2} \mathcal{M}_0 \delta Z_{H^\pm}. \quad (9.15b)$$

Finally, the decay widths at NLO are given by

$$\Gamma_1^{\text{EW/QCD}}(A^0 \rightarrow ab) = \Gamma_1^{\text{virt,EW/QCD}}(\tilde{q}_a \rightarrow \tilde{q}_b A^0) + \Gamma_1^{\text{real,EW/QCD}}(\tilde{q}_a \rightarrow \tilde{q}_b A^0), \quad (9.16a)$$

$$\Gamma_1^{\text{EW/QCD}}(H^\pm \rightarrow ab) = \Gamma_1^{\text{virt,EW/QCD}}(\tilde{q}_a \rightarrow \tilde{q}'_b H^\pm) + \Gamma_1^{\text{real,EW/QCD}}(\tilde{q}_a \rightarrow \tilde{q}'_b H^\pm). \quad (9.16b)$$

9.4 Numerical evaluation

The SM parameters used in this analyses are the same as used in Section 7.1. For the MSSM parameters, we consider benchmark scenarios, where the masses and couplings of the first two sfermion generations (light-flavor sfermions) are identical. Therefore, for Higgs-boson decays into light-flavor sfermions the partial decay widths include decays into first- and

second-generation sfermions. Furthermore, the decay widths also include the decays into charge conjugated final states,

$$\Gamma(S \rightarrow \tilde{f}_a^* \tilde{f}_b' + \text{cc}) = \sum_{j=1,2} \left[\Gamma(S \rightarrow \tilde{f}_a^j \tilde{f}_b'^j) + \Gamma(S \rightarrow \tilde{f}_a^j \tilde{f}_b'^{j*}) \right], \quad (9.17a)$$

$$\Gamma(S \rightarrow \tilde{f}_a^{3*} \tilde{f}_b^{3'} + \text{cc}) = \Gamma(S \rightarrow \tilde{f}_a^{3*} \tilde{f}_b'^3) + \Gamma(S \rightarrow \tilde{f}_a^3 \tilde{f}_b'^{3*}), \quad (9.17b)$$

where S denotes any of the five physical Higgs bosons, f^j/\tilde{f}^j the fermions/sfermions of the first two generations, and f^3/\tilde{f}^3 the third-generation fermions/sfermions. This can be accounted for by multiplying the Higgs-boson decay widths with the factors in Tab. 9.1 for decays into squarks and Tab. 9.2 for decays into sleptons. Furthermore, they include a factor of $1/2$ for the decay of the neutral Higgs bosons into two identical sneutrinos.

$(H^0, A^0) \rightarrow \tilde{q}_i \tilde{q}_j^* + \text{cc}, \quad q = u, d$	(1st and 2nd generation)	$2 \times (2 - \delta_{ij})$
$(H^0, A^0) \rightarrow \tilde{q}_i \tilde{q}_j^* + \text{cc}, \quad q = t, b$		$2 - \delta_{ij}$
$H^- \rightarrow \tilde{u}_i^* \tilde{d}_j$	(1st and 2nd generation)	2
$H^- \rightarrow \tilde{t}_i^* \tilde{b}_j$		1

Table 9.1: Factors accounting for decays into charge conjugate final states and into the two light-flavor squark generations for the decays $H \rightarrow \tilde{q}_i^* \tilde{q}_j'$.

$(H^0, A^0) \rightarrow \tilde{\nu} \tilde{\nu},$	(1st and 2nd generation)	$2 \times 1/2$
$(H^0, A^0) \rightarrow \tilde{\nu}_\tau \tilde{\nu}_\tau,$		$1/2$
$(H^0, A^0) \rightarrow \tilde{e}_i \tilde{e}_j^* + \text{cc},$	(1st and 2nd generation)	$2 \times (2 - \delta_{ij})$
$(H^0, A^0) \rightarrow \tilde{\tau}_i \tilde{\tau}_j^* + \text{cc},$		$2 - \delta_{ij}$
$H^- \rightarrow \tilde{\nu} \tilde{e}_j$	(1st and 2nd generation)	2
$H^- \rightarrow \tilde{\nu}_\tau \tilde{e}_j$		1

Table 9.2: Factors accounting for decays into charge conjugate final states and into the two light-flavor slepton generations for the decays $H \rightarrow \tilde{l}_i^* \tilde{l}_j'$.

For the decay of the neutral Higgs bosons into charginos, the decay into charge-conjugated final states are incorporated into the same decay width,

$$\Gamma(S^0 \rightarrow \tilde{\chi}_i^+ \tilde{\chi}_j^- + \text{cc}) = \Gamma(S^0 \rightarrow \tilde{\chi}_i^+ \tilde{\chi}_j^-) + \Gamma(S^0 \rightarrow \tilde{\chi}_i^- \tilde{\chi}_j^+), \quad i \neq j, \quad (9.18)$$

where S^0 denotes any of the neutral Higgs bosons h^0 , H^0 , and A^0 . Again, this can be done by multiplying the decay widths with the factors given in Tab. 9.3 where factors of $1/2$ for decays into identical neutralinos are included.

$$\begin{array}{ll}
(h^0, H^0, A^0) \rightarrow \tilde{\chi}_i^0 \tilde{\chi}_j^0 & \frac{1}{1 + \delta_{ij}} \\
(h^0, H^0, A^0) \rightarrow \tilde{\chi}_i^+ \tilde{\chi}_j^- + \text{cc.} & 2 - \delta_{ij} \\
H^- \rightarrow \tilde{\chi}_i^- \tilde{\chi}_j^0 & 1
\end{array}$$

Table 9.3: Factors accounting for decays into two identical particles, charge conjugate final states and to the two light-flavor squark generations for the decays of the Higgs bosons into neutralinos and charginos.

We illustrate the effects of the EW and QCD NLO corrections to Higgs-boson decays into sfermions or into neutralinos/charginos in the maximal-mixing scenario used in [134], where the maximal possible Higgs-boson mass is obtained. For the parameter point

$$\begin{aligned}
\tan \beta &= 30, & m_{A^0} &= 500 \text{ GeV}, & \mu &= -200 \text{ GeV}, \\
M_1 &= \frac{1}{2} M_2 = 75 \text{ GeV}, & M_2 &= 150 \text{ GeV}, & M_3 &= 2 \text{ TeV}, \\
M_{\tilde{q}_{L/R}^{1,2}} &= M_{\text{SUSY}} = 2 \text{ TeV} \\
M_{\tilde{q}_{L/R}^3} &= 400 \text{ GeV}, & A_b = A_\tau &= 400 \text{ GeV}, & A_t &= \sqrt{6} M_{\tilde{q}_L^3} + \frac{\mu}{\tan \beta},
\end{aligned} \tag{9.19}$$

we compute the decay widths at NLO for the Higgs-boson decays into sfermions, neutralinos, and charginos. At this parameter point, the lightest Higgs boson h^0 does not decay into SUSY particles. Since the CP-odd Higgs boson A^0 has similar decay characteristics as the CP-even Higgs boson H^0 , we only list the decay widths and branching ratios of H^0 and H^- in Tab. 9.4, where decay channels with $\text{BR} < 0.1\%$ are omitted. Γ_0^Z denotes the improved Born decay width, whereas Γ_1 the decay width including EW and QCD NLO corrections. The decays into SM particles have been computed with FeynHiggs 2.7.4 [29] and include the full one-loop corrections. The branching ratios BR_1 have been computed using the decay widths Γ_1 .

The decay $H^0 \rightarrow \tilde{t}_1 \tilde{t}_1^*$ receives positive relative QCD corrections of 10% and negative EW corrections of about -1% . The decays into neutralinos and charginos receive only EW corrections. In general, they lie between -2% and 10% . However the decays $H^0 \rightarrow \tilde{\chi}_1^0 \tilde{\chi}_4^0$ and $H^0 \rightarrow \tilde{\chi}_2^0 \tilde{\chi}_3^0$ receive large corrections which reach about 40% and 30%.

In order to illustrate the effects of NLO corrections to the different Higgs-boson decay channels, we choose different benchmark points where only the particular channel is kinematically allowed. In Subsection 9.4.1 the decays of the heavier neutral Higgs bosons into chargino and neutralinos are examined. This analysis is done starting from the benchmark point (9.19) with a high and low value of $\tan \beta$ and varying m_{A^0} . In Subsection 9.4.2, the invisible decay of the lightest Higgs boson into two lightest-neutralinos is analyzed. In order to allow for this decay, the universality relation between M_1 and M_2 has to be relaxed. For the decay of the heavy neutral Higgs boson into third-generation squarks,

$H^0 \rightarrow \dots$			$H^- \rightarrow \dots$				
	Γ_1 [GeV]	BR ₁		Γ_1 [GeV]	BR ₁		
$\tau \bar{\tau}$	0.847	4.7%	$\bar{\nu}_\tau \tau$	0.914	6.5%		
$b \bar{b}$	11.999	66.2%	$\bar{t} b$	9.655	68.2%		
$H^0 \rightarrow \dots$			$H^- \rightarrow \dots$				
	Γ_0^Z [GeV]	Γ_1 [GeV]		Γ_0^Z [GeV]	Γ_1 [GeV]	BR ₁	
$\tilde{t}_1 \tilde{t}_1^*$	1.378	1.571	8.7%	$\tilde{\chi}_1^- \tilde{\chi}_1^0$	0.571	0.614	4.3%
$\tilde{\chi}_1^0 \tilde{\chi}_1^0$	0.094	0.094	0.5%	$\tilde{\chi}_1^- \tilde{\chi}_2^0$	0.038	0.036	0.3%
$\tilde{\chi}_1^0 \tilde{\chi}_2^0$	0.342	0.349	1.9%	$\tilde{\chi}_1^- \tilde{\chi}_3^0$	0.685	0.757	5.3%
$\tilde{\chi}_1^0 \tilde{\chi}_3^0$	0.150	0.165	0.9%	$\tilde{\chi}_1^- \tilde{\chi}_4^0$	0.691	0.736	5.2%
$\tilde{\chi}_1^0 \tilde{\chi}_4^0$	0.021	0.029	0.2%	$\tilde{\chi}_2^- \tilde{\chi}_1^0$	0.005	0.011	0.1%
$\tilde{\chi}_2^0 \tilde{\chi}_2^0$	0.279	0.291	1.6%	$\tilde{\chi}_2^- \tilde{\chi}_2^0$	1.212	1.280	9.0%
$\tilde{\chi}_2^0 \tilde{\chi}_3^0$	0.172	0.219	1.2%	$\tilde{\chi}_2^- \tilde{\chi}_3^0$	0.156	0.154	1.1%
$\tilde{\chi}_3^0 \tilde{\chi}_3^0$	0.011	0.012	0.1%	$\tilde{\chi}_2^- \tilde{\chi}_4^0$	0.007	0.008	0.1%
$\tilde{\chi}_3^0 \tilde{\chi}_4^0$	0.218	0.213	1.2%				
$\tilde{\chi}_1^+ \tilde{\chi}_1^-$	1.042	1.040	5.7%				
$\tilde{\chi}_1^+ \tilde{\chi}_2^-$	1.144	1.275	7.0%				
Tot. width	18.123			Tot. width	14.165		

Table 9.4: Decay widths and branching ratios for the decay of the neutral CP-even Higgs boson H^0 and the charged Higgs boson H^\pm . Decays with branching ratios $< 0.1\%$ are omitted. The decay widths for the SM decays into τ and b are obtained with FeynHiggs 2.7.4 and are given at full one-loop precision. The branching ratios are then computed with the one-loop decay widths.

the mass parameters for the third-generation squarks have to be lowered. These decays are analyzed in Subsection 9.4.3. Finally, the decay $H^0 \rightarrow \tilde{\tau}_1 \tilde{\tau}_1^*$ is analyzed in Subsection 9.4.4. For this analysis we choose a parameter point, where the Higgs-boson decay into staus is kinematically allowed, whereas the other sfermions are considerably heavier than the Higgs bosons.

9.4.1 $H^0 \rightarrow \tilde{\chi} \tilde{\chi}$

Following [134] we chose the parameter point

$$\begin{aligned}
\tan \beta &= \{3, 30\}, & m_{A^0} &\in [100, 500] \text{ GeV}, & \mu &= -200 \text{ GeV}, \\
M_1 &= \frac{1}{2} M_2 = 75 \text{ GeV}, & M_2 &= 150 \text{ GeV}, & M_3 &= 2 \text{ TeV}, \\
M_{\tilde{q}_{L/R}} &= M_{\text{SUSY}} = 2 \text{ TeV}, & A_b = A_\tau &= 2 \text{ TeV}, & A_t &= \sqrt{6} M_{\text{SUSY}} + \frac{\mu}{\tan \beta}.
\end{aligned} \tag{9.20}$$

Note, the authors of [134] take $-\mu = M_2 = 150$ GeV. Since this leads to instabilities in the renormalization constants of δM_2 and $\delta\mu$ (cf. Subsection 7.3.5), thus the value μ has been shifted to $\mu = -200$ GeV. The value for the trilinear coupling A_t is chosen according to the maximal-mixing scenario. We vary the parameter m_{A^0} between 100 and 500 GeV. In Fig. 9.5 the neutral Higgs-boson masses m_{h^0} and m_{H^0} are plotted in function of m_{A^0} . For $m_{A^0} \geq 150$ GeV the light Higgs-boson mass m_{h^0} reaches its maximal value ~ 125 GeV. The heavy Higgs-boson mass m_{H^0} shows a nearly linear dependence on m_{A^0} except for small values of m_{A^0} .

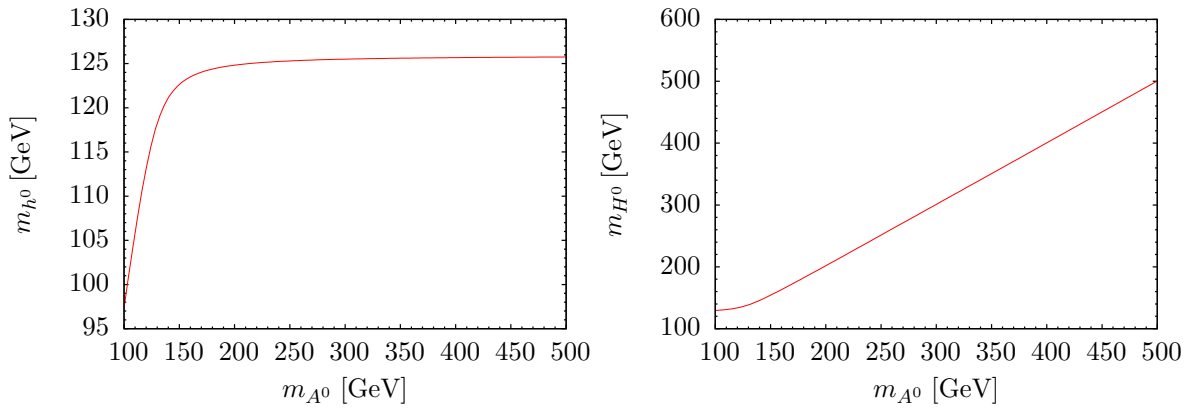


Figure 9.5: Values for m_{h^0} (left) and m_{H^0} (right) in function of m_{A^0} . The other parameters are chosen as described in the first paragraph of Subsection 9.4.1.

In Fig. 9.6 the partial decay width Γ and the relative corrections

$$\delta = \frac{\Gamma_1^{\text{EW}} - \Gamma_0^Z}{\Gamma_0^Z} \quad (9.21)$$

for the invisible decay $H^0 \rightarrow \tilde{\chi}_1^0 \tilde{\chi}_1^0$ are plotted for $\tan\beta = 3$ and $\tan\beta = 30$ in function of m_{A^0} . Γ_0^Z denotes the improved Born decay width including the effects from the Higgs-field correction factors Z . The partial decay width for $\tan\beta = 30$ is enhanced by a factor 4 compared to the decay width for $\tan\beta = 3$. As it can be seen in the right-hand side plot, the relative corrections amount from -1.5% to 3% .

The partial decay widths and relative corrections for the decay of H^0 into all neutralinos and charginos except the invisible decay $H^0 \rightarrow \tilde{\chi}_1^0 \tilde{\chi}_1^0$ are plotted in Fig. 9.7. Again, the decay width for $\tan\beta = 30$ is larger than for $\tan\beta = 3$. The relative corrections lie between -4% and 8% .

9.4.2 $h^0 \rightarrow \tilde{\chi}_1^0 \tilde{\chi}_1^0$

If $m_{\tilde{\chi}_1^0} \lesssim m_{h^0}/2$ the invisible decay of the lightest Higgs boson $h^0 \rightarrow \tilde{\chi}_1^0 \tilde{\chi}_1^0$ becomes relevant. In order to allow for a light $\tilde{\chi}_1^0$, the universality relation for the parameter point (9.20) is

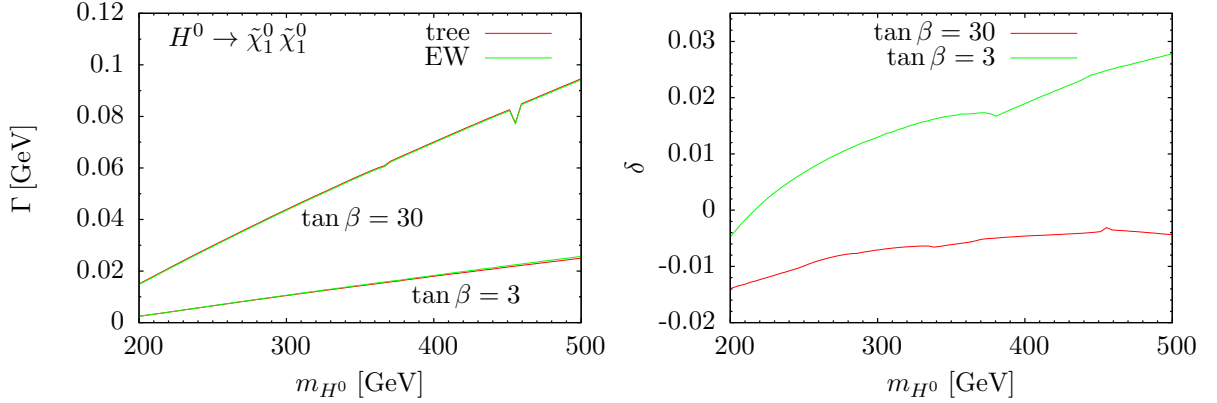


Figure 9.6: Partial decay width Γ in GeV (left) and relative corrections δ (right) for the decay $H^0 \rightarrow \tilde{\chi}_1^0 \tilde{\chi}_1^0$. The other parameters are chosen as described in the first paragraph of Subsection 9.4.1.

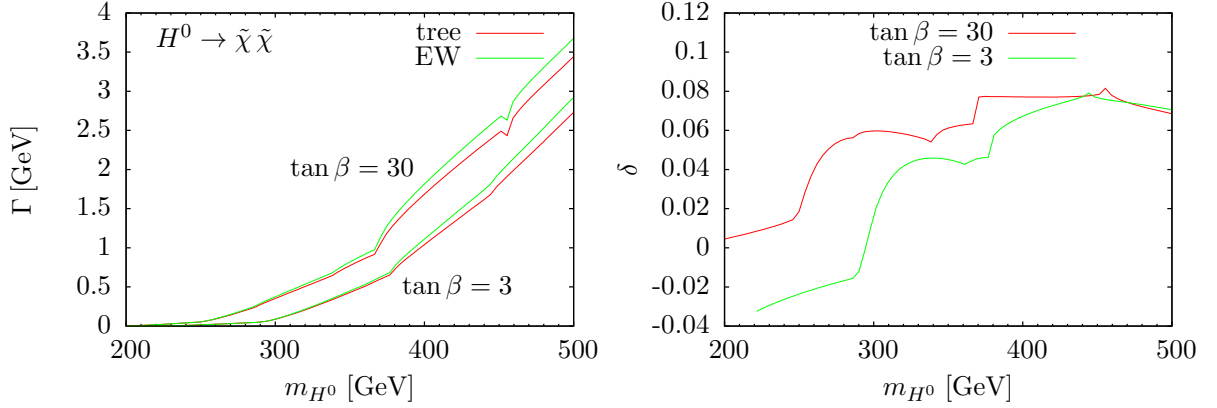


Figure 9.7: Partial decay width in GeV (left) and relative corrections (right) for the decay of the Higgs boson H^0 into all neutralinos and charginos except $H^0 \rightarrow \tilde{\chi}_1^0 \tilde{\chi}_1^0$ in function of m_{H^0} . The other parameters are chosen as described in the first paragraph of Subsection 9.4.1.

relaxed to $M_1 = \{0.1, 0.3\} \times M_2$. Thus, according to [134] the following parameter point was chosen and m_{A^0} is varied between 100 and 500 GeV.

$$\begin{aligned}
 \tan \beta &= 10, & m_{A^0} &\in [100, 500] \text{ GeV}, & \mu &= -200 \text{ GeV}, \\
 M_1 &= \{0.1, 0.3\} \times M_2, & M_2 &= 150 \text{ GeV}, & M_3 &= 2 \text{ TeV}, \\
 M_{\tilde{q}_{L/R}} &= M_{\text{SUSY}} = 2 \text{ TeV}, & A_b &= A_\tau = 2 \text{ TeV}, & A_t &= \sqrt{6} M_{\text{SUSY}} + \frac{\mu}{\tan \beta}.
 \end{aligned} \tag{9.22}$$

In Fig. 9.8 the partial decay width and the relative corrections for the decay $h^0 \rightarrow \tilde{\chi}_1^0 \tilde{\chi}_1^0$ is plotted in function of $m_{h^0}^0$. For $m_{h^0} \rightarrow 125$ GeV the partial decay width approaches zero causing the relative corrections to diverge. The relative corrections lie between 2% and 10%.

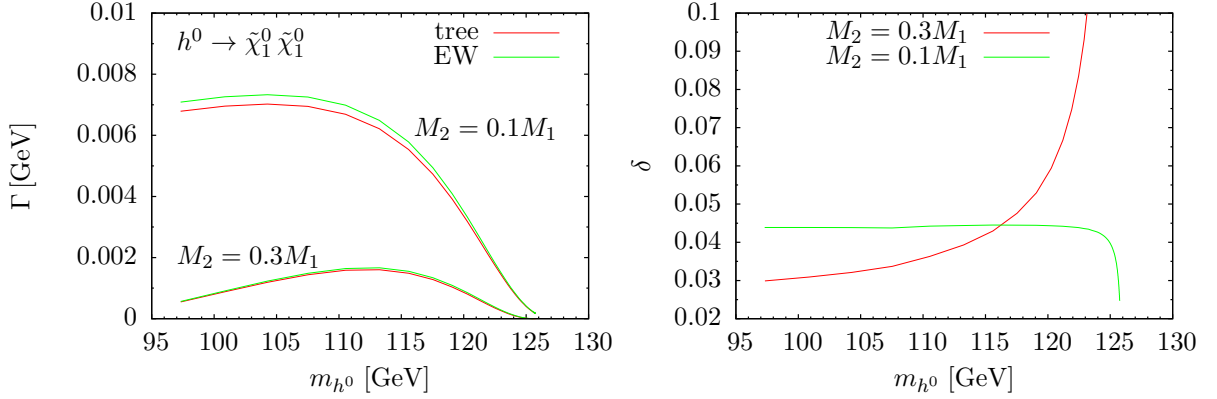


Figure 9.8: Partial decay width in GeV(left) and relative corrections (right) for the decay $h^0 \rightarrow \tilde{\chi}_1^0 \tilde{\chi}_1^0$. The other parameters are chosen as described in the first paragraph of Subsection 9.4.2.

9.4.3 $H^0 \rightarrow \tilde{t}_1 \tilde{t}_1$

In order to study the decay of heavy Higgs boson into top squarks, the squark mass parameters for the third generation have been lowered to 400 GeV and the CP-odd Higgs-boson mass m_{A^0} is varied between 400 and 1000 GeV. This results in the MSSM parameters

$$\begin{aligned}
 \tan \beta &= \{3, 30\}, & m_{A^0} &\in [400, 1000] \text{ GeV}, & \mu &= -200 \text{ GeV}, \\
 M_1 &= \frac{1}{2} M_2 = 75 \text{ GeV}, & M_2 &= 150 \text{ GeV}, & M_3 &= 2 \text{ TeV}, \\
 M_{\tilde{q}_{L/R}^{1,2}} &= M_{\text{SUSY}} = 2 \text{ TeV} \\
 M_{\tilde{q}_{L/R}^3} &= 400 \text{ GeV}, & A_b = A_\tau &= 400 \text{ GeV}, & A_t &= \sqrt{6} M_{\text{SUSY}} + \frac{\mu}{\tan \beta}.
 \end{aligned} \tag{9.23}$$

The partial decay width and relative corrections (9.21) to the decay widths of $H^0 \rightarrow \tilde{t}_1 \tilde{t}_1^*$ are shown in Fig. 9.9. They slightly decrease with higher values of m_{H^0} . The relative QCD corrections lie between 5% and 20% whereas the EW contributions amount to -4% to 2% .

9.4.4 $H^0 \rightarrow \tilde{\tau}_1 \tilde{\tau}_1^*$

In order to allow for the decay $H^0 \rightarrow \tilde{\tau}_1 \tilde{\tau}_1^*$ the mass of $\tilde{\tau}_1$ has to be considerably lighter than the mass of the heavy Higgs bosons, i.e. $m_{H^0} > 2m_{\tilde{\tau}_1}$. Therefore, we perform our numerical analysis of the decay $H^0 \rightarrow \tilde{\tau}_1 \tilde{\tau}_1^*$ in scenario α of [142]. In terms of the parameters at the GUT scale scenario α is given by

$$\begin{aligned}
 M_0 &= 800 \text{ GeV}, & M_{1/2} &= 600 \text{ GeV}, & A_0 &= 1600 \text{ GeV}, \\
 \tan \beta &= 55, & \text{sgn } \mu &> 0.
 \end{aligned} \tag{9.24}$$

This yields the MSSM parameters given in Tab. 9.5. The relevant $\tilde{\tau}$ and Higgs-boson

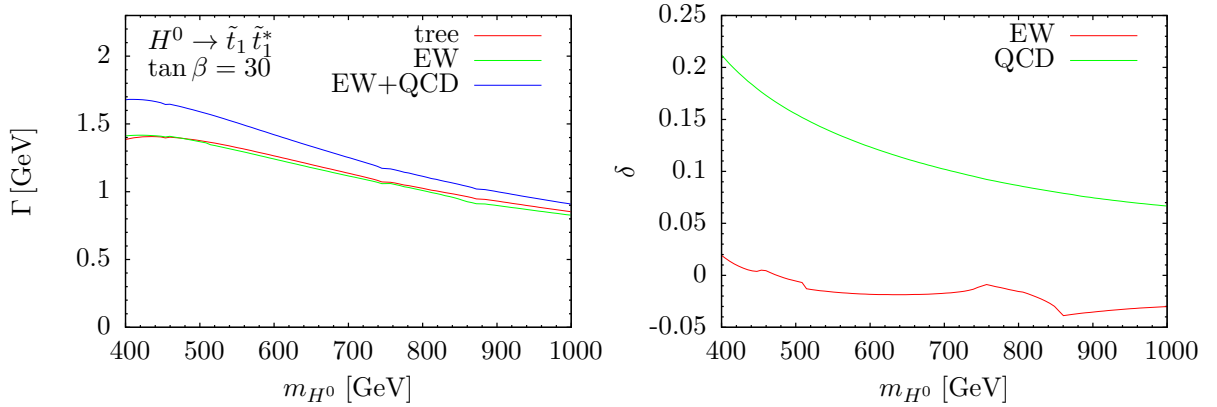


Figure 9.9: Partial decay width in GeV (left) and relative corrections (right) for the decay of the Higgs boson $H^0 \rightarrow \tilde{t}_1^* \tilde{t}_1$. The other parameters are chosen as described in the first paragraph of Subsection 9.4.3.

$M_{A^0} = 401.67$ GeV	$\tan \beta = 55$	$\mu = 665.88$ GeV
$M_1 = 252.83$ GeV	$M_2 = 466.04$ GeV	$M_3 = 1397.17$ GeV
$M_{\tilde{t}_L^{(1,2)}} = 890.60$ GeV	$M_{\tilde{e}_R^{(1,2)}} = 829.83$ GeV	
$M_{\tilde{t}_L^{(3)}} = 687.54$ GeV	$M_{\tilde{\tau}_R} = 214.93$ GeV	
$M_{\tilde{q}_L^{(1,2)}} = 1466.69$ GeV	$M_{\tilde{u}_R^{(1,2)}} = 1428.30$ GeV	$M_{\tilde{d}_R^{(1,2)}} = 1424.08$ GeV
$M_{\tilde{q}_L^{(3)}} = 1224.25$ GeV	$M_{\tilde{t}_R} = 1104.50$ GeV	$M_{\tilde{b}_R} = 1239.66$ GeV
$A_\tau = 507.28$ GeV	$A_t = -466.89$ GeV	$A_b = -503.83$ GeV

Table 9.5: Soft SUSY-breaking on-shell parameters for the CMSSM scenario α [142]. Since the bottom quark/squark and τ sector is treated in the $\overline{\text{DR}}$ scheme, the trilinear coupling of the bottom quark A_b and A_τ remain $\overline{\text{DR}}$ values.

masses in this scenario are

$$m_{H^0} = 401.52 \text{ GeV}, \quad m_{\tilde{\tau}_1} = 196.54 \text{ GeV}, \quad m_{\tilde{\tau}_2} = 684.51 \text{ GeV}. \quad (9.25)$$

Thus, only the decay channel $H^0 \rightarrow \tilde{\tau}_1 \tilde{\tau}_1^*$ is kinematically accessible in this benchmark scenario. Starting from this parameter point the CP-odd Higgs-boson mass is varied between $390 \text{ GeV} \leq m_{A^0} \leq 1000 \text{ GeV}$. In Fig. 9.10 the partial decay width (left) and relative corrections (right) for the decay $H^0 \rightarrow \tilde{\tau}_1 \tilde{\tau}_1^*$ are shown in function of m_{H^0} . The partial decay width reaches zero when $m_{H^0} \rightarrow 2m_{\tilde{\tau}_1} \approx 400 \text{ GeV}$. For low values of m_{H^0} the relative correction goes up to $\delta \approx 3\%$ and for values of $m_{H^0} \geq 500 \text{ GeV}$ the relative correction stabilizes at $\delta \approx -2\%$.

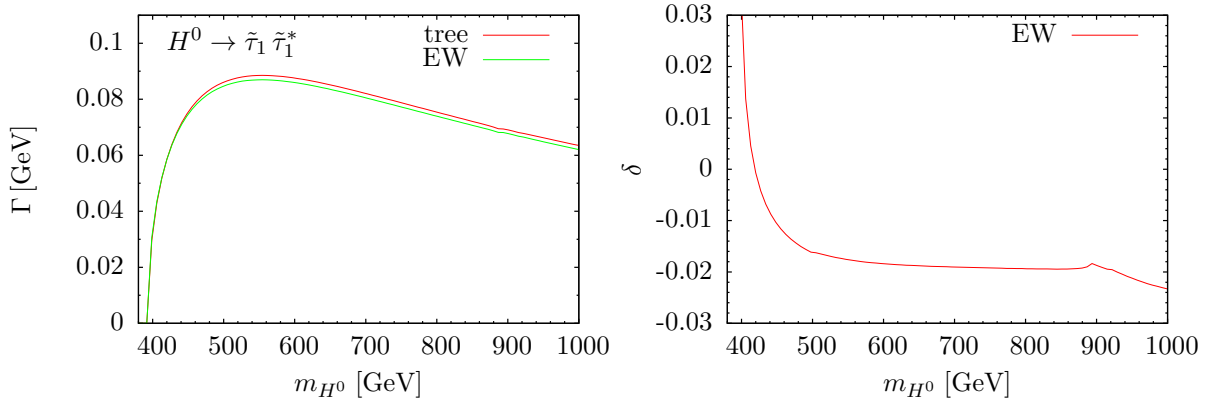


Figure 9.10: Partial decay width in GeV (left) and relative corrections (right) for the decay of the Higgs boson $H^0 \rightarrow \tilde{\tau}_1 \tilde{\tau}_1^*$ in function of m_{H^0} . The other parameters are chosen as described in the first paragraph of Subsection 9.4.4.

9.5 Comparison with HFOLD

The HFOLD package [133] computes the strict one-loop EW and QCD corrections to Higgs-boson decays within the MSSM. As in the SFOLD package the calculation is performed in the $\overline{\text{DR}}$ scheme using on-shell masses for the kinematics. Hence, we use the same procedure as in Section 7.5 to obtain the soft-breaking parameters in the on-shell scheme (only the trilinear couplings A_b and A_τ are renormalized according to the $\overline{\text{DR}}$ scheme) used in our calculation. As for the comparison with the SFOLD package we compare the decay widths obtained with our code and with HFOLD at the SPS1a' [55, 123] benchmark point using the SM parameters given in (7.13). The on-shell masses are given in Tab. 7.14 and the soft-breaking parameters in the $\overline{\text{DR}}$ and on-shell schemes are given in Tab. 7.15.

The partial decay widths computed with HFOLD and with our Higgs-boson decay code (HDC) are compared in Tab. 9.6. In order to be able to compare the results for processes with small decay widths, all values are given in MeV. Since the computation in HFOLD is performed in the $\overline{\text{DR}}$ scheme, whereas in our code for most parameters the on-shell scheme is used, only the partial decay widths including the full corrections can be compared. For the decay of the CP-even neutral Higgs boson H^0 and charged Higgs boson H^\pm the difference between the partial decay widths computed with HFOLD and with our code is mostly below 2%. Only for the decays into $\tilde{\tau}$ the differences between the decay widths computed with HFOLD and our code are between 5% and 10%. For the decays of the CP-odd Higgs boson A^0 only the partial decay widths for the decays $A^0 \rightarrow \tilde{\chi}_1^0 \tilde{\chi}_1^0$ and $A^0 \rightarrow \tilde{\chi}_1^0 \tilde{\chi}_2^0$ are below 2%. The other partial decay widths show differences up to 11% between the computation of HFOLD and our code. So far, the reason for this discrepancy between the two computations has not been identified and needs further examination.

Process	HFOLD	HDC	Process	HFOLD	HDC
	Γ_1 [MeV]	Γ_1 [MeV]		Γ_1 [MeV]	Γ_1 [MeV]
$H^0 \rightarrow \tilde{\chi}_1^0 \tilde{\chi}_1^0$	14.01	13.86	$A^0 \rightarrow \tilde{\chi}_1^0 \tilde{\chi}_1^0$	20.54	20.53
$H^0 \rightarrow \tilde{\chi}_1^0 \tilde{\chi}_2^0$	46.50	45.43	$A^0 \rightarrow \tilde{\chi}_1^0 \tilde{\chi}_2^0$	97.16	95.41
$H^0 \rightarrow \tilde{\chi}_2^0 \tilde{\chi}_2^0$	20.65	19.91	$A^0 \rightarrow \tilde{\chi}_2^0 \tilde{\chi}_2^0$	116.57	104.88
$H^0 \rightarrow \tilde{\chi}_1^+ \tilde{\chi}_1^-$	52.73	49.45	$A^0 \rightarrow \tilde{\chi}_1^+ \tilde{\chi}_1^-$	286.20	255.32
$H^0 \rightarrow \tilde{\nu}_e \tilde{\nu}_e^*$	0.50	0.50	$A^0 \rightarrow \tilde{\tau}_1 \tilde{\tau}_2^*$	59.37	55.02
$H^0 \rightarrow \tilde{\nu}_\tau \tilde{\nu}_\tau^*$	0.54	0.55			
$H^0 \rightarrow \tilde{e}_L \tilde{e}_L^*$	0.41	0.42	$H^- \rightarrow \tilde{\chi}_1^- \tilde{\chi}_1^0$	130.58	127.96
$H^0 \rightarrow \tilde{e}_R \tilde{e}_R^*$	0.45	0.44	$H^- \rightarrow \tilde{\chi}_1^- \tilde{\chi}_2^0$	0.63	0.66
$H^0 \rightarrow \tilde{\tau}_1 \tilde{\tau}_1^*$	18.43	17.20	$H^- \rightarrow \tilde{e}_L \tilde{\nu}_e$	1.26	1.28
$H^0 \rightarrow \tilde{\tau}_1 \tilde{\tau}_2^*$	38.13	35.16	$H^- \rightarrow \tilde{\tau}_1 \tilde{\nu}_\tau$	64.32	59.97
$H^0 \rightarrow \tilde{\tau}_2 \tilde{\tau}_2^*$	3.51	3.32	$H^- \rightarrow \tilde{\tau}_2 \tilde{\nu}_\tau$	1.18	1.04

Table 9.6: Partial decay widths including the full NLO corrections computed with HFOLD and with our code denoted as HDC. The decay widths of the neutral CP-even Higgs boson H^0 computed with HDC also include higher-order corrections from the finite field-renormalization factors.

Chapter 10

Conclusions

Supersymmetry (SUSY) is among the most promising extensions of the Standard Model of elementary particles. It has the potential to solve important open questions, i.e. it is able to solve the hierarchy problem, allows for unification of the electroweak and strong forces, and provides a viable dark matter candidate.

If SUSY is realized at the TeV scale, there is a good chance to produce and detect supersymmetric particles at the LHC. The particles with the generally largest production cross section at the LHC are squarks and the gluino, the superpartners of quarks and the gluon. Since they decay immediately after their production, precise knowledge of their decay channels and corresponding decay rates is essential. The theoretical predictions are significantly affected by higher-order contributions and therefore next-to-leading order (NLO) corrections have to be included. Hence, decay rates and branching ratios of squarks and gluino including QCD and electroweak NLO corrections are the first topic of this work.

Since the Yukawa couplings of the quarks of the first two generations are negligible at the energy scale considered, there are no mixing effects for squarks of the first two generations (light-flavor squarks) and the masses of left- and right-handed squarks are nearly degenerate. Hence, for light-flavor squarks we only considered decays into quark plus gluino, quark plus neutralino and quark plus chargino. On the other hand, the Yukawa couplings of the top and bottom quark cannot be neglected. This results in potentially large mixing between left- and right-handed third-generation squarks and large mass splittings between mass eigenstates are possible. Because of this potentially large difference between the mass eigenstates, decays of the heavier squarks into lighter squarks plus electroweak gauge-boson or Higgs-boson become possible. Thus, for third-generation squarks we considered in addition to the aforementioned decay channels the decays of the heavier top/bottom squark into Z/W-boson plus lighter-squark and Higgs-boson plus lighter-squark.

Generally, we performed the calculation of the QCD and electroweak NLO corrections in the on-shell renormalization scheme except for the bottom quark mass and the according trilinear coupling which we renormalized in the $\overline{\text{DR}}$ scheme. This procedure cures numerical instabilities in certain parameter regions. Furthermore, we also resummed $\tan\beta$ -enhanced contributions into effective bottom Yukawa couplings. Since the masses of the left-handed down-type squarks and the masses of the three heavier neutralinos can be chosen to depend

on the other masses, finite shifts between the tree-level and on-shell values have to be respected. This can alter the decay width by a few percent.

The computation has been performed within the framework of the Minimal Supersymmetric Standard Model (MSSM). In order to study the numerical results the decay widths and branching ratios including the NLO contributions have been evaluated at specific benchmark points which represent distinct characteristics (e.g. mass spectra). The contributions from virtual and real QCD corrections to the total decay widths of squarks lies between -5% and 20% . The QCD corrections to the total squark decay width grow substantially in parameter regions, where the decay into quark plus gluino is dominating, i.e. when the gluino is lighter than the squarks. Otherwise, QCD corrections are of the same order as the electroweak corrections, which lie between -5% and 5% , but often have opposite sign than the QCD corrections. Hence, significant cancellations between electroweak and QCD NLO contributions can occur and therefore, it is important to include both, electroweak and QCD corrections. Finally, we also examined effects of NLO corrections on differential distributions. The real photon bremsstrahlung corrections alter the p_T distributions of the quark jet in light-flavor squark decays into quark plus neutralino/chargino significantly. In contrast the distributions in the decays of the top squark into top quark plus neutralino is not strongly altered by real QCD corrections because of the reduced phase space. For the gluino decay into quark plus squark, the numerical study at selected benchmark points show that the QCD corrections vary between -8% and -13% and the electroweak corrections again have opposite sign and a value of approximately 4% . Hence, cancellations between electroweak and QCD NLO contributions have again to be taken into account.

In order to formulate a consistent supersymmetric Lagrangian, also the Higgs-sector has to be extended. In the MSSM it consists of two scalar doublet fields, which after spontaneous symmetry breaking, result in five physical Higgs bosons. Since the additional Higgs bosons can have large masses, their decays into supersymmetric particles may have sizeable branching fractions. Therefore, in the second part of this work we examined NLO corrections to Higgs boson decays into supersymmetric particles. We considered the decays of Higgs bosons into sfermions, neutralinos, and charginos. Furthermore, we also analyze the invisible decay of the lightest Higgs boson into two lightest neutralinos. This decay becomes relevant in scenarios with light neutralino LSPs, especially when the universality condition $M_1 = \frac{5}{3} \tan^2 \theta_W M_2$ is relaxed. We adopted the same framework as in squark and gluino decays to compute the QCD and electroweak corrections to the aforementioned Higgs-boson decays. In order to study the decay width and the impact of NLO contributions numerically, specific benchmark scenarios have been chosen. We choose the maximal-mixing scenario, where the maximal possible Higgs-boson mass is obtained. For the Higgs-boson decays into neutralinos and charginos, we found relative electroweak corrections between 2% and 10% . For Higgs-boson decays into top squarks, the QCD corrections lie between 5% and 20% , whereas the contributions from electroweak corrections amount to -4% to 2% . Finally, the Higgs-boson decays into tau sleptons have been studied in a benchmark scenario where this decay is kinematically accessible. Here,

the electroweak corrections are of the order of -2% .

This work provides an important step in collecting all NLO corrections to two-body squark decays in a consistent framework. Furthermore, the existing implementations of NLO corrections to Higgs-boson decays into SM particles are complemented by the presented corrections to Higgs-boson decays into their supersymmetric partners.

Appendix A

Bremsstrahlung integrals

For the processes $\tilde{t}_2 \rightarrow \tilde{t}_1 Z$ and $\tilde{t}_2 \rightarrow \tilde{t}_1 h^0$ the real photon/gluon radiation decay widths are also computed analytically. These decay widths are linear combinations of the bremsstrahlung integrals presented in this section using the notation of [30]. For a massive particle with momentum p_0 and mass m_0 decaying into two massive particles with momenta p_1, p_2 and masses m_1, m_2 and a photon with momentum q the following phase-space integrals need to be computed,

$$I_{i_1, \dots, i_n}^{j_1, \dots, j_m} = \frac{1}{\pi^2} \int \frac{d^3 p_1}{2E_1} \frac{d^3 p_2}{2E_2} \frac{d^3 q}{2E_q} \delta(p_0 - p_1 - p_2 - q) \frac{(\pm 2q p_{j_1}) \cdots (\pm 2q p_{j_m})}{(\pm 2q p_{i_1}) \cdots (\pm 2q p_{i_n})}, \quad (\text{A.1a})$$

$$E_i = \sqrt{\mathbf{p}_i^2 + m_i^2}, \quad E_q = \sqrt{\mathbf{q}^2 + \lambda^2},$$

where λ is the fictitious photon mass introduced to regularize the infrared divergences. For bremsstrahlung integrals with no upper indices the scalar products in the numerator are replaced by 1. With the phase-space function $\kappa \equiv \kappa(m_0^2, m_1^2, m_2^2)$ given in (3.2) and the dilogarithm $\text{Li}_2(x)$

$$\text{Li}_2(x) = - \int_0^1 \frac{dt}{t} \log(1 - xt), \quad (\text{A.2})$$

and defining the abbreviations

$$\beta_0 = \frac{m_0^2 - m_1^2 - m_2^2 + \kappa}{2m_1 m_2}, \quad \beta_1 = \frac{m_0^2 - m_1^2 + m_2^2 - \kappa}{2m_0 m_2}, \quad (\text{A.3a})$$

$$\beta_2 = \frac{m_0^2 + m_1^2 - m_2^2 - \kappa}{2m_0 m_1}, \quad (\text{A.3b})$$

compact expressions for the analytical integration of (A.1a) can be obtained. Since (A.1a) is symmetric under the exchange of the two external massive particles, the integrals with the indices 1 and 2 interchanged are obtained by interchanging m_1 and m_2 . Omitting integrals which can be obtained by interchanging indices, the IR-singular bremsstrahlung

integrals are given by

$$I_{00} = \frac{1}{4m_0^2} \left[\kappa \log \left(\frac{\kappa^2}{\lambda m_0 m_1 m_2} \right) - \kappa - (m_1^2 - m_2^2) \log \left(\frac{\beta_1}{\beta_2} \right) - m_0^2 \log(\beta_0) \right], \quad (\text{A.4a})$$

$$I_{11} = \frac{1}{4m_0^2 m_1^2} \left[\kappa \log \left(\frac{\kappa^2}{\lambda m_0 m_1 m_2} \right) - \kappa - (m_0^2 - m_2^2) \log \left(\frac{\beta_0}{\beta_2} \right) - m_1^2 \log(\beta_1) \right], \quad (\text{A.4b})$$

$$I_{01} = \frac{1}{4m_0^2} \left[-2 \log \left(\frac{\lambda m_0 m_1 m_2}{\kappa^2} \right) \log(\beta_2) + 2 \log^2(\beta_2) - \log^2(\beta_0) - \log^2(\beta_1) \right. \\ \left. + 2 \text{Li}_2(1 - \beta_2^2) - \text{Li}_2(1 - \beta_0^2) - \text{Li}_2(1 - \beta_1^2) \right], \quad (\text{A.4c})$$

$$I_{12} = -I_{01} - I_{02}. \quad (\text{A.4d})$$

The other bremsstrahlung integrals are IR-finite. Again, omitting integrals which are obtained by interchanging indices, the IR-finite bremsstrahlung integrals read

$$I = \frac{1}{4m_0^2} \left[\frac{\kappa}{2} (m_0^2 + m_1^2 + m_2^2) + 2m_0^2 m_1^2 \log(\beta_2) + 2m_0^2 m_2^2 \log(\beta_1) \right. \\ \left. + 2m_1^2 m_2^2 \log(\beta_0) \right], \quad (\text{A.5a})$$

$$I_0 = \frac{1}{4m_0^2} \left[-2m_1^2 \log(\beta_2) - 2m_2^2 \log(\beta_1) - \kappa \right], \quad (\text{A.5b})$$

$$I_1 = \frac{1}{4m_0^2} \left[-2m_0^2 \log(\beta_2) - 2m_2^2 \log(\beta_0) - \kappa \right], \quad (\text{A.5c})$$

$$I_0^1 = \frac{1}{4m_0^2} \left[m_1^4 \log(\beta_2) - m_2^2 (2m_0^2 - 2m_1^2 + m_2^2) \log(\beta_1) \right. \\ \left. - \frac{\kappa}{4} (m_0^2 - 3m_1^2 + 5m_2^2) \right], \quad (\text{A.5d})$$

$$I_1^0 = \frac{1}{4m_0^2} \left[m_0^4 \log(\beta_2) - m_2^2 (2m_1^2 - 2m_0^2 + m_2^2) \log(\beta_0) \right. \\ \left. - \frac{\kappa}{4} (m_1^2 - 3m_0^2 + 5m_2^2) \right], \quad (\text{A.5e})$$

$$I_2^1 = -I - I_2^0, \quad (\text{A.5f})$$

$$I_{00}^{12} = \frac{1}{4m_0^2} \left[m_1^4 \log(\beta_2) + m_2^4 \log(\beta_1) + \frac{\kappa^3}{6m_0^2} + \frac{\kappa}{4} (3m_1^2 + 3m_2^2 - m_0^2) \right], \quad (\text{A.5g})$$

$$I_{11}^{02} = \frac{1}{4m_0^2} \left[m_0^4 \log(\beta_2) + m_2^4 \log(\beta_0) + \frac{\kappa^3}{6m_1^2} + \frac{\kappa}{4} (3m_0^2 + 3m_2^2 - m_1^2) \right], \quad (\text{A.5h})$$

$$I_{00}^{12} = -I_1^0 - I_{11}^{02}, \quad (\text{A.5i})$$

$$I_{00}^{12} = -I_0^1 - I_{00}^{12}, \quad (\text{A.5j})$$

$$I_{00}^{12} = -I_1^2 - I_{11}^{02}. \quad (\text{A.5k})$$

Appendix B

Renormalization constants

In Chapters 6 and 9 the counterterm Lagrangian for squark–quark–neutralino/chargino, squark–quark–gluino, squark–squark–gauge-boson, squark–squark–Higgs-boson, and Higgs-boson–neutralino/chargino interactions are derived. In this section we list the renormalization constants belonging to the couplings given in the Lagrangians.

B.1 $\tilde{q}_a^* q' \tilde{\chi}_i$

$$\delta C_{sk}^L = -\delta g_2 U_{k1} U_{s1}^{\tilde{d}} + \left(\frac{\delta g_2}{g_2} + \frac{\delta m_d}{m_d} - \frac{\delta M_W^2}{2M_W^2} - \frac{\delta c_\beta}{c_\beta} \right) \frac{g_2 U_{k2}}{\sqrt{2} M_W c_\beta} m_d U_{s2}^{\tilde{d}}, \quad (\text{B.1})$$

$$\delta D_{sk}^L = -\delta g_2 V_{k1} U_{s1}^{\tilde{u}} + \left(\frac{\delta g_2}{g_2} + \frac{\delta m_u}{m_u} - \frac{\delta M_W^2}{2M_W^2} - \frac{\delta s_\beta}{s_\beta} \right) \frac{g_2 V_{k2}}{\sqrt{2} M_W s_\beta} m_u U_{s2}^{\tilde{u}}, \quad (\text{B.2})$$

$$\delta E_{sk}^R = \left(\frac{\delta g_2}{g_2} + \frac{\delta m_d}{m_d} - \frac{\delta M_W^2}{2M_W^2} - \frac{\delta c_\beta}{c_\beta} \right) E_{sk}^R, \quad (\text{B.3})$$

$$\delta F_{sk}^R = \left(\frac{\delta g_2}{g_2} + \frac{\delta m_u}{m_u} - \frac{\delta M_W^2}{2M_W^2} - \frac{\delta s_\beta}{s_\beta} \right) F_{sk}^R, \quad (\text{B.4})$$

$$\delta G_{sk}^{uL} = \delta G_k^{uL} U_{s1}^{\tilde{u}} - \left(\frac{\delta g_2}{g_2} + \frac{\delta m_u}{m_u} - \frac{\delta M_W^2}{2M_W^2} - \frac{\delta s_\beta}{s_\beta} \right) \frac{g_2}{\sqrt{2} M_W s_\beta} m_u N_{k4}^* U_{s2}^{\tilde{u}}, \quad (\text{B.5})$$

$$\delta G_{sk}^{uR} = \delta G_k^{uR} U_{s2}^{\tilde{u}} - \left(\frac{\delta g_2}{g_2} + \frac{\delta m_u}{m_u} - \frac{\delta M_W^2}{2M_W^2} - \frac{\delta s_\beta}{s_\beta} \right) \frac{g_2}{\sqrt{2} M_W s_\beta} m_u N_{k4} U_{s1}^{\tilde{u}}, \quad (\text{B.6})$$

$$\delta G_{sk}^{dL} = \delta G_k^{dL} U_{s1}^{\tilde{d}} - \left(\frac{\delta g_2}{g_2} + \frac{\delta m_d}{m_d} - \frac{\delta M_W^2}{2M_W^2} - \frac{\delta c_\beta}{c_\beta} \right) \frac{g_2}{\sqrt{2} M_W c_\beta} m_d N_{k3}^* U_{s2}^{\tilde{d}}, \quad (\text{B.7})$$

$$\delta G_{sk}^{dR} = \delta G_k^{dR} U_{s2}^{\tilde{d}} - \left(\frac{\delta g_2}{g_2} + \frac{\delta m_d}{m_d} - \frac{\delta M_W^2}{2M_W^2} - \frac{\delta c_\beta}{c_\beta} \right) \frac{g_2}{\sqrt{2} M_W c_\beta} m_d N_{k3} U_{s1}^{\tilde{d}}, \quad (\text{B.8})$$

$$\delta G_k^{qL} = \frac{\delta g_2}{g_2} G_k^{qL} - \sqrt{2} g_2 [\delta t_W (Q_q - T_{3L}^q) N_{k1}^*], \quad (\text{B.9})$$

$$\delta G_k^{qR} = \left(\frac{\delta g_2}{g_2} + \frac{\delta t_W}{t_W} \right) G_k^{qR}. \quad (\text{B.10})$$

B.2 $\tilde{q}_a^* \tilde{q}'_b V$

$$\begin{aligned} \delta C(Z, \tilde{q}_s^*, \tilde{q}_t) &= \left(\delta Z_e - \frac{\delta s_W}{s_W} - \frac{\delta c_W}{c_W} \right) C(Z, \tilde{q}_s^*, \tilde{q}_t) \\ &+ \left[4 (I_{\tilde{q}}^3)^2 Q_{\tilde{q}} U_{s1}^{\tilde{q}} U_{t1}^{\tilde{q}} + Q_{\tilde{q}} U_{s2}^{\tilde{q}} U_{t2}^{\tilde{q}} \right] \delta s_W^2, \end{aligned} \quad (\text{B.11})$$

$$\delta C(W^+, \tilde{u}_s^*, \tilde{d}_t) = \delta C(W^-, \tilde{d}_s^*, \tilde{u}_t) = \left(\delta Z_e - \frac{\delta s_W}{s_W} \right) C(W^+, \tilde{u}_s^*, \tilde{d}_t). \quad (\text{B.12})$$

B.3 $\tilde{q}_a^* \tilde{q}'_b S$

$$\begin{aligned} \delta C(H^+, \tilde{u}_s^*, \tilde{d}_t) &= \delta C(H^-, \tilde{d}_s^*, \tilde{u}_t) = \left(\frac{\delta g_2}{g_2} - \frac{\delta M_W^2}{2 M_W^2} \right) C(H^+, \tilde{u}_s^*, \tilde{d}_t) \\ &+ \frac{g_2}{2 M_W} \left[U_{s1}^{\tilde{u}} U_{t1}^{\tilde{d}} \left(\frac{2 m_u \delta m_u}{t_\beta} - \frac{m_u^2 \delta s_\beta}{t_\beta s_\beta} + 2 m_d \delta m_d t_\beta - m_d^2 t_\beta \frac{\delta c_\beta}{c_\beta} - \delta M_W^2 s_{2\beta} \right. \right. \\ &+ \left. \left. M_W^2 (\delta s_\beta c_\beta + \delta c_\beta s_\beta) \right) \right. \\ &- \left. U_{s1}^{\tilde{u}} U_{t2}^{\tilde{d}} \left(\delta m_d (\mu - A_d t_\beta) + m_d \left(\delta \mu - \delta A_d t_\beta - \frac{\delta c_\beta}{c_\beta} (\mu - A_d t_\beta) \right) \right) \right. \\ &- \left. U_{s2}^{\tilde{u}} U_{t1}^{\tilde{d}} \left(\delta m_u \left(\mu - \frac{A_u}{t_\beta} \right) + m_u \left(\delta \mu - \frac{\delta A_u}{t_\beta} - \frac{\delta s_\beta}{s_\beta} \left(\mu - \frac{A_u}{t_\beta} \right) \right) \right) \right. \\ &\left. + U_{s2}^{\tilde{u}} U_{t2}^{\tilde{d}} \left((\delta m_u m_d + \delta m_d m_u) \left(t_\beta + \frac{1}{t_\beta} \right) - m_u m_d \left(t_\beta \frac{\delta c_\beta}{c_\beta} + \frac{1}{t_\beta} \frac{\delta s_\beta}{s_\beta} \right) \right) \right], \end{aligned} \quad (\text{B.13})$$

$$\delta C(H^0, \tilde{u}_s^*, \tilde{u}_t) = \delta C_A(\tilde{u}_s^*, \tilde{u}_t) s_\alpha + \delta C_\mu(\tilde{u}_s^*, \tilde{u}_t) c_\alpha - \delta C_g(\tilde{u}_s^*, \tilde{u}_t) c_{\alpha+\beta} + C_g(\tilde{u}_s^*, \tilde{u}_t) s_{\alpha+\beta} c_\beta^2 \delta t_\beta, \quad (\text{B.14})$$

$$\delta C(h^0, \tilde{u}_s^*, \tilde{u}_t) = \delta C_A(\tilde{u}_s^*, \tilde{u}_t) c_\alpha - \delta C_\mu(\tilde{u}_s^*, \tilde{u}_t) s_\alpha + \delta C_g(\tilde{u}_s^*, \tilde{u}_t) s_{\alpha+\beta} + C_g(\tilde{u}_s^*, \tilde{u}_t) c_{\alpha+\beta} c_\beta^2 \delta t_\beta, \quad (\text{B.15})$$

$$\delta C \left(H^0, \tilde{d}_s^*, \tilde{d}_t \right) = \delta C_A \left(\tilde{d}_s^*, \tilde{d}_t \right) c_\alpha + \delta C_\mu \left(\tilde{d}_s^*, \tilde{d}_t \right) s_\alpha - \delta C_g \left(\tilde{d}_s^*, \tilde{d}_t \right) c_{\alpha+\beta} + C_g \left(\tilde{d}_s^*, \tilde{d}_t \right) s_{\alpha+\beta} c_\beta^2 \delta t_\beta, \quad (\text{B.16})$$

$$\delta C \left(h^0, \tilde{d}_s^*, \tilde{d}_t \right) = -\delta C_A \left(\tilde{d}_s^*, \tilde{d}_t \right) s_\alpha + \delta C_\mu \left(\tilde{d}_s^*, \tilde{d}_t \right) c_\alpha + \delta C_g \left(\tilde{d}_s^*, \tilde{d}_t \right) s_{\alpha+\beta} + C_g \left(\tilde{d}_s^*, \tilde{d}_t \right) c_{\alpha+\beta} c_\beta^2 \delta t_\beta. \quad (\text{B.17})$$

$$\delta C \left(A^0, \tilde{u}_s^*, \tilde{u}_t \right) = \left(\frac{\delta g_2}{g_2} + \frac{\delta m_u}{m_u} - \frac{\delta M_W^2}{2 M_W^2} \right) C \left(A^0, \tilde{u}_s^*, \tilde{u}_t \right) + \frac{i g_2 m_u}{2 M_W} \left(U_{s1}^{\tilde{u}} U_{t2}^{\tilde{u}} \left(\delta \mu - \frac{\delta A_u}{t_\beta} - \frac{\delta s_\beta}{s_\beta} \left(\mu - \frac{A_u}{t_\beta} \right) \right) - U_{s2}^{\tilde{u}} U_{t1}^{\tilde{u}} \left(\delta \mu - \frac{\delta A_u}{t_\beta} - \frac{\delta s_\beta}{s_\beta} \left(\mu - \frac{A_u}{t_\beta} \right) \right) \right) \quad (\text{B.18})$$

$$\delta C \left(A^0, \tilde{d}_s^*, \tilde{d}_t \right) = \left(\frac{\delta g_2}{g_2} + \frac{\delta m_u}{m_u} - \frac{\delta M_W^2}{2 M_W^2} \right) C \left(A^0, \tilde{u}_s^*, \tilde{u}_t \right) + \frac{i g_2 m_d}{2 M_W} \left(U_{s1}^{\tilde{d}} U_{t2}^{\tilde{d}} \left(\delta \mu - \delta A_d t_\beta - \frac{\delta c_\beta}{c_\beta} (\mu - A_d t_\beta) \right) - U_{s2}^{\tilde{d}} U_{t1}^{\tilde{d}} \left(\delta \mu - \delta A_d t_\beta - \frac{\delta c_\beta}{c_\beta} (\mu - A_d t_\beta) \right) \right) \quad (\text{B.19})$$

$$\delta C_A \left(\tilde{u}_s^*, \tilde{u}_t \right) = \left(\frac{\delta g_2}{g_2} - \frac{\delta M_W^2}{2 M_W^2} - \frac{\delta s_\beta}{s_\beta} \right) C_A \left(\tilde{u}_s^*, \tilde{u}_t \right) + \frac{g_2}{M_W s_\beta} \left[\left(\frac{\delta m_u A_u}{2} + \frac{m_u \delta A_u}{2} \right) (U_{s1}^{\tilde{u}} U_{t2}^{\tilde{u}} + U_{s2}^{\tilde{u}} U_{t1}^{\tilde{u}}) - 2 m_u \delta m_u (U_{s1}^{\tilde{u}} U_{t1}^{\tilde{u}} + U_{s2}^{\tilde{u}} U_{t2}^{\tilde{u}}) \right], \quad (\text{B.20})$$

$$\delta C_A \left(\tilde{d}_s^*, \tilde{d}_t \right) = \left(\frac{\delta g_2}{g_2} - \frac{\delta M_W^2}{2 M_W^2} - \frac{\delta c_\beta}{c_\beta} \right) C_A \left(\tilde{d}_s^*, \tilde{d}_t \right) + \frac{g_2}{M_W c_\beta} \left[\left(\frac{\delta m_d A_d}{2} + \frac{m_d \delta A_d}{2} \right) (U_{s1}^{\tilde{d}} U_{t2}^{\tilde{d}} + U_{s2}^{\tilde{d}} U_{t1}^{\tilde{d}}) - 2 m_d \delta m_d (U_{s1}^{\tilde{d}} U_{t1}^{\tilde{d}} + U_{s2}^{\tilde{d}} U_{t2}^{\tilde{d}}) \right], \quad (\text{B.21})$$

$$\delta C_\mu \left(\tilde{u}_s^*, \tilde{u}_t \right) = \left(\frac{\delta g_2}{g_2} + \frac{\delta m_u}{m_u} + \frac{\delta \mu}{\mu} - \frac{\delta M_W^2}{2 M_W^2} - \frac{\delta s_\beta}{s_\beta} \right) C_\mu \left(\tilde{u}_s^*, \tilde{u}_t \right), \quad (\text{B.22})$$

$$\delta C_\mu \left(\tilde{d}_s^*, \tilde{d}_t \right) = \left(\frac{\delta g_2}{g_2} + \frac{\delta m_d}{m_d} + \frac{\delta \mu}{\mu} - \frac{\delta M_W^2}{2 M_W^2} - \frac{\delta c_\beta}{c_\beta} \right) C_\mu \left(\tilde{d}_s^*, \tilde{d}_t \right), \quad (\text{B.23})$$

$$\delta C_g \left(\tilde{u}_s^*, \tilde{u}_t \right) = \left(\frac{\delta g_2}{g_2} + \frac{\delta M_W^2}{2 M_W} \right) C_g \left(\tilde{u}_s^*, \tilde{u}_t \right) + g_2 M_W \left[(1 - 2 Q_u) U_{s1}^{\tilde{u}} U_{t1}^{\tilde{u}} + 2 Q_u U_{s2}^{\tilde{u}} U_{t2}^{\tilde{u}} \right] t_W \delta t_W, \quad (\text{B.24})$$

$$\delta C_g \left(\tilde{d}_s^*, \tilde{d}_t \right) = \left(\frac{\delta g_2}{g_2} + \frac{\delta M_W^2}{2 M_W} \right) C_g \left(\tilde{d}_s^*, \tilde{d}_t \right) - g_2 M_W \left[(1 + 2 Q_d) U_{s1}^{\tilde{d}} U_{t1}^{\tilde{d}} - 2 Q_d U_{s2}^{\tilde{d}} U_{t2}^{\tilde{d}} \right] t_W \delta t_W. \quad (\text{B.25})$$

B.4 $S \tilde{\chi}_i \tilde{\chi}_j$

$$\delta C_{nl}^R(h^0) = \delta C_{ln}^L(h^0)^* = \delta g_2 C_{nl}^R(h^0) + g_2 (\sin \alpha \delta Q_{nl}'' + \cos \alpha \delta S_{nl}''), \quad (\text{B.26})$$

$$\delta C_{nl}^R(H^0) = \delta C_{ln}^L(H^0)^* = \delta g_2 C_{nl}^R(H^0) - g_2 (\cos \alpha \delta Q_{nl}'' - \sin \alpha \delta S_{nl}''), \quad (\text{B.27})$$

$$\delta C_{nl}^R(A^0) = \delta C_{ln}^L(A^0)^* = \delta g_2 C_{nl}^R(A^0) - i g_2 (\sin \beta \delta Q_{nl}'' - \cos \beta \delta S_{nl}''), \quad (\text{B.28})$$

$$\delta C_{nl}^R(G^0) = \delta C_{ln}^L(G^0)^* = \delta g_2 C_{nl}^R(G^0) + i g_2 (\cos \beta \delta Q_{nl}'' + \sin \beta \delta S_{nl}''), \quad (\text{B.29})$$

$$\delta D_{km}^R(h^0) = \delta D_{mk}^L(h^0)^* = \delta g_2 D_{km}^R(h^0), \quad (\text{B.30})$$

$$\delta D_{km}^R(H^0) = \delta D_{mk}^L(H^0)^* = \delta g_2 D_{km}^R(H^0), \quad (\text{B.31})$$

$$\delta D_{km}^R(A^0) = \delta D_{mk}^L(A^0)^* = \delta g_2 D_{km}^R(A^0), \quad (\text{B.32})$$

$$\delta D_{km}^R(G^0) = \delta D_{mk}^L(G^0)^* = \delta g_2 D_{km}^R(h^0), \quad (\text{B.33})$$

$$\delta E_{lk}^R(H^-) = \delta g_2 E_{lk}^R(H^-) - g_2 \sin \beta \delta Q_{lk}'^R, \quad (\text{B.34})$$

$$\delta E_{lk}^L(H^-) = \delta g_2 E_{lk}^R(H^-) - g_2 \cos \beta \delta Q_{lk}'^L, \quad (\text{B.35})$$

$$\delta E_{lk}^R(G^-) = \delta g_2 E_{lk}^R(G^-) + g_2 \cos \beta \delta Q_{lk}'^R, \quad (\text{B.36})$$

$$E_{lk}^L(G^-) = \delta g_2 E_{lk}^R(G^-) - g_2 \sin \beta \delta Q_{lk}'^L. \quad (\text{B.37})$$

$$\delta Q_{lk}'^R = -\frac{1}{\sqrt{2}} U_{k2} N_{l1} \delta t_W, \quad \delta Q_{lk}'^L = \frac{1}{\sqrt{2}} V_{k2}^* N_{l1}^* \delta t_W, \quad (\text{B.38})$$

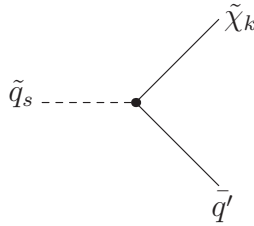
$$\delta Q_{nl}'' = -\frac{1}{2} (N_{n3} N_{l1} + N_{l3} N_{n1}) \delta t_W, \quad \delta S_{nl}'' = -\frac{1}{2} (N_{n4} N_{l1} + N_{l4} N_{n1}) \delta t_W. \quad (\text{B.39})$$

Appendix C

Feynman rules

The Feynman rules including counterterms are deduced from the Lagrangians given in Chapter 6. In the vertices all momenta are considered as incoming.

C.1 $\tilde{q}_s \bar{q}' \tilde{\chi}_k$



$$= i (C^L P_L + C^R P_R),$$

$$\begin{pmatrix} C^L \\ C^R \end{pmatrix} [\tilde{u}_s, \bar{d}, \tilde{\chi}_k^-] = \begin{pmatrix} E_{sk}^{R*} \\ D_{sk}^L \end{pmatrix}$$

$$\begin{pmatrix} C^L \\ C^R \end{pmatrix}^{\text{CT}} [\tilde{u}_s, \bar{d}, \tilde{\chi}_k^-] = \begin{pmatrix} \frac{1}{2} \left([\delta \mathcal{Z}_{\tilde{\chi}^+}^R]^* E_{sl}^{R*} + [\delta \mathcal{Z}_{\tilde{u}}]_{ts} E_{tk}^{R*} + \delta Z_d^{R*} E_{sk}^{R*} \right) + \delta E_{sk}^{R*} \\ \frac{1}{2} \left([\delta \mathcal{Z}_{\tilde{\chi}^+}^L]^* D_{sl}^L + [\delta \mathcal{Z}_{\tilde{u}}]_{ts} D_{tk}^L + \delta Z_d^{L*} D_{sk}^L \right) + \delta D_{sk}^L \end{pmatrix}$$

$$\begin{pmatrix} C^L \\ C^R \end{pmatrix} [\tilde{d}_s, \bar{u}, \tilde{\chi}_k^+] = \begin{pmatrix} F_{sk}^{R*} \\ C_{sk}^L \end{pmatrix}$$

$$\begin{pmatrix} C^L \\ C^R \end{pmatrix}^{\text{CT}} [\tilde{d}_s, \bar{u}, \tilde{\chi}_k^+] = \begin{pmatrix} \frac{1}{2} \left([\delta \mathcal{Z}_{\tilde{\chi}^+}^L]_{lk} F_{sl}^{R*} + [\delta \mathcal{Z}_{\tilde{d}}]_{ts} F_{tk}^{R*} + \delta Z_u^{R*} F_{sk}^{R*} \right) + \delta F_{sk}^{R*} \\ \frac{1}{2} \left([\delta \mathcal{Z}_{\tilde{\chi}^+}^R]_{lk} C_{sl}^L + [\delta \mathcal{Z}_{\tilde{d}}]_{ts} C_{tk}^L + \delta Z_u^{L*} C_{sk}^L \right) + \delta C_{sk}^L \end{pmatrix}$$

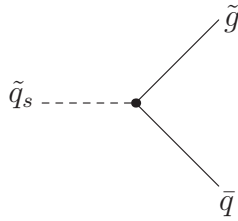
$$\begin{pmatrix} C^L \\ C^R \end{pmatrix} [\tilde{u}_s, \bar{u}, \tilde{\chi}_k^0] = \begin{pmatrix} G_{sk}^{uR^*} \\ G_{sk}^{uL^*} \end{pmatrix}$$

$$\begin{pmatrix} C^L \\ C^R \end{pmatrix}^{\text{CT}} [\tilde{u}_s, \bar{u}, \tilde{\chi}_k^0] = \begin{pmatrix} \frac{1}{2} ([\delta \mathcal{Z}_{\tilde{\chi}^0}]_{lk} G_{sl}^{uR^*} + [\delta \mathcal{Z}_{\tilde{u}}]_{ts} G_{tk}^{uR^*} + \delta Z_u^{R^*} G_{sk}^{uR^*}) + \delta G_{sk}^{uR^*} \\ \frac{1}{2} ([\delta \mathcal{Z}_{\tilde{\chi}^0}]_{lk}^* G_{sl}^{uL^*} + [\delta \mathcal{Z}_{\tilde{u}}]_{ts} G_{tk}^{uL^*} + \delta Z_u^{L^*} G_{sk}^{uL^*}) + \delta G_{sk}^{uL^*} \end{pmatrix}$$

$$\begin{pmatrix} C^L \\ C^R \end{pmatrix} [\tilde{d}_s, \bar{d}, \tilde{\chi}_k^0] = \begin{pmatrix} G_{sk}^{dR^*} \\ G_{sk}^{dL^*} \end{pmatrix}$$

$$\begin{pmatrix} C^L \\ C^R \end{pmatrix}^{\text{CT}} [\tilde{d}_s, \bar{d}, \tilde{\chi}_k^0] = \begin{pmatrix} \frac{1}{2} ([\delta \mathcal{Z}_{\tilde{\chi}^0}]_{lk} G_{sl}^{dR^*} + [\delta \mathcal{Z}_{\tilde{d}}]_{ts} G_{tk}^{dR^*} + \delta Z_d^{R^*} G_{sk}^{dR^*}) + \delta G_{sk}^{dR^*} \\ \frac{1}{2} ([\delta \mathcal{Z}_{\tilde{\chi}^0}]_{lk}^* G_{sl}^{dL^*} + [\delta \mathcal{Z}_{\tilde{d}}]_{ts} G_{tk}^{dL^*} + \delta Z_d^{L^*} G_{sk}^{dL^*}) + \delta G_{sk}^{dL^*} \end{pmatrix}.$$

C.2 $\tilde{q}_s \bar{q} \tilde{g}^a$

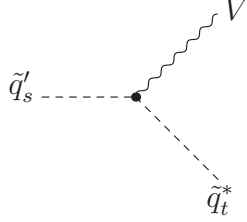


$$= i (C^L P_L + C^R P_R),$$

$$\begin{pmatrix} C^L \\ C^R \end{pmatrix} [\tilde{q}_s, \bar{q}, \tilde{g}^a] = -\sqrt{2} g_s T^a \begin{pmatrix} -U_{2s}^{\tilde{q}} \\ U_{1s}^{\tilde{q}} \end{pmatrix}$$

$$\begin{pmatrix} C^L \\ C^R \end{pmatrix}^{\text{CT}} [\tilde{q}_s, \bar{q}, \tilde{g}^a] = -\sqrt{2} g_s T^a \begin{pmatrix} -\delta Z_{g_s} U_{2s}^{\tilde{q}} - \frac{1}{2} [\delta \mathcal{Z}_{\tilde{q}}]_{ts} U_{2t}^{\tilde{q}} - \frac{1}{2} \delta Z_q^{R^*} U_{2s}^{\tilde{q}} \\ \delta Z_{g_s} U_{1s}^{\tilde{q}} + \frac{1}{2} [\delta \mathcal{Z}_{\tilde{q}}]_{ts} U_{1t}^{\tilde{q}} + \frac{1}{2} \delta Z_q^{L^*} U_{1s}^{\tilde{q}} \end{pmatrix}.$$

C.3 $\tilde{q}'_s \tilde{q}_t^* V$



$$= iC (p_1 - p_2)_\mu,$$

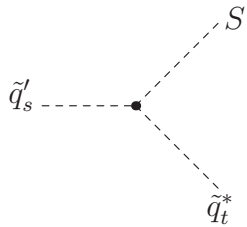
$$C [\tilde{q}_s, \tilde{q}_t^*, Z_\mu] = C (Z, \tilde{q}_t^*, \tilde{q}_s),$$

$$C^{\text{CT}} [\tilde{q}_s, \tilde{q}_t^*, Z_\mu] = \delta C (Z, \tilde{q}_t^*, \tilde{q}_s) + \frac{1}{2} \delta Z_{11}^{ZA} C (Z, \tilde{q}_t^*, \tilde{q}_s) + \frac{1}{2} \delta Z_{21}^{ZA} C (A, \tilde{q}_t^*, \tilde{q}_s) \\ + \frac{1}{2} [\delta \mathcal{Z}_{\tilde{q}}^*]_{tu} C (Z, \tilde{q}_t^*, \tilde{q}_s) + \frac{1}{2} [\delta \mathcal{Z}_{\tilde{q}}]_{sv} C (Z, \tilde{q}_t^*, \tilde{q}_v),$$

$$C [\tilde{u}_s, \tilde{d}_t^*, W_\mu^-] = C (W^-, \tilde{d}_t^*, \tilde{u}_s),$$

$$C^{\text{CT}} [\tilde{u}_s, \tilde{d}_t^*, W_\mu^-] = \delta C (W^-, \tilde{d}_t^*, \tilde{u}_s) + \frac{1}{2} \delta Z_W C (W^-, \tilde{d}_t^*, \tilde{u}_s) \\ + \frac{1}{2} [\delta \mathcal{Z}_{\tilde{d}}^*]_{tu} C (W^-, \tilde{d}_t^*, \tilde{u}_s) + \frac{1}{2} [\delta \mathcal{Z}_{\tilde{u}}]_{sv} C (W^-, \tilde{d}_t^*, \tilde{u}_v).$$

C.4 $\tilde{q}'_s \tilde{q}_t^* S$



$$= iC$$

$$C [\tilde{q}_s, \tilde{q}_t^*, h^0] = C (h^0, \tilde{q}_t^*, \tilde{q}_s),$$

$$C^{\text{CT}} [\tilde{q}_s, \tilde{q}_t^*, h^0] = \delta C (h^0, \tilde{q}_t^*, \tilde{q}_s) + \frac{1}{2} [\delta \mathcal{Z}_{\tilde{q}}^*]_{tu} C (h^0, \tilde{q}_t^*, \tilde{q}_s) + \frac{1}{2} [\delta \mathcal{Z}_{\tilde{q}}]_{sv} C (h^0, \tilde{q}_t^*, \tilde{q}_v) \\ + \frac{1}{2} \delta Z_{h^0 h^0} C (h^0, \tilde{q}_t^*, \tilde{q}_s) + \frac{1}{2} \delta Z_{h^0 H^0} C (H^0, \tilde{q}_t^*, \tilde{q}_s),$$

$$\begin{aligned}
C[\tilde{q}_s, \tilde{q}_t^*, H^0] &= C(H^0, \tilde{q}_t^*, \tilde{q}_s), \\
C^{\text{CT}}[\tilde{q}_s, \tilde{q}_t^*, H^0] &= \delta C(H^0, \tilde{q}_t^*, \tilde{q}_s) + \frac{1}{2} [\delta \mathcal{Z}_{\tilde{q}}]_{tu}^* C(H^0, \tilde{q}_u^*, \tilde{q}_s) + \frac{1}{2} [\delta \mathcal{Z}_{\tilde{q}}]_{sv} C(H^0, \tilde{q}_t^*, \tilde{q}_v) \\
&\quad + \frac{1}{2} \delta Z_{H^0 H^0} C(H^0, \tilde{q}_t^*, \tilde{q}_s) + \frac{1}{2} \delta Z_{h^0 H^0} C(h^0, \tilde{q}_t^*, \tilde{q}_s),
\end{aligned}$$

$$\begin{aligned}
C[\tilde{q}_s, \tilde{q}_t^*, A^0] &= C(A^0, \tilde{q}_t^*, \tilde{q}_s), \\
C^{\text{CT}}[\tilde{q}_s, \tilde{q}_t^*, A^0] &= \delta C(A^0, \tilde{q}_t^*, \tilde{q}_s) + \frac{1}{2} [\delta \mathcal{Z}_{\tilde{q}}]_{tu}^* C(A^0, \tilde{q}_u^*, \tilde{q}_s) + \frac{1}{2} [\delta \mathcal{Z}_{\tilde{q}}]_{sv} C(A^0, \tilde{q}_t^*, \tilde{q}_v) \\
&\quad + \frac{1}{2} \delta Z_{A^0 A^0} C(A^0, \tilde{q}_t^*, \tilde{q}_s) + \frac{1}{2} \delta Z_{A^0 G^0} C(G^0, \tilde{q}_t^*, \tilde{q}_s),
\end{aligned}$$

$$\begin{aligned}
C[\tilde{u}_s, \tilde{d}_t^*, H^-] &= C(H^-, \tilde{d}_t^*, \tilde{u}_s), \\
C^{\text{CT}}[\tilde{u}_s, \tilde{d}_t^*, H^-] &= \delta C(H^-, \tilde{d}_t^*, \tilde{u}_s) + \frac{1}{2} [\delta \mathcal{Z}_{\tilde{d}}]_{tu}^* C(H^-, \tilde{d}_u^*, \tilde{u}_s) + \frac{1}{2} [\delta \mathcal{Z}_{\tilde{u}}]_{sv}^* C(H^-, \tilde{d}_t^*, \tilde{u}_v) \\
&\quad + \frac{1}{2} \delta Z_{H^+ H^-} C(H^-, \tilde{d}_t^*, \tilde{u}_s) + \frac{1}{2} \delta Z_{H^- G^+} C(G^-, \tilde{d}_t^*, \tilde{u}_s).
\end{aligned}$$

C.5 $S \tilde{\chi}_n \tilde{\chi}_l$

$$\begin{array}{c}
\tilde{\chi}_l^0 \\
\diagup \\
S^0 \text{---} \bullet \\
\diagdown \\
\tilde{\chi}_n^0
\end{array} = \frac{i}{2} (C^L P_L + C^R P_R),$$

$$\begin{pmatrix} C^L \\ C^R \end{pmatrix} [S^0, \tilde{\chi}_n^0, \tilde{\chi}_l^0] = \begin{pmatrix} C_{nl}^L(S^0) \\ C_{nl}^R(S^0) \end{pmatrix}, \quad S^0 = h^0, H^0, A^0,$$

$$\begin{pmatrix} C^L \\ C^R \end{pmatrix}^{\text{CT}} [h^0, \tilde{\chi}_n^0, \tilde{\chi}_l^0] = \begin{pmatrix} \left\{ \begin{array}{l} \frac{1}{2} ([\delta Z_{\tilde{\chi}^0}]_{mn} C_{ml}^L(h^0) + C_{nk}^L(h^0) [\delta Z_{\tilde{\chi}^0}]_{kl} \\ + \delta Z_{h^0 h^0} C_{nl}^L(h^0) + \delta Z_{h^0 H^0} C_{nl}^L(H^0) + \delta C_{nl}^L(h^0) \end{array} \right\} \\ \left\{ \begin{array}{l} \frac{1}{2} ([\delta Z_{\tilde{\chi}^0}]_{mn}^* C_{ml}^R(h^0) + C_{nk}^R(h^0) [\delta Z_{\tilde{\chi}^0}]_{kl}^* \\ + \delta Z_{h^0 h^0} C_{nl}^R(h^0) + \delta Z_{h^0 H^0} C_{nl}^R(H^0) + \delta C_{nl}^R(h^0) \end{array} \right\} \end{pmatrix},$$

$$\begin{pmatrix} C^L \\ C^R \end{pmatrix}^{\text{CT}} [H^0, \tilde{\chi}_n^0, \tilde{\chi}_l^0] = \left(\begin{array}{c} \left\{ \begin{array}{l} \frac{1}{2} \left([\delta Z_{\tilde{\chi}^0}]_{mn} C_{ml}^L(H^0) + C_{nk}^L(H^0) [\delta Z_{\tilde{\chi}^0}]_{kl} \\ + \delta Z_{H^0 H^0} C_{nl}^L(H^0) + \delta Z_{h^0 H^0} C_{nl}^L(h^0) \end{array} \right) + \delta C_{nl}^L(H^0) \\ \frac{1}{2} \left([\delta Z_{\tilde{\chi}^0}]_{mn}^* C_{ml}^R(H^0) + C_{nk}^R(H^0) [\delta Z_{\tilde{\chi}^0}]_{kl}^* \\ + \delta Z_{H^0 H^0} C_{nl}^R(H^0) + \delta Z_{h^0 H^0} C_{nl}^R(h^0) \end{array} \right) + \delta C_{nl}^R(H^0) \end{array} \right),$$

$$\begin{pmatrix} C^L \\ C^R \end{pmatrix}^{\text{CT}} [A^0, \tilde{\chi}_n^0, \tilde{\chi}_l^0] = \left(\begin{array}{c} \left\{ \begin{array}{l} \frac{1}{2} \left([\delta Z_{\tilde{\chi}^0}]_{mn} C_{ml}^L(A^0) + C_{nk}^L(A^0) [\delta Z_{\tilde{\chi}^0}]_{kl} \\ + \delta Z_{A^0 A^0} C_{nl}^L(A^0) + \delta Z_{A^0 G^0} C_{nl}^L(G^0) \end{array} \right) + \delta C_{nl}^L(A^0) \\ \frac{1}{2} \left([\delta Z_{\tilde{\chi}^0}]_{mn}^* C_{ml}^R(A^0) + C_{nk}^R(A^0) [\delta Z_{\tilde{\chi}^0}]_{kl}^* \\ + \delta Z_{A^0 A^0} C_{nl}^R(A^0) + \delta Z_{A^0 G^0} C_{nl}^R(G^0) \end{array} \right) + \delta C_{nl}^R(A^0) \end{array} \right).$$

$$\begin{array}{c} \tilde{\chi}_k^+ \\ \swarrow \\ S^0 \text{---} \bullet \\ \searrow \\ \tilde{\chi}_m^+ \end{array} = i(C^L P_L + C^R P_R),$$

$$\begin{pmatrix} C^L \\ C^R \end{pmatrix} [S^0, \tilde{\chi}_k^+, \tilde{\chi}_m^+] = \begin{pmatrix} D_{km}^L(S^0) \\ D_{km}^R(S^0) \end{pmatrix}, \quad S^0 = h^0, H^0, A^0,$$

$$\begin{pmatrix} C^L \\ C^R \end{pmatrix}^{\text{CT}} [h^0, \tilde{\chi}_k^+, \tilde{\chi}_m^+] = \left(\begin{array}{c} \left\{ \begin{array}{l} \frac{1}{2} \left([\delta Z_{\tilde{\chi}^\pm}^R]_{lk}^* D_{lm}^L(h^0) + D_{kn}^L(h^0) [\delta Z_{\tilde{\chi}^\pm}^L]_{nm} \\ + \delta Z_{h^0 h^0} D_{km}^L(h^0) + \delta Z_{h^0 H^0} D_{km}^L(H^0) \end{array} \right) + \delta D_{km}^L(h^0) \\ \frac{1}{2} \left([\delta Z_{\tilde{\chi}^\pm}^L]_{lk}^* D_{lm}^R(h^0) + D_{kn}^R(h^0) [\delta Z_{\tilde{\chi}^\pm}^R]_{nm} \\ + \delta Z_{h^0 h^0} D_{km}^R(h^0) + \delta Z_{h^0 H^0} D_{km}^R(H^0) \end{array} \right) + \delta D_{km}^R(h^0) \end{array} \right),$$

$$\begin{pmatrix} C^L \\ C^R \end{pmatrix}^{\text{CT}} [H^0, \tilde{\chi}_k^+, \tilde{\chi}_m^+] = \left(\begin{array}{c} \left\{ \begin{array}{l} \frac{1}{2} \left([\delta Z_{\tilde{\chi}^\pm}^R]_{lk}^* D_{lm}^L(H^0) + D_{kn}^L(H^0) [\delta Z_{\tilde{\chi}^\pm}^L]_{nm} \\ + \delta Z_{H^0 H^0} D_{km}^L(H^0) + \delta Z_{h^0 H^0} D_{km}^L(h^0) \end{array} \right) + \delta D_{km}^L(H^0) \\ \frac{1}{2} \left([\delta Z_{\tilde{\chi}^\pm}^L]_{lk}^* D_{lm}^R(H^0) + D_{kn}^R(H^0) [\delta Z_{\tilde{\chi}^\pm}^R]_{nm} \\ + \delta Z_{h^0 h^0} D_{km}^R(H^0) + \delta Z_{h^0 H^0} D_{km}^R(h^0) \end{array} \right) + \delta D_{km}^R(H^0) \end{array} \right),$$

$$\begin{pmatrix} C^L \\ C^R \end{pmatrix}^{\text{CT}} [A^0, \tilde{\chi}_k^+, \tilde{\chi}_m^+] = \left(\begin{array}{c} \left\{ \begin{array}{l} \frac{1}{2} \left([\delta Z_{\tilde{\chi}^\pm}^R]_{lk}^* D_{lm}^L(A^0) + D_{kn}^L(A^0) [\delta Z_{\tilde{\chi}^\pm}^L]_{nm} \\ + \delta Z_{A^0 A^0} D_{km}^L(A^0) + \delta Z_{A^0 G^0} D_{km}^L(G^0) \end{array} \right) + \delta D_{km}^L(A^0) \\ \frac{1}{2} \left([\delta Z_{\tilde{\chi}^\pm}^L]_{lk}^* D_{lm}^R(A^0) + D_{kn}^R(A^0) [\delta Z_{\tilde{\chi}^\pm}^R]_{nm} \\ + \delta Z_{A^0 A^0} D_{km}^R(A^0) + \delta Z_{A^0 G^0} D_{km}^R(G^0) \end{array} \right) + \delta D_{km}^R(A^0) \end{array} \right).$$

$$\begin{array}{c}
 \tilde{\chi}_l^0 \\
 \swarrow \\
 H^- \text{---} \bullet \\
 \searrow \\
 \tilde{\chi}_k^+
 \end{array}
 = i(C^L P_L + C^R P_R),$$

$$\begin{pmatrix} C^L \\ C^R \end{pmatrix} [H^-, \tilde{\chi}_l^0, \tilde{\chi}_k^+] = \begin{pmatrix} E_{lk}^L(H^-) \\ E_{lk}^R(H^-) \end{pmatrix},$$

$$\begin{pmatrix} C^L \\ C^R \end{pmatrix}^{\text{CT}} [H^-, \tilde{\chi}_l^0, \tilde{\chi}_k^+] = \begin{pmatrix} \left\{ \begin{array}{l} \frac{1}{2} \left([\delta Z_{\tilde{\chi}^0}]_{ml} E_{mk}^L(H^-) + E_{ln}^L(H^-) [\delta Z_{\tilde{\chi}^\pm}^L]_{nk} \right. \\ \left. + \delta Z_{H^+H^-} E_{lk}^L(H^-) + \delta Z_{H^+G^-} E_{lk}^L(G^-) \right) + \delta E_{lk}^L(H^-) \end{array} \right\} \\ \left\{ \begin{array}{l} \frac{1}{2} \left([\delta Z_{\tilde{\chi}^0}]_{ml}^* E_{mk}^R(H^-) + E_{ln}^R(H^-) [\delta Z_{\tilde{\chi}^\pm}^R]_{nk} \right. \\ \left. + \delta Z_{H^+H^-} E_{lk}^R(H^-) + \delta Z_{H^+G^-} E_{lk}^R(H^-) \right) + \delta E_{lk}^R(H^-) \end{array} \right\} \end{pmatrix}.$$

$$\bar{A}^0, p \text{---} \times \text{---} Z_\mu = -i \frac{M_Z}{2} (\delta Z_{A^0 G^0} + \cos^2 \beta \delta \tan \beta) p_\mu$$

$$\bar{H}^+, p \text{---} \times \text{---} W_\mu^- = -i \frac{M_W}{2} (\delta Z_{H^+ G^-} + \cos^2 \beta \delta \tan \beta) p_\mu$$

$$\bar{H}^-, p \text{---} \times \text{---} W_\mu^+ = i \frac{M_W}{2} (\delta Z_{H^- G^+} + \cos^2 \beta \delta \tan \beta) p_\mu$$

Appendix D

Input parameters

For the SPS1a', SPS4, point.10.1.1 and point.40.1.1 benchmark scenarios, the low-energy spectrum is defined by only five GUT scale parameters ($M_0, M_{1/2}, A_0, \tan \beta, \text{sgn}\mu$). Using the renormalization group running, the GUT parameters are evolved down to the SUSY scale

$$Q_{\text{SUSY}} = 1 \text{ TeV} \quad (\text{D.1})$$

according to the SPA convention [55]. Numerically, we use the program Softsusy 3.1.7 [128]. In order to translate the soft-breaking parameters in the $\overline{\text{DR}}$ scheme into the on-shell (OS) scheme, sfermion masses, their mixing angles and the neutralino masses are computed in the $\overline{\text{DR}}$ scheme using tree-level relations. A further subtlety is that the SM particle masses in the squark mass matrix also need to be in $\overline{\text{DR}}$ scheme. Therefore, before computing the squark masses, the SM masses are translated to the $\overline{\text{DR}}$ scheme.

After computing the masses and mixing angles in the $\overline{\text{DR}}$ scheme, they are translated to the OS scheme using relations

$$(m_{\tilde{q}_i}^2)^{\text{OS}} = (m_{\tilde{q}_i}^2)^{\overline{\text{DR}}} + (\delta m_{\tilde{q}_i}^2)^{\text{OS}} - (\delta m_{\tilde{q}_i}^2)^{\overline{\text{DR}}}, \quad i = 1, 2, \quad (\text{D.2a})$$

$$\theta_{\tilde{t}}^{\text{OS}} = \theta_{\tilde{t}}^{\overline{\text{DR}}} + \delta\theta_{\tilde{t}}^{\text{OS}} - \delta\theta_{\tilde{t}}^{\overline{\text{DR}}}, \quad (\text{D.2b})$$

$$m_{\tilde{\chi}_1^0}^{\text{OS}} = m_{\tilde{\chi}_1^0}^{\overline{\text{DR}}} + \delta m_{\tilde{\chi}_1^0}^{\text{OS}} - \delta m_{\tilde{\chi}_1^0}^{\overline{\text{DR}}}, \quad (\text{D.2c})$$

$$m_{\tilde{\chi}_i^\pm}^{\text{OS}} = m_{\tilde{\chi}_i^\pm}^{\overline{\text{DR}}} + \delta m_{\tilde{\chi}_i^\pm}^{\text{OS}} - \delta m_{\tilde{\chi}_i^\pm}^{\overline{\text{DR}}}, \quad i = 1, 2. \quad (\text{D.2d})$$

The squark, chargino, and neutralino mass renormalization constants in the OS scheme are given in (4.47), (4.84a), and (4.95a). The according renormalization constants in the $\overline{\text{DR}}$ scheme are obtained by taking the UV-divergent parts of the renormalization constants in the OS scheme. The renormalization constant of the top squark mixing angle in the OS scheme is given by

$$\delta\theta_{\tilde{t}}^{\text{OS}} = \det(U_{\tilde{t}}) \frac{\delta Y_{\tilde{t}}}{m_{\tilde{t}_1}^2 - m_{\tilde{t}_2}^2} \quad (\text{D.3})$$

with the renormalization constant $\delta Y_{\tilde{t}}$ defined in (4.64b). Again, the top squark mixing angle renormalization constant in the $\overline{\text{DR}}$ scheme is obtained by taking the UV-divergent part of $\delta Y_{\tilde{t}}$.

As mentioned in Subsection 4.1.3 each generation of the light-flavor squarks has three and the third-generation squark sector five input parameters $M_{\tilde{q}_L}, M_{\tilde{u}_R}, M_{\tilde{d}_R}$ and the trilinear couplings for the third generation A_t, A_b . Thus, the $\overline{\text{DR}}$ to on-shell transition (D.2a) is performed for $m_{\tilde{u}_{L,R}}$ and $m_{\tilde{d}_R}$ ($m_{\tilde{t}_{1,2}}$ and $m_{\tilde{b}_2}$ for third generation squarks). The fourth dependent squark mass $m_{\tilde{d}_L}$ ($m_{\tilde{b}_1}$) is computed via (4.55) and (4.65). Since in the bottom-quark/squark sector the trilinear coupling A_b is treated in the $\overline{\text{DR}}$ scheme, only the mixing angle of the top squark is translated into the on-shell scheme.

Similarly, the chargino and neutralino sector is defined by the three parameters M_1, M_2 and μ (Subsection 4.1.3). Thus, the $\overline{\text{DR}}$ to on-shell transitions are performed for the three masses $m_{\tilde{\chi}_{1,2}^\pm}$ and $m_{\tilde{\chi}_0}$. The remaining three neutralino masses obtained with relation (4.96).

In summary, the procedure to obtain soft-breaking input parameters in the on-shell scheme is as follows:

1. Define CMSSM parameters $(M_0, M_{1/2}, A_0, \tan \beta, \text{sgn} \mu)$ at the GUT scale.
2. Evolve parameters at the GUT scale down to Q_{SUSY} .
3. Translate $\overline{\text{DR}}$ parameters at Q_{SUSY} to the on-shell scheme:
 - (a) Translate SM parameters into the $\overline{\text{DR}}$ scheme.
 - (b) Compute sparticle masses and mixing angles using tree-level relations.
 - (c) Translate sparticle masses and stop mixing angle into the on-shell scheme.
 - (d) Compute soft-breaking parameters in the on-shell scheme using tree-level relations.
 - (e) Compute the dependent on-shell masses for the subset of squark and neutralino masses mentioned above.

Bibliography

- [1] A. Einstein, *The Foundation of the General Theory of Relativity*, *Annalen Phys.* **49** (1916) 769–822.
- [2] E. Schrödinger, *Quantisierung als Eigenwertproblem I*, *Annalen Phys.* **79** (1926) 361–376.
E. Schrödinger, *Quantisierung als Eigenwertproblem II*, *Annalen Phys.* **79** (1926) 489–527.
E. Schrödinger, *Quantisierung als Eigenwertproblem III*, *Annalen Phys.* **80** (1926) 734–756.
E. Schrödinger, *Quantisierung als Eigenwertproblem IV*, *Annalen Phys.* **81** (1926) 109–139.
- [3] W. Heisenberg, *Über den anschaulichen Inhalt der quantentheoretischen Kinematik und Mechanik*, *Z.Phys.* **43** (1927) 172–198.
- [4] S. Glashow, *Partial Symmetries of Weak Interactions*, *Nucl.Phys.* **22** (1961) 579–588.
S. Weinberg, *A Model of Leptons*, *Phys.Rev.Lett.* **19** (1967) 1264–1266.
A. Salam, *Weak and Electromagnetic Interactions*, .
- [5] S. Glashow, J. Iliopoulos, and L. Maiani, *Weak Interactions with Lepton-Hadron Symmetry*, *Phys.Rev.* **D2** (1970) 1285–1292.
- [6] H. Fritzsch, M. Gell-Mann, and H. Leutwyler, *Advantages of the Color Octet Gluon Picture*, *Phys.Lett.* **B47** (1973) 365–368.
- [7] D. Gross and F. Wilczek, *Asymptotically Free Gauge Theories. 1*, *Phys.Rev.* **D8** (1973) 3633–3652.
D. Gross and F. Wilczek, *Asymptotically Free Gauge Theories. 2.*, *Phys.Rev.* **D9** (1974) 980–993.
- [8] H. Politzer, *Reliable Perturbative Results for Strong Interactions?*, *Phys.Rev.Lett.* **30** (1973) 1346–1349.

- [9] P. W. Higgs, *Broken Symmetries and the Masses of Gauge Bosons*, *Phys.Rev.Lett.* **13** (1964) 508–509.
P. W. Higgs, *Spontaneous Symmetry Breakdown without Massless Bosons*, *Phys.Rev.* **145** (1966) 1156–1163.
F. Englert and R. Brout, *Broken Symmetry and the Mass of Gauge Vector Mesons*, *Phys.Rev.Lett.* **13** (1964) 321–322.
G. Guralnik, C. Hagen, and T. Kibble, *Global Conservation Laws and Massless Particles*, *Phys.Rev.Lett.* **13** (1964) 585–587.
- [10] **ATLAS** Collaboration, G. Aad *et. al.*, *Combined Search for the Standard Model Higgs Boson Using up to 4.9 fb⁻¹ of pp Collision Data at sqrt(s) = 7 TeV with the ATLAS Detector at the LHC*, *Phys.Lett.* **B710** (2012) 49–66, [[arXiv:1202.1408](#)].
- [11] **CMS** Collaboration, S. Chatrchyan *et. al.*, *Combined Results of Searches for the Standard Model Higgs Boson in pp Collisions at sqrt(s) = 7 TeV*, *Phys.Lett.* **B710** (2012) 26–48, [[arXiv:1202.1488](#)].
- [12] J. Wess and B. Zumino, *A Lagrangian Model Invariant Under Supergauge Transformations*, *Phys.Lett.* **B49** (1974) 52.
- [13] H. P. Nilles, *Supersymmetry, Supergravity and Particle Physics*, *Phys.Rept.* **110** (1984) 1–162.
- [14] H. E. Haber and G. L. Kane, *The Search for Supersymmetry: Probing Physics Beyond the Standard Model*, *Phys. Rept.* **117** (1985) 75–263.
- [15] G. R. Farrar and P. Fayet, *Phenomenology of the Production, Decay, and Detection of New Hadronic States Associated with Supersymmetry*, *Phys.Lett.* **B76** (1978) 575–579.
- [16] **Particle Data Group** Collaboration, K. Nakamura *et. al.*, *Review of Particle Physics*, *J.Phys.G* **G37** (2010) 075021.
- [17] S. Heinemeyer, W. Hollik, D. Stöckinger, A. Weber, and G. Weiglein, *Precise Prediction for M(W) in the MSSM*, *JHEP* **0608** (2006) 052, [[hep-ph/0604147](#)].
J. R. Ellis, S. Heinemeyer, K. Olive, A. Weber, and G. Weiglein, *The Supersymmetric Parameter Space in Light of B⁻ physics Observables and Electroweak Precision Data*, *JHEP* **0708** (2007) 083.
S. Heinemeyer, W. Hollik, A. Weber, and G. Weiglein, *Z Pole Observables in the MSSM*, *JHEP* **0804** (2008) 039.
- [18] G. 't Hooft and M. Veltman, *Regularization and Renormalization of Gauge Fields*, *Nucl.Phys.* **B44** (1972) 189–213.

- [19] **Muon G-2** Collaboration, G. Bennett *et. al.*, *Final Report of the Muon E821 Anomalous Magnetic Moment Measurement at BNL*, *Phys.Rev.* **D73** (2006) 072003, [hep-ex/0602035]. Summary of E821 Collaboration measurements of the muon anomalous magnetic moment, each reported earlier in Letters or Brief Reports. Revised version submitted to *Phys.Rev.D*.
- T. Moroi, *The Muon Anomalous Magnetic Dipole Moment in the Minimal Supersymmetric Standard Model*, *Phys.Rev.* **D53** (1996) 6565–6575, [hep-ph/9512396].
- A. Czarnecki and W. J. Marciano, *The Muon Anomalous Magnetic Moment: A Harbinger for 'New Physics'*, *Phys.Rev.* **D64** (2001) 013014, [hep-ph/0102122].
- J. P. Miller, E. de Rafael, and B. Roberts, *Muon ($g-2$): Experiment and Theory*, *Rept.Prog.Phys.* **70** (2007) 795, [hep-ph/0703049].
- F. Jegerlehner, *Essentials of the Muon $g-2$* , *Acta Phys.Polon.* **B38** (2007) 3021, [hep-ph/0703125].
- M. Passera, W. Marciano, and A. Sirlin, *The Muon $g-2$ and the Bounds on the Higgs Boson Mass*, *Phys.Rev.* **D78** (2008) 013009, [arXiv:0804.1142].
- [20] **LEP Electroweak Working Group, SLD Electroweak Group, SLD Heavy Flavour Group** Collaboration, *Precision Electroweak Measurements on the Z Resonance*, *Phys.Rept.* **427** (2006) 257–454, [hep-ex/0509008].
- [21] H. Flächer, M. Goebel, J. Haller, A. Höcker, K. Mönig, *et. al.*, *Revisiting the Global Electroweak Fit of the Standard Model and Beyond with Gfitter*, *Eur.Phys.J.* **C60** (2009) 543–583, [arXiv:0811.0009].
- [22] M. Drees, R. Godbole, and P. Roy, *Theory and Phenomenology of Sparticles: An Account of Four-Dimensional $N=1$ Supersymmetry in High Energy Physics*, *World Scientific Publishing* (2004).
- [23] S. P. Martin, *A Supersymmetry Primer*, hep-ph/9709356.
- [24] S. R. Coleman and J. Mandula, *All Possible Symmetries of the S Matrix*, *Phys.Rev.* **159** (1967) 1251–1256.
- [25] A. Salam and J. Strathdee, *Supergauge Transformations*, *Nucl.Phys.* **B76** (1974) 477–482.
- [26] L. Girardello and M. T. Grisaru, *Soft Breaking of Supersymmetry*, *Nucl.Phys.* **B194** (1982) 65.
- [27] **LEP Working Group for Higgs Boson Searches** Collaboration, S. Schael *et. al.*, *Search for neutral MSSM Higgs bosons at LEP*, *Eur.Phys.J.* **C47** (2006) 547–587, [hep-ex/0602042].

- [28] H. E. Haber and R. Hempfling, *The Renormalization Group Improved Higgs Sector of the Minimal Supersymmetric Model*, *Phys.Rev.* **D48** (1993) 4280–4309, [[hep-ph/9307201](#)]. Revised version.
H. E. Haber, R. Hempfling, and A. H. Hoang, *Approximating the Radiatively Corrected Higgs Mass in the Minimal Supersymmetric Model*, *Z.Phys.* **C75** (1997) 539–554, [[hep-ph/9609331](#)].
- [29] M. Frank, T. Hahn, S. Heinemeyer, W. Hollik, H. Rzehak, and G. Weiglein, *The Higgs Boson Masses and Mixings of the Complex MSSM in the Feynman-Diagrammatic Approach*, *JHEP* **02** (2007) 047, [[hep-ph/0611326](#)].
G. Degrandi, S. Heinemeyer, W. Hollik, P. Slavich, and G. Weiglein, *Towards high-precision predictions for the MSSM Higgs sector*, *Eur. Phys. J.* **C28** (2003) 133–143, [[hep-ph/0212020](#)].
S. Heinemeyer, W. Hollik, and G. Weiglein, *The Masses of the neutral CP - even Higgs bosons in the MSSM: Accurate analysis at the two loop level*, *Eur. Phys. J.* **C9** (1999) 343–366, [[hep-ph/9812472](#)].
S. Heinemeyer, W. Hollik, and G. Weiglein, *FeynHiggs: a Program for the Calculation of the Masses of the Neutral CP-Even Higgs Bosons in the MSSM*, *Comput. Phys. Commun.* **124** (2000) 76–89, [[hep-ph/9812320](#)].
- [30] A. Denner, *Techniques for Calculation of Electroweak Radiative Corrections at the One Loop Level and Results for W Physics at LEP-200*, *Fortschr. Phys.* **41** (1993) 307–420, [[arXiv:0709.1075](#)].
- [31] G. Passarino and M. Veltman, *One Loop Corrections for $e^+ e^-$ Annihilation Into $\mu^+ \mu^-$ in the Weinberg Model*, *Nucl.Phys.* **B160** (1979) 151.
- [32] T. Hahn and M. Perez-Victoria, *Automatized One Loop Calculations in Four-Dimensions and D-Dimensions*, *Comput.Phys.Commun.* **118** (1999) 153–165, [[hep-ph/9807565](#)].
T. Hahn, *Optimizations for the Computation of Radiative Corrections*, *Nucl.Phys.Proc.Suppl.* **116** (2003) 363–367, [[hep-ph/0210220](#)].
T. Hahn, *New Features in FormCalc 4*, *Nucl.Phys.Proc.Suppl.* **135** (2004) 333–337, [[hep-ph/0406288](#)].
T. Hahn, *New Developments in FormCalc 4.1*, [hep-ph/0506201](#).
T. Hahn and M. Rauch, *News from FormCalc and LoopTools*, *Nucl.Phys.Proc.Suppl.* **157** (2006) 236–240, [[hep-ph/0601248](#)].
T. Hahn and J. Illana, *Excursions into FeynArts and FormCalc*, *Nucl.Phys.Proc.Suppl.* **160** (2006) 101–105, [[hep-ph/0607049](#)].
T. Hahn, *A Mathematica Interface for FormCalc-Generated Code*, *Comput.Phys.Commun.* **178** (2008) 217–221, [[hep-ph/0611273](#)].

- [33] K. K. E. Byckling, *Particle Kinematics*. John Wiley and Sons Ltd, 1973.
- [34] T. Fritzsche, *Berechnung von Observablen zur supersymmetrischen Teilchenerzeugung an Hochenergie-Collidern unter Einschluss hoeherer Ordnungen*. PhD thesis, 2005.
- [35] W. Hollik and D. Stöckinger, *Regularization and Supersymmetry Restoring Counterterms in Supersymmetric QCD*, *Eur.Phys.J.* **C20** (2001) 105–119, [hep-ph/0103009].
- [36] W. Hollik, E. Kraus, M. Roth, C. Rupp, K. Sibold, and D. Stöckinger, *Renormalization of the Minimal Supersymmetric Standard Model*, *Nucl.Phys.* **B639** (2002) 3–65, [hep-ph/0204350].
- [37] C. Bollini and J. Giambiagi, *Lowest Order Divergent Graphs in ν -Dimensional Space*, *Phys.Lett.* **B40** (1972) 566–568.
- [38] W. Siegel, *Supersymmetric Dimensional Regularization via Dimensional Reduction*, *Phys.Lett.* **B84** (1979) 193.
- [39] W. Siegel, *Inconsistency of Supersymmetric Dimensional Regularization*, *Phys.Lett.* **B94** (1980) 37.
- [40] D. Stöckinger, *Regularization by Dimensional Reduction: Consistency, Quantum Action Principle, and Supersymmetry*, *JHEP* **0503** (2005) 076, [hep-ph/0503129].
- [41] H. Lehmann, K. Symanzik, and W. Zimmermann, *On the Formulation of Quantized Field Theories*, *Nuovo Cim.* **1** (1955) 205–225.
- [42] M. Böhm, H. Spiesberger, and W. Hollik, *On the One Loop Renormalization of the Electroweak Standard Model and Its Application to Leptonic Processes*, *Fortsch.Phys.* **34** (1986) 687–751.
- [43] W. A. Bardeen, A. Buras, D. Duke, and T. Muta, *Deep Inelastic Scattering Beyond the Leading Order in Asymptotically Free Gauge Theories*, *Phys.Rev.* **D18** (1978) 3998.
- [44] P. H. Chankowski, S. Pokorski, and J. Rosiek, *One Loop Corrections to the Supersymmetric Higgs Boson Couplings and LEP Phenomenology*, *Phys.Lett.* **B286** (1992) 307–314.
- [45] A. Dabelstein, *The One Loop Renormalization of the MSSM Higgs Sector and its Application to the Neutral Scalar Higgs Masses*, *Z. Phys.* **C67** (1995) 495–512, [hep-ph/9409375].

- [46] A. Brignole, *Radiative Corrections to the Supersymmetric Neutral Higgs Boson Masses*, *Phys.Lett.* **B281** (1992) 284–294.
M. Frank, S. Heinemeyer, W. Hollik, and G. Weiglein, *FeynHiggs1.2: Hybrid MS-Bar / On-Shell Renormalization for the CP Even Higgs Boson Sector in the MSSM*, [hep-ph/0202166](#).
- [47] A. Freitas and D. Stöckinger, *Gauge Dependence and Renormalization of $\tan\beta$ in the MSSM*, *Phys.Rev.* **D66** (2002) 095014, [[hep-ph/0205281](#)].
- [48] **CDF and D0** Collaboration, *Combination of CDF and D0 Results on the Mass of the Top Quark Using up to 5.6 fb^{-1} of Data*, [arXiv:1007.3178](#).
- [49] A. H. Hoang and I. W. Stewart, *Top Mass Measurements from Jets and the Tevatron Top-Quark Mass*, *Nucl.Phys.Proc.Suppl.* **185** (2008) 220–226, [[arXiv:0808.0222](#)].
- [50] U. Langenfeld, S. Moch, and P. Uwer, *Measuring the Running Top-Quark Mass*, *Phys.Rev.* **D80** (2009) 054009, [[arXiv:0906.5273](#)].
S. Moch, U. Langenfeld, and P. Uwer, *The Top-Quark’s Running Mass*, *PoS RADCOR2009* (2010) 030, [[arXiv:1001.3987](#)].
- [51] S. Heinemeyer, W. Hollik, H. Rzehak, and G. Weiglein, *High-Precision Predictions for the MSSM Higgs Sector at $O(\alpha(b)\alpha(s))$* , *Eur.Phys.J.* **C39** (2005) 465–481, [[hep-ph/0411114](#)].
- [52] W. Hollik and H. Rzehak, *The Sfermion Mass Spectrum of the MSSM at the One-Loop Level*, *Eur. Phys. J.* **C32** (2003) 127–133, [[hep-ph/0305328](#)].
- [53] S. Heinemeyer, H. Rzehak, and C. Schappacher, *Proposals for Bottom Quark/Squark Renormalization in the Complex MSSM*, *Phys.Rev.* **D82** (2010) 075010, [[arXiv:1007.0689](#)].
- [54] T. Fritzsche and W. Hollik, *Complete One-Loop Corrections to the Mass Spectrum of Charginos and Neutralinos in the MSSM*, *Eur. Phys. J.* **C24** (2002) 619–629, [[hep-ph/0203159](#)].
- [55] J. A. Aguilar-Saavedra *et. al.*, *Supersymmetry Parameter Analysis: SPA Convention and Project*, *Eur. Phys. J.* **C46** (2006) 43–60, [[hep-ph/0511344](#)].
- [56] T. Kinoshita, *Mass Singularities of Feynman Amplitudes*, *J.Math.Phys.* **3** (1962) 650–677.
- [57] F. Bloch and A. Nordsieck, *Note on the Radiation Field of the Electron*, *Phys. Rev.* **52** (Jul, 1937) 54–59.

- [58] T. Lee and M. Nauenberg, *Degenerate Systems and Mass Singularities*, *Phys.Rev.* **133** (1964) B1549–B1562.
- [59] R. Kleiss, *Hard Bremsstrahlung Amplitudes for $e^+ e^-$ Collisions with Polarized Beams at LEP / SLC Energies*, *Z.Phys.* **C33** (1987) 433.
F. A. Berends, R. Kleiss, P. De Causmaecker, R. Gastmans, W. Troost, *et. al.*, *Multiple Bremsstrahlung in Gauge Theories at High-Energies. 2. Single Bremsstrahlung*, *Nucl.Phys.* **B206** (1982) 61.
- [60] S. Catani and M. Seymour, *The Dipole Formalism for the Calculation of QCD Jet Cross-Sections at Next-to-Leading Order*, *Phys.Lett.* **B378** (1996) 287–301, [[hep-ph/9602277](#)].
S. Catani and M. Seymour, *A General Algorithm for Calculating Jet Cross-Sections in NLO QCD*, *Nucl.Phys.* **B485** (1997) 291–419, [[hep-ph/9605323](#)].
- [61] S. Catani, S. Dittmaier, M. H. Seymour, and Z. Trocsanyi, *The Dipole Formalism for Next-to-Leading Order QCD Calculations with Massive Partons*, *Nucl.Phys.* **B627** (2002) 189–265, [[hep-ph/0201036](#)].
- [62] S. Dittmaier, A. Kabelschacht, and T. Kasprzik, *Polarized QED Splittings of Massive Fermions and Dipole Subtraction for non-Collinear-Safe Observables*, *Nucl.Phys.* **B800** (2008) 146–189, [[arXiv:0802.1405](#)].
- [63] G. 't Hooft and M. Veltman, *Scalar One Loop Integrals*, *Nucl.Phys.* **B153** (1979) 365–401.
- [64] U. Baur, S. Keller, and D. Wackerroth, *Electroweak Radiative Corrections to W Boson Production in Hadronic Collisions*, *Phys.Rev.* **D59** (1999) 013002, [[hep-ph/9807417](#)].
S. Keller and E. Laenen, *Next-to-Leading Order Cross-Sections for Tagged Reactions*, *Phys.Rev.* **D59** (1999) 114004, [[hep-ph/9812415](#)].
- [65] S. Dittmaier, *Separation of Soft and Collinear Singularities from one Loop N point Integrals*, *Nucl.Phys.* **B675** (2003) 447–466, [[hep-ph/0308246](#)].
- [66] J. Küblbeck, M. Böhm, and A. Denner, *FeynArts: Computer Algebraic Generation of Feynman Graphs and Amplitudes*, *Comput.Phys.Commun.* **60** (1990) 165–180.
T. Hahn, *Generating Feynman Diagrams and Amplitudes with FeynArts 3*, *Comput. Phys. Commun.* **140** (2001) 418–431, [[hep-ph/0012260](#)].
- [67] T. Hahn and C. Schappacher, *The Implementation of the minimal supersymmetric standard model in FeynArts and FormCalc*, *Comput.Phys.Commun.* **143** (2002) 54–68, [[hep-ph/0105349](#)].

- [68] G. van Oldenborgh and J. Vermaseren, *New Algorithms for One Loop Integrals*, *Z.Phys.* **C46** (1990) 425–438.
- [69] T. Hahn, *CUBA: A Library for Multidimensional Numerical Integration*, *Comput.Phys.Commun.* **168** (2005) 78–95, [[hep-ph/0404043](#)].
- [70] P. Z. Skands, B. Allanach, H. Baer, C. Balazs, G. Belanger, *et. al.*, *SUSY Les Houches Accord: Interfacing SUSY Spectrum Calculators, Decay Packages, and Event Generators*, *JHEP* **0407** (2004) 036, [[hep-ph/0311123](#)].
B. Allanach, C. Balazs, G. Belanger, M. Bernhardt, F. Boudjema, *et. al.*, *SUSY Les Houches Accord 2*, *Comput.Phys.Commun.* **180** (2009) 8–25, [[arXiv:0801.0045](#)].
- [71] T. Hahn, *SUSY Les Houches Accord I/O Made Easy*, [hep-ph/0408283](#).
T. Hahn, *SUSY Les Houches Accord 2 I/O Made Easy*, *Comput.Phys.Commun.* **180** (2009) 1681–1693, [[hep-ph/0605049](#)].
- [72] **ATLAS** Collaboration, W. Armstrong *et. al.*, *ATLAS: Technical Proposal for a General-Purpose $p p$ Experiment at the Large Hadron Collider at CERN*, tech. rep., 1994. CERN-LHCC-94-43.
- [73] *CMS, the Compact Muon Solenoid: Technical proposal*, tech. rep., 1994. CERN-LHCC-94-38.
- [74] **LHCb** Collaboration, S. Amato *et. al.*, *LHCb Technical Proposal*, tech. rep., 1998. CERN-LHCC-98-04.
R. Hierck, *Physics Performance Study of the $B/s0 \rightarrow D/s \pi$ and $B/s0 \rightarrow D/s K$ Decay Channels for the Technical Pproposal of the LHCb Detector*, . CERN-THESIS-2000-045.
- [75] *ALICE: Technical Proposal for a Large Ion Collider Experiment at the CERN LHC*, tech. rep., 1995. CERN-LHCC-95-71.
- [76] P. Harrison and C. Llewellyn Smith, *Hadroproduction of Supersymmetric Particles*, *Nucl.Phys.* **B213** (1983) 223.
S. Dawson, E. Eichten, and C. Quigg, *Search for Supersymmetric Particles in Hadron - Hadron Collisions*, *Phys.Rev.* **D31** (1985) 1581.
E. Reya and D. Roy, *Supersymmetric Particle Production at p anti- p Collider Energies*, *Phys.Rev.* **D32** (1985) 645.
H. Baer, M. Bisset, X. Tata, and J. Woodside, *Supercollider Signals from Gluino and Squark Decays to Higgs bosons*, *Phys. Rev.* **D46** (1992) 303–314.
- [77] S. Bornhauser, M. Drees, H. K. Dreiner, and J. S. Kim, *Electroweak Contributions to Squark Pair Production at the LHC*, *Phys.Rev.* **D76** (2007) 095020, [[arXiv:0709.2544](#)].

- [78] W. Beenakker, R. Höpker, M. Spira, and P. Zerwas, *Squark and gluino Production at Hadron Colliders*, *Nucl.Phys.* **B492** (1997) 51–103, [hep-ph/9610490].
- [79] J. Germer, W. Hollik, and E. Mirabella, *Hadronic Production of Bottom-Squark Pairs with Electroweak Contributions*, *JHEP* **1105** (2011) 068, [arXiv:1103.1258].
J. Germer, W. Hollik, E. Mirabella, and M. K. Trenkel, *Hadronic Production of Squark-Squark Pairs: The Electroweak Contributions*, *JHEP* **1008** (2010) 023, [arXiv:1004.2621].
W. Hollik, E. Mirabella, and M. K. Trenkel, *Electroweak Contributions to Squark-Gluino Production at the LHC*, *JHEP* **0902** (2009) 002, [arXiv:0810.1044].
W. Hollik, M. Kollar, and M. K. Trenkel, *Hadronic Production of Top-Squark Pairs with Electroweak NLO Contributions*, *JHEP* **0802** (2008) 018, [arXiv:0712.0287].
W. Hollik and E. Mirabella, *Squark Anti-Squark Pair Production at the LHC: The Electroweak Contribution*, *JHEP* **0812** (2008) 087, [arXiv:0806.1433].
- [80] W. Beenakker, R. Höpker, and M. Spira, *PROSPINO: A Program for the Production of Supersymmetric Particles in Next-to-Leading order QCD*, hep-ph/9611232.
- [81] A. Kulesza and L. Motyka, *Threshold resummation for squark-antisquark and gluino-pair production at the LHC*, *Phys.Rev.Lett.* **102** (2009) 111802, [arXiv:0807.2405].
A. Kulesza and L. Motyka, *Soft gluon resummation for the production of gluino-gluino and squark-antisquark pairs at the LHC*, *Phys.Rev.* **D80** (2009) 095004, [arXiv:0905.4749].
- [82] W. Beenakker, S. Brensing, M. Krämer, A. Kulesza, E. Laenen, *et. al.*, *Soft-gluon resummation for squark and gluino hadroproduction*, *JHEP* **0912** (2009) 041, [arXiv:0909.4418].
- [83] W. Beenakker, S. Brensing, M. Krämer, A. Kulesza, E. Laenen, *et. al.*, *Supersymmetric top and bottom squark production at hadron colliders*, *JHEP* **1008** (2010) 098, [arXiv:1006.4771].
- [84] W. Beenakker, S. Brensing, M. Krämer, A. Kulesza, E. Laenen, *et. al.*, *NNLL Resummation for Squark-Antisquark Pair Production at the LHC*, arXiv:1110.2446.
- [85] U. Langenfeld and S.-O. Moch, *Higher-order soft corrections to squark hadro-production*, *Phys.Lett.* **B675** (2009) 210–221, [arXiv:0901.0802].
- [86] H. F. Heath, C. Lynch, S. Moretti, and C. H. Shepherd-Themistocleous, *Higgs Production in Association with Top Squark Pairs in the MSSM at the LHC: the Decay Patterns*, arXiv:0901.1676.

- A. Dedes and S. Moretti, *Higgs Production in Association with Squark Pairs in the Minimal Supersymmetric Standard Model at Future Hadron Colliders*, *Eur. Phys. J.* **C10** (1999) 515–535, [[hep-ph/9904491](#)].
- A. Dedes and S. Moretti, *Higgs Boson Production in Association with Squark Pairs in the MSSM at the LHC*, [hep-ph/9909526](#).
- [87] J. R. Ellis and H. Kowalski, *Supersymmetric Particles at the CERN p anti- p Collider*, *Nucl.Phys.* **B246** (1984) 189.
- V. D. Barger, K. Hagiwara, and W.-Y. Keung, *Constraints on Squark Masses from CERN p anti- p Collider Data*, *Phys.Lett.* **B145** (1984) 147.
- A. Allan, E. Glover, and A. D. Martin, *Scalar Quark Signatures at the anti- p p Collider*, *Phys.Lett.* **B146** (1984) 247.
- [88] R. Barnett, J. F. Gunion, and H. E. Haber, *Gluino Decay Patterns and Signatures*, *Phys.Rev.* **D37** (1988) 1892.
- [89] H. Baer, V. D. Barger, D. Karatas, and X. Tata, *Detecting Gluinos at Hadron Supercolliders*, *Phys.Rev.* **D36** (1987) 96.
- [90] R. Barnett, J. F. Gunion, and H. E. Haber, *Finding Gluinos at Hadron Colliders*, *Phys.Rev.Lett.* **60** (1988) 401.
- [91] G. Gamberini, *Heavy Gluino and Squark Decays at p Anti- p Collider*, *Z.Phys.* **C30** (1986) 605–613.
- [92] H. Baer, J. R. Ellis, G. Gelmini, D. V. Nanopoulos, and X. Tata, *Squark Decays into Gauginos at the p anti- p Collider*, *Phys.Lett.* **B161** (1985) 175.
- [93] A. Bartl, W. Majerotto, B. Mosslacher, N. Oshimo, and S. Stippel, *Gluino and Squark Decays into Heavy Top Quarks*, *Phys.Rev.* **D43** (1991) 2214–2222.
- [94] S. Kraml, H. Eberl, A. Bartl, W. Majerotto, and W. Porod, *SUSY-QCD Corrections to Scalar Quark Decays into Charginos and Neutralinos*, *Phys. Lett.* **B386** (1996) 175–182, [[hep-ph/9605412](#)].
- [95] A. Djouadi, W. Hollik, and C. Jünger, *QCD Corrections to Scalar Quark Decays*, *Phys. Rev.* **D55** (1997) 6975–6985, [[hep-ph/9609419](#)].
- [96] J. Guasch, J. Sola, and W. Hollik, *Yukawa Coupling Corrections to Scalar Quark Decays*, *Phys.Lett.* **B437** (1998) 88–99, [[hep-ph/9802329](#)].
- [97] J. Guasch, W. Hollik, and J. Sola, *Fermionic Decays of Sfermions: A Complete Discussion at One-Loop Order*, *JHEP* **10** (2002) 040, [[hep-ph/0207364](#)].
- J. Guasch, W. Hollik, and J. Sola, *Radiative Corrections to Scalar Quark Decays in the MSSM*, [hep-ph/0001254](#).

- [98] J. Guasch, S. Penaranda, and R. Sanchez-Florit, *Effective Description of Squark Interactions*, *JHEP* **04** (2009) 016, [[arXiv:0812.1114](#)].
- [99] W. Beenakker, R. Höpker, and P. Zerwas, *SUSY QCD Decays of Squarks and Gluinos*, *Phys.Lett.* **B378** (1996) 159–166, [[hep-ph/9602378](#)].
- [100] W. Beenakker, R. Höpker, T. Plehn, and P. Zerwas, *Stop Decays in SUSY QCD*, *Z.Phys.* **C75** (1997) 349–356, [[hep-ph/9610313](#)].
- [101] H.-S. Hou, W.-G. Ma, L.-H. Wan, and R.-Y. Zhang, *Electroweak Corrections to the Decays of Stop and Gluino*, *Phys.Rev.* **D65** (2002) 075019, [[hep-ph/0202032](#)].
- [102] H. Hlucha, H. Eberl, and W. Frisch, *SFOLD - a Program Package for Calculating Two-Body Sfermion Decays at Full One-Loop Level in the MSSM*, [arXiv:1104.2151](#).
- [103] A. Bartl, W. Majerotto, and W. Porod, *Squark and Gluino Decays for Large $\tan\beta$* , *Z.Phys.* **C64** (1994) 499–508.
A. Bartl, H. Eberl, K. Hidaka, S. Kraml, T. Kon, *et. al.*, *Bosonic Decays of Stop(2) and Sbottom(2)*, *Phys.Lett.* **B435** (1998) 118–124, [[hep-ph/9804265](#)].
- [104] A. Bartl *et. al.*, *SUSY-QCD Corrections to Stop and Sbottom Decays into W^{+-} and $Z0$ Bosons*, *Phys. Lett.* **B419** (1998) 243–252, [[hep-ph/9710286](#)].
- [105] A. Arhrib and R. Benbrik, *Third Generation Sfermions Decays into Z and W Gauge Bosons: Full One-Loop Analysis*, *Phys. Rev.* **D71** (2005) 095001, [[hep-ph/0412349](#)].
A. Arhrib and R. Benbrik, *Complete One-Loop Analysis to Stop and Sbottom Decays into Z and W^\pm Bosons*, *Afr.J.Math.Phys.* **3** (2006) 85–91, [[hep-ph/0511116](#)].
- [106] A. Arhrib, A. Djouadi, W. Hollik, and C. Jünger, *SUSY Higgs Boson Decays into Scalar Quarks: QCD Corrections*, *Phys.Rev.* **D57** (1998) 5860–5870, [[hep-ph/9702426](#)].
- [107] A. Bartl, H. Eberl, K. Hidaka, S. Kraml, W. Majerotto, *et. al.*, *SUSY - QCD Corrections to Top and Bottom Squark Decays into Higgs Bosons*, *Phys.Rev.* **D59** (1999) 115007, [[hep-ph/9806299](#)].
- [108] Q. Li, L. G. Jin, and C. S. Li, *Supersymmetric Electroweak Corrections to Heavier Top Squark Decay into Lighter Top Squark and Neutral Higgs Boson*, *Phys.Rev.* **D66** (2002) 115008, [[hep-ph/0207363](#)].
- [109] C. Weber, K. Kovarik, H. Eberl, and W. Majerotto, *Complete One-Loop Corrections to Decays of Charged and CP-Even Neutral Higgs Bosons into Sfermions*, *Nucl.Phys.* **B776** (2007) 138–169, [[hep-ph/0701134](#)].

- [110] G. Altarelli and R. Rückl, *Searching for a Scalar Top at the CERN p anti- p Collider*, *Phys.Lett.* **B144** (1984) 126.
I. I. Bigi and S. Rudaz, *Search for Scalar Superpartners of the Top Quark*, *Phys.Lett.* **B153** (1985) 335–340.
- [111] K.-i. Hikasa and M. Kobayashi, *Light Scalar Top at $e^+ e^-$ Colliders*, *Phys.Rev.* **D36** (1987) 724.
- [112] W. Porod and T. Wöhrmann, *Higher Order Top Squark Decays*, *Phys.Rev.* **D55** (1997) 2907–2917, [[hep-ph/9608472](#)].
- [113] C. Boehm, A. Djouadi, and Y. Mambrini, *Decays of the Lightest Top Squark*, *Phys.Rev.* **D61** (2000) 095006, [[hep-ph/9907428](#)].
- [114] M. Mühlleitner and E. Popenza, *Light Stop Decay in the MSSM with Minimal Flavour Violation*, *JHEP* **1104** (2011) 095, [[arXiv:1102.5712](#)].
- [115] M. Mühlleitner, A. Djouadi, and Y. Mambrini, *SDECAY: A Fortran Code for the Decays of the Supersymmetric Particles in the MSSM*, *Comput. Phys. Commun.* **168** (2005) 46–70, [[hep-ph/0311167](#)].
- [116] A. Djouadi, M. Mühlleitner, and M. Spira, *Decays of Supersymmetric Particles: The Program SUSY-HIT (SUSpect-SdecaY-Hdecay-InTerface)*, *Acta Phys.Polon.* **B38** (2007) 635–644, [[hep-ph/0609292](#)].
- [117] A. Djouadi, J.-L. Kneur, and G. Moultaka, *SuSpect: A Fortran Code for the Supersymmetric and Higgs Particle Spectrum in the MSSM*, *Comput.Phys.Commun.* **176** (2007) 426–455, [[hep-ph/0211331](#)].
- [118] A. Djouadi, J. Kalinowski, and M. Spira, *HDECAY: A Program for Higgs Boson Decays in the Standard Model and its Supersymmetric Extension*, *Comput.Phys.Commun.* **108** (1998) 56–74, [[hep-ph/9704448](#)].
- [119] J. Gunion and H. E. Haber, *Higgs Bosons in Supersymmetric Models. 1.*, *Nucl.Phys.* **B272** (1986) 1.
- [120] S. Heinemeyer, W. Hollik, and G. Weiglein, *Decay Widths of the Neutral CP-Even MSSM Higgs Bosons in the Feynman-Diagrammatic Approach*, *Eur. Phys. J.* **C16** (2000) 139–153, [[hep-ph/0003022](#)].
- [121] **LHC New Physics Working Group** Collaboration, D. Alves *et. al.*, *Simplified Models for LHC New Physics Searches*, [arXiv:1105.2838](#).
- [122] H. P. Nilles, *Dynamically Broken Supergravity and the Hierarchy Problem*, *Phys.Lett.* **B115** (1982) 193.

- A. H. Chamseddine, R. L. Arnowitt, and P. Nath, *Locally Supersymmetric Grand Unification*, *Phys.Rev.Lett.* **49** (1982) 970.
- R. Barbieri, S. Ferrara, and C. A. Savoy, *Gauge Models with Spontaneously Broken Local Supersymmetry*, *Phys.Lett.* **B119** (1982) 343.
- [123] B. C. Allanach *et. al.*, *The Snowmass Points and Slopes: Benchmarks for SUSY Searches*, *Eur. Phys. J.* **C25** (2002) 113–123, [[hep-ph/0202233](#)].
- [124] M. J. Dolan, D. Grellscheid, J. Jaeckel, V. V. Khoze, and P. Richardson, *New Constraints on Gauge Mediation and Beyond from LHC SUSY Searches at 7 TeV*, *JHEP* **1106** (2011) 095, [[arXiv:1104.0585](#)].
- [125] **ATLAS** Collaboration, G. Aad *et. al.*, *Search for Supersymmetry in Final States with Jets, Missing Transverse Momentum and one Isolated Lepton in $\sqrt{s} = 7$ TeV pp Collisions Using 1 fb^{-1} of ATLAS Data*, *Phys.Rev.* **D85** (2012) 012006, [[arXiv:1109.6606](#)]. 18 pages plus author list (30 pages total), 9 figures, 4 tables, final version to appear in Physical Review D.
- [126] **CMS** Collaboration, S. Chatrchyan *et. al.*, *Search for Supersymmetry at the LHC in Events with Jets and Missing Transverse Energy*, *Phys.Rev.Lett.* **107** (2011) 221804, [[arXiv:1109.2352](#)].
- [127] S. AbdusSalam, B. Allanach, H. Dreiner, J. Ellis, U. Ellwanger, *et. al.*, *Benchmark Models, Planes, Lines and Points for Future SUSY Searches at the LHC*, [arXiv:1109.3859](#).
- [128] B. C. Allanach, *SOFTSUSY: a Program for Calculating Supersymmetric Spectra*, *Comput. Phys. Commun.* **143** (2002) 305–331, [[hep-ph/0104145](#)].
- [129] A. Freitas, A. von Manteuffel, and P. Zerwas, *Slepton Production at e^+e^- and e^-e^- Linear Colliders*, *Eur.Phys.J.* **C34** (2004) 487–512, [[hep-ph/0310182](#)].
- [130] A. Chatterjee, M. Drees, S. Kulkarni, and Q. Xu, *On the On-Shell Renormalization of the Chargino and Neutralino Masses in the MSSM*, [arXiv:1107.5218](#).
- [131] R. Barbieri, G. Gamberini, G. F. Giudice, and G. Ridolfi, *Constraining Supergravity Models from Gluino Production*, *Nucl.Phys.* **B301** (1988) 15.
- [132] H. Baer, X. Tata, and J. Woodside, *Phenomenology of Gluino Decays via Loops and Top Quark Yukawa Coupling*, *Phys.Rev.* **D42** (1990) 1568–1576.
- [133] W. Frisch, H. Eberl, and H. Hlucha, *HFOLD - a Program Package for Calculating Two-Body MSSM Higgs Decays at Full One-Loop Level*, *Comput.Phys.Commun.* **182** (2011) 2219–2226, [[arXiv:1012.5025](#)].
- [134] A. Djouadi, *The Higgs Sector of Supersymmetric Theories and the Implications for High-Energy Colliders*, *Eur. Phys. J.* **C59** (2009) 389–426, [[arXiv:0810.2439](#)].

- [135] H. Eberl, K. Hidaka, S. Kraml, W. Majerotto, and Y. Yamada, *Improved SUSY QCD Corrections to Higgs Boson Decays into Quarks and Squarks*, *Phys. Rev.* **D62** (2000) 055006, [hep-ph/9912463].
- [136] H. Baer, D. Dicus, M. Drees, and X. Tata, *Higgs Boson Signals in Superstring Inspired Models at Hadron Supercolliders*, *Phys.Rev.* **D36** (1987) 1363.
J. F. Gunion and H. E. Haber, *Higgs Bosons in Supersymmetric Models. 3. Decays into Neutralinos and Charginos*, *Nucl.Phys.* **B307** (1988) 445.
K. Griest and H. E. Haber, *Invisible Decays of Higgs Bosons in Supersymmetric Models*, *Phys.Rev.* **D37** (1988) 719.
- [137] A. Djouadi, J. Kalinowski, and P. Zerwas, *Exploring the SUSY Higgs Sector at e^+e^- Linear Colliders: A Synopsis*, *Z.Phys.* **C57** (1993) 569–584.
A. Djouadi, P. Janot, J. Kalinowski, and P. Zerwas, *SUSY Decays of Higgs Particles*, *Phys.Lett.* **B376** (1996) 220–226, [hep-ph/9603368].
A. Djouadi, J. Kalinowski, P. Ohmann, and P. Zerwas, *Heavy SUSY Higgs Bosons at e^+e^- Linear Colliders*, *Z.Phys.* **C74** (1997) 93–111, [hep-ph/9605339].
A. Djouadi, *Impact of the SUSY Decays on the Search for the MSSM Higgs bosons at the LHC*, *Mod.Phys.Lett.* **A14** (1999) 359–368, [hep-ph/9903382].
G. Belanger, F. Boudjema, F. Donato, R. Godbole, and S. Rosier-Lees, *SUSY Higgs at the LHC: Effects of Light Charginos and Neutralinos*, *Nucl.Phys.* **B581** (2000) 3–33, [hep-ph/0002039].
- [138] L.-H. Wan, W.-G. Ma, R.-Y. Zhang, and Y. Jiang, *Electroweak Corrections to the Charged Higgs Boson Decay into Chargino and Neutralino*, *Phys.Rev.* **D64** (2001) 115004, [hep-ph/0107089].
- [139] M. Drees, M. M. Nojiri, D. Roy, and Y. Yamada, *Light Higgsino Dark Matter*, *Phys.Rev.* **D56** (1997) 276–290, [hep-ph/9701219].
- [140] A. Djouadi, M. Drees, P. Fileviez Perez, and M. Mühlleitner, *Loop Induced Higgs and Z boson Couplings to Neutralinos and Implications for Collider and Dark Matter Searches*, *Phys.Rev.* **D65** (2002) 075016, [hep-ph/0109283].
- [141] H. Eberl, M. Kincel, W. Majerotto, and Y. Yamada, *One Loop Corrections to Neutral Higgs Boson Decays into Neutralinos*, *Nucl.Phys.* **B625** (2002) 372–388, [hep-ph/0111303].
- [142] J. M. Lindert, F. D. Steffen, and M. K. Trenkel, *Direct Stau Production at Hadron Colliders in Cosmologically Motivated Scenarios*, *JHEP* **1108** (2011) 151, [arXiv:1106.4005].

Acknowledgments

First and foremost, I would like to thank my supervisor Prof. Wolfgang Hollik for giving me the opportunity to work in such a fascinating field of research. His continuous support and invaluable advice during all stages of the thesis have made this work possible in the first place.

I am indebted to my fellow PhD students in the Phenomenology Group, Sophia Borowka, Thi Nhung Dao, Jan Germer, Tobias Kasprzik, Jonas Lindert, Edoardo Mirabella, Davide Pagani, Sebastian Paßehr, Maike Trenkel and my office mate Jochen Baumann for fruitful discussions and creating the most pleasant work atmosphere. Furthermore, my gratitude goes to all senior members of the Phenomenology Group who helped me whenever necessary. For proofreading (parts of) my thesis, I thank Jonas Lindert, Daniel Härtel, Patrick Kerner, and Clemens Kießig.

Many thanks go to Frank Daniel Steffen for taking care of the International Max Planck Research School on Elementary Particle Physics and always standing up for us PhD students, to Thomas Hahn and Peter Breitenlohner for enduring my computer issues. I would like to thank the secretary of the Phenomenology Group Monika Goldammer and Rosita Jurgeleit for their kind and uncomplicated support. Furthermore, I am grateful to Corina Brunnlechner, Regina Henning, and Jördis Scholz for helping me with all possible administrative issues.

Last but not least, I would like to express my deepest gratitude to my family and my friends. Your support gave me the strength to accomplish this task.